

THE UNIVERSITY OF HULL

**Development of novel continuous flow reaction
methodology for fine chemical production**

being a Thesis submitted for the Degree of Doctor of
Philosophy in the University of Hull

By

Mohammed Alotaibi

BSc, MSc

June 2016

This thesis is dedicated to my

Wonderful deeply missed mother

Forever you remain in my soul

Acknowledgments

Without help and support, this thesis would not have been possible. I am deeply grateful to each and all. Firstly, thank you Professor Gillian M Greenway, Professor Stephen M Kelly, Professor Stephen Haswell and Dr. Georgios Kyriakou for supervising, supporting and guiding me through this PhD. I also wish to thank Dr. Ping He for his support throughout my first year. To my fantastic father; from the start you have been there for me and without your steadfast support, I would not have gotten here. Your lifelong encouragement and unwavering belief in me has given me the confidence to do this. Words are a poor expression of my gratitude for all you have done for me.

To all my siblings and my family, thank you for your love and support.

I extend my gratitude to the Analytical Chemistry Group at the University of Hull for their encouragement and help throughout this project especially, Amin, Zeid, Asim, Ahmed, Jari, and Martin Taylor.

Thank you to Dr. Tom McCreedy, Dr. Charlotte Wiles, and Dr. Kevin Wellham for your advice and technical support.

I would like to thank technicians, Bob Knight, Dean Moore, Tony Sinclair, and Ann Lowry for their help through my PhD.

I want to express my sincere thanks to Dr. Simon Beaumont who performed the XPS analysis at Newcastle University.

Last but not least, I wish to acknowledge the kingdom of Saudi Arabia for generously funding this work to conduct my research.

Abstract

At present, synthesising complex chemical compounds is a process that is facilitated by employing conventional batch based laboratory approaches. This path, which can to some extent be automated, frequently suffers from inefficient and uncontrollable chemical conversions cannot be controlled over the course of the numerous possible steps of the synthesis process and, which in turn leads to generally lacks in terms of product yields and a poor of product selectivity.

In this research chemical synthesis was conducted in combination with small meso (μm) and micron-scale flow reactors, to offer more effective control over chemical reactions compared to conventional batch chemistry. The work capitalised the unique high surface area and excellent thermal transfer characteristics available in meso/micro flow systems, facilitating the creation of controllable, non-uniform, and time-dependent localised reactant, intermediates, and product concentrations, which generate a novel dimension in reaction control that is similar to the chemical control engaged in with biological systems. One factor investigated in the current research was the production of a stable monolithic structure *via* a sol-gel approach. The macroporous silica-monoliths were fabricated through controlled processes from two precursors tetramethoxysilane (TMOS) and tetraethyl orthosilicate (TEOS) with different polymer templates. Commercial available *Candida antarctica* lipase (CAL) was employed, to produce an active and stable microreactor for biocatalysis reactions. Its activity was investigated through the hydrolysis of 4-nitrophenyl butyrate by using a water-decane biphasic system.

The kinetic studies were performed using *Candida antarctica* lipase (CAL) immobilized on macroporous silica monolith. Interestingly, the kinetic studies had identified that a similar value for k_{cat} is obtained for the immobilized *Candida antarctica* lipase was (in the range 0.13 to 0.61 min^{-1}) and the free lipase in solution (0.12 min^{-1}) whilst the

immobilized apparent Michaelis constant K_m was 12 times lower than the free lipase in solution. The considerable higher rates gained with the immobilised lipases, due to the establishment of a favourable biphasic system in the continuous flowing microreactor setup. In addition to this, it was found that the optimisation of the outward features of the monolith eliminate lipase aggregation and pore obstruction, thereby increasing lipase specific activity and the accessibility of the substrate to the biphasic system. A range of studies in the literature also, attest to this finding. It should be noted that these optimised monoliths were revealed as highly efficient with regard to various reactions including transesterification reactions. This is important as, owing to this, beneficial aspects could be generated in biodiesel production.

The quest for alternative sources of energy has received extensive coverage owing to the increasing pace with which the current fossil fuel stores are being consumed. An additional factor is that there are a range of concerns relating to growing prices and, critically, climate change brought about by the use of carbon-based fuels. In light of these considerations, biodiesel, also known as fatty acid methyl ester, is notable as it is obtained from the transesterification of triglycerides and, hence, is a possible replacement for petroleum-based diesel. Biodiesel exhibits several advantages over diesel fuel such as low toxicity, high biodegradation, lower emission of particulate matter and its derivation from renewable energy sources. In this work, the use of lipase immobilised on a silica monolith as a microreactor for performing transesterification reactions is reported. Silica monolithic microreactor channels provide a large surface area for enzyme immobilisation. *Candida antarctica* lipase was trapped onto the silica monolith and was tested for the transesterification of tributyrin (TB). TB was quantitatively transformed into methyl butyrate when using flow rates of $0.8 \mu\text{L min}^{-1}$. The immobilised lipase microreactor was also shown to be reusable without loss of activity for 105 hours when operated at 30°C and flow rates of $0.8 \mu\text{L min}^{-1}$.

Two simple, reproducible methods of preparing evenly distributed gold (Au) nanoparticle-containing mesoporous silica monoliths were also, investigated. These Au nanoparticle containing monoliths were applied as flow reactors for the selective oxidation of cyclohexene. In the first strategy, the silica monolith was directly impregnated with preformed Au nanoparticles during the formation of the monolith. The second approach was to pre-functionalise the monolith with thiol groups tethered within the silica mesostructure. These can act as evenly distributed anchors for the Au nanoparticles to be incorporated by flowing an Au nanoparticle solution through the thiol functionalised monolith. Both methods led to an even distribution of Au nanoparticles along the length of the monolith as demonstrated by ICP-OES. However, the impregnation method led to a strong agglomeration of the Au nanoparticles during subsequent heating steps while the thiol-anchoring procedure maintained the nanoparticles in the range of 6.8 ± 1.4 nm. Both Au nanoparticle containing monoliths as well as samples with no Au incorporated were tested for the selective oxidation of cyclohexene under constant flow at 30 °C. The Au-free materials were found to be catalytically inactive with Au being the minimum necessary requirement for the reaction to proceed. The impregnated Au-containing monolith was found to be less active than the thiol-functionalised Au-containing material, attributable to the low metal surface area of the Au nanoparticles. The reaction on the thiol-functionalised Au-containing monolith was found to depend strongly on the type of oxidant used: *tert*-butyl hydroperoxide (TBHP) was more active than H₂O₂, likely due to the thiol-induced hydrophobicity of the monolith.

In conclusions, this project was successfully completed, and a stable monolithic structure through a sol-gel method was successfully produced. One implication of this was the production of a considerable quantity of molecular information for all of the reactions that were operated. The project's goals were achievable with the model set-up due to the

fact that it fulfilled a degree of appropriateness and versatility. The main topics addressed by the project were the improvement of catalyst immobilisation methods, and the flow reaction system represented a movement in the direction of the development of an entirely automated flow synthetic optimisation system.

TABLE OF CONTENTS

Acknowledgments	I
Abstract.....	II
LIST OF FIGURES	IX
LIST OF TABLES	XV
LIST OF SYMBOLS AND ABBREVIATIONS	XV
Chapter 1. Introduction.....	1
1.1 Microreactors	1
1.1.1 Overview of microreactors.....	2
1.1.2 Microreactor types and fabrication	3
1.1.3 Safety advantage of the microreactor.....	5
1.1.4 Microreactor operation.....	6
1.1.5 Temperature Operation	6
1.1.6 High Pressure	7
1.1.7 Mass Transport.....	7
1.2 Flow in microreactors	9
1.2.1 Types of flow on microreactors	11
1.3 Monolithic microreactors.....	13
1.3.1 Types of monolith	17
1.3.2 Fabrication of silica monolith microreactors (SBM)	17
1.3.3 Fabrication of polymer based monoliths (PBM) microreactors.....	24
1.3.4 Comparison between silica monoliths and polymeric monoliths.....	25
1.3.5 Modification of silica monoliths	29
1.3.6 Characterisation of the silica-based monolith	31
1.3.7 Applications of monolithic reactors	35
1.4 Catalysts.....	38
1.4.1 Definition of a Catalysts	38
1.4.2 Types of catalyst	39
1.4.3 Biocatalysts (enzymes)	41
1.4.4 Lipases as biocatalysts	41
1.4.5 Advantages of immobilisation of enzyme.....	42
1.4.6 Immobilisation methods.....	43
1.4.7 Influence of immobilisation carriers	44
1.4.8 Assay of the enzyme for free and immobilise lipase	46
1.4.9 Determination of parameters for free lipase kinetics	48
1.4.10 Determination of parameters for immobilised lipase kinetics in continuous-flow systems	52
1.5 Biodiesel	54
1.5.1 Biodiesel production by using the microreactor	60
1.5.2 Additional variables impacting microreactor biodiesel production	63
1.5.3 Catalysts for microreactor biodiesel synthesis.....	66

1.5.4	Catalytic mechanism of <i>Candida antarctica</i> lipase (CAL) for hydrolysis and transesterification	68
1.6	Catalysis by gold.....	70
1.6.1	History of gold nanoparticles	71
1.6.2	Immobilisation of Au-NPs on solid supports.....	72
1.6.3	Application of supported Au-NPs in catalysis	73
1.6.4	Synthesis of gold nanoparticles.....	75
1.6.5	Characterisation of Gold nanoparticles	76
1.6.6	Using Gold Nanoparticles as Catalysts for Selective Oxidation of Cyclohexene.....	81
1.7	Aims and objectives of the PhD project.....	84
1.8	Thesis structure	87
Chapter 2. Experimental		88
2.1	Chemicals.....	88
2.2	General instrumentation and equipment	91
2.3	Silica monolith synthesis	92
2.4	Characterisation of monolithic materials	97
2.4.1	SEM analysis	97
2.4.2	BET and BJH analysis	97
2.5	Calibration curve of 4-nitrophenol.....	97
2.6	Immobilisation of lipase.....	98
2.6.1	Assay of the free and immobilised lipase activity	98
2.6.2	Determination of lipase loading in the immobilized monolith microreactor	101
2.7	General procedure for catalytic transesterification:.....	101
2.7.1	Calibration curve of tributyrin	102
2.7.2	Calibration curve of methyl butyrate	102
2.7.3	HPLC conditions and mobile phase combination.....	102
2.8	Au-nanoparticle synthesis.....	102
2.8.1	Au nanoparticle - impregnated silica monolith synthesis	103
2.8.2	Modified Au-thiol functionalized silica monolith.....	103
2.8.3	Characterisation of Au-catalysts	104
2.8.4	SEM analysis	104
2.8.5	BET and BJH analysis	104
2.8.6	ICP-OES Analysis.....	104
2.8.7	Powder X-ray diffraction (PXRD) and XPS analysis.....	104
2.8.8	Catalytic testing.....	105
2.8.9	GC-FID conditions.....	106
2.8.10	Calibration curve of Cyclohexene.....	107
2.8.11	Calibration curve of Cyclohexene oxide.....	107
2.8.12	Calibration curve of 2-Cyclohexene -1-ol.....	107
2.8.13	Calibration curve of 2-Cyclohexen -1-one.....	107
2.8.14	Calibration curve of Mesitylene.....	108
Chapter 3. Development of the Silica Monolith microreactors for hydrolysis reactions		109
3.1	Physical characterisation of monoliths	110
3.2	Effect of ammonia treatment on the silica microreactors	111
3.3	Determination of average through pores size by SEM	114
3.4	Calibration curve of 4-NP at 400 nm	117
3.5	Assay of the free lipase activity	120
3.6	Kinetic study of free lipase activity	131
3.7	Determination of lipase loading in the immobilised monolith microreactor	141
3.8	Evaluation of the kinetic parameters for immobilized lipase.....	146

3.9	Conclusions.....	151
Chapter 4. Development of the Silica Monolith microreactors for biodiesel production..... 152		
4.1	Calibration curve of tributyrin	153
4.2	Calibration curve of methyl butyrate	155
4.3	Catalytic activity	158
4.3.1	Catalytic activity of the lipase immobilised on the silica monolith microreactors (M1, M3 and M5).....	159
4.3.2	Effect of reaction time.....	162
4.3.3	Effect of molar ratio of methanol:tributyrin.....	163
4.3.4	Effect of temperature	165
4.3.5	Effect of flow rate	166
4.4	Conclusions.....	168
Chapter 5. Selective Oxidation of Cyclohexene through Gold functionalised Silica Monolith Microreactors..... 169		
5.1	Calibration curve of Cyclohexene.....	170
5.2	Calibration curve of Cyclohexene oxide.....	172
5.3	Calibration curve of 2-Cyclohexene -1-ol	173
5.4	Calibration curve of 2-Cyclohexene -1-one.....	175
5.5	Calibration curve of Mesitylene (External standard)	176
5.6	Characterisation of Au monolith microreactors with BET	178
5.7	Determination of silica Au monolith microreactors by SEM	179
5.8	ICP-OES analysis for Au-impregnated and Au-modified monolith microreactors ..	183
5.9	Characterisation of Au monolith microreactors with TEM	185
5.10	Characterisation of Au monolith microreactors with PXRD	188
5.11	Characterisation of Au monolith microreactors with XPS	190
5.12	Catalytic activity of oxidation of cyclohexene.....	193
5.13	Conclusions.....	198
Chapter 6. Conclusions and Future work..... 199		
Chapter 7. References 203		
Publication and presentations..... 217		

LIST OF FIGURES

Figure 1-1. Different micro channel geometries: (A) Y-junction, (B) T-junction, and (C) interdigitated multilamellar mixer. ³²	8
Figure 1-2. Examples of microreactors (clockwise from top left): (A) Jensen's silicon-based microreactor; (B) Syrris' glass microreactor; (C) Ehrfeld's stainless steel microreactor; (D) Micronit Microfluidic's glass microreactor; (e) CYTOS Lab System's stainless steel microreactor; (F) Haswell's glass microreactor. (G) Vapourtec tube reactor (right). ⁶⁴	10
Figure 1-3. Types of fluid flow (A) Turbulent, (B) transitional and (C) laminar	12
Figure 1-4. An image of the porous monolith situated by access-way to the Summer Palace Park, Beijing, China. ⁷⁸	14
Figure 1-5. Micro, meso, macro porous within monolith. ⁷⁹	15
Figure 1-6. Reaction schemes in hydrolysis and condensation reactions as part of the sol-gel formative procedures . ¹⁰²	20
Figure 1-7. Illustrations based on scanning electron microscopy of monoliths containing PEO with 100% 10,000 molecular weight (A), PEO with 50% 10,000 and 50% 100,000 molecular weight (B), and PEO with 100% 100,000 molecular weight. ¹⁰⁷	22
Figure 1-8. Scanning electron micrographs of a polymer-based monolith. The image depicts the internal porous structure of the fractured capillary ends. ¹²²	25
Figure 1-9. SEM image depicting macroscopic variations between (A) silica and (B) polymer based monoliths morphologies. ¹²⁷	26
Figure 1-10. Inaccessibility of micropores in porous silica-based surface. ¹⁴³	30
Figure 1-11. Simplified representation of a scanning electron microscope. ¹⁵⁴	32
Figure 1-12. IUPAC categorisation of sorption isotherms. The adsorption and desorption isotherms have six characteristic shapes (I-VI): (I) microporous, (II) non-porous or macroporous, (III) non-porous, (IV) mesoporous, (V) mesoporous, and (VI) non-porous. ¹⁵⁵	34
Figure 1-13. Enzyme binds with substrate during a chemical reaction. ¹⁷⁵	40
Figure 1-14. The operation principle of a spectrophotometer. ²¹⁹	48
Figure 1-15. Plot of reaction rate V against substrate concentration $[S]$ according to the Michaelis-Menten equation. The enzyme concentration remains constant. 50	50

Figure 1-16. Lineweaver-Burk plot of $1/V$ against $1/[S]$ from which K_m and V_{max} can be obtained directly from the intersection of the resulting straight line with the x- and y-axes.....	51
Figure 1-17. Homogenous-based catalysed reaction procedure for the transesterification of triglyceride (TG).	58
Figure 1-18. Catalytic mechanism of <i>Candida antarctica</i> lipase (CALB) for hydrolysis or transesterification. ²⁸¹	69
Figure 1-19. A schematic representation of Bragg's reflection from a crystal.....	77
Figure 1-20. Simplified representation of a basic transmission electron microscopy (TEM). ³³⁰	80
Figure 1-21. The proposed reaction scheme for hydrolysis reaction of 4-nitrophenyl butyrate to 4-nitrophenol.....	85
Figure 1-22. The proposed reaction scheme for the transesterification reaction of tributyrin with methanol.....	86
Figure 1-23. The proposed reaction scheme for the selective oxidation of cyclohexene.	86
Figure 2-1. Schematic diagram showing the monolith preparation steps.	94
Figure 2-2. A silica monolith contained in a shrinkable tube and connected to the borosilicate tube for flow through use and surface modification.....	95
Figure 2-3. Schematic diagram of the reaction system used to assay immobilised lipase activity.....	100
Figure 2-4. Schematic of continuous flow system for silica monolith catalytic testing.	101
Figure 2-5. Schematic of continuous flow system for silica monolith catalytic testing.	105
Figure 3-1. Isotherm curves exhibited by two TMOS monolithic silica (M1) rods following the nitrogen physisorption method. The only significant difference in methodology is the absence of hydrothermal treatment (isotherm curve A)/ presence of hydrothermal treatment at 80 °C (isotherm curve B).	113
Figure 3-2 .SEM image of (A) the silica monolith after calcination sample. M1.....	115
Figure 3-3.SEM image of (B) the silica monolith after calcination sample. M3.....	115
Figure 3-4.SEM image of (C) the silica monolith after calcination sample. M5.....	116
Figure 3-5. An absorption spectrum (λ) for 4-NP.....	118
Figure 3-6. Calibration curve of 4-NP at 400 nm.	119

Figure 3-7. The concentration of 4-NP in mM as a function of reaction time in presence of free lipase 0.02 mg/mL.	125
Figure 3-8. The concentration of 4-NP in mM as a function of reaction time in presence of free lipase 0.04 mg/mL.	125
Figure 3-9. The concentration of 4-NP in mM as a function of reaction time in presence of free lipase 0.08 mg/mL.	126
Figure 3-10. The concentration of 4-NP in mM as a function of reaction time in presence of free lipase 0.17 mg/mL.	126
Figure 3-11. The concentration of 4-NP in mM as a function of reaction time in presence of free lipase 0.33 mg/mL.	127
Figure 3-12. The concentration of 4-NP in mM as a function of reaction time in presence of free lipase 0.58 mg/mL.	127
Figure 3-13. The concentration of 4-NP in mM as a function of reaction time in presence of free lipase 0.83 mg/mL.	128
Figure 3-14. The concentration of 4-NP in mM as a function of reaction time in presence of free lipase 1.25 mg/mL.	128
Figure 3-15. The concentration of 4-NP in mM as a function of reaction time in presence of free lipase 1.67 mg/mL.	129
Figure 3-16. The initial velocity (mM/min) plotted versus the concentration of lipase in mg/mL.	130
Figure 3-17. The initial velocity (mM/min) were plotted versus the concentration of lipase in mg/mL.	131
Figure 3-18. The concentration of 4-NP in mM as a function of reaction time in 0.3 mM of 4-NPB.	135
Figure 3-19. The concentration of 4-NP in mM as a function of reaction time in 0.5 mM of 4-NPB.	135
Figure 3-20. The concentration of 4-NP in mM as a function of reaction time in 1 mM of 4-NPB.	136
Figure 3-21. The concentration of 4-NP in mM as a function of reaction time in 2 mM of 4-NPB.	136
Figure 3-22. The concentration of 4-NP in mM as a function of reaction time in 3 mM of 4-NPB.	137
Figure 3-23. The concentration of 4-NP in mM as a function of reaction time in 4 mM of 4-NPB.	137

Figure 3-24. The concentration of 4-NP in mM as a function of reaction time in 5 mM of 4-NPB.....	138
Figure 3-25. Lineweaver–Burk double reciprocal plot for free lipase.....	140
Figure 3-26. The concentration of 4-NP in mM as a function of reaction time in presence of free lipase.....	142
Figure 3-27. The concentration of 4-NP in mM as a function of reaction time after the first washing with Tris-HCL buffer.....	143
Figure 3-28. The concentration of 4-NP in mM as a function of reaction time after the second washing with Tris-HCL buffer.....	145
Figure 3-29. Lilly–Hornby plots of the immobilised lipase for immobilised lipase on monolith microreactor (M1).....	147
Figure 3-30. Lilly–Hornby plots of the immobilized lipase for immobilised lipase on monolith microreactor (M3).....	148
Figure 3-31. Lilly–Hornby plots of the immobilized lipase for immobilised lipase on monolith microreactor (M5).....	149
Figure 4-1. Wavelength scan of tributyrin from 199 to 900 nm.....	153
Figure 4-2 . Calibration curve of tributyrin.....	154
Figure 4-3. Wavelength scan of methyl butyrate from 199 to 900 nm.....	156
Figure 4-4. Calibration curve of methyl butyrate.....	157
Figure 4-5. HPLC peaks of transesterification reaction of tributyrin (a): before the reaction, (b): after the reaction). Peak at 3.2 min assigned to tributyrin and peak at 2.00 min assigned to methyl butyrate.....	158
Figure 4-6. Yield of methyl butyrate using different lipase immobilized microreactors. (Reaction conditions: methanol /tributyrin molar ratio 2 :1; Flow rate 0.8 μ L/min; 30 °C; 20h). The error bars are the standard deviation of the yield % for three experiments.....	160
Figure 4-7. Effect of time on the yield of methyl butyrate with two molar ratio methanol: tributyrin 2:1 (Reaction conditions: Flow rate 0.8 μ l min ⁻¹ ; 30 °C).	162
Figure 4-8. Effect of time on the yield of methyl butyrate with two molar ratio methanol: tributyrin 3:1 (Reaction conditions: Flow rate 0.8 μ l min ⁻¹ ; 30 °C).	163
Figure 4-9. Yield of methyl butyrate using different lipase immobilized microreactors. (Reaction conditions: Flow rate 0.8 μ L/min; 30 °C; 20 h). The error bars are the standard deviation of the yield % for three experiments.....	164

Figure 4-10. Effect of temperature on the yield of methyl butyrate. (Reaction conditions: Flow rate 0.8 μ L/min; 30 $^{\circ}$ C, methanol:tributylin molar ratio 2:1).....	165
Figure 4-11. Effect of time on the yield of methyl butyrate. (Reaction conditions: Flow rate 0.8 μ L/min; 30 $^{\circ}$ C).....	167
Figure 5-1. Calibration curve of Cyclohexene.....	171
Figure 5-2. Calibration curve of Cyclohexene oxide.....	173
Figure 5-3. Calibration curve of Cyclohexene -1-ol.....	174
Figure 5-4. Calibration curve of Cyclohexene 1-one.....	176
Figure 5-5. Calibration curve of Mesitylene (External standard).....	177
Figure 5-6. SEM image of (a) Au-free monolith.....	180
Figure 5-7. SEM image of (b) Au-impregnated monolith.....	181
Figure 5-8. SEM image of (c) Au-thiol functionalised monolith.....	182
Figure 5-9. ICP-OES results taken at 1 cm at different position a cross sections of the two monoliths. (n=1).....	184
Figure 5-10. TEM and particle size distribution diagrams of: (a) Au thiol-functionalised monolith. (n=1).....	186
Figure 5-11. TEM and particle size distribution diagrams of: (b) Au-impregnated monolith. (n=1).....	187
Figure 5-12. For gold catalyst monoliths thiol-modified (top) monoliths impregnated (bottom): (a) PXRD data, specific dominant crystallographic planes are indicated on the figure. In each case data for two samples are offset for clarity. XPS binding energy scale corrected to C 1s at 284.4 eV.....	188
Figure 5-13. For gold catalyst monoliths thiol-modified (top) monoliths impregnated (bottom): (b) Au 4f region XP spectra. In each case data for two samples are offset for clarity. XPS binding energy scale corrected to C 1s at 284.4 eV.....	191
Figure 5-14. For gold catalyst monoliths thiol-modified (top) monoliths impregnated (bottom): (c) S 2s region XP spectra. In each case data for two samples are offset for clarity. XPS binding energy scale corrected to C 1s at 284.4 eV.....	192
Figure 5-15. GC peaks of epoxidation reaction of Cyclohexene (A): before the reaction. Peak at 3.72 min assigned to solvent (Acetonitrile, peak at 4.96 min assigned to Cyclohexene, peak at 5.25 min assigned to tert-Butyl hydroperoxide, and peak at 17.20 min assigned to Mesitylene (external standard). (B) : after the	

reaction. Peak at 3.72 min assigned to solvent (Acetonitrile), peak at 4.97 min assigned to Cyclohexene, peak at 5.25 min assigned to tert-Butyl hydroperoxide, peak at 9.86 min assigned to Cyclohexene oxide, peak at 11.34 min assigned to 2-Cyclohexene-1-ol, peak at 14.78 min assigned to 2-Cyclohexene-1-one, and peak at 17.20 min assigned to Mesitylene (external standard)..... 193

LIST OF TABLES

Table 1-1. Microreactor fabrication and significant features adapted from these references. 14, 15	4
Table 1-2. Summary of literature review comparing advantages and disadvantages of inorganic and organic monoliths.....	28
Table 2-1 . Chemicals, reagents and solvents used in the experiment.....	88
Table 2-2 Instruments and materials used.....	91
Table 2-3. Summary of monolith preparation conditions.	96
Table 3-1. Physical characterisation of monolith by BET	110
Table 3-2 .Micron scale pore diameter	117
Table 3-3. Absorbance of 4-NP measured under varied concentration	118
Table 3-4. Estimated error values for calibration equation.....	120
Table 3-5. Absorbance of 4-NP as a function of time for different free lipase concentrations.	121
Table 3-6. Concentration of 4-NP in mg/mL as a function of time for different free lipase concentrations.	122
Table 3-7. Concentration of 4-NP in mM as a function of time for different free lipase concentrations.	124
Table 3-8. Initial velocity (mmol/min) of each lipase concentration.....	129
Table 3-9. Absorbance of 4-NP as a function of time for different free lipase concentrations	132
Table 3-10. Concentration of 4-NP in mg/mL as a function of time	133
Table 3-11. Concentration of 4- NP in mM as a function of time	134
Table 3-12. Initial velocity (mmol/min) of each 4-NPB concentration.....	139
Table 3-13 Analysis of collected solution after the loading of free lipase.....	141
Table 3-14. Analysis of collected solution after the first washing of the immobilised lipase.	143
Table 3-15. Analysis of collected solution after the second washing of the immobilised lipase.	144
Table 3-16 Summary of lipase concentration on different monoliths.	145
Table 3-17. Lilly–Hornby for the immobilised lipase on the silica monolith microreactor (M1).....	146
Table 3-18. Lilly–Hornby for the immobilized lipase on the silica monolith microreactor (M3).....	147

Table 3-19. Lilly–Hornby for the immobilized lipase on the silica monolith microreactor (M5).....	148
Table 3-20. Kinetic evaluations for free and immobilized lipase	150
Table 4-1. The peak area of tributyrin measured under varied concentration	154
Table 4-2. Analytical figures for tributyrin.....	155
Table 4-3. The peak area of methyl butyrate measured under varied concentration	156
Table 4-4. Analytical figures for methyl butyrate:.....	157
Table 4-5. The TOF results	161
Table 5-1. The peak area of Cyclohexene measured under varied concentration (n=1)	171
Table 5-2. The peak area of Cyclohexene oxide measured under varied concentration (n=1).....	172
Table 5-3. The peak area of 2-Cyclohexene -1-ol measured under varied concentration (n=1).....	173
Table 5-4. The peak area of 2-Cyclohexene -1-one measured under varied concentration (n=1).....	175
Table 5-5. The peak area of Mesitylene measured under varied concentration (n=1)..	176
Table 5-6. Physical characterisation of monolith (n=1).....	178
Table 5-7. Au particle size distribution via TEM and PXRD	189
Table 5-8. Cyclohexene oxidation on Au impregnated and Au free monoliths using tert-butyl hydroperoxide (TBHP) and hydrogen peroxide (H ₂ O ₂) as the oxidants at 30 °C.	195

LIST OF SYMBOLS AND ABBREVIATIONS

ASTM	American Society for Testing and Materials
Abs.	Absorbance
BET	Brunauer-Emmett -Teller model
BJH	Barrett-Joyner-Halenda
CAL	Candida antarctica lipase
C _{in}	Concentrations at the inlet
C _{out}	Concentrations at the outlet
EDX	Energy dispersive X-ray spectroscopy
Da	Dalton
°C	Degree Celsius
FAME	Fatty Acid Methyl Ester
FID	Flame ionisation detector
g	Gram
GC	Gas chromatography
GC-MS	Gas Chromatography-Mass Spectrometry
HPLC	High Performance Liquid Chromatography
i.d.	Internal diameter
kDa	Kilo Dalton
K _{cat}	Turn-over number
K _m	Michaelis constant

MeOH	Methanol
mM	Millimolar
μ	Micro
μm	Micrometre
mL	Milli litres
Mw	Molecular weight
min	Minute
M	Molar
mg	Milligram
Mpa	MegaPascals
nm	Nanometer
O.D.	Outer diameter
R^2	Correlation coefficient
PEG	Polyethylene glycol
PEO	Polyethylene oxide
LOD	Limit of detection
PMMA	Poly(methyl methacrylate)
PDMS	Poly(dimethylsiloxane)
t_r	Retention time
Q	Volume flow rate
rpm	Rotations per minute

SEM	Scanning Electron Microscope
STD	Standard deviation
TEOS	Tetraethylorthosilicate
TMOS	Tetramethylorthosilicate
TAG	Triacylglycerols
TG	Triglyceride
TBHP	<i>tert</i> -butyl hydroperoxide
UV	UltraViolet
UV-Vis	UltraViolet-Visible
V	Volume
V _{void}	Void volume of the monolith
V _{max}	Maximum rate of the reaction
λ	Wavelength
Wt.	Weight
4-NP	4-nitrophenol
4-NPB	4-nitrophenyl butyrate

Chapter 1. Introduction

1.1 Microreactors

Over the last few decades, numerous of publications and books on microreactors have increased interest in the area of process intensification for research and industrial applications worldwide.¹ This research is backed up by a growing number of industrial patents: 62 on micro-scale heat exchangers and 350 on microreactors, 55 on the micromixers and 600 on micro pumps.² This interest has been reflected in the dedicated microreactor conferences and growing sales of practical microreactor technology. This can be attributed to the numerous benefits of microreactors over traditional methods, including their reaction efficiency and cost effectiveness and the fact that less raw materials are needed to operate the device.^{3,4}

Microscale-based chemical operations are chemical reactions which take place in sub-millimeter dimensions. A microreactor consists of a series of small micron-sized channels, common dimensions range from 10-500 micrometres, incised or moulded in a solid substrate.^{5,6} These channels are linked in different geometries that allow the reagents to mix and react for a particular time in a controlled area using different pumping techniques, including hydrodynamic pumping and electrokinetic pumping.⁷

A number of micro-scale units have been proposed within a multitude of large-scale operations, namely micromixers, microsensors, microreactors for the pharmaceutical and fine chemical industry fields.⁸ The heat exchange characteristics of the micro-structured reactors are recognized to be better than in macroscopic batch or flow-through reactors due to their high surface area to volume ratio.⁸ These processes generally utilise a continuous flow method over batch-based approaches given that the former offers a greater control of reaction parameters. Other advantages of these approaches include

better controlled reactions, operational safety, ease of use, long-term operating at a reduced expense, better reproducibility, the possibility to pressurise the microreactor, ease of automation and the possibility of a closed system. This approach results in efficient and reproducible mixing and very accurate reaction monitoring. Reactions in microreactors therefore are usually cleaner with better selectivity and minimal by-products compared to conventional reactions.⁸ Microscale methods such as these contribute to developments which have evolved beyond existing typical chemical processes, meaning operational plants and procedures can be made sustainable, efficient, safe and environmentally sound.⁸

1.1.1 Overview of microreactors

Microstructured continuous-flow reactors and chip-based microreactors are gaining favour since they provide a means to facilitate scale out from small-scale laboratory trial conditions. These new developments permit easy adjustment of reaction parameters and offer significant advantages over conventional round-bottomed glass flasks, minimising requirements for time, effort and starting reagents in the quest to identify optimum reaction conditions.^{5,6}

Currently, most chemical reaction procedures are facilitated by the traditional production methods of the last few decades. However, these provide significant challenges in scaling from laboratory trial to mass production. Recently, microreactor technology has been put forward as a means to facilitate this process *via* the replication of unit processes to yield large volume throughput. This development has the potential for great relevance to the pharmaceutical industry where the benefit offered by the ability to perform multiple operations (e.g., synthesis, screening, detection and evaluation) with a single piece of equipment will permit significant reductions in lead time in new compound discovery,

testing and production. Therefore, advantages of reaction miniaturisation will be examined with relevant practical examples.⁵

Microreactor research has become a significant focus with scientists seeking to overcome the disadvantages associated with other types of reactors. Actually, microreactor technology had been in operation prior to this recent increased interest, thanks to the developments in related areas such as the design of the silicon chip in computer technology, which, in turn, facilitated the development of microreactor technology in other sectors.⁶ Since different products require different manufacturing techniques, several different examples are examined. Furthermore, the application and the manner in which reagents are introduced to a system vary considerably, but particularly in relation to the size of the microreactor.⁶

1.1.2 Microreactor types and fabrication

Microreactors can be made from numerous materials, allowing flexibility in their production and for machines to be optimally designed at a reduced cost.

To fabricate the microreactors, the most common materials include glass⁹ or ceramic,¹⁰ quartz,¹¹ metals,¹² polymers¹³, and these have been sourced for the production of modern, more resilient microreactors and each material has its own advantages and disadvantages. Table 1-1 shows the materials and fabrication techniques for microreactor construction. Determining the most appropriate material requires striking a balance between the following aspects: chemical affinity, simplicity of production, strength and thermal conductivity.

Table 1-1. Microreactor fabrication and significant features adapted from these references. ^{14, 15}

Material	Fabrication techniques	Advantages	Disadvantages
Silicon	Photolithography; wet and dry etching	Applicable at high pressure and temperature; excellent heat conductivity; high -aspect ratio designs	Reactive with strong aqueous bases at moderate temperatures
Ceramic	Stereolithography; powder melting; electro - discharge machining; laser machining	High temperature stability with conservation of reaction heat; chemically resistant	High production cost; shrinkage after sintering
Stainless steel	Lithography; electroplating and melting; stamping; micromachining	High pressure and temperature viability	Reactive with acidic media and some organic solvents (acetone, THF, CH ₂ Cl ₂ , DMSO) expensive specialized steels utilised.
Glass	Photolithography; powder blasting; wet etching; ultrasonic machining	Good resistance to wide range of chemicals; direct inspection of reaction possible; photochemistry viable	Reactive with strong aqueous bases at moderate temperature; Subject to freeze fracture: only for temperatures > 0°C
Plastic	Soft lithography; injection melting; hot embossing; phase- separation- micromoulding	Fast manufacture; low manufacture costs	Reactive with organic solvents; limited structural strength; unsuitable for high temperatures and pressures

Polydimethylsiloxane - PDMS,¹⁶ and Polymethyl methacrylate - PMMA¹⁷ are both polymeric substances which have been broadly utilised for the manufacture of microreactors. Expendable PDMS-based micro utensils have been useful in biology labs. PDM-based materials perish under harsh chemical conditions is due to its mechanical property however, and also when exposed to extreme pressures. PDMS is permeable to gas, transparent, and biocompatible, and this explains the robust interest of the scientific society in using this material to produce microfluidic devices for cell biological studies.¹⁸

However, the microfluidic systems formed of polymers, such as (PDMS), are generally limited to conditions close to ambient temperature and atmospheric pressure.^{19, 20}

Glass has been a popular choice, but its low thermal conductivity is a significant drawback.²¹ Stainless steel is robust and has great thermal conductivity. However, stainless is also largely unsuitable for constructing micromachines, as its opacity is problematic given the inability to monitor the internal operations during a reaction cycle.²² In silicon, the high thermal conductivity displays the potentiality of rapid removal of heat created by an exothermic reaction. Furthermore, silicon due to its mature manufacture infrastructure, inexpensive and mass production capability. Additionally, the silicon technology of micromachining displays the probability of a high-density combination of monitoring operation, e.g., *in situ* flow measurements with dedicated and/or sensors temperatures.²³⁻²⁵

1.1.3 Safety advantage of the microreactor

The small-scale nature of microreactor operations²⁶ leads to enhanced operation safety.²⁶
²⁷ Exotherms can be monitored enabling the safe use of highly toxic and explosive substrates due to the small volume used by the microreactors. In conventional batch systems, temperatures must be closely observed, as, if the reaction exceeds critical temperatures, a runaway reaction may ensue.^{28, 29} For example, direct fluorination is a

risky process which requires the application of precise cooling in order to avoid dangerous outcomes, requiring F_2 addition and produces HF as a byproduct.³⁰ Undertaking these kinds of reactions as part of a batch method would incur much higher levels of explosive risk. Moreover, microreactors can produce safe containment to implement singlet oxygen addition reactions, which are complicated by the requirement of high-intensity light exposure. These reactions are dangerous in batches because they demand litres of toxic and possibly explosive organic solutions.³¹⁻³³ It is possible to investigate physical environmental effects and surface interactions with the reaction flow through diffusive mixing under laminar flow high surface area to volume ratio; it is also possible to affect mass and heat transfer.³⁴

1.1.4 Microreactor operation

Microreactors are operated in a continuous mode.³⁵ They require little cleaning and maintenance, which does not have to take place between each cycle. Temperature and concentration are both easy conditions to manipulate if the system has been efficiently designed.³⁶ The majority of industrial procedures take place on a continual basis, which is highly beneficial over existing batch results.

1.1.5 Temperature Operation

The high surface area to volume ratios in the microreactor promote heat transfer. When a heavy-duty pressurised or heated procedure is underway, reactions may be observed even though temperatures exceed the boiling point of the solvent.³⁷ High-temperature procedures generally produce faster reaction cycles, meaning additional catalytic routes are able to be pursued within laboratory conditions.³⁸

Microreactors provide many benefits in enhancing heat and mass-transfer limited reactions. These are obtained by reducing the reactor dimensions to the microscale, enabling the development of steep gradients in concentration and temperature,

conditions that are beneficial in highly exothermic and mass-transport limited processes.³⁹ This development facilitates the potential for the application of innovative process methodologies, such as those implemented to achieve the fluorination of toluene with elemental fluorine. A ‘falling film’ microreactor has been constructed of adjacent heat exchanger and reaction channels within a microstructured reaction plate to facilitate liquid distribution over an increased surface area.⁴⁰ Due to the explosive nature of the reaction, for safety reasons, conventional manufacturing processes require an operating temperature of -70° C. However, since the specially constructed microreactor altered the reaction mechanism from an unselective and uncontrollable, radically-mediated process to a safe, selective, electrophilic substitution process, and the microreactor operations were successfully and safely achieved at only -10 °C.

1.1.6 High Pressure

Microreactors are exceptional cases of small-scale reactors; they can stand excessive pressure. Microreactors made from silicon are strong and have very high mechanical strength.⁴¹⁻⁴³ The nanoscale channels of silicon allows supercritical processes to take place, for example with supercritical water at 250 bars and 400 °C. This environment has allowed quantum dots to be produced in microreactors that contain pressurised or supercritical fluids.⁴⁴⁻⁴⁶

1.1.7 Mass Transport

Issues with mass transportation continue to blight conventional reactor methods.

Microreactors give much shorter reactions which enables observation and detection problems of mass transfer limitations which may arise, and also allow for rapid diffusive mixing; given their specific length scales.^{47, 48} Micromixers have been constructed in an interdigitated fashion allowing the division and joining of flows which reduces

diffusional length scales.⁴⁹⁻⁵² Active micromixer processes have been tested with periodic and acoustic flow.⁵³ Reactions that may suffer from the poor mass transfer associated with conventional procedures are often found to be greatly improved when transferred to the microscale.

Whilst more complicated channel constructions are conceivable, microchannel junctions are often simple T- or Y-shaped structures with a rectangular or trapezoidal cross section as seen in Figure 1-1.^{6, 32}

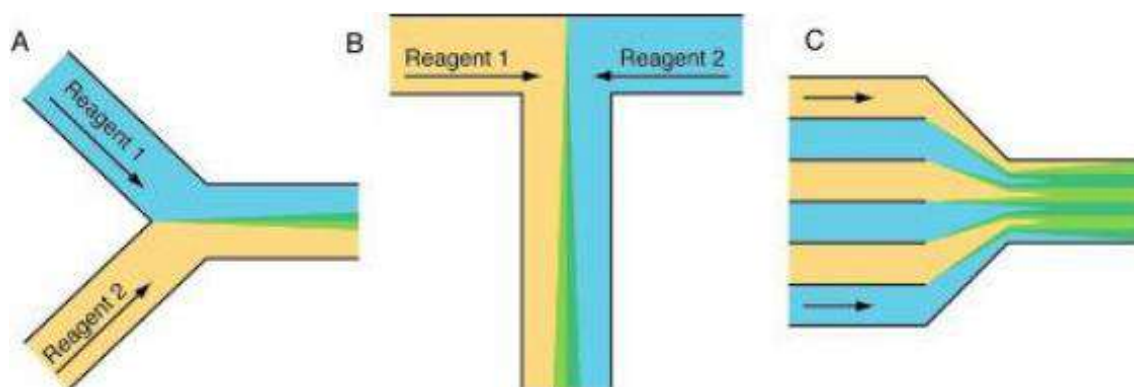


Figure 1-1. Different micro channel geometries: (A) Y-junction, (B) T-junction, and (C) interdigitated multilamellar mixer.³²

For the reasons previously described microreactors enable innovative methodology for carrying out organic synthetic leading to increased yields and improved selectivities.⁵⁴

1.2 Flow in microreactors

Flow chemistry has become more prevalent over the last twenty years.⁵⁴⁻⁵⁸ and it involves running a chemical reaction in a continuous flowing stream as opposed to having a batch process. Two classifications for flow chemistry have been reported as meso flow and micro flow, and they are utilised for both organic and inorganic synthesis whilst also providing benefits for modern analytical techniques. As indicated earlier, the conventional batch process involved start-and-stop reaction chemistry whereas the normal approach for flow in synthetic reactions is to use a continuous flow of reactants to produce the end product. The main issue to be overcome though is scale-up which differs for both flow and batch processes. Continuous flow itself is reaction chemistry which has the advantage over batch reaction chemistry, for, with volume flow, it is also possible to check reaction time speed, to control reaction conditions more efficiently and effectively, to mix reagents more efficiently with minimal waste and to have additional reactions running concurrently as well as analysis and purification.^{57, 59-61}

During the process of a flow reaction, one of the main difficulties of scale-up is the issue of maintaining the reaction conditions. For example, in the case of temperature, the problem is that the outer flow temperature may be different from the temperature of the inner flow. This use of this concept in the polymerisation in large-scale batch reactors was illustrated by Sacks *et al.*⁶² The ease of syntheses and their improvement is a main focus for the chemical industry which has been consistently developing new technologies, particularly over the last five years. Whilst flow chemistry has been used in the manufacturing industry for a long time, it was believed that smaller scale versions were required.⁶²

Mesoflow works in an almost similar way to microflow except that, rather than two reagents mixing in micrometer-sized channels in a chip, they mix under characteristic

conditions in a tube reactor, and, as such, it is possible to implement these reactions on a larger scale. The use of tethered reagents in flow chemistry is possible in two ways: the reactant could dislodge the tethered reagent as it flowed through the column, whilst, at the same time, combining and producing product; or, alternatively, the reactant, as it flowed through the column, could be subjected to surface interaction with a reagent to produce a product which may need to be physically removed from the solid support.^{43, 63}

The features of several different microreactors are outlined in Figure 1-2 :

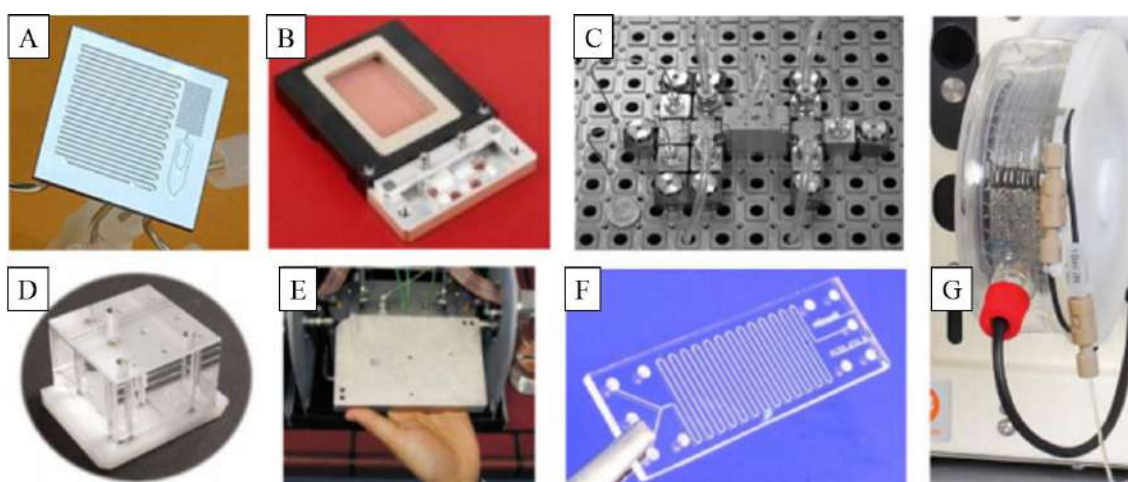


Figure 1-2. Examples of microreactors (clockwise from top left): (A) Jensen's silicon-based microreactor; (B) Syrris' glass microreactator; (C) Ehrfeld's stainless steel microreactator; (D) Micronit Microfluidic's glass microreactator; (e) CYTOS Lab System's stainless steel microreactator; (F) Haswell's glass microreactator. (G) Vapourtec tube reactor (right).⁶⁴

These examples of flow reactors are becoming more popular for performing syntheses and, in reactions where unstable intermediates are formed, they are becoming the most preferred.⁶⁴ Efficiency, reproducibility, and safety are some of the characteristics which can be improved through the use of flow chemistry. Automation is the main reason why the efficiency of a scientist can be greatly improved by using flow chemistry because, once the systems have been set up, the scientist can work at other functions whilst the automation system continues to do most of the manipulations.^{43, 65}

Improved reproducibility also occurs in reactions within an automation environment as the parameters are set exactly every time the reaction is run, thus reducing the possibility of human error.

1.2.1 Types of flow on microreactors

The behaviour, mixing and separation of the flow is governed by the reagent flow profiles. This is seen as one of the inherent advantages of micro flow and is associated with fluid mechanics and is classified by Reynolds number.⁶⁶

Laminar, transitional and turbulent are terms used to describe the various flow types. Fluid flow is termed as chaotic and the fluid mixes randomly with wakes, vortexes and eddies, making it extremely difficult to measure with any accuracy.

Turbulent flow normally takes place at high flow rates or in larger diameter pipes and is usually preferred in the situations where solids need to stay suspended in the fluid to make sure there is no settling or blockages. Laminar flow usually exists at lower flow rates through pipes with smaller diameters so it could be described as the fluid particles flowing in cylinders, with the outer cylinder, which is touching the pipe wall, moving slower. The next cylinder is the slowest since it is flowing against the unmoving fluid cylinder, showing reduced frictional “pull” than the pipe wall, and this trend continues with the inner-most cylinder having the greatest velocity. Transitional flow is regarded as a combination of both laminar and turbulent flows with the edges of the fluid flow being accounted for in a laminar state while the flow’s centre is turbulent. As is the case with turbulent flows, transitional flows are extremely difficult to assess with precision. Figure 1-3 provide an indication of the various types of fluid flow.^{67, 68}

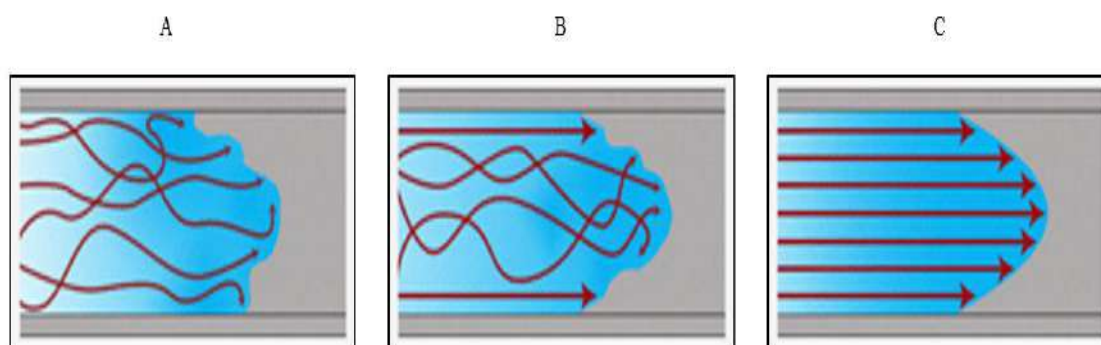


Figure 1-3. Types of fluid flow (A) Turbulent, (B) transitional and (C) laminar

The type of flow can be characterised by Reynolds numbers. Fluid velocity, channel diameter, fluid density and fluid viscosity in Equation 1-1 are the parameters which determine a specific Reynolds number.⁶⁹

Figure 1-3 C. This illustrates that the flow is separated into parallel streams and, furthermore, it displays the channel surface interaction with the fluid in motion.⁷⁰

$$Re = \frac{\rho v D_H}{\mu} \quad \text{Equation 1-1}$$

The Reynolds number (Re) linked to a cylindrical channel is produced according to the fluid density (ρ) kg/L, fluid velocity (v) m/s, chamber diameter (D_H) m, and the fluid viscosity (μ) Ns/m². Extensive research has been conducted in an attempt to evaluate microreactor devices. This is especially the case with regard to the attempt to control mixing in the flow channels. In the domain of analytical chemistry, a number of practices require laminar flow in order to facilitate several washing and analyte tagging processes. Notably, this brings the laminar flow into one's viewpoint to a certain degree when considered in conjunction with the micro flow.⁶⁹

This unique dependency on diffusion for mixing in laminar flow is governed by Einstein's equation of Brownian motion.⁷¹

Equation 1-2 asserts that the distance travelled (x) is directly related to time (τ) and the diffusion constant (D) of that molecule.⁷²

$$\chi = \sqrt{2D\tau} \quad \text{Equation 1-2}$$

Peyman *et al.* employed this dependency on diffusion in the context of laminar flow in order to log analytes in a successful way with magnetic particles.⁷³ The particles were sifted through laminar flow streams of a buffer solution and, following this, a fluorescent tagging reagent and another buffer solution. The procedure was also applied to DNA hybridisation.⁷⁴

1.3 Monolithic microreactors

In many processes, there is a need to include a solid phase in the flow system. This has often been added as a packed bed, but this can cause high back pressures in flow systems. In many cases, reactors have arbitrarily packed catalytic beds and therefore the fluid dynamics are not controlled, and, from a chemical-reaction-engineering standpoint, this is quite disadvantageous as these are viewed as stagnation zones with hot-spot formation, broad residence time distribution, low selectivity, and as a result low process efficiency.⁷⁵
⁷⁶ An obvious solution to counteract these difficulties is the development of structured beds which are designed on a nanoscale up to the macro-geometry scale. A monolith, which is described generally as a block of structured material that consists of continuous substructures, or regular or irregular channels, is deemed to be the best-structured material known for this purpose.⁷⁷ It is possible to define a monolithic column as being one portion of a consistent and inflexible porous material; the other key feature is that it has an interconnected skeletal layout with pores. The etymology of the term “monolith” dates back to the 19th century, where it was formulated from two Greek roots, ‘monos’ and ‘lithos’. The two Greek terms can be translated as “single” and “stone”, respectively, and, in this way, the word was used to denote a physical or technology-based mass like a

mountain-range or a carved boulder. It has commonly been used to denote features like enormous individual rocks. One such monolith, a boulder obtained by a Chinese empress, was placed in the entrance to a palace she owned and this is displayed in Figure 1-4.⁷⁸



Figure 1-4. An image of the porous monolith situated by access-way to the Summer Palace Park, Beijing, China.⁷⁸

Solid materials with porosity allow interaction with ions, molecules and atoms both at their surfaces and all through their mass, which is why they have attracted so much attention in science and technology fields. The pores within the monolith are classified according to size to three kinds: macropores or through-pores (> 50 nm), micropores (< 2 nm), or mesopores (2-50 nm) as can be seen in Figure 1-5.

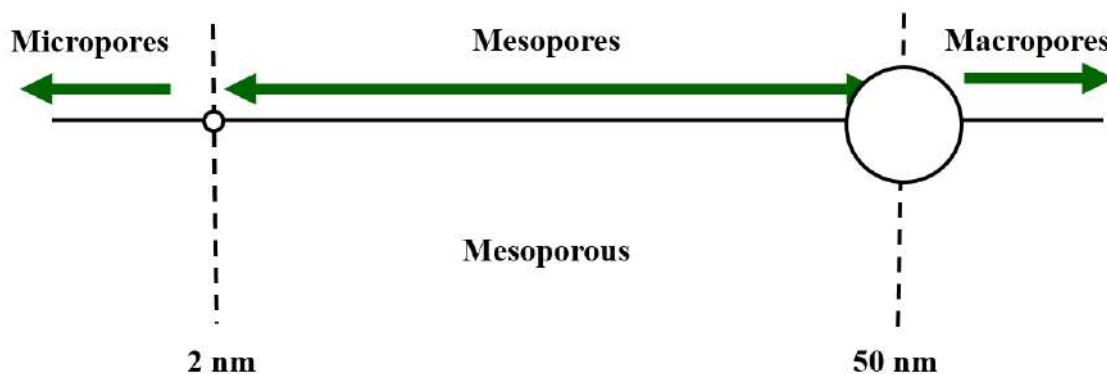


Figure 1-5. Micro, meso, macro porous within monolith.⁷⁹

The distribution of sizes, shapes and volumes of the void spaces in porous materials directly relates to their ability to perform the desired function in a particular application.

Monolithic materials have a large geometric surface area and a large void volume which leads to low pressure during the cross of a fluid and a large contact area of the catalyst or the reagent with the fluid.⁸⁰ Variation in pore size is beneficial in promoting different reaction mechanisms. Whilst micropores are the most significant, oversized molecules, too large to diffuse through the micropores, will react with mesopores. Larger still, macropores are key to controlling microreactor column permeability, minimising backpressure within the column.⁸¹ These advantages, accompanied with mechanical strength, special surface properties, chemical and thermal stability, can lead to novel applications of the materials.

Hjerten *et al.*⁸² led the first investigations into monolithic materials when the researchers created and employed compressed soft gels in the context of chromatographic separation. This took place in 1989, and the compressed soft gels are referred to in the extant and related literature as ‘continuous beds’. Svec and Frechet implemented innovations at the beginning of the 1990s with the formulation of rigid macroporous polymer monoliths. Notably, these polymer monoliths were created as a result of a relatively straightforward

“moulding” procedure and, following this, they were utilised as a high-performance liquid chromatography medium of separation.⁸³ Owing to the distinctive features of the range of organic monolithic materials, they have been applied in numerous applications.⁸⁴ In addition to the research discussed above, studies beginning in 1996 were carried out to fabricate inorganic silica-based monoliths.^{85,86}

Silica monolith was chemically resistant and suitable for organic reactions requiring solid catalysts. The catalyst could be held within the monolith reactor.⁸⁷ Typically, monolith reactors support high fluid throughputs by maintaining a lower pressure drop. This relieves tension against the reactor’s microporous structure. During mass transfer reactions, these monoliths hold the advantage of having a higher specific external catalyst surface area to increase efficiency and output.⁸⁸ This could reduce external mass transfer in multiphasic reactions and internal diffusion limitation when the monolith reactor walls are thin. Due to the lower pressure drop, the axial dispersion and back-mixing rate are low, thus yielding high product selectivity.^{89, 90}

Furthermore, the catalyst lifetime, by preventing possible plugging and reducing instances of fouling, increases the system’s efficiency and work output. The particulates that accumulate on the capillary channel walls are cleaned easily, leaving the monolith reactors free from high cost of maintenance.⁹⁰ Also, frits are not needed in the monolith microreactors, which help avoid bubble formation, as conventional packed bed reactor.⁹¹

Furthermore, monolithic microreactors can be selectively produced through a condensation step, depending on the catalyst.⁹² This process can result in a highly condensed column that favours the production of mesoporous structures. This feature enhances diffusion rates of various reacting species in the monolith reactor.⁹²

1.3.1 Types of monolith

Monoliths are a major component of several chemical reactions and processes. They are put to commercial use worldwide as a widely superior method and are implemented as modern advancements on older set-ups that generated less yield.⁹³ The monolithic reactor used for different processes varies depending on the type of reaction being carried out.⁷⁶ The most promising monolith families for application in catalysis used for the production of fine chemical in continuous processes are those where the skeleton consists of polymer, hybrid polymer-glass, or an inorganic inner frame (silica) that measure between 10-500 μm . Other types of monolith presenting very large flow-through pores ($> 50 \mu\text{m}$; extrudates, foams) made of ceramic, carbon or metal foils will not be considered here as they are not often utilised in small-scale chemistry in the field of fine chemical synthesis.⁷⁶

1.3.2 Fabrication of silica monolith microreactors (SBM)

Silica-based monoliths (SBM) comprise an exclusive microstructure which contains micro- and mesopores. This level of porosity increases its permeability and passage of liquid flow which results in excellent mass transfer rates. It is the amalgamation of both interlinked pore types that results in the ability of silica monoliths to interact with different analytes. Silica bestows extreme mechanical integrity which is impervious to the type of damage seen in other materials under high stress or pressure.⁹⁴

SBM also has the capability to tailor the pore size distribution and mesopore volume to equally distribute catalysis of materials in producing high quality products. Moreover, the surface of silica monoliths has a predefined chemical stability that enables it to modify surface chemistry as required by the reaction type.⁹⁴ Currently, chemists and those in commerce industries have found great appeal in SBMs and have even entered into production investments enabling them to tailor SBMs for applied use in industry.⁹⁵

Silica-based monoliths can be fabricated through different approaches. The first approach proposed by Fields in 1996 for chromatographic applications involved introducing a solution of potassium silicate into a fused-silica column which was exposed to a temperature of 100°C for 60 minutes and followed by being helium-dried at 120°C for one day.⁸⁵ A dried dimethyloctadecylchlorosilane solution (10%) in dried toluene was used to modify the structure of the silica-containing monolith. After the modification, the column was washed off in preparation for reversed-phase HPLC. On the upside, this approach enables the production of continuous silica monoliths but, the morphology of the silica based monolith is not homogeneous.^{85,96} A more homogeneous and highly pure monolith structure can be obtained through the sol-gel method suggested by Minakuchi *et al.*⁹⁷. In addition to the high purity and homogeneity, this latter approach afforded satisfactory mechanical strength to the silica monoliths. Furthermore, the structure of the silica monoliths exhibited double pores with co-continuous through-pores of the order of micrometres as well as silica skeletons with nanometre-sized mesopores. The high surface area of the silica-based monolith structure as well as its high rate of diffusion was useful in processes of catalysis, separation and extraction due to the combined mesoporous and macroporous qualities.

In the present study, the silica monolith was produced with this sol-gel approach as the material was made more permeable by the through-pores, while its surface area was high due to the mesopores structure. The stages make up the sol-gel method: precursor sol formation hydrolysis, polycondensation, gelation, ageing, drying, and calcination.

1.3.2.1 Hydrolysis of precursor materials

Precursor hydrolysis and condensation reactions are essential for sol development. The fabrication of a silica-based monolith structure can be achieved with a range of precursors, including alkoxysilanes with low molecular weight, like tetramethylorthosilicate (TMOS) and tetraethylorthosilicate (TEOS). The reaction with water and the cost-effectiveness of

metal alkoxides also contribute to their appeal.⁹⁸ Furthermore, the formation of silica gel macropores and micropores occurs with the participation of a porogen in the shape of a polymer soluble in water (e.g., polyethylene oxide [PEO]) which is present in the original solution. An acid (e.g., nitric acid or acetic acid) or a base catalyst (e.g., dimethylaminopyridine or *N*-methylimidazole) contributes to sol formation as well.⁹⁹ It is important to note that, compared to TEOS, TMOS is hydrolysed faster in the sol gel procedure. Consequently, in this study, TEOS was hydrolysed with a strong acid (e.g., nitric acid), whilst TMOS was hydrolysed with a weaker acid (e.g., acetic acid).^{86, 94}

As illustrated in Figure 1-6 A, the liquid alkoxide is hydrolysed with water during the initial reaction stage, resulting in the production of silanol groups (Si-OH). These groups interact with one another in the process of condensation, giving rise to polycondensed kinds with siloxane links (-Si- O-Si-) between two silane molecules (Figure 1-6, B and C). This causes the solution to become highly viscous, thereby furthering sol transformation into gel.^{100, 101}

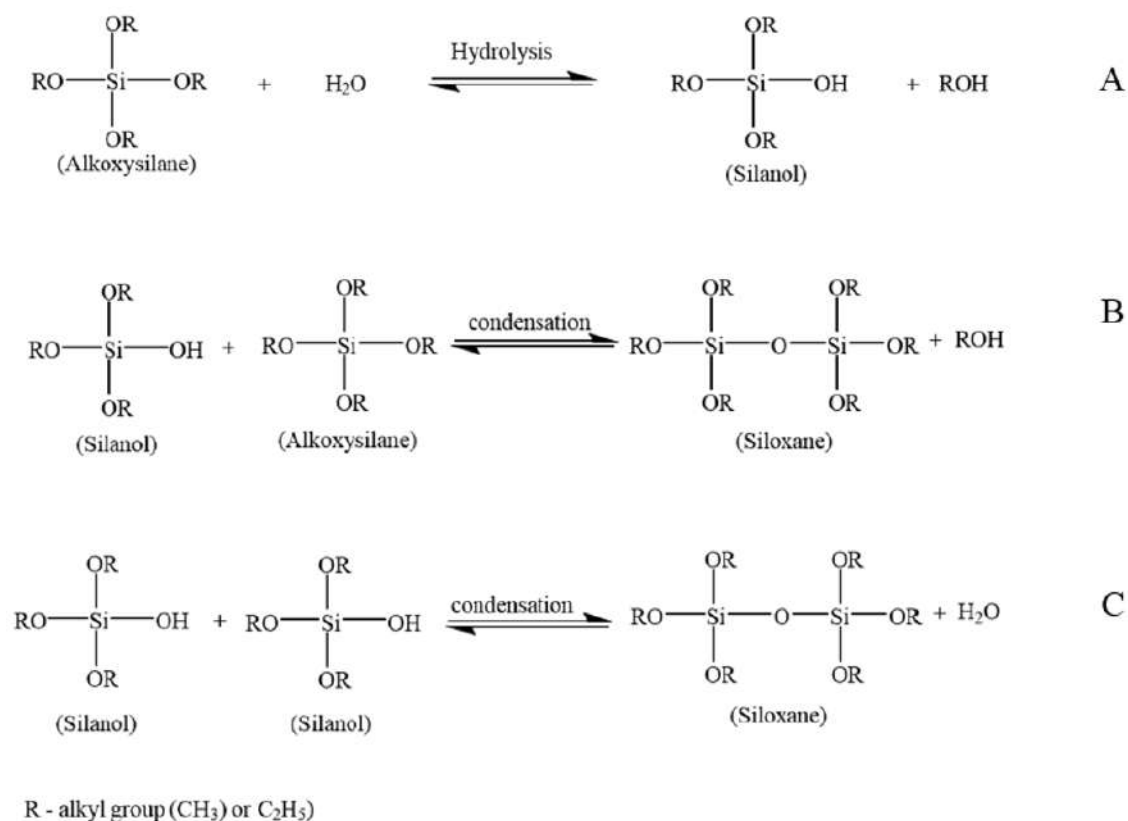


Figure 1-6. Reaction schemes in hydrolysis and condensation reactions as part of the sol-gel formative procedures .¹⁰²

Prior to becoming too viscous, the solution that has undergone partial polymerisation is poured into a mould. The shape and type of the mould are among the factors that affect the casting procedure used to determine the final frame product. The mould employed to produce silica monoliths in this study was the barrel of a plastic syringe (BD -1 mL). This was chosen to exclude any reaction between the solution and the mould.

1.3.2.2 Gelation

The main event of the process of gelation is the development of particles from the condensation reactions which determines the formation of clusters and makes the solution more viscous. The binding of silica oligomers gives rise to a 3D network, resulting in the formation of a wet gel material of partial solidity. The amount of time in which this process of gelation takes place is known as the gelation time.¹⁰³ Fluctuations in processing

variables e.g., precursor material type, pH, catalyst, precursor concentration, and solvent influence how the reactions of hydrolysis and condensation unfold.

The manner in which the internal structure of silica monoliths is affected by the varying chemical configurations and physical variables during the process of gel formation has been the focus of many studies.¹⁰⁴ For example, 18 combinations of tetramethoxysilane (TMOS) and methyltrimethoxysilane (MTMS) were used by Motokawa *et al.*¹⁰⁵ to produce monolithic fused-silica capillary columns. The through-pore size and the skeleton size of the obtained silica monoliths varied between 2 and 8 μm and between 1 and 2 μm , respectively. Column efficiency and back pressure were found to be higher in the case of silica-based monolith columns.

1.3.2.3 Aging and ammonia treatment

A silica skeleton displaying a bi-continuous through-pore (macropore) network on its surface is the outcome of the phase separation among the silica-poly(ethylene oxide) (PEO) system and water that forms as silica undergoes polycondensation reactions with the PEO organic polymer soluble in water acting as a porogen. In addition to through-pore formation, the solubilisation of the alkoxysilane reagent is also a function of the porogen. Meanwhile, phase separation can make the silica oligomers unstable and therefore the PEO must have a high molecular weight to prevent this from happening. For instance, minimal phase separation occurred in both TMOS and TEOS systems as a result of integrating PEO with a mean molecular weight of 4000 in the precursor materials.¹⁰⁶

Adjustment of the concentration and molecular weight of the porogen enables regulation of the through-pore and skeleton size. PEO molecular weights of 10,000 and 100,000 were used by Shrinivasan *et al.*¹⁰⁷ to produce TMOS monoliths. The morphology of monoliths with varying PEO molecular weight are illustrated in Figure 1-7. More specifically, monoliths containing PEO with a molecular weight of 10,000 and measured

diameter size of through-pores and surface area of 5-7 μm and 40 $\text{m}^2 \text{g}^{-1}$, respectively, are shown in Figure 1-7(A) as appearing under the scanning electron microscope (SEM).

SEM images of monoliths containing PEO 50% 10,000 molecular weight and 50% 100,000 molecular weight and with measured diameter size of through-pores and surface area of 2-4 μm and 380 $\text{m}^2 \text{g}^{-1}$, respectively, are illustrated in Figure 1-7(B). Moreover, SEM images of monoliths containing PEO with a molecular weight of 100,000 and measured diameter size of through-pores and surface area of 1 μm and 520 $\text{m}^2 \text{g}^{-1}$, respectively, are illustrated in Figure 1-7(C).¹⁰⁷

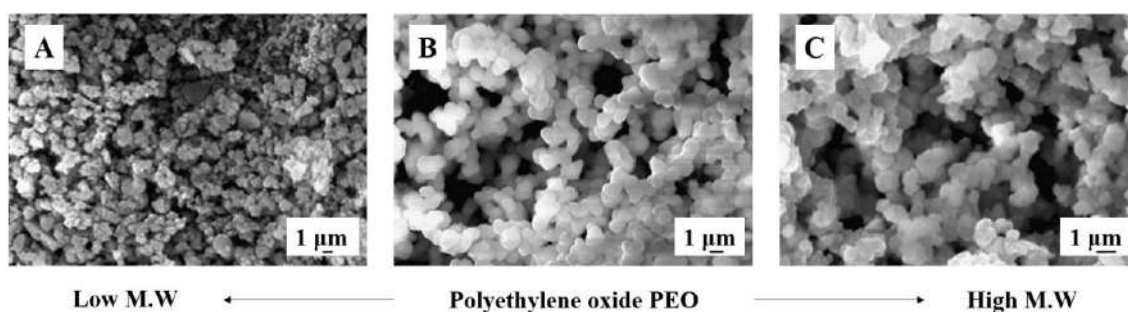


Figure 1-7. Illustrations based on scanning electron microscopy of monoliths containing PEO with 100% 10,000 molecular weight (A), PEO with 50% 10,000 and 50% 100,000 molecular weight (B), and PEO with 100% 100,000 molecular weight.¹⁰⁷

It can be clearly observed from Figure 1-7 that the smaller the size of the through-pores, the higher the level of condensation. In other words, the monoliths are less permeable but their surface area is expanded as a result of increase in the molar mass of PEO in the initial mixture. In a study conducted by Fletcher *et al.*¹⁰⁸, the skeleton structure of biporous silica-based monoliths consisted of both through-pores (μm) and mesopores (nm), by using PEO with high molecular weights of 100,000 and 200,000, the authors revealed that monolith surface area was increased while through-pore size was decreased when the PEO molar mass in the original mixture was increased. Furthermore, the use of a very high PEO molecular weight of 300,000 in the fabrication of monolithic columns

resulted in rapid crack formation or failed monolith development¹⁰⁸. Different PEO concentration and molar mass were used by Minakuchi *et al.*⁹⁷ in the original mixture during preparation of silica-based monoliths. Thus, the dissolution of 9.4 g PEO was undertaken in 100 mL of 0.01 M aqueous acetic acid as well as in 45 mL TMOS. The initial size of 3.46 μm of the through-pores was diminished to 1.26 μm when the PEO quantity was increased to 10.4 g. Furthermore, in relation to the conversion of sol into gel, phase separation was delayed as a result of augmentation of PEO concentration and molar mass. Consequently, there was a longer growth interval for the silica network in the gelation phase prior to the freezing of the silica-based monolith structure. Hence, the monolith became less permeable and porous as the skeleton structure was made stronger and thicker due to the increase in PEO concentration and molar mass. It was possible to extract the monolith from the mould for the purpose of hydrothermal treatment thanks to the reduction in size of the wet gel.^{97, 109}

In order to increase the surface area, the silica aged monolithic treated with thermal decomposition of urea or ammonium hydroxide solution was conducted at near 100°C, resulting in mature silica-based monolith subjected to treatment with a basic medium, thus leading to an expansion in surface area. A dissolution-precipitation process permits the adjustment of mesopores within the silica skeleton, whereby variation in pH and temperature causes the dissolution and reprecipitation of silica on the convex and concave surfaces, respectively.^{110, 111} The response of monolithic material to different variables of hydrothermal treatment e.g. temperature, pH, and duration, in terms of pore size distribution and chromatographic performance and catalysis, have been explored by a number of studies. The main finding in this regard was that mesopore size and volume distribution expanded according to elevation in hydrothermal temperature and pH. In addition to the increasing of the surface area, the monolithic structure was also mechanically strengthened by hydrothermal treatment.¹¹⁰⁻¹¹⁷

1.3.2.4 Drying and calcination

The removal of most of the solvents employed (mostly water and alcohol) is achieved by drying the wet gel monolith in an oven with air circulation at a temperature in the range of 40-80°C, according to solvent type. The eliminated solvents and evaporated liquid are replaced within the pore structure with a concave meniscus made of liquid/vapour, giving rise to capillary pressures that cause the internal structure to shrink further.^{118, 119}

Once the monolith is dry, it is subjected to additional thermal treatment at 500-650 °C to remove the organic residue (polymer) while the monolithic silica structure is not deformed. Furthermore, calcination makes the monolith more stable from a mechanical point of view, but reduces its pore volume and surface area.^{100, 108}

1.3.3 Fabrication of polymer based monoliths (PBM) microreactors

Fabricating PBMs is a comparable process to that which is carried out to produce silica-based monoliths. Compressed gels can be used to generate PBMs, and these are considerably smaller in size after polymerisation. An additional fabrication method is constituted of free-radical initiation and, following this, the polymerisation of monomer-based mixtures takes place in the presence of porogens.^{76, 120}

A range of organic compounds have been employed as monomers in order to fabricate monoliths, and these include polystyrene, acrylamide, and methacrylate. Lee *et al.* reported on the preparation of a monolithic capillary column by employing glycidyl methacrylate (GMA) and trimethylolpropane trimethacrylate (TRIM) in order to extract immunoglobulin G (IgG) from human serum.¹²¹ It is noteworthy that the procedure included the surface-immobilisation of protein G. The monolithic capillary column generated displayed a low-flow resistance with a heightened likelihood to preconcentrate and clean up IgG from a human serum sample that had been diluted 500 and 65,000 times.

Figure 1-8 illustrates a scanning electron micrograph of the internal structure of a polymer-based monolith, and this was produced by Gusev *et al.*¹²²

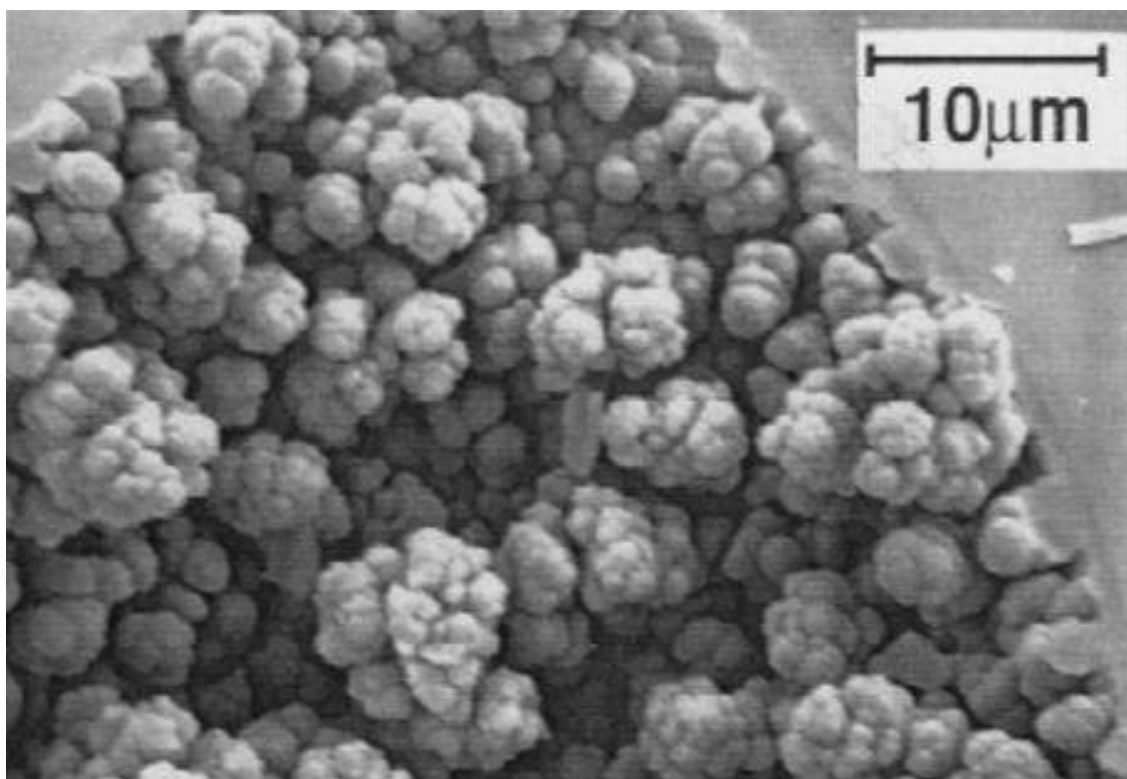


Figure 1-8. Scanning electron micrographs of a polymer-based monolith. The image depicts the internal porous structure of the fractured capillary ends.¹²²

1.3.4 Comparison between silica monoliths and polymeric monoliths

The high surface area is the most significant characteristic of monolithic materials and this can be improved by increasing the number of micropores. However, macropores are also required to maintain the permeability of the monolith and permit liquid to flow through the monolith at a satisfactory pressure.¹²³ Therefore, the surface area and the hydrodynamic properties of the monolith both depend on the pore size distribution of the monolith requiring the need to find a suitable balance between low flow resistance and high surface area. The optimum monolith should, therefore, have both macropores and micropores to enable adequate permeability and high capacity.^{124, 125}

The different morphologies between silica- and polymer-based monoliths can be seen in Figure 1-9. The optimisation of the composition of the polymerisation mixture and the reaction conditions by increasing both surface area and permeability of monolith characteristics have been extensively reported.¹²⁶

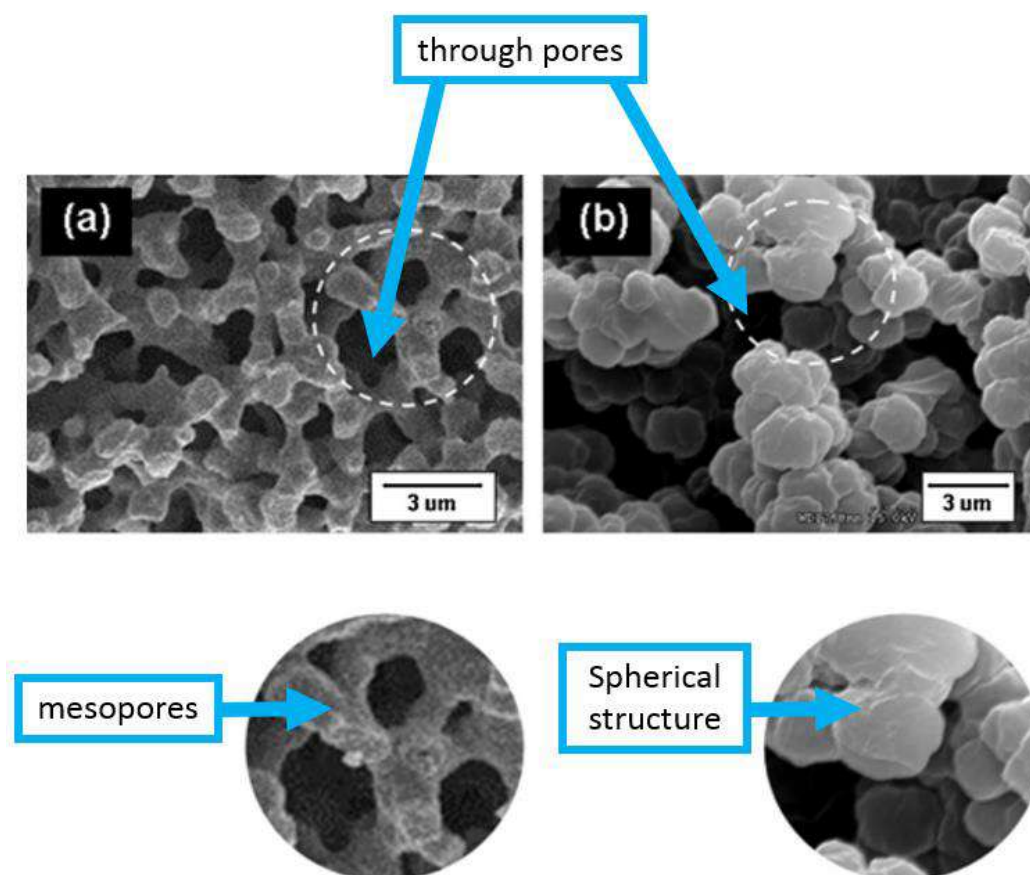


Figure 1-9. SEM image depicting macroscopic variations between (A) silica and (B) polymer based monoliths morphologies.¹²⁷

Difficulties frequently encountered include ensuring that the pores are large enough to reduce backpressure and that the mesopore distribution is over an optimal size range. Furthermore, organic monolithic (polymer) materials are not structurally stable since they can be degraded by temperature and/or organic solvents. This may result in shrinking or swelling of the monolith material with affect performance consequences.^{128, 129}

Since fabrication of large-scale monoliths can be problematic, organic polymer-based monoliths are usually produced on a small scale. The challenge in producing large-scale monoliths is a consequence of the production methodology: the required polymerisation reaction mixtures must not be stirred; however, this has the side-effect of reducing the heat-dissipation capacity of the polymerisation reaction, leading to unwanted heterogeneity in the pore structure.^{84, 130}

In the case of polymer-based monoliths, it is difficult to always ensure that the pore size is large enough to reduce back pressure for efficient fluid flow,¹³¹ as compared with its counterpart, the silica-based monoliths.¹³²

Silica monoliths exhibit a characteristic bimodal pore size distribution which includes mesopores (2 – 50 nm) on the surface of the silica skeleton and macro through-pores (> 50 nm) which confer a high permeability on the material. In contrast, the mesopores in the structure offer a high surface area and therefore facilitate reactant interactions which enables efficient catalytic reactions.^{133, 134}

In comparison, the internal structure of polymeric monoliths consists of only macro-pores. This reduces the surface area and, concomitantly, accessibility of substrate to functional groups on the monolith, compared with the silica alternative.⁷⁸ Reduced interaction between the substrate and the catalyst surface detrimentally affects the efficiency of the catalytic reaction, whilst the mesoporous pore space in the thin skeleton offers access to the majority of functional group sites by imposing only short diffusion distances.¹²⁷

Whilst each monolith type offers its own particular disadvantages and advantages, a summary comparison between silica and polymeric monoliths is detailed in Table 1-2.

Table 1-2. Summary of literature review comparing advantages and disadvantages of inorganic and organic monoliths.

Comparison	Silica monolith	Polymer monolith
Preparation method	Simple	Simple
Preparation time	Long, with a number of stages involved ⁷⁸	Short, and a single-stage process ^{78, 135}
Surface area	High (200 – 800 m ² g ⁻¹) ¹³⁶	Lowers (100 – 400 m ² g ⁻¹) ^{137, 138}
Permeability	High ^{136, 139, 140}	Moderate ^{128, 129}
Thermal and chemical stability	High mechanical strength and relatively high thermal stability. ⁷⁸	Labile to temperature and / or organic solvents leading to shrinking or swelling which would affect the reproducibility. ^{128, 129}
Stability over pH range	Unstable at high pH values. (2 > pH > 8) ¹⁴¹	Stability observed for a wide range of pH values ¹⁴²
Surface modification of the monolith	Easily derivatised with a number of functional groups ^{143, 144}	Exhibited a large number of crosslinking bonds ¹⁴⁴
Fabrication inside microchip	Difficult to locate monolith precisely within the microchip, because their fabrication depends on using thermal initiation ^{109, 145}	Easy as the initiation of a polymerisation reaction can be carried out by photoinitiation (light) ^{123, 146}

1.3.5 Modification of silica monoliths

It is possible to enact further modifications to silica monoliths in a straightforward manner by implementing a grafting procedure with a range of organosilanes or, alternatively, inorganic precursors in flow. This is the case as the surface silanols can react with a broad range of active functional groups, including acids, bases, chelating ligands, and other inorganic alkoxides.¹⁴⁷

Siloxane (Si-O-Si) and silanol (Si-OH) are both functional groups that are present on the surface of silica. The siloxane group is subject to nucleophilic substitution at the Si atom; or the silanol group is subject to a direct reaction with the hydroxyl group. However, it should be noted that it is generally thought that the silanol group constitutes the predominant modification pathway. Silanols can be categorised as (a) isolated groups (or free silanols), where the surface silicon atom has three bonds linking to the main structure with the fourth bond attached to a single hydroxyl group; (b) vicinal silanols (or bridged silanols), where two isolated silanol groups are linked by hydrogen bonding; and (c), geminal silanols where two hydroxyl groups are attached to a single silicon atom. Such chemical alteration of the silica surface of the silica gel renders it useful as an adsorbing agent since it does not swell or strain and has impressive structural and thermal properties.¹⁴⁸ The presence of uncondensed hydroxyl groups on the surface of silica confer polar properties to the monolith material.¹⁴⁹

Additional efficiency and selectivity of a silica monolith can be achieved by a derivatisation reagents.^{143, 150} Modification of the silica surface commonly occurs in the mesopores (2-50 nm) as the mesopores are more readily available to the derivatisation reagent as well as to the analytes. Micropores (>2 nm) are inaccessible, so the silanol groups in these pores cannot be modified since they are blocked by the bonded moieties in the mesopores,¹⁴³ as illustrated in Figure 1-10.

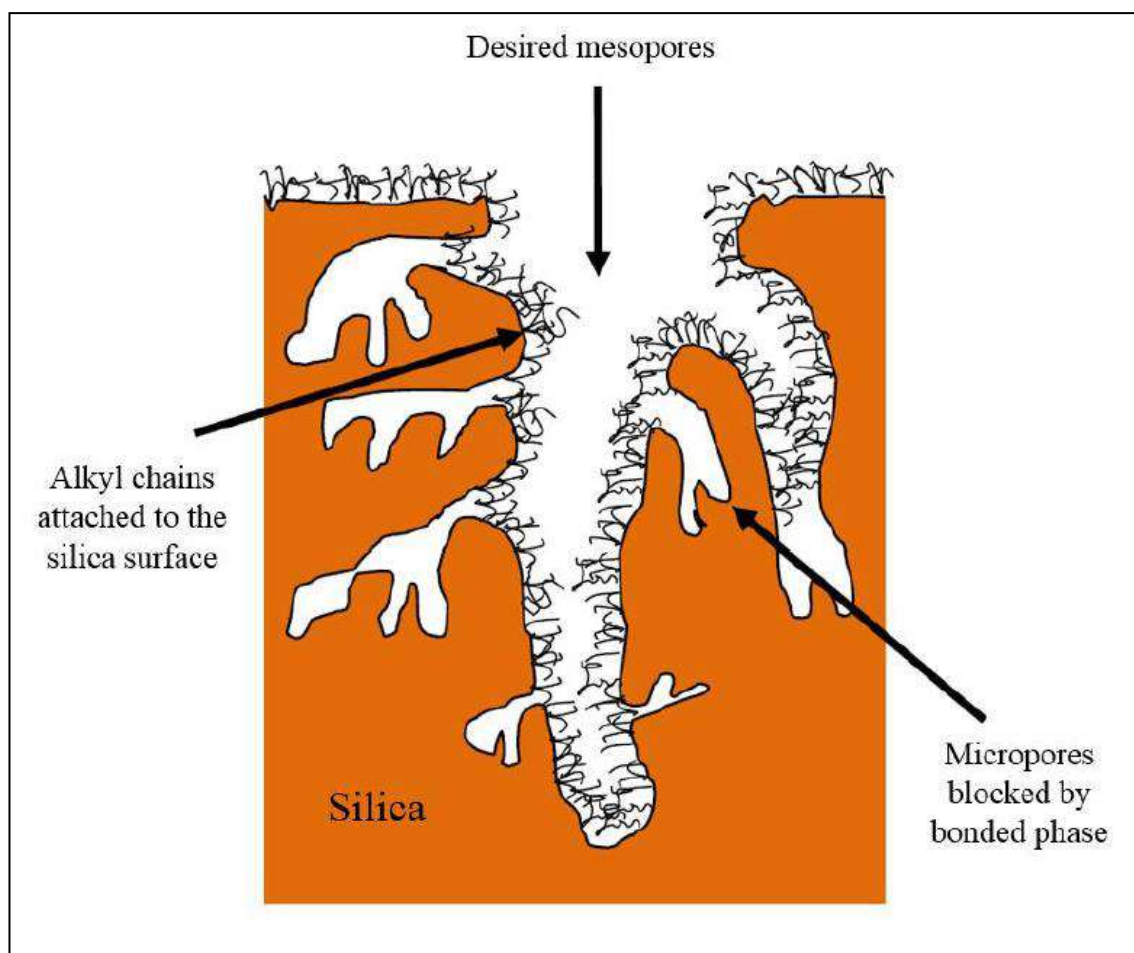


Figure 1-10. Inaccessibility of micropores in porous silica-based surface.¹⁴³

It is notable that a number of silanol groups in the mesopores are sometimes not subject to modification. This often occurs when the attached organic moieties are large, for example in relation to octadecyl groups; the movement obstructs the adjacent silanol groups, thereby hindering other organic moieties approaching. A series of free silanol groups remains after that.¹⁴³ Despite, in instances where the attached organic moieties are minimal with limited movement, the adjacent silanol groups are not obstructed. In this way, the free silanol groups detrimentally impact catalysis, separation, and extraction owing to the way they can generate supplemental ion-exchange interaction between the free silanol groups and the reagents.¹⁵¹

In order to minimise the effect of this unwanted secondary interaction, the number of free silanol groups needs to be reduced. A second “end capping” reaction can be performed

which involves bonding smaller silane-type molecules such as trimethylchlorosilane (TMCS), or hexamethyldisilazane (HMDS) to the larger bonded moieties.¹⁵²

1.3.6 Characterisation of the silica-based monolith

Physical characterisation of monolithic materials can be achieved by several different methods. Optical techniques such as scanning electron microscopy (SEM), atomic force microscopy (AFM) and transmission electron microscopy (TEM) are all useful for surface characterisation methodologies, providing details on the morphology of the monolithic material that is closely related to porosity characteristics. Furthermore, such techniques are useful in determining pore size that in turn relates to the hydrodynamic properties of the column and its structural strength. Mercury intrusion porosimetry (MIP) enables measurement of porosity and pore size distribution for pores ranging between 10 nm to 150 μm . Inverse size exclusion chromatography (ISEC) is used to measure smaller pores of size < 50 nm. Whilst the Brunauer-Emmett-Teller (BET) method can be used to determine internal surface area of the monolithic material by measuring the volume of N_2 adsorbed and then calculating the surface area from the adsorbed volume of an N_2 molecule.^{84, 153}

1.3.6.1 Characterisation of the silica-based monolith with scanning electron microscopy (SEM)

Scanning electron microscopy (SEM) is one of the key methodologies for investigating the morphology of silica monoliths. SEM additionally provides an indication of the through pore size and overall homogeneity of the skeleton monolith.¹⁵⁴

The column of a scanning electron microscope is illustrated in simplified form in Figure 1-11. It can be seen that electrons are emitted through the column by an electron gun and a set of lenses focus the electron beam. Contact between the electrons and the sample occurs once the former have gone through the last lens; at the same time, the

sample surface produces secondary electrons, backscattered electrons and typical X-rays, which are captured by various detectors.¹⁵⁴

The selection of the detector types depends on the types of emitted electrons to be detected.

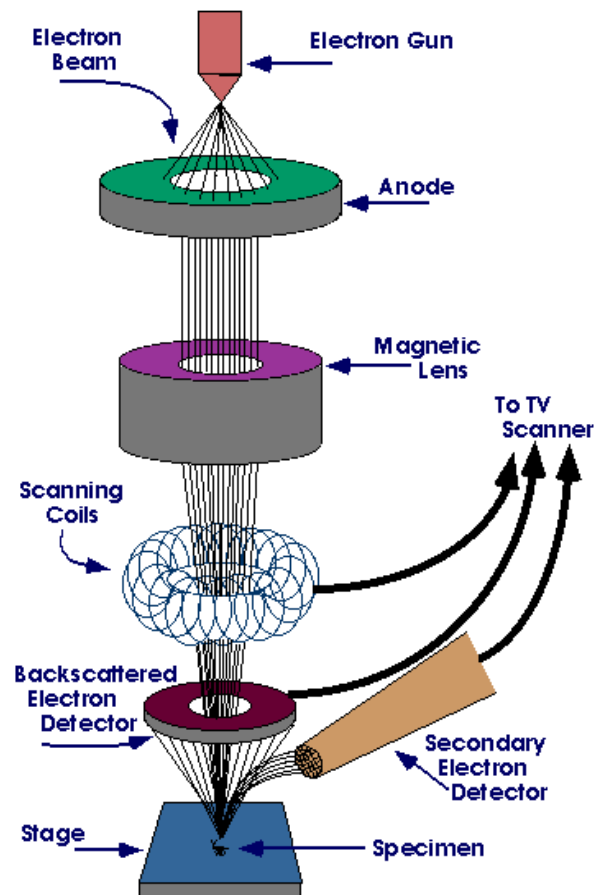


Figure 1-11. Simplified representation of a scanning electron microscope.¹⁵⁴

A charge effect may arise if the sample lacks conductivity. The sample adopts a negative charge if the proportion of electrons exiting the sample by diffusion to ground is lower than the proportion of electrons coming into contact with the sample. The electric field generated by this negative charge can have an adverse effect on the incidence beam, resulting in a distorted image. On the other hand, the charge effect is indiscernible at high

voltage if the sample possesses conductivity. There are two ways in which this effect can be averted. One way is to endow samples lacking conductivity with a suitable conducting surface by coating them with carbon or gold. The second way is to employ a low voltage which eliminates the necessity of interfering with the surface of the sample.

1.3.6.2 Characterisation of the silica-based monolith with nitrogen physisorption method (BET)

The physisorption technique can be utilised for the measurement of the physical properties of silica monoliths, such as mesoporous size, mesoporous volume, and surface area. The procedure incorporates the adsorption of nitrogen gas onto the silica monolith structure while the temperature remains consistent. It should be noted that the amount of adsorbed gas in the sol-gel material is correlated with the applied pressure, and it is also important to acknowledge that the changes produced by this particular adsorption process can be reversed to van der Waals forces. The amount of gas adsorbed is directly proportional to the applied pressure, then the solid's surface area can be computed with reference to the amount of adsorbed gas. When equilibrium pressure (P) is maintained, the gas adsorption process is halted and, moreover, the number of adsorbed molecules is the same as the number of desorbed molecules. In light of this, it is clear that the physical adsorption of gas molecules can be used to compute the surface area of a the solid.^{144, 155}

An equilibrium relative pressure (P/P_0) is applied to the isotherm measurement which varies between 0 to 1, where P_0 denotes the saturation pressure of the adsorptive gas (N_2). It is often the case that a researcher can obtain the isotherm curve evaluation by charting the adsorptive region (namely, the y-axis) along with the equilibrium relative pressure (P/P_0). It is pertinent to note here that the isotherm curve is a function of pore volume and pore size and, in addition, isotherm curves are generated in six varying forms. These have been classified by the International Union of Pure and Applied Chemistry (IUPAC), as displayed in Figure 1-12.¹⁵⁵

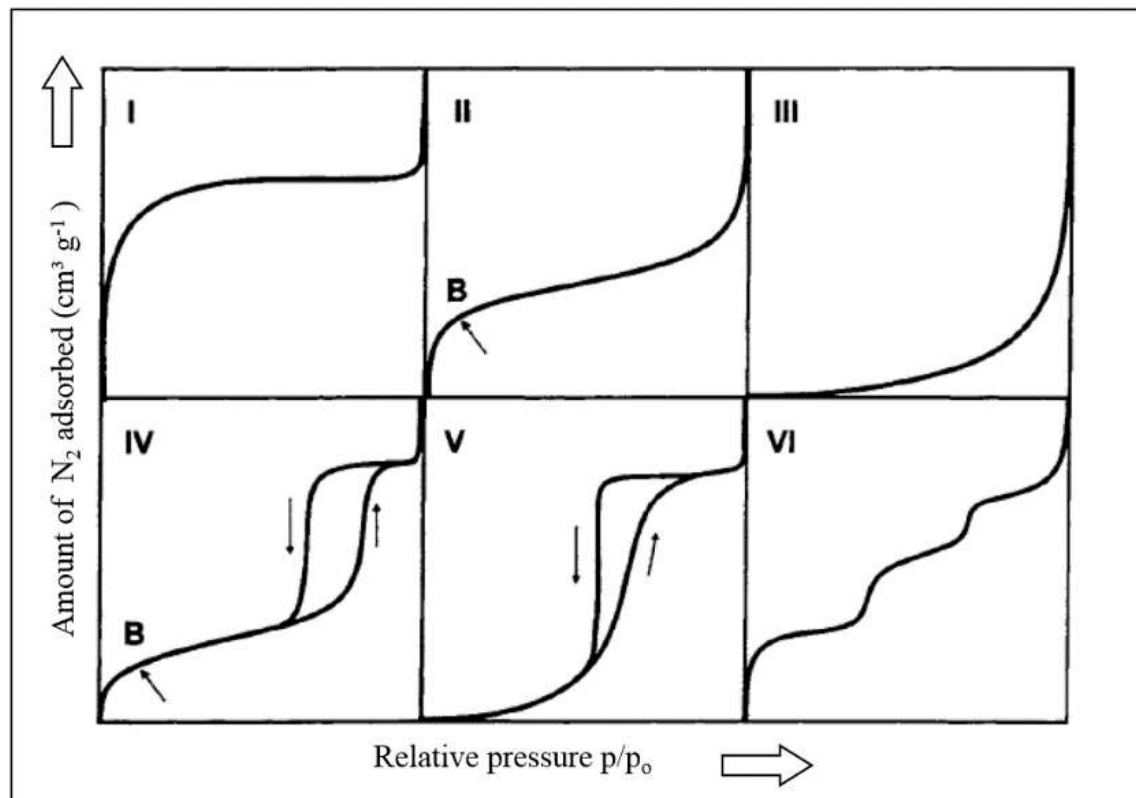


Figure 1-12. IUPAC categorisation of sorption isotherms. The adsorption and desorption isotherms have six characteristic shapes (I-VI): (I) microporous, (II) non-porous or macroporous, (III) non-porous, (IV) mesoporous, (V) mesoporous, and (VI) non-porous.¹⁵⁵

The Type I isotherm displays a quick rise in the adsorption level when heightening pressure is applied until the saturation pressure. This reaction is characteristic in those instances where adsorption is limited to a monolayer or, alternatively, when it is restricted to within solids that contain extremely fine pore structures, including microporous materials (namely, where the pore size < 2 nm). Type II isotherms are a feature of strong adsorption interactions and, are linked to non-porous or macroporous absorbents (namely, where the pore size > 50 nm). This classification displays an unbounded monolayer-multilayer adsorption. If one consults Figure 1-12, it is possible to identify Point B the beginning of the almost linear mid-section of the curve, which indicates the time at which the monolayer coverage will be complete and, when the multilayer adsorption is starting. One of the central features of Type III isotherms is the considerably weak adsorption

interactions of non-porous materials. It is also notable that type V isotherms generate a hysteresis loop with weak adsorption interactions, where the structure of the loop offers an indication of the appearance of mesopores.¹⁵⁵ Type IV isotherms are characteristic of mesoporous materials ($2 \text{ nm} < \text{pore size} < 50 \text{ nm}$) that have reinforced adsorption interactions. These involve a hysteresis loop, and this provides an indication of the capillary condensation occurring in the mesopores (i.e. the filling pores), along with a reduced uptake over several increased relative pressures (P/P_0). The initial point of Type IV isotherms is attributed to monolayer-multilayer adsorption because it follows the same path as the corresponding part of the Type II isotherm shown by the given adsorptive on the same surface area of a non-porous adsorbent; notably, this is suggested by the provided adsorptive residing on the identical surface area of a non-porous adsorbent. Type VI isotherms are associated with the generation of multilayers on non-porous adsorbents, thereby providing an indication of conjunct, multilayer adsorption onto an unbroken solid surface.^{144, 155}

1.3.7 Applications of monolithic reactors

In the early days of monolith reactor research, people considered their applications to be limited. However, with research and development in this technology, the number of applications identified has increased significantly. From its original chemical industry application, monolithic reactors have become widely used in a range of areas including pharmaceutical industry and food processing. The following are some of the many identified applications of monolithic reactors.⁹⁴

In the beginning, monolithic reactors were developed in the automotive industry as catalyst supports to convert engine emissions through gas-solid reactions to remove carbon monoxide, nitrogen oxide and hydrocarbons, and these materials have been used mainly as a selective catalytic reduction tool within stationary emission control

reactors.¹⁵⁶ Generally, this application offers a lower pressure drop as compared to traditional catalysts. Moreover, monoliths are also responsible for improving catalyst effectiveness, hotspot elimination and high selectivity.⁹⁰ Gas-liquid-solid reaction monoliths have been identified as having exceptional mass-transfer properties facilitated by their great surface area to volume ratios and no need for separation *via* catalyst.¹⁵⁷

Considering the success in the automobile application of monolith structures, the possibility of applying monolith reactors in catalytic hydrogenation or dehydrogenation, and oxidation of aromatic compounds, combustion of methane, water-gas shift reactions, hydrogen generation for fuel cells, steam reforming of methanol and light hydrocarbons have been reported.⁹⁰ Monolith catalysts have found new potential in replacing three-phase slurry reactors in synthesizing important chemicals, where monolith catalysts can achieve activities, and selectivities several times higher than slurry reactors.¹⁵⁸ Monolithic reactors can be used in the commercial production of hydrogen peroxide through the catalytic hydrogenation of anthraquinone towards its corresponding hydroquinones. The monolith support used in this method is SiO₂, while the active catalyst is palladium.⁹⁰ Through electroless deposition, Pd is placed onto the wall surface of the monolith to facilitate enhanced effectiveness of the surface. Comparatively, monolith reactors produce significantly higher activity with longer catalyst life, and higher product selectivity than packed bead bed reactors.⁹⁰

Monolithic TiO₂ rod columns were also used to separate adenosine monophosphate, adenosine diphosphate and adenosine triphosphate. This function is due to the ability to bind phosphate groups.¹⁰² Monolithic materials, are also finding their place in a variety of applications, such as gas chromatography (GC), high-performance liquid chromatography (HPLC), and capillary electrochromatography (CEC). These uses have been reviewed previously in detail.¹⁵⁹⁻¹⁶⁵

Furthermore, silica-based monolithic materials have also been used as sorbents during solid phase extraction and as carriers for immobilised enzymatic reactors.¹⁶⁶ Enzymatic microreactors with optimized porous properties synthesised by lipase immobilisation in capillary columns have a high rate of proteolytic activity and are used in proteomics for analysis of substrate solutions.¹⁶⁷

In summary, silica-based monoliths have been used in separation science to separate compounds or in catalysis as a microreactor. The scope of this thesis is to adopt a silica-based monolith as a heterogeneous catalytic microreactor for fine chemical synthesis due to the high porosity, high surface area and ease of surface modification which made it an ideal for a solid support structure. By combining the silica monolith embedded with catalysts into a flow reaction system, this lead to the potential of an automated optimisation flow reaction system.

Therefore, the following sections will illustrate the use of catalytic microreactors in general and specifically biocatalytic microreactors and their kinetics. The application of biocatalytic microreactors in biodiesel production and oxidation reactions will be revealed in more details in the biodiesel and catalysis by gold sections in this chapter.

1.4 Catalysts

1.4.1 Definition of a Catalysts

Catalysts increase the rate of particular chemical reactions but are not in themselves permanently changed by the reaction. During the catalytic process, the catalyst may undergo changes that distinguish it from its native state, but, by the end of the reaction, it has reverted to its initial state; therefore, catalysts at the start of a reaction are the same as those at the end

Catalysis is fundamental to chemical transformations. Almost all biological reactions rely upon catalysts, as do most industrial syntheses. Catalysis is considered the most important technology to protecting the environment through catalytic conversion to reduce emissions, such as catalytic converters used by the automobile industry. Although the dependence upon catalytic processes has a long and illustrious history, for example, the catalysis (fermentation) of sugar to ethanol and the conversion of ethanol to acetic acid, the core principle of catalysis has only been recognised within the last two centuries. Since then, scientific advances in catalysis have gone on to acquire the significance attributed to them today.^{168, 169}

Although catalysts can take the form of gas, solid or liquid, the majority of industrial catalysts are solid or liquid. The chemical industry is so dependent upon catalysis that 75% of all chemicals manufactured require catalytic input, though this figure increases to more than 90% in recently developed processes.¹⁶⁹ A large number of the organic intermediate products that are fundamental to the production of crop-protection agents, dyes, pharmaceuticals, pigments, plastics, resins, and synthetic fibres rely upon catalytic processes. This dependency extends to the purification, refining and chemical transformation stages of crude oil processing and petrochemistry. Measures to protect the

environment, such as purifying the off gases generated by industry and power stations, are only achievable with the help of catalysts.¹⁶⁹

Properties that determine whether a catalyst is suitable for an industrial process are its activity, its selectivity, and its stability (its deactivation behaviour).¹⁶⁹

1.4.2 Types of catalyst

Catalysts are broadly categorised as heterogeneous, homogeneous, and biological (biocatalysts).¹⁷⁰ Homogeneous catalysis describes those catalytic processes that occur in uniform gas or liquid phases. This category of catalysts usually comprises distinct chemical compounds or coordination complexes. Along with the reactants, homogeneous catalysts are distributed within the reaction medium.¹⁶⁹

In heterogeneous catalysis, the phase of the catalysts differs to that of the reactant. Typically, reactants are in liquid or gaseous phase, whereas the catalysts are solid. Heterogeneous catalysts are often preferred due the straightforwardly to separation of products from the catalyst through filtration or centrifugation.¹⁶⁹ In industry, heterogeneous catalysts have generally been preferred due to their high efficiency, substrate-handling characteristics, continuous product formation with catalyst separation, exceedingly low catalyst and reagent consumption, ability for catalyst re-use, less waste production and less volatile, lower cost operation and environmental benefits. In addition, heterogeneous catalysts offer the possibility of maintaining reaction performance even under what would normally be considered unfavourable operating conditions.^{171, 172} Heterogeneous catalysts comprise oxides, metal alloys or even sulfides on porous abutments. Enzymes can be considered somewhat anomalous because they feature elements of hetero- as well as homogenous catalysis.¹⁷³

Biocatalysts are enzymes a type of protein, that facilitate metabolic processes at the molecular level in living cells. Like all proteins, enzymes are formed from amino acids

with peptide bond linkages conferring a characteristic structure to each enzyme type. The active site for biocatalysis activity usually consists of a pocket in the morphology of the amino acid arrangement of the enzyme. Figure 1-13 demonstrates the process by which an enzyme binds with its substrate. Enzymes employ four different substrate-binding mechanisms: electrostatic interactions, hydrogen bonding, van der Waals interactions and hydrophobic interactions.^{174, 175}

Some enzymes are present in cells in a soluble form, whereas others are located on cell membranes where they are chemically bound. Enzymes fall between being macroscopic heterogeneous and molecular homogeneous catalysts.¹⁶⁹

Reaction rates are governed by kinetic factors. Within a catalytic system reaction rates are not scale-dependent and thus form the foundations of "scale-up reaction-engineering".¹⁷³

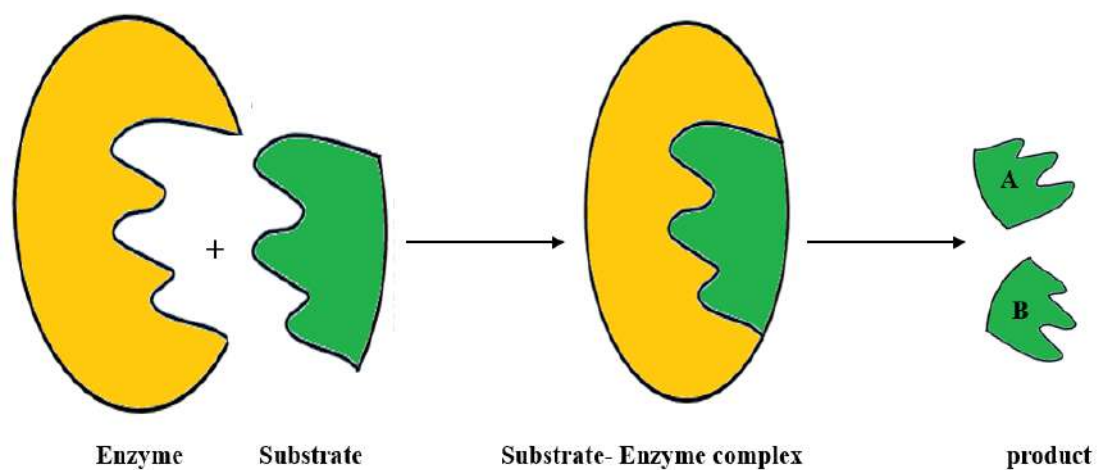


Figure 1-13. Enzyme binds with substrate during a chemical reaction.¹⁷⁵

1.4.3 Biocatalysts (enzymes)

Enzymes as catalyst are environmentally friendly and sustainable.¹⁷⁶ The high activity, selectivity, and specificity of enzymes open up a range of potential applications including biocatalysing, biosensing and in biomedicine.¹⁷⁶ These features have promoted the use of biocatalysts in industry over the past few decades.

Pharmaceutical, food and bulk chemical industries are relying on biocatalysts for production including the synthesis of drugs and chemicals.¹⁷⁷⁻¹⁷⁹

In terms of their application to industry, enzymes are most significant to agriculture, basic and fine chemicals, energy production, food, mining, medicine, and pharmaceuticals.¹⁶⁹

Biocatalysts are remarkable in their activity and selectivity. For example, the catabolism of hydrogen peroxide by catalase is 109 times faster than inorganic catalysts.¹⁶⁹

Biocatalysts are diverse and are derived from numerous natural sources, including microbial, plant or animal cells. As well as whole cells, they include cell-free extracts and enzymes. Generally, enzymes demonstrate a considerable degree of specificity for their substrates, are chemoselective, regioselective, and enantioselective.

However, significant challenges remain as enzyme-catalysed bioprocesses are unstable in large-scale industrial processes, making them operationally expensive. To help offset this, in recent years there has been a marked development in enzyme immobilisation.¹⁷⁶

This technology is acknowledged as promoting enzyme stability by protecting against environmental and chemical attack. Furthermore, in a large-scale continuous process, the immobilised enzymes can be reclaimed and used again.¹⁷⁶

1.4.4 Lipases as biocatalysts

Enzymes with unusual and potentially useful properties are often produced by microorganisms inhabiting extreme environments. Lipases secreted by psychrophilic microorganisms are one example, with the lipase produced by the Antarctic yeast *Candida*

antarctica being a subject of intensive study.^{180, 181} Different sources of lipase enzyme confer different kinetic properties with respect to enzyme morphology, substrate specificity, pH optimum and thermo stability which in turn may permit a wide range of industrial applications from food processing to detergent manufacture. Identification of novel species of unique lipase-secreting microorganisms may therefore reduce the production costs associated with existing technologies or may even facilitate the catalysis of new, useful chemicals. Lipases are members of the hydrolase class of enzymes that catalyse hydrolysis reactions – i.e., those reactions involving the addition of water to split large molecules into smaller ones. The hydrolytic reactions of lipases have demonstrated potential applications in the biodegradation of oil and fat wastes from the food industry.¹⁸² Lipases have been applied for catalysis of enantio- and region selective reactions, including hydrolysis, aminolysis, esterifications and transesterifications.^{183, 184}

Where lipase is used as homogeneous catalyst, it is difficult to recover the expensive lipase at the end of the reaction; an alternative method is to use lipase as a heterogeneous catalyst. As such, it is immobilised on a supporting solid surface, which facilitates the easy separation and recovery of the lipase.¹⁸⁵⁻¹⁸⁸ The rate of chemical reactions can be efficiently up-scaled by using lipase-immobilised microreactors. This method can generate high quantities of products whilst using only a portion, or even a minimal number of reagents and materials.^{189, 190}

1.4.5 Advantages of immobilisation of enzyme

Immobilised enzymes are those that retain their catalytic activity whilst confined or localised, enabling them to be used continuously and repeatedly. Their history dates back to the 1960s; it was followed in the 1970s by the works of Zaborsky and Royer that inspired academic and industrial scientists.¹⁹¹

Enzymes such as amino acylase, amylase, invertase, protease, and several lipases have been applied successfully in many industrial processes. Immobilising enzymes results in continuous activity instead of batch operation which, in large-scale processes, reduces labour costs by simplifying control of the process. Most bio-products are not produced on a large scale, so immobilised enzymes are used to manufacture fine chemicals and pharmaceuticals. They are not sufficiently cost-effective to rival conventional catalysts used in manufacturing bulk chemicals.^{179, 192}

The advantages of enzyme immobilisation are manifold. It promotes stability, facilitates easy product separation, permits reusability, and confers superior control over catalysis and economy of the process. In addition to efficiently initiating enzymatic reactions and products, immobilisation also enhances innate properties of the lipase whilst making the most of the numerous products that could be generated during and following the reaction. Aside from the enzyme and product separation that this technology affords, the lipase or substrate contact time is improved by using continuous flow system.¹⁸⁷

Yet immobilisation is not without its drawbacks. Conformational changes to the enzyme, modifications in properties, limitations of mass transfer, reduced action on insoluble substrates and potential enzyme denaturation may occur. The operational cost of biocatalytic reactions and the degree of enzyme stability can be influenced considerably by selecting suitable immobilisation methods and adopting appropriate support.¹⁹³

1.4.6 Immobilisation methods

There are several ways to immobilise enzymes on the solid supports.¹⁹¹

1. Binding to a solid support

- a. Physical adsorption (by hydrogen bonds or hydrophobic interaction)
- b. by covalent binding (e.g., to epoxy groups)

- c. by ionic binding (e.g., to ion exchange resins)
2. Cross-linking (e.g., by glutaraldehyde).
3. Entrapment.
- a. in gels (e.g., calcium alginate)
 - b. in membrane reactors (e.g., hollow fibre reactors)
 - c. in reversed micelles, microemulsions.

1.4.7 Influence of immobilisation carriers

The carrier materials for immobilisation makes a significant contribution to the effectiveness of immobilised lipases. These materials need to be readily available, non-toxic and compatible biologically with the enzyme.¹⁹⁴ As well as the material, the structure of the carrier has an influence on the immobilised enzymes. Silica and polymers are commonly carrier supports for enzymes.¹⁹⁵⁻¹⁹⁷

In determining the process of production, the method of immobilisation can vary. Industrially applied lipase immobilisation methods are predominantly based on lipase adsorption to hydrophobic polymers such as alkyl-agarose, polypropylene, and polystyrene.^{198, 199}

The effect of immobilisation depends on process variables, such as substrate concentration and reaction time as studied by Peterson *et al.*¹⁶⁷ The research revealed that enzymatic microreactors displayed superior performance in the investigated reactions. However, the problem of lipase stability persists and it remains a topic for further research.¹⁶⁷ Dissociation of multimeric enzymes can result in subunits capable of inactivating lipase or contaminating the reaction. A range of techniques aiming to stabilise multimeric enzymes are under development. Recently, approach has been to crosslink the enzyme subunits by maximising disulfide bonds, which reinforces the

interaction between subunits.²⁰⁰ Yet these methods may come with an efficiency cost, reducing the catalytic capability of the enzyme or introducing steric hindrance to the catalytic sites, inhibiting substrate interaction.²⁰⁰ For the same reason, catalytic deformity presents a problem if production is dependent on these processes.

To overcome these limitations, there is active research into alternative methods of entrapping lipases. Microporous polymer monoliths present one possibility as they adsorb large volumes of enzyme. Research has demonstrated that these structures support a high reaction rate for each lipase molecule, superior to that of free lipase.^{191, 201}

Yang *et al.*²⁰² showed that a modification-coupled method with silica-PEG gel immobilised lipase more effectively than adsorption and cross-linking methods.

Hydrophobic sol-gel (alkyl-modified silane) supports present an alternative to generate monolithic reactors.^{203, 204} The activity is improved by the structure of the lipase, in which the lipophilic domain is stabilised in the open form, where it can interact with the hydrophobic regions of the gel.²⁰⁵ Production of monolithic reactors by this method is not problem-free, as steric hindrances may occur. Nonetheless, this method remains popular with some industries and researchers. Because of the high homogeneity, multimodal ordered porosity, and specific high surface area afforded by sol-gel processing, this has become a popular technique for the immobilisation of enzyme.^{102, 206} Immobilisation of enzymes onto silica has previously been highlighted as a potentially successful avenue for further investigation. Many previous reports have indicated that a significantly high loading of enzyme such as cytochrome C, papain and trypsin demonstrated a noticeably higher efficiency after immobilization in MCM-41. Both enzyme size and mesopore size were demonstrably correlated with efficiency of the immobilised enzymes.²⁰⁷ α -amylase immobilized in ordered mesoporous silicas exhibited a specific activity equivalent to 80%

of the specific activity of the free enzyme, but with higher thermal and pH stability compared with the free α -amylase.²⁰⁸

Enzymatic activity of alkaline phosphatase was elevated by a factor of 2–10 following immobilization onto mesoporous silica ($\sim 30 \text{ \AA}$) compared to enzyme immobilisation onto mesoporous sol-gel silica due to more effective diffusion of the substrate molecules.²⁰⁹ Lipase immobilization offers the advantage that it cannot only increase lipase stability, but it also can promote lipase activity. In 1995, Reetz *et al.*^{210, 211} reported that it is possible to increase the activity of lipases by up to 100 fold by immobilization in a sol-gel. Adsorption of lipases onto strongly hydrophobic supports, in some instances, resulted in a 20-fold increase in activity whilst also exhibiting more enantiomeric selectivity than lipase in the free state.¹⁹⁹

1.4.8 Assay of the enzyme for free and immobilise lipase

An 'assay' is the term used for the investigation of an enzyme's activity. Enzyme activity can be assessed by measuring the rate of substrate used in the reaction or the amount of product formed. There are a number of assays available to measure enzyme activity; Lipase/esterase activity plays a key role in enzyme production and it is possible to measure the hydrolytic activity of lipases and esterases by a variety of methods, including titrimetry, spectroscopy, chromatography, turbidimetry, conductometry, immunochemistry, microscopy and biosensor techniques.^{212, 213} Factors that may influence the choice of assay include cost, convenience, and availability of equipment.²¹⁴

The hydrolytic activity of lipase / esterase enzymes is frequently determined by the pH-stat methodology. However, this technique is a lengthy process, and produces various waste streams; therefore, spectrophotometric techniques utilising chromogenic substrates such as 4-nitrophenol and resorufin esters are considered a more efficient approach.²¹⁵

This type of spectrophotometric assay is a simple, selective and non-destructive technique that has become accepted as a standard approach for determination of enzyme activity. For example, spectrophotometric measurements at 400 nm, over different time intervals, using of 4-nitrophenol as a chromophore, can be used where the lipase / esterase mediates hydrolysis of 4-nitrophenyl butyrate.²¹⁶⁻²¹⁸

1.4.8.1 Spectrophotometric theory

Visible light represents electromagnetic radiation of 400-750 nm wavelength, within which light-absorbing compounds are coloured. However, in the ultraviolet (UV) wavelength of 200-400 nm, light is absorbed by numerous compounds that are not coloured. It must be noted that the absorption process can be better understood not on the basis of the wavelength of visible and UV light, as is standard, but on the basis of their frequency. Furthermore, an inverse correlation exists between wavelength (λ) and frequency (ν) (*i.e.*, $\lambda = c/\nu$; c denoting the speed of light). As the frequency of electronic fluctuation in the molecules and of the irradiating light is the same, irradiation of absorbing molecules enhances the energy level of their electrons, thereby inducing light absorption. Dependent on the absorbing molecule structure, the wavelength at which compounds display maximum light absorption is the wavelength associated with the above-mentioned frequency (λ_{\max}). Moreover, the likelihood of the occurrence of electronic transition determines the degree of light absorption.

The quantity of light absorbed by an analyte sample can be determined through spectrophotometry, which involves penetrating the sample with a light beam and measuring the intensity of light that reaches the detector in Figure 1-14.

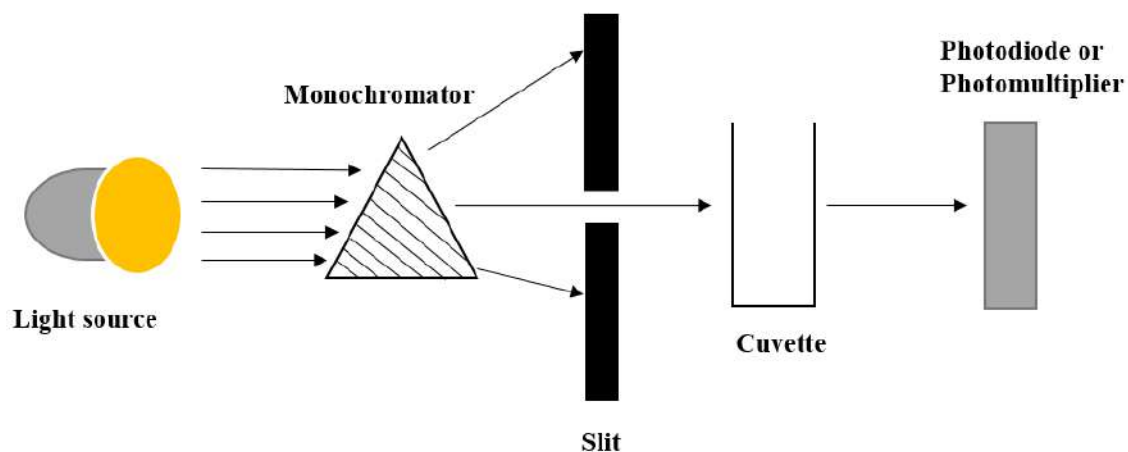


Figure 1-14. The operation principle of a spectrophotometer.²¹⁹

The detector of the spectrophotometric is based upon the Equation of Beer-Lambert law in Equation 1-3, with A representing the absorbance, b path length (cm) , c molar concentration(M), and ϵ refers to the molar absorptivity ($M^{-1}cm^{-1}$).²²⁰

$$A = \epsilon bc \quad \text{Equation 1-3}$$

1.4.9 Determination of parameters for free lipase kinetics

Kinetic factors determine the rates of enzyme-catalysed reactions. Henri in 1903 proposed a first-order reaction rate equation.²²¹ Michaelis and Menten built on Henri's work to present the most basic and well-recognised model of enzyme kinetics in 1913, known today as the Michaelis-Menten model.²²² This relates the rate of an enzyme-catalysed reaction to the concentration of the starting substrate. In the most basic scenario, one substrate is catalysed by one enzyme with only a single catalytic site. During the first step of this reaction, an equilibrium is set up between the concentrations of the enzyme (E) and the substrate (S) in the production of an enzyme-substrate complex (ES). This enzyme-substrate complex can, as part of the equilibrium process, subsequently dissociate back to the substrate and enzyme again, or alternatively, can progress to the completion of the catalysis with the formation of the reaction end product (P) and the subsequent release of the enzyme once more. It is assumed that the equilibrium is not

affected by the concentrations of the end product produced during the initial period when the measurement of the reaction rate is taken as can be seen in Equation 1-4.



Equation 1-4

k_1 , k_{-1} and k_2 represent the rate constants for the individual steps of the reaction and are also used to define K_m , the Michaelis constant in Equation 1-5:

$$K_m = \frac{k_{-1} + k_2}{k_1} \quad \text{Equation 1-5}$$

If the enzyme-substrate complex is in rapid equilibrium with the enzyme and substrate reactants, this means that the equilibrium reactions occur much more rapidly than the product is formed, giving rise to the Michaelis-Menten in Equation 1-6 :

$$v = \frac{V_{max} [S]}{K_m + [S]} \quad \text{Equation 1-6}$$

In this equation, v is the initial reaction rate, $[S]$ is the substrate concentration and V_{max} is the maximum rate of the reaction. A hyperbolic curve depicts the rate of the enzyme catalysed reaction versus the substrate concentration (Figure 1-15) and from this, the K_m value can be defined as the substrate concentration correlating to the point at which the reaction rate is half of V_{max} . These parameters can also be obtained by adapting the Michaelis-Menten equation to produce a linear response. This formulation is achieved by taking the reciprocal of both sides of the equation to produce the Lineweaver-Burk equation as illustrate in Equation 1-7:

$$\frac{1}{v} = \left(\frac{K_m}{V_{max}} \right) \frac{1}{[S]} + \frac{1}{V_{max}} \quad \text{Equation 1-7}$$

The intercept on the y-axis can be read to give a value for V_{max} similarly K_m can be obtained directly by the determination of the slope of the resulting straight line graph (Figure 1-16). The turnover-number K_{cat} can be calculated through Equation 1-8.

$$K_{cat} = \frac{v_{max}}{[lipase]} \quad \text{Equation 1-8}$$

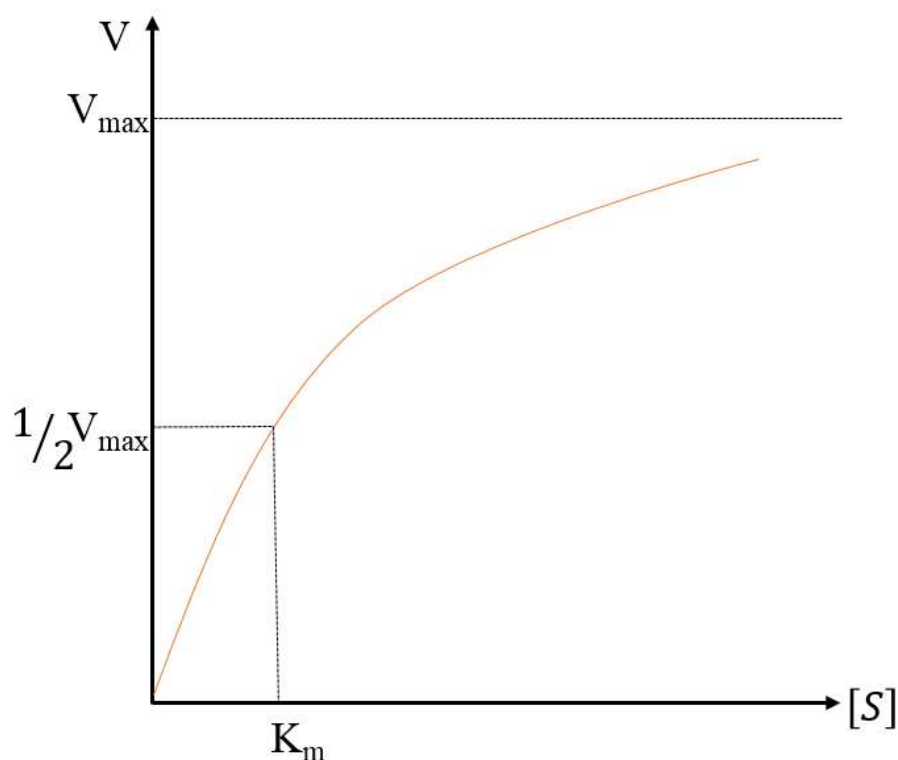


Figure 1-15. Plot of reaction rate V against substrate concentration $[S]$ according to the Michaelis-Menten equation. The enzyme concentration remains constant.

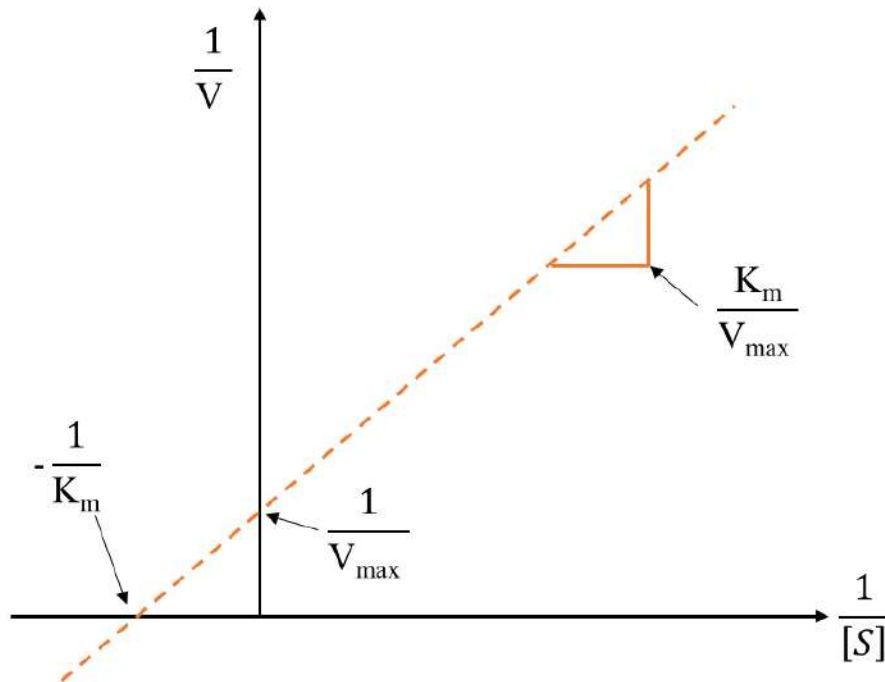


Figure 1-16. Lineweaver-Burk plot of $1/V$ against $1/[S]$ from which K_m and V_{\max} can be obtained directly from the intersection of the resulting straight line with the x- and y-axes.

It can be seen that the value of V_{\max} for any enzymatic reaction will vary according to the concentration of the enzymes. The greater the enzyme concentrations, the faster the rate of reaction (so long as the substrate concentration is not a limiting factor). This means that V_{\max} provides details of the enzyme's efficiency as a catalyst. The 'turnover-number' of an enzyme is the number of substrate molecules that the enzyme molecule can transform into product per unit time (again, assuming that the substrate concentration is not limiting). Highly efficient enzymes have turnover numbers in the order of several hundred thousand, whilst less-efficient enzymes can have turnover numbers of less than one substrate molecule converted per second. The well-known enzyme, catalase, has a turnover-number 4×10^7 molecules per second, whilst for another well-known enzyme, lysozyme, it is 0.5 molecules per second.²²³

K_m is known as the Michaelis constant. This indicates the substrate concentration at which the reaction rate is at half its maximum value. Therefore, the Michaelis constant

is an indicator of the efficiency with which an enzyme can catalyse the conversion of a substrate into a product. Values for K_m generally vary over a broad range but typically fall within 10^{-7} to 10^{-1} . High K_m values are indicative of enzymes which may take a relatively longer time to disassociate from the substrate and which therefore may be classified as relatively less active or efficient than enzymes with lower K_m values. Where an enzyme is able to catalyse reactions where there is more than one substrate, a different K_m value will be applicable for each substrate.²²³

1.4.10 Determination of parameters for immobilised lipase kinetics in continuous-flow systems

Hadd *et al.*²²⁴ first reported the use of a microfluidic system for the analysis of enzyme kinetics following their successful demonstration of a computer-controlled electrokinetic transport mechanism for reagent dilution and mixing. This study involved the mixing of precise concentrations of a fluorogenic compound with $\hat{\alpha}$ -galactosidase and monitoring the fluorescence resulting from the product of the hydrolysis reaction to elucidate the enzyme kinetics. A centrifugal microfluidic system able to perform multiple concomitant homogeneous enzymatic assays employing colorimetric detection has subsequently been reported by Duffy *et al.*²²⁵

Most quantitative studies on enzyme kinetics determined using microfluidic systems have been performed in homogeneous solutions.²²⁶⁻²³⁰ Heterogeneous assays employing the use of immobilized enzymes offer potential benefits, including simplicity of enzyme arrangement within arrays, capability to investigate enzymes in association with cell membranes (impossible in homogeneous solution) as well as simplification of enzyme renewal and computerised continuous-flow analysis. Trypsin immobilized on beads was used in a microfluidic reactor by Harrison *et al.*²³¹ to catalyse the breakdown of proteins before mass spectrometry.

An approach involving immobilisation of enzymes on fluid bilayers supported on the walls of microfluidic channels was similarly reported by Mao *et al.* prior to one shot determination of the enzyme kinetics employing laminar flow-controlled dilution.²³² Lastly, the preparation of reactive porous monoliths within microchannels as supports for the immobilization of trypsin with analysis of the compounds resulting from protein breakdown was reported by Peterson *et al.*²³³

The diffusional constraints or interactions resulting from the support matrix for immobilised enzymes may result in different kinetics to those obtained for the same enzymes in solution. As a consequence, the term ‘apparent kinetics’ is frequently used to refer to the kinetics of immobilised enzymes. The apparent kinetic parameters in packed-bed enzyme reactors under steady-state conditions are commonly determined using a calculation referred to as the Lilly-Hornby model in Equation 1-9 which will be used to determine the kinetic parameters of the immobilised lipase in this work.^{234, 235}

$$C_{in} - C_{out} = K_m \frac{C_{out}}{C_{in}} + \frac{V_{max} V_{void}}{Q} \quad \text{Equation 1-9}$$

Where K_m is the apparent Michaelis constant; V_{max} is the maximum rate of reaction; C_{in} and C_{out} are the respective reactant concentrations at the inlet and outlet of the reactor; V_{void} is the void volume of the monolith microreactor; and Q is the volume flow rate. As previously discussed, it is possible to obtain K_m values from the gradient of a graph of reaction rate versus substrate concentration; with V_{max} values obtainable from the y-axis intercept. Values of V_{void} the void volume of the monolith microreactor and Q the volume flow rate were measured.

1.5 Biodiesel

Biodiesel is derived from the Greek word 'bio', meaning life, as well as 'Diesel', the fuel named after Rudolf Diesel. Biodiesel is a synthetic diesel-equivalent fuel created from biological material.²³⁶ Particularly over the past couple of decades, there has been an increasing problem posed by ever-scarcer non-renewable energy reserves, alongside environmental degradation.²³⁷

From the 1800s onwards, petroleum-based fuel resources have developed to become the most significant global energy sector. Consumption has grown over this time, necessitating further petroleum output. Certain estimates suggest that, over the next three decades, non-renewable energy reserves will be exhausted. Consequently, environmental pressures, resource exhaustion and increasing consumption all add impetus to the search for fossil fuel substitutes.²³⁸ With depleting fuel resources and ever-growing worries regarding global warming, there has been a concerted effort to discover environmentally sustainable and renewable alternatives to petroleum fuels. An alternative which is considered to have significant potential in the coming decades is biodiesel, which stands to supplant a considerable proportion of diesel fuel use. Biodiesel, or mono-alkyl ester, is created *via* the catalysis of vegetable oil- triglyceride- by alcohol. Glycerol is the acknowledged by-product in the process of transesterification. Such production should typically adhere to the American Society for Testing and Materials (ASTM) regulations.²³⁹ Biodiesel is considered to have particular potential as a renewable, biologically sourced energy resource with both environmental and financial advantages. It has been the focus of increasing research, energy sector attention and societal awareness, with proven economic viability as a biofuel. The ASTM has determined biodiesel to be a renewable, vegetable or animal fat-derived mono-alkyl long chain fatty acid ester.^{237, 240}

Barnwal and Sharma outlined how vegetable and used fats can be used without any synthesis, although in practice there are disadvantages.²³⁷ There is significant smoke production resulting from poor combustion, and certain incombustible materials can build up in the engine, while fouling of the injector through coking is common. Therefore, academic investigations have considered the most effective way of synthesising biodiesel by chemical alteration of biological fats, producing a fuel with related characteristics to diesel fuel.²⁴¹ The characteristics particular to biodiesel are what gives it certain advantages as a fuel, particularly compared to diesel. It has a larger octane number; furthermore, it is biodegradable and non-hazardous. In addition, it contributes no sulfur, incombustible hydrocarbons or particulate pollution to environmental pollution, while there are lower carbon monoxide emissions. The capture and reuse of carbon dioxide emissions through photosynthesis is also possible.^{241, 242} Diesel fuel also has increased hazards during production and movement due to its lower flash point, whereas biodiesel is much more stable with a flash point of 150° C.²³⁸

Barnwal and Sharma²³⁷ pointed to an additional benefit of biodiesel, in that it acts as a lubricant for engines, diminishing degradation and contributing to lengthened working life. Furthermore, biodiesel and diesel share similar viscous properties, meaning diesel fuel engines have to undergo minimal or no conversion to enable the use of biodiesel-petroleum diesel fuel mixes.

Various characteristics of biodiesel make it superior in many respects to diesel petroleum, such as its reduced environmental impact due to decreased sulphur dioxide and carbon monoxide emissions, biodegradability, its lubricating and viscous properties, a great flash point temperature, as well as a large cetane number.²⁴³

Diesel fuel emissions contain carcinogens, the emission of which can be diminished if it is mixed with biodiesel, or through the use of biodiesel outright. It is possible to utilise pure biodiesel in car engines, which is termed B100 fuel when at 100% biodiesel content.

Alternatively, engines can run on biodiesel diluted to varying degrees with standard diesel. Thus, the most widely adopted biodiesel variations are: B2- 98% diesel fuel and 2% biodiesel; B5- 95% diesel fuel and 5% biodiesel; B20- 80% diesel fuel and 20% biodiesel, the most widely used combination, as well as B100- 100% biodiesel.²⁴⁴

Oliveira *et al.*²⁴⁴ outlined the various methods of synthesising biodiesel, such as microemulsification and pyrolysis. The most widely utilized procedure for synthesis is alcoholysis, or transesterification. This entails instigating the reaction of biological fats with alcohol, using enzyme, acidic or alkaline catalysts to produce the mono-alkyl ester fatty acids, or biodiesel, a process which also produces glycerol. The fatty acid methyl esters (FAME) necessary for the creation of biodiesel are produced through the transesterification of triacylglycerol or triglyceride by methanol or ethanol. Ethanol and methanol are the most widely applied alcohols for the transesterification process. Due to its chemical and physical properties of being the shortest chain alcohol and polar, methanol is the most preferable alcohol for transesterification, as it is also cost effective.^{245, 246}

Using methanol in the transesterification process also has the advantages of effectively responding to alkaline catalysis, as well as a rapid reaction with triglyceride. Nevertheless, a drawback is its potentially hazardous nature, with its lower boiling point producing methanol fumes which can result in a volatile production environment.²⁴⁷

Vegetable oils used for the synthesis of biodiesel are varied, such as canola, soybean and cottonseed oil. In the transesterification process with a small molecular weight alcohol e.g. : propanol, butanol, methanol or ethanol enables the chemical decomposition of the triglyceride molecules into ethyl or methyl esters, when catalysis of the reaction is enabled through the use of, for example, potassium hydroxide and sodium hydroxide.²⁴⁸

The most widely used as homogenous catalysts are potassium hydroxide and sodium hydroxide, in the transesterification process, although other alkoxides can be used. Their

advantage lays in the fact that no special environment is required for their use, while they instigate rapid reactions with large production of methyl esters.²⁴⁹

Nevertheless, this catalyst during the catalysis process forms of soap through saponification, and this process cause serious problems which actually decreases the catalyst's efficiency and the production of biodiesel.^{250, 251} A solution to the problem of soap formation during the transesterification process is to use acidic catalysts, for example hydrochloric acid, sulfonic acid or sulphuric acid. However, the disadvantage of acids catalyst is the rate of the reaction is slow compared with base catalyst, while also requiring a high temperature.^{246, 252, 253}

The utilisation of lipase enzymes to catalyse the transesterification reaction allows for a particularly efficient and chemically clean process; however, chemical catalysts are significantly cheaper to purchase.²⁵²

A transesterification process which used a methanol is called methanolysis. As can be seen in Figure 1-17 , three chronologically contiguous reactions occur, with triglyceride broken down into diglyceride (DG), followed by the formation of monoglycerides (MG). With potassium hydroxide (KOH) as the catalyst, a reaction occurs between the methanol and triglycerides, producing diacylglycerols or diglycerides and a single fatty acid alkyl ester (FAAE). The next reaction occurs between the methanol and diacylglycerols, forming monoacylglycerol or monoglycerides, alongside a further FAAE. The final reaction is that between the methanol and monoglycerides, forming a further FAAE and the additional co-product glycerol. Each step is a reversible reaction. The initial biological fat used for the reaction is much more viscous than the biodiesel produced.^{254, 255}

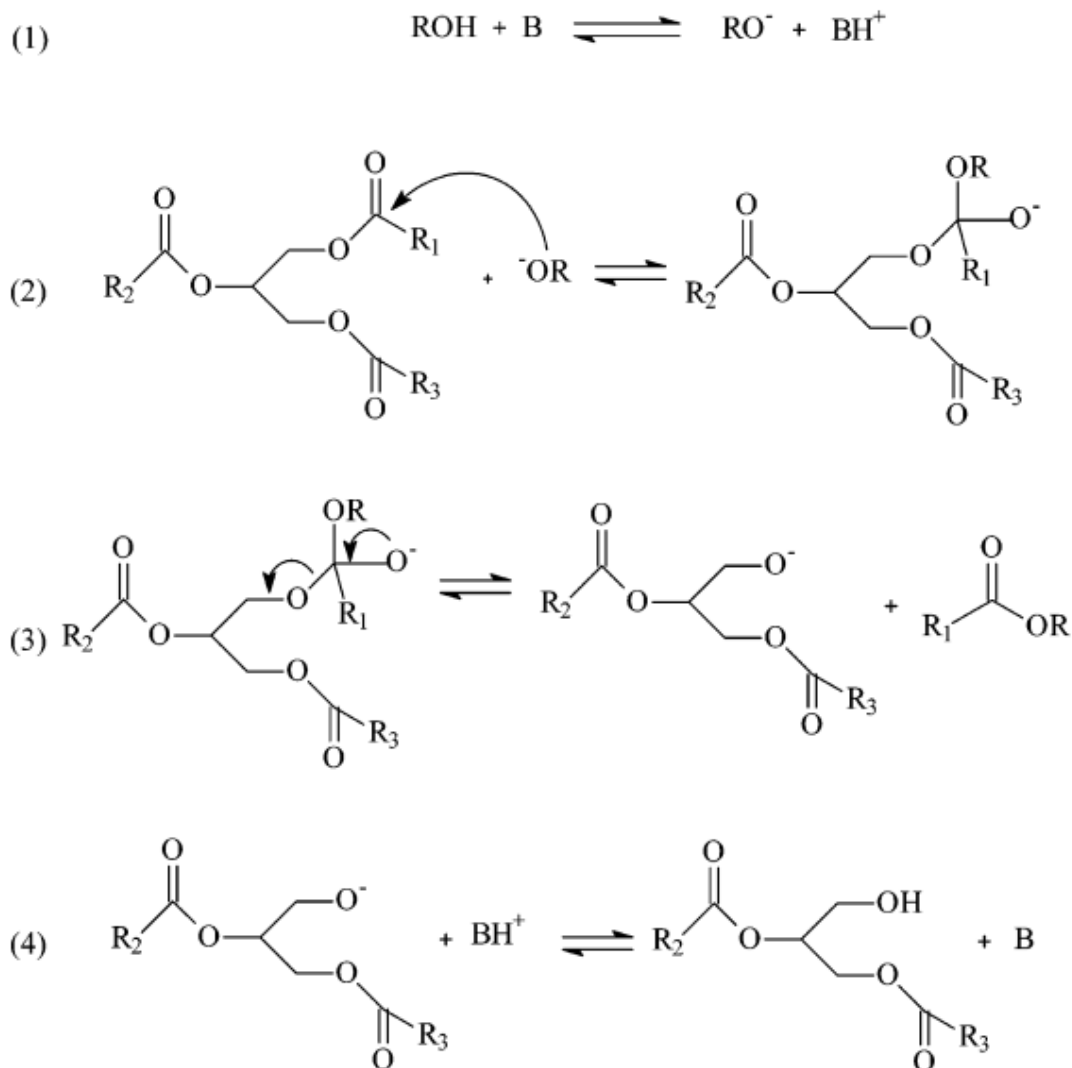


Figure 1-17. Homogenous-based catalysed reaction procedure for the transesterification of triglyceride (TG).

Where: R: alkyl group of the alcohol (methanol); B: base catalyst (KOH); R1, R2, R3: carbon chain of the fatty acids; OR^- : CH_3O^- ; BH^+ : $[\text{K}(\text{OH})\text{H}]^+$

The three-stage reversible process which produces the fatty acid alkyl ester molecules can be explored in greater detail, broken down into a further three processes. During the first process, a strong nucleophile alkoxide is produced, with the assistance of the base KOH catalyst. During the second process, a tetrahedral intermediate is produced from the nucleophilic attack by the alkoxide on the TG carbonyl group. The final process sees the carbon gain electrons from the negative carbonyl oxygen, while a respective DG and FFAE molecule are released by the degradation of the tetrahedral intermediate. DG and MG are both produced as intermediates in the act of transesterification, often reducing the purity of the biodiesel. TG which did not react might also undermine the purity of the biodiesel. There can be detrimental impacts on engine injectors from the presence of glycerides such as DG, TG and MG; however, engine issues can be mitigated through the use of ASTM D6751.^{246, 256}

Two phases are formed during the transesterification reactions. The bottom phase liquid generally contains water, soap or glycerol as a result of additional free fatty acids, remaining a catalyst substance. Glycerol as co-products of the transesterification reaction requires intensive purification and washing in this process itself, and the glycerol has useful applications in cosmetic production, the pharmaceutical industry, as well as plastic and food production. The methyl and ethyl ester is located in the top phase liquid, which, following refinement to eliminate residual methanol and cleansing with water, can be utilised as biodiesel.²⁵⁷ There is an important qualification: it must correspond to the characteristic information for biodiesel as stipulated by the ASTM.

1.5.1 Biodiesel production by using the microreactor

There are multiple microreactors for biodiesel production with an array of characteristics, being made of different substances, having different structures, properties as well as alternating size.¹⁴

However, some typical properties, for example the micro-structured reactor to increase mixing efficiency, as well as a microtube or microchannel, can achieve a more comprehensive reaction. Biodiesel production can adopt several microreactors or a single mechanism. The most straightforward microreactor structure are capillaries, which have an established practical use within biodiesel production, as well as being the most comprehensively analysed in the research. There are other microreactors which rely on newer technology, materials and production methods, while microdispersive reactors have also been utilised for biodiesel production.²⁵⁸

1.5.1.1 Microtube reactors

Sun *et al.*²⁵⁹ utilised biodiesel production from a ready-prepared mixture of KOH, rapeseed oil and methanol, utilising a quartz capillary measuring 0.25 mm in terms of inner diameter (I.D.). The KOH concentration was 1 wt %, while the ratio of methanol to oil was 6:1. FAME production was 99.4% at 60° C within 5.89 min. However, the full benefits of adopting a microreactor for biodiesel synthesis cannot be seen in this research, due to the rapeseed oil and methanol having been mixed prior to the use of the capillary reactor. Guan *et al.*²⁶⁰ applied biodiesel synthesis by mixing methanol and sunflower oil within a t-shaped, clear, fluorinated ethylene-propylene (FEP) microchannel reactor, with measurements of 0.8mm I.D. The KOH concentration was 4.5 wt %, while the methanol to oil molar ratio stood at 23.9:1. FAME production was 100% after 100 s at 60° C. A flow rate of 8.2 cm³/h was achieved, with a semi-homogeneous liquid also being produced. Compared to a laboratory-sized batch reactor, the microchannel reactor achieved increased efficiency in biodiesel synthesis. Bertoldi *et al.*²⁶¹ implemented a biodiesel

synthesis process using supercritical ethanol, soybean oil as well as an additional solvent of carbon dioxide. Catalysts were absent from the procedure, while the temperature for reaction was between 300-350° C, at 7.5 to 20 MPa. A stainless steel pipe reactor measuring 316 mm in length, with an I.D. of 0.76 mm and 1.59 mm external diameter was utilised, having a capacity of 88 mL. Trentin *et al.*²⁶² staged a similar experiment, except the tubular reactor's capacity was 13.5 mL. In recent times, Santacesaria *et al.*²⁶³ synthesised biodiesel through the reaction of methanol with soybean oil, using KOH as a catalyst. The tubular reactor adopted was a stainless steel AISI 316 cylindrical tube, with a length of 20 cm and the diameter of 12.7 mm, the I.D. measuring 10 mm and comprised of tiny stainless steel spheres, several alternative packed beds were investigated. One was a cylindrical reactor comprising 2.5 mm diameter spheres; the second added 1 mm diameter spheres to pack the octahedral spaces existing among the 2.5mm diameter spheres, while a final alternative also added spheres with a diameter of 0.39 mm to minimise the tetrahedral space existing between the bigger balls. Consequently, three decreasing sizes of microtubes were created, of 1000 µm, 500 µm and 300 µm on average, relating to the diminishing size of the spheres used. The results determined that with prime reaction circumstances, a rapid degree of biodiesel synthesis is achieved at 60° C in under a minute, with the methanol to oil ratio being 6:1.

1.5.1.2 Reactors comprised of microstructures

An improvement on microtube reactors for achieving a uniform mix of methanol and oil is considered to be the use of microstructured reactors, comprising multiple mixing methods. A microstructured reactor utilised by Canter²⁶⁴ contained microtubes in a parallel layout across a plastic plate with diminished thickness, so as to mix methanol/NaOH and vegetable oil distributed by separate syringes. FAME production at 40° C after 4 minutes was 90%, while at 45° C after 10 minutes stood at 96%. However, Canter did not elaborate on the nature of the reactor.

In a comparison of an equal volume of biodiesel synthesised *via* the utilisation of microreactors to that synthesised by batch method, it was shown that the former improved the synthesis of biodiesel in terms of financial expenditure and energy requirements.

Wen *et al.*²⁶⁵ produced biodiesel by mixing methanol, soybean oil and the catalyst NaOH, and the microchannels were designed through an electric spark handling on the stainless steel, criss-crossed microtube reactor comprising the periodic turn values 10, 50, 100, 200 and 350/1.07 m, with a 240 μm to 900 μm hydraulic diameter. At 56° C and after 28 s, at 240 μm hydraulic diameter, a production rate of 99.5% was achieved, with a NaOH concentration of 1.2 wt % and a methanol to soybean fat molar ratio of 9:1. Jovanovic *et al.*²⁶⁶ synthesised biodiesel by mixing methanol with soybean oil, *via* a patent-protected microreactor with a trio of channels at a 90° angle. These channels had the respective width and depth measurements of 135 mm x 135 mm, 100 mm x 1.7 mm and 100 mm x 0.8 mm. After a period of 10 min and at a room temperature of 25° C, with NaOH concentration at 1 wt % and a 2.5 mL/min flow rate, a significant production of biodiesel was seen with a 7.2: 1 ratio of methanol to oil. Sun *et al.*²⁶⁷ synthesised biodiesel from methanol and cottonseed oil, utilising a KOH catalyst. The microstructured reactor which they utilised comprised a couple of multilamination micromixers, with a PTFE tube at 3 mm I.D containing delay loop Dixon rings. The multilamination micromixers were a slit interdigital micromixer (SIMM-V2) built by IMM in Mainz, Germany, as well as a rectangular interdigital micromixer (RIMM), made by Mikroglas who are also situated in Mainz. A greater production of FAME was seen, due to these mixers being much more vigorous and effective than the J-mixer and T-mixer. At a temperature of 70° C and after 17 s, with a 10 mL/min flow rate, biodiesel production stood at 99.5%, with an 8:1 methanol to oil molar ratio.

Kalua *et al.*²⁶⁸ used biodiesel production utilising a slit-channel microreactor, which contained a 15.24 cm channel length, 2 mm width and various depths of 1 mm, 2 mm, 5

mm and 10 mm. A top block of polycarbonate was used, alongside a nylon bottom block. Such a parallel composition increased the active surface area beyond those of typical microreactors, resulting in an effective distribution of the catalyst. When a standardised catalyst of sodium alkoxide was utilised, the slit-channel microreactor showed increased effectiveness in producing biodiesel than a typical batch reactor.

A new investigation by Avellaneda and Salvado²⁶⁹ produced biodiesel from waste oil, *via* the catalyst NaOH. A helicoidal reactor was utilised, comprising two initial separate flow channels made of 3.175 mm 316 stainless steel pipe, with 0.216 cm I.D. These channels were joined *via* a T-device in the Caterpillar Micro Mixer, version 1.2 Sizes R600/12 and R1200/8, produced by IMM in Mainz, Germany. A following mixing element was formed from a single helicoidal pipe with 6 mm I.D., containing multiple helices of varying length. After 13 minutes, a FAME production of 89% was achieved, whereas a standard batch production method took 75 min to achieve equal FAME production.

1.5.1.3 Microreactors utilising membranes

A novel biocatalytic membrane microreactor was created by Achmadin *et al.*²⁷⁰ to aid triolein's transesterification by methanol. The BMM was based on an irregular PES 300 membrane created by Millipore Inc., based in Massachusetts, USA. The BMM was 280 μm thick, 63.5 mm in diameter and had a 300 kDa nominal molecular weight limit. A methanol-triolein mixture was diffused through the membrane, resulting in the membrane apertures forming microreactors where the reaction of the methanol and triolein ensued. After 19 minutes and at 35 $^{\circ}$ C, the yield of biodiesel was 80%.

1.5.2 Additional variables impacting microreactor biodiesel production

A number of significant variables affect the production of biodiesel in microreactors, including the dimensions of the microtubes, residence time, temperature of the reaction, as well as the method for mixing.

1.5.2.1 Microchannel dimensions

A variable which clearly has a significant impact on microreactor effectiveness is the dimensions of the microchannel, which can influence the degree to which the alcohol and fat mix.²⁷¹ Through the use of a capillary microreactor where inner diameter 0.25 mm, with a residence time of 6 min, KOH concentration of 1 wt % and a 6: 1 methanol to oil molar ratio, biodiesel production of 95% was achievable.²⁵⁹

This was much greater than with a capillary microreactor where inner diameter 0.53 mm. Similar results were obtained when zigzag microchannel reactors were utilised, when sodium hydroxide was used as the catalyst and the dimensions of the tubes were 240 and 900 μm respectively.²⁶⁵

In a consideration of the synthesis of biodiesel from soybean oil in a slit-channel reactor, it has been shown that the rate of production rises significantly when channel size is above 1 mm, in a comparison of channel 15.24 cm in length, 2 mm in width and varying depths of 1 mm, 2 mm, 5 mm and 10 mm.²⁶⁸ After all, there was nominal difference in yield rates between the channel depths of 5 mm and 10 mm, as a result of various factors. This includes the generally small diffusion space, rapid and effective heat diffusion and weight transmission, as well as large surface-to-volume ratios involved in microchannel mixing. When a microchannel decreases in dimension, greater production of biodiesel can be achieved. Nevertheless, this corresponds to a large decrease in pressure the smaller the microchannels are, which can lead to greater production problems and financial impact. One possible remedy is to insert Dixon rings ('made of a stainless steel wire mesh which provides a large surface area in a small volume') in to larger tubes,²⁶⁷ minimising the effect in pressure and maintaining greater FAME production rates over a briefer duration of time.

1.5.2.2 Residence time

A major benefit to producing biodiesel through microreactors is the diminished residence time compared to standard batch reactors, as much as 10 to 100 times quicker.²⁶⁴

Typically, as residence time is lengthened in capillary and microstructure reactors, the production of FAME raises significantly. Nevertheless, residence time can vary according to the sort of microreactor utilised. The vast array required for a large FAME production using the majority of capillary reactors is more prolonged than that necessary for microstructure reactors. When a prime reaction environment is ensured, a brief residence time between 17- 28 s is often sufficient to result in FAME production greater than 99%.^{261, 263}

Sun *et al.*²⁵⁹ provided an in-depth investigation into the impact of residence time on FAME production. Aiming to produce biodiesel from a ready-made mixture of methanol, rapeseed oil and catalyst KOH at 1 wt %, they utilised a capillary reactor with 0.25 mm I.D. At a temperature of 60° C and ratio of methanol to rapeseed oil of 6:1, an initial rise in FAME production was observed when residence time was increased, standing at 92.5% and 99.4% at 3.68 min and 5.89 min respectively. However, beyond this removal time the FAME production diminished to around 92%. Therefore, it can be observed that, in a capillary microreactor, having an extended residence time can have a detrimental impact on FAME yield rates.

1.5.2.3 Temperature of the reaction

A vast array of temperatures can be used to undertake the transesterification of methanol and triglyceride in batch reactors. With regard to capillary microreactors, the temperature of the reaction usually has a minor impact on FAME production, in comparison to the three other variables of concentration of KOH, residence time and the ratio of oil to methanol.²⁵⁹ When the temperature rises to 60° C from an initial base of 30° C, it has been observed that FAME production raised from 96% to greater than 99%. At 70° C, there

was a minor fall in FAME production. The explanation for why there is a reduction in FAME production when the boiling temperature of methanol is exceeded might be due to the alteration of flow in the microreactor from slug flow to bubble, while saponification of the glycerides production is increased due to the action of the KOH catalyst. When Guan *et al.*²⁶⁰ utilised a stainless steel microtube reactor with 0.8 mm I.D., at a temperature of 60°C for the synthesis of biodiesel from methanol and sunflower oil, they observed that the raised temperature also raised the synthesis rate.

1.5.2.4 Method of Mixing

The method of mixing in a microreactor is a crucial factor in the rate of mass transfer, therefore it can have an impact on the synthesis speed and reactions results. A slug flow often results in capillary reactors, as a result of the large interfacial pressures resulting at the barrier between the methanol and oil liquid phases. As the production of biodiesel progresses in the microreactor, there is no change observed in this slug flow.²⁵⁹

As the synthesis of biodiesel progresses, the result is an almost-homogenous one phase flow²⁶⁰, due to the aggregation of the droplets, a decrease in the volume of the methanol phase, as well as growing existence of FAME in the microreactor. Slug flow is also apparent at the T-mixer and J-mixer exits. Nevertheless, when RIMM and SIMM-V2 micromixers were used to syntheses biodiesel from methanol and cottonseed oil, slug flow containing methanol precipitate with 50 to 500 µm diameter were observed at the micromixer exits, deep in the oil phase.²⁶⁷

1.5.3 Catalysts for microreactor biodiesel synthesis

While catalysts are not strictly necessary for the transesterification of an oil by alcohol, they do serve to reduce the duration of residence time, the temperature requirements as well as necessary pressure.²⁷² Consequently, either a lipase catalysts, acid catalysts or base catalyst is often selected to obtain a high production rate of biodiesel with mild reaction conditions. Acid catalysts have the disadvantage of requiring slightly more

particular reaction conditions for optimum effectiveness, as well as a longer reaction duration, unlike an alkaline catalyst. However, if reaction conditions are present where this is a greater amount of free fatty acid, alkaline catalysts are not convenient.²⁷³ In practice and commercially, both alkaline and acidic conventional catalysts are utilised, whereas the heterogeneous catalysts still largely in the testing stages.

1.5.3.1 Homogeneous catalysts

The homogenous alkaline catalysts used for biodiesel production are alkoxides, organic amines, carbonates, guanidine compounds and alkaline metal hydroxides. The homogenous acid catalysts are commonly phosphoric acid, benzene sulfuric acid, sulfuric acid and dihydrochloride, to name a few.²⁷⁴ Due to their ease of use and robust catalytic properties, many of these catalysts are applied for microreactor biodiesel production.

1.5.3.2 Heterogeneous catalysts

While homogeneous catalysts are effective, the development of heterogeneous catalysts has been pursued, due to the possibility of having a more cost-effective, easier refinement procedure, reduced water pollution, alongside diminished energy and resource expenditure. In general, this will result in a procedure with reduced environmental impact.²⁷⁵

Nevertheless, the majority of heterogeneous catalysts remain in the testing stages. One successfully developed and marketed catalyst was created by the Institute Français du Pétrole (IFP), which was created through the Esterfi p-H technology. Production started in 2006, with a current production rate of 160,000 tonnes per year. However, its use in microreactors is a rare occurrence.²⁷⁶ Achmadin *et al.*²⁷⁰ developed a technique whereby immobilised lipase was contained within the pores of an asymmetric poly(ethersulfone) membrane, thereby acting as a microreactor in the process of triolein transesterification by methanol. After twelve days of production without halt, there was no diminishment of the reaction process.

The use of lipase catalysts in the synthesis of biodiesel is commonly advocated, due to the normal reaction conditions under which it can operate, as well as its environmentally friendly characteristics.²⁷⁷ Furthermore, the mass-production of lipase catalysts is becoming increasingly viable, with the advent of advanced growth and gene-modification technologies.²⁷⁸

With regard to enzyme catalysis of biological fats' transesterification by alcohol, the prospects for using lipase as a primary catalyst are generally favourable. This is due to the reduction in water effluent, absence of side reactions, easy to separate the products, simple glycerol recovery.²⁷⁹ Long chain fatty alcohol is very amenable to the application of a lipase catalyst, which acts with reduced efficiency on short chain fatty alcohols. Extreme conditions are not typically modelled for lipase catalyst reactions, as they are unnecessary for their effective use. However, enzyme catalysts are more costly to produce, while the ability to recycle them is diminished, despite the need for production periods of significant duration.²⁸⁰

1.5.4 Catalytic mechanism of *Candida antarctica* lipase (CAL) for hydrolysis and transesterification

The mechanism of a heterogeneous transesterification is same as the homogeneous process, the organic base immobilised on the surface of the silica converts the alcohol into an alkoxide, which, in turn, will react with the triglyceride as shown in Figure 1-18

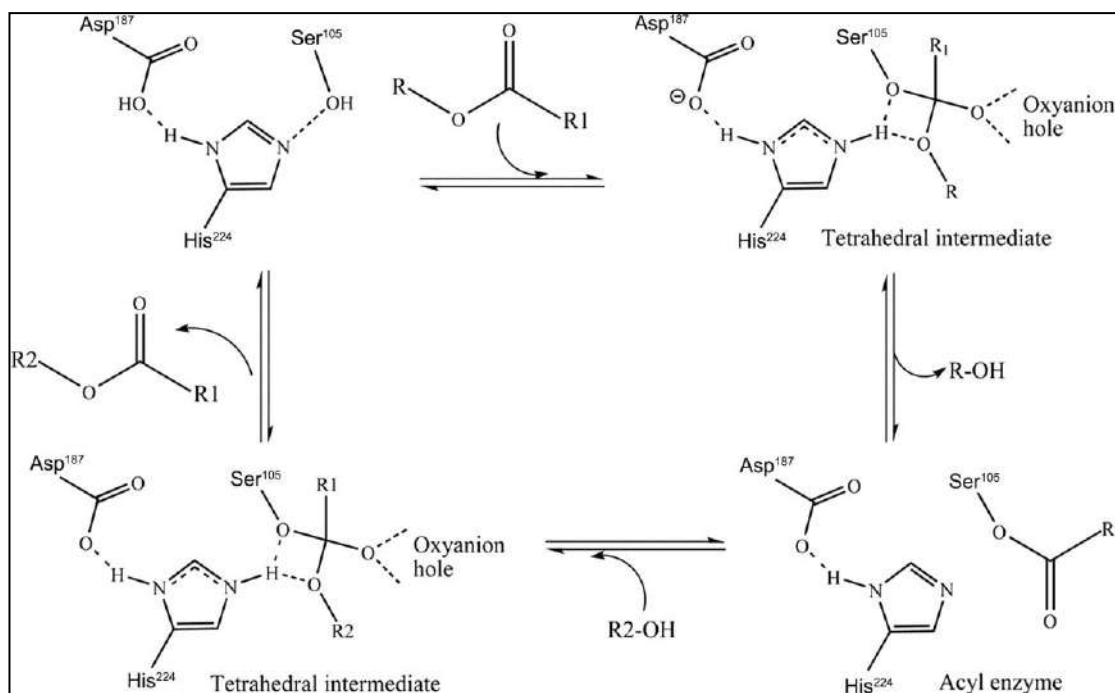


Figure 1-18. Catalytic mechanism of *Candida antarctica* lipase (CALB) for hydrolysis or transesterification.²⁸¹

The CAL enzyme displays an identical reaction mechanism to the serine proteases with catalytic triad serine (Ser105), histidine (His224), and aspartic acid (Asp187), and an oxyanion hole threonine (Thr40) with glutamin (Gln106).

The reaction mechanism is illustrated in Figure 1-18, provides an indication of the nature of the reaction mechanism by displaying a transesterification reaction. The active site is subject to binding by a carboxylic ester and, following this, the carbonyl carbon of the ester is subject to attack by the catalytic Ser105 (nucleophile). This takes place *via* the TS1 and then attack is supported by His224 insofar as it serves as a general base and, subsequently, accepts a proton from Ser105.

Over the course of the attack, the carbonyl bond transforms into a single bond while the carbonyl oxygen transforms into an oxyanion and forms three hydrogen bonds with the oxyanion hole (two to Thr40 and one to Gln106). Product 1, which is the alcohol, exist the active site and, following this, acyl enzyme is generated. Substrate 2, which is a

nucleophile, carries out a novel nucleophilic attack on the carbonyl carbon of the acyl enzyme proceeding through a second transition state (TS2), thereby generating the transacylation product (product 2). As a result of this, product 2 is emitted and the free enzyme regenerates.

1.6 Catalysis by gold

Gold (Au) has the atomic number 79 with atomic configuration [Xe] 4f¹⁴5d¹⁰6s¹. Amongst the metallic elements, gold is the most electronegative; it is also the least reactive metal conferring it with extreme resistance to corrosion and oxidation. Gold will dissolve in hydrochloric acid only in the presence of a powerful oxidising agent such as nitric acid (aqua regia) and as a bulk material does not react with other electronegative elements, such as oxygen and sulfur.^{282, 283}

The oxidation states for gold range from +1 to +3, but Au(I) and Au(III) predominate (the +5 state is only observed in (AuF⁶⁻). Gold, copper and silver, as noble metals, have fully occupied d-bands. However, in contrast to gold, copper and silver have low ionisation potentials and can lose electrons. This confers catalytic capability as demonstrated by the industrial use of copper and silver to synthesise respectively methanol and ethylene oxide.^{284, 285}

Gold, on the other hand, has high ionisation potential and accordingly, a low attraction to other elements. Early surface science and density functional calculation demonstrated this quality. At temperatures below 200° C, no dissociative adsorption of O₂ and H₂ occurs. This indicates that gold should be catalytically inactive in oxidation and hydrogenation reactions.^{286, 287}

Copper and silver have been employed in a number of large scale processes. Furthermore, platinum and palladium are noble metals which are often used as catalysts. Gold is the newcomer as it was only during the 1980s that it began to receive attention from the

catalysis research community.²⁸⁸ Since then, the number of industrial and academic applications using gold has risen. Material science, medicine, heterogeneous and homogeneous catalysis have benefitted from the attributes of gold.²⁸⁹

1.6.1 History of gold nanoparticles

The appeal of gold has spanned millennia. Even Stone Age people appreciated its aesthetic splendour and corrosion resistant qualities. Gold has attracted great value, becoming currency, and the gold standard has underpinned many monetary systems.²⁹⁰

The extraction of gold is thought to have begun around the 5th millennium B.C. near Varis (Bulgaria). The remarkable golden death mask of Tutankhamen manufactured around 1300 B.C. is testament to the use of gold. Soluble gold, appeared in China and Egypt in about the 4th century B.C. The earliest evidence of gold nanoparticles being used is the dichroic glass of the Lycurgus cup which dates from A.D. 4th century. The unique cup changes colour from green to red depending on whether the light is reflected or transmitted.²⁹¹

In spite of the long history of gold and people's fascination with it, its inert nature led it to be overlooked in terms of understanding and developing its chemistry, which was limited to its concentration, recovery and purification. The chemistry of gold was initiated by Michael Faraday in 1857. In a two-phase reaction, he used phosphorus in carbon sulphide (CS_2) to reduce an aqueous solution of chloroaurate (AuCl_4^-). The result was formation of a deep-red solution of nanoparticles.²⁹² Faraday also scrutinised the optical properties of a thin film that had been prepared from dried colloidal solutions. Furthermore, he noted that, upon mechanical compression, the films reversibly changed colour.²⁹³

By preparing an Au₅₅ cluster ([Au₅₅(PPh₃)₁₂Cl₆]), Schmid, in 1981, created the synthesis of phosphine-stabilised gold clusters with a particle diameter average of 1.4 nm. Through the 20th century, several gold nanoparticle synthesis methods were described.^{294, 295}

But it was not until the last decade of the century that a biphasic protocol was devised and widely adopted. Expanding upon Faraday's original method of manufacturing gold nanoparticles in biphasic and monophosphine solutions, Brust and Schiffrin used thiols as stabilising agents leading to the Brust-Schiffrin biphasic method.^{296, 297} Other methods to synthesise gold nanoparticles include the popular Turkevich method. This was popular as the method used citrate ions as the capping agents to produce nanoparticles in the 10–20 nm size range.²⁹⁸ Through using a dendrimer as the template and stabiliser, Zhao *et al.*²⁹⁹ have broadened the process of synthesising gold nanoparticles.

1.6.2 Immobilisation of Au-NPs on solid supports

The principal purpose of the support is to prevent the gold nanoparticles from agglomerating and coalescing during catalysis.³⁰⁰ As a result, substantial effort has been invested in developing appropriate methods of synthesising gold supported catalysts. The supports are typically metal oxides, such as CeO₂, Co₂O₃, Fe₂O₃, TiO₂ and ZrO₂, (M41S), Al₂O₃, MgO and SiO₂.³⁰¹

Silica is a superior material for supports and its inert nature makes it a suitable support. The minimal interaction between the support and the metal facilitates the investigation of the effect of the metal. The exceptional properties of silica support include a high surface area, good pore volume, thermal stability and appropriate mechanical features. These properties are achieved through the high dispersion of gold nanoparticles on silica. Silica supports also promote the access of substrates to the active sites; therefore, gold catalysts may demonstrate enhanced activity when incorporated with silica.

Floris *et al.*³⁰² reported using gold nanoparticle-modified polymer monoliths for flow-through catalytic reactions to reduce hexacyanoferrate to assess the activity of the catalyst. The catalytic activity of gold nanoparticles immobilised on polymer monoliths were superior, with 95% Fe(III) being reduced to Fe(II).

Hussain *et al.*³⁰³ studied the catalytic reduction N₂O by monolith-supported rhodium catalysts. A mesoporous powder silica catalyst was modified after adding salt by including aluminium. The N₂O decomposition reaction was examined revealing the inherent qualities of the material. Compared to non-modified silica catalysts, this material demonstrated superior catalytic activity. Monolith catalysts show an exceptional nature for selective oxidation. A continuous flow pharmaceutical fixed-bed reactor was created by Badran *et al.*³⁰⁴ where the researchers used catalytic monoliths to selectively oxidise benzyl alcohol to benzaldehyde with Pt impregnated. The study is a landmark development in carbon monoliths, which could be extended to industrial settings.

1.6.3 Application of supported Au-NPs in catalysis

The unique properties and multiple surface functionality of gold nanoparticles are particularly suited to bionanotechnology and have been used extensively in this area. Gold nanoparticle functionalisation delivers an adaptable platform for nanobiological assembly of antibodies,³⁰⁵ oligonucleotides³⁰⁶ and proteins.³⁰⁷ Gold nanoparticle bioconjugates also offer promise in the design of new biomaterials suitable to investigate biological systems.³⁰⁸

Heterogeneous catalysis relies on the adsorption of reacting molecules to a catalytically active solid surface. As chemical bonds are broken and formed on the catalyst's surface, the products are discharged into the gas or liquid phase. As highlighted earlier, the nature of the support has an essential role in determining the interaction between the support and gold nanoparticles. This relationship stresses the need for selectivity in the choice of

support to be one that promotes stability and efficiency of gold nanoparticle catalysts. Several studies of gold nanoparticles being used for organic reactions are available. For instance, the very effective oxidation of cyclohexane over a calcined gold MCM-41 catalyst has been described by Lit *et al.*³⁰⁹ The environmentally friendly protocol used oxygen as the oxidant in a solvent-free system. Five different gold/MCM-41 catalysts, labelled A-E, were formulated using different gold load. The gold/MCM-41 was distinguished using diffuse reflectance UV-visible (DRUV-vis), inductively coupled plasma optical emission spectrometry (ICP-OES), N₂ adsorption/desorption, X-ray diffraction (XRD) and X-ray photoelectron spectroscopy (XPS). The BET surface area ranged 624 – 839 m²g⁻¹ and the pore diameter was 3.6 – 5.7 nm. From the DRUV-vis spectrum of gold/MCM-41, the surface plasmon vibration band at $\lambda = 500 - 600$ nm was in the visible region of the electromagnetic spectrum. The cyclohexane oxidation selectivity was 76 % while the conversion was 16 %.

The high surface area of the gold nanoparticles can accommodate many multifunctional molecules such as drugs³¹⁰ and targeting agents,³¹¹ making gold nanoparticles practical platforms for therapeutic agents. Tsukuda *et al.*³¹² conducted a comparable study into the aerobic oxidation of cyclohexane. Gold clusters (n=10, 18, 25, 39) immobilised on hydroxyapatite (HAP) were used to oxidize the cyclohexane to cyclohexanone and cyclohexanol. High angle annular dark field-scanning transmission electron microscopy (HAADF-STEM) and transmission electron microscopy (TEM) were used to analyse the average diameter of the gold clusters, which were in the range of 1.0–1.1 nm. The diameter was independent of the size of the glutathionate-capped gold (Au_M(SG)_M) precursor. No cluster aggregation was revealed by TEM imaging. To evaluate the effect of cluster size on catalytic activity, aerobic oxidation of cyclohexane was conducted in O₂ atmosphere (1 MPa) at 150° C. A comparison of activity was made between Au_N/HAP (n = 10, 18, 25, 39) and larger gold clusters with an average diameter of 1.4 nm. This

catalyst was designated Au~85/HAP. After four hours, the conversion of cyclohexane had increased from 11.6% to 14.9% where n had increased from 10 to 39. For $n \sim 85$, there was a decrease to 6.7%. There was a concomitant increase in frequency and cluster size, peaking at $18500 \text{ h}^{-1}/\text{Au atom}$.

The study by Patil *et al.*³¹³ describes the use of gold nanoparticles deposited on BaO, CaO, MgO and SrO to catalyse the selective epoxidation of styrene with *tert*-butyl hydroperoxide. The deposition-precipitation method was used to prepare the catalysts, with urea and NaOH being the precipitating agents. Catalysts that had been prepared with urea had a higher gold loading and were smaller. The styrene conversion was greater than 53% and selectivity towards styrene oxide ranged from 45 – 60%.

1.6.4 Synthesis of gold nanoparticles

In recent decades, an assortment of solution-based methods have been devised to control the size,³¹⁴ shape,³¹⁵ and surface functionality.^{291, 316, 317} In 1951, Turkevich *et al.*²⁹⁸ created a method to synthesise gold nanoparticles by adding citric acid (that acts as the reducing and stabilising agent) to hydrogen tetrachloraurate (HAuCl_4) in an aqueous solution. The protocol was refined by Frens to control particle size and was achieved by changing the ratio of gold-to-citrate.³¹⁸

This method has since been used extensively to prepare dilute solutions of acceptably stable spherical gold nanoparticles. Typically, the diameter of these gold nanoparticles is 10–20 nm, but the size can be increased nanoparticles of 100 nm. During the functionalisation process with a thiolate surfactant, gold nanoparticles stabilised with citrate can irreversibly aggregate. To overcome this drawback, a number of approaches have been developed, including using Tween 20, a surfactant that is applied prior to modification, preventing gold nanoparticles from clumping together.³¹⁹ Thiocetic acid (TA) can also be applied as an intermediate in a two-step functionalisation.³²⁰

A large-scale production challenge has been the need for high dilution. A significant step towards resolving this problem was made in 1994 by Brust and Schriffin, when they created organic soluble alkanethiol-stabilised gold nanoparticles by employing a biphasic reduction procedure that used a sodium borohydride (NaBH_4) reducing agent and tetraoctylammonium bromide (TOAB) phase transfer reagent.³²¹ The results of this method are low dispersity (1.5 to 5 nm) gold nanoparticles, with the variance depending upon reaction conditions such as the ratio of gold-to-thiol, reaction temperature and reduction rate.³²²

The synergetic effect of gold-thiol interactions and van der Waals attractions of the neighbouring ligands, confers alkanethiol-protected gold nanoparticles with greater stability compared to most other gold nanoparticles.³²³ These nanoparticles are superbly suited to reuse, as they can be completely dried and redispersed in solution without aggregating.

1.6.5 Characterisation of Gold nanoparticles

1.6.5.1 X-ray powder Diffraction (P-XRD) Analysis

Bulk phase detection, monitoring of bulk transformation kinetics, and particle size measurement can all be effectively conducted with the help of the X-ray diffraction (XRD) method. P-XRD is based on a collimated X-ray beam of wavelength ranging between 0.5 and 2.5 Å, which is incident on a powder specimen and its diffraction occurs through crystalline phases in keeping with Bragg's law in Equation 1-11:

$$n\lambda = 2d \sin \theta \quad \text{Equation 1-11}$$

Where: λ is a wavelength of the radiation, n is an integer referring to the order of reflection, d and θ representing the lattice spacing between crystalline phase atoms and the diffraction angle, respectively). The diffraction angle 2θ and the orientation of the specimen dictate how intense the diffracted X-rays are. The crystalline phases and

structural attributes of the specimen can then be determined based on the obtained diffraction pattern.³²⁴

The determination of d-spacing, intensity and full width at half maximum (FWHM), obtained with the Scherrer in Equation 1-12, enabled the dimensions of the crystallites to be determined.³²⁵

$$\text{Crystallite size} = \frac{(K * \lambda)}{(FWHM * \cos \theta)} \quad \text{Equation 1-12}$$

Where: K and λ represent the Scherrer constant and the X-ray wavelength, respectively.³²⁵

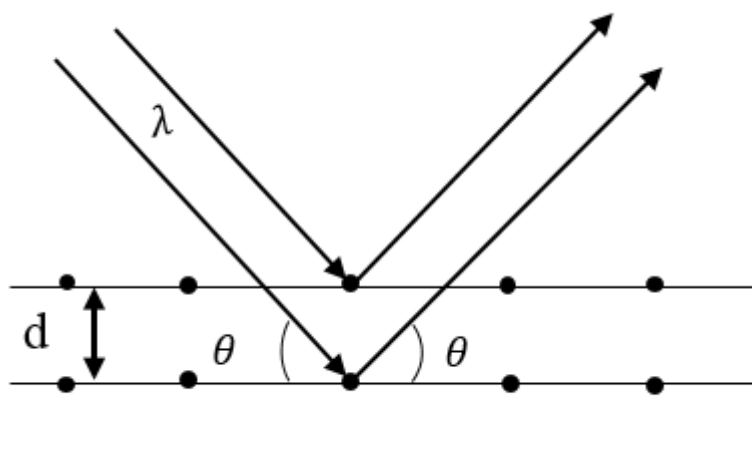


Figure 1-19. A schematic representation of Bragg's reflection from a crystal.

1.6.5.2 X-ray photoelectron spectra (XPS)

The surface analysis method of XPS plays a key role in catalysis, as it provides data related to element composition and oxidation status. X-ray irradiation of the sample surface is done in accordance with the photoelectric effect, followed by measurement of the photoelectron emission.³²⁶

Absorption of an energy photon ($h\nu$) by an atom determines the emission with kinetic energy (E_k) of a core or valence electron with binding energy (E_b) through Equation 1-13:

$$E_k = h\nu - E_b - \varphi \quad \text{Equation 1-13}$$

In the above equation, E_k and E_b respectively represent the kinetic energy of the photoelectron and the binding energy of the photoelectron in terms of the Fermi level sample, while h , ν and φ are Planck's constant, the exciting radiation frequency, and the work function of the spectrometer, respectively. In general, the XPS spectrum takes the form of a plot of photoelectron intensity against binding energy. The method has high surface specificity because the source of the electrons whose energies are subjected to XPS analysis is no deeper than 5 nm.³²⁷ The suitability of XPS for the analysis of sample composition, including peak area and photoemission cross-sections, arises from the fact that elements have fixed sets of binding energies, which also comprise chemical data (e.g., oxidation status), since the chemical state of the atom determines to some extent the core electrons' energy levels. Changes in the binding energies make it possible for XPS to provide data on an element's oxidation status and chemical medium. Usually, chemical changes are within the range 0-3 eV, with Al-K α (1486.6 eV) and Mg-K α (1253.6 eV) being the most widely used. These two changes are obtained from a conventional X-ray tube and there is a correlation between the peaks identified in the XPS spectra and the sample's bound core electrons. The amount of emitting atoms in the near-surface area determines peak intensity and the emitting atoms' oxidation status and local medium dictate the correct binding energy of every peak.^{328, 329}

1.6.5.3 Transmission Electron Microscopy (TEM)

The data derived from sample analysis with transmission electron microscopy (TEM) help shed light on such aspects as the size, shape, composition and crystal structure of the gold nanoparticles. Williams and Carter³³⁰ have provided a comprehensive overview of the concepts underpinning TEM and other related methods as well as the applications of these methods. Sample imaging at extremely small scales (\AA) is achieved by TEM with the help of accelerated electrons, which are emitted by an electron source and pass

through a vacuum within the column of the microscope. The electrons have a wavelength of 2.51×10^{-3} nm at a standard operating voltage of 200 kV. This wavelength reduces the resolution at the order of angstrom (10^{-10} m), since it is significantly lower compared to the visible light wavelength (400 nm). There are three distinct electron sources that can be employed by the electron microscope, and these are plain tungsten filament, tungsten filament with a LaB₆ crystal tip, and field emission gun. The attained brightness level differs according to which of these sources is employed, with the tungsten filament and field emission producing minimal and maximal brightness, respectively. To trigger electron excitation, the filament is kept in a wehnelt cap without a charge (0 kV) and vacuum-heated. Subsequently, the excited released electrons are guided *via* the anode which is positively charged (typically 200 kV) and therefore situated under the wehnelt cap. A TEM column is illustrated in simplified form in Figure 1-20. During its movement down the column, the electron beam goes through several lenses and apertures. The condenser lens is the first lens that the beam passes through which focuses it on the sample. The condenser apertures are situated beneath the lens, and, by adjusting their sizes, sample contrast variation can be achieved. The objective lens refocuses the beam that has gone through the sample, thus making the diffraction plane visible. Objective aperture adjustment enables enhancement of the sample contrast and viewing of the dark field imaging. The projector lens is the last lens through which the beam passes and projects the image on the viewing screen. The quality of the image is determined by how dense the sample material is. After it is enlarged by a series of electromagnetic lenses, the image is photographically documented either on film or in digital format.

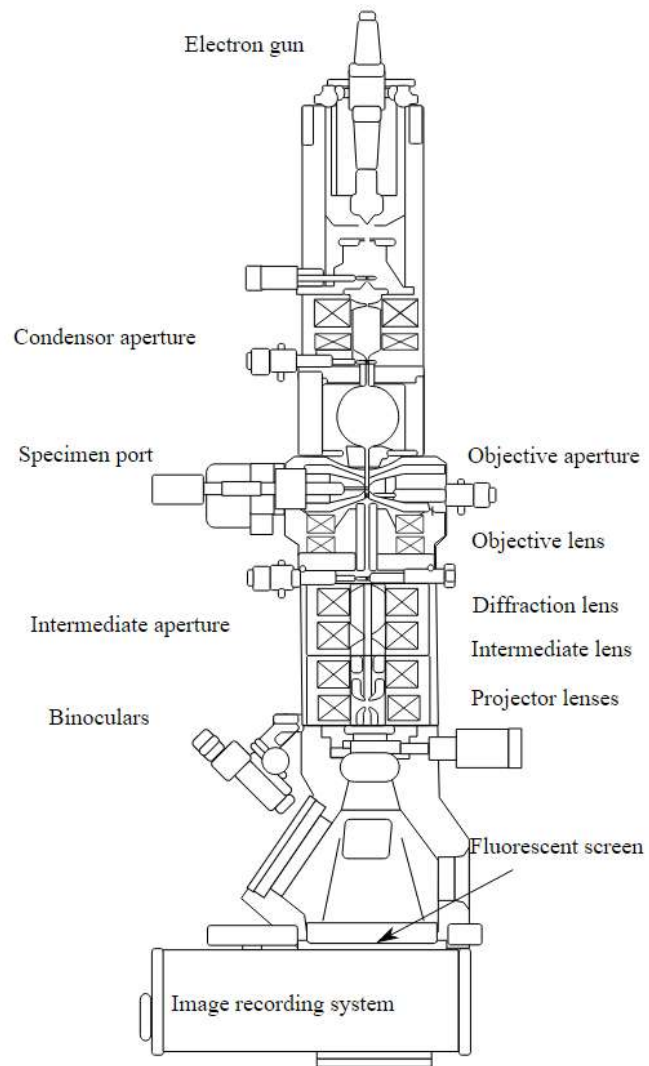


Figure 1-20. Simplified representation of a basic transmission electron microscopy (TEM).³³⁰

1.6.5.4 Inductively Coupled Plasma-Optical Emission Spectroscopy (ICP-OES)

The elements of a sample inserted in an ICP source emit light which can be measured with the accurate tool of elemental analysis ICP-OES, which can detect both metals and non-metals at minimal concentrations (ppm). Furthermore, compared to atomic absorption spectroscopy, this method is more useful because it can undertake the concomitant measurement of multiple elements. If the sample is in the solid state it is dissolved by, the process of wet digestion facilitating oxidation of the sample's organic elements or removal of any metals contained in inorganic matrices.³³¹ To achieve this, the solid sample is combined with a particular mixture of concentrated acid and the type of add mixtures employed depends on the constituent elements of the solid sample.³³¹

The most common add mixtures are nitric acid (HNO₃), hydrochloric acid (HCl), sulphuric acid (H₂SO₄), and phosphoric acid (H₃PO₄). Aside from wet digestion, sample preparation can be undertaken through other techniques as well, according to sample characteristics.³³¹ After sample preparation, the sample is introduced into the ICP (argon plasma, 8000-10000°C), by a solution nebulisation process. Once in the plasma the atoms are atomised and excited resulting in specific optical emissions at various wavelengths. Comparison of the measured intensities of emission with the intensities of standards of set concentration makes it possible to determine the sample's actual elemental concentration.³³²

1.6.6 Using Gold Nanoparticles as Catalysts for Selective Oxidation of Cyclohexene

Epoxidation of alkene is a reaction of prime importance to the fine chemical industry. Alkenes are frequently used as precursors in the synthesis of many products including epoxy resins, perfumes, pharmaceuticals and plasticisers.³³³⁻³³⁵ Epoxidation reactions have conventionally been performed using peracids, yet these are expensive, unsafe and generate considerable waste.³³⁵

Metal nanoparticles borne by oxide supports offer the chemical industry an environmentally friendlier alternative to the damaging traditional methods.²⁸² The incorporation of metal nanoparticles in monolithic structures in particular has received attention for its applications in chromatography,^{336, 337} metal adsorption for contaminant purification,³³⁸ C–C coupling reactions,³³⁹⁻³⁴¹ reduction of nitrophenols³⁴², low temperature CO oxidation reactions,³⁴³ selective oxidation reactions,²⁸² and hydrogen peroxide formation from O₂ and H₂.³⁴⁴ Selective oxidation reactions are of prime economic importance in a diverse range of applications from the production of fine chemicals and synthetic fibres to polymers and paints. In the case of oxidation, it has been reported that silica monoliths loaded with either Pt or Pd nanoparticles presented conversions 2.5 times higher in microreactors than when using powder catalysts. This shows that using microreactor technology for selective oxidation reactions enhances the catalytic ability of precious metal catalysts.³⁴³ A major challenge in all cases however is to evenly functionalize the catalytically active species along the length of the monolithic microreactor, which is key to maximising efficient reaction control.

Hughes *et al.*³⁴⁵ studied the epoxidation of cyclic alkenes by molecular oxygen and peroxide as catalysed by gold nanoparticles supported on graphite. They found that *cis*-cyclooctene could be epoxidised to cyclooctene epoxide with a selectivity of more than 80% under mild, solvent-free conditions. It was further demonstrated that, under mild reaction conditions, cyclohexane, cyclooctene, styrene and *trans*-stilbene could be oxidised to their corresponding epoxides. However, in the absence of the catalyst, some oxidation was detected but with low selectivity for the epoxide. High selectivity required a radical initiator, usually peroxide, though the reaction can occur in the absence of an initiator. Again, the catalyst could be reused.

A number of studies into the liquid-phase epoxidation of styrene by anhydrous *tert*-butyl hydroperoxide (TBHP) over various gold-bearing supports have been reported by Chowthary *et al.*^{313, 346} The researchers used anhydrous TBHP oxidant for the epoxidation of styrene over gold nanoparticles supported on BaO, CaO, MgO and SrO. All of the catalysts were active for styrene oxidation, producing a styrene conversion of 45% – 67%. Styrene oxide was found to be selectively favoured. Gold nanoparticles supported on MgO demonstrated superb reusability with a considerable improvement in selectivity and catalytic activity in epoxidising styrene.³¹³

1.7 Aims and objectives of the PhD project

This project aims to investigate chemical syntheses currently used in industry with a view to minimising their associated environmental impacts. The research described above details the innovations of solid catalysts and their relative activity; these are directly relevant to the chemical industry. In this thesis, the application of microreactor technology with immobilised catalysts was investigated to exploit the advantages of this technology to obtain the greater efficiency and enhanced chemical selectivity needed for fine chemical synthesis as compared to batch based techniques.

The following objectives were identified:

- To exploit the spatial and temporal characteristics of chemical microreactions by using monoliths.
- To prepare different silica-based monolith microreactors with different physical properties.
- To immobilize enzyme lipase on the monolith microreactors as heterogeneous catalysts through multipoint interactions between the surface of silica monolith and the lipase within an active conformation which in turn would augment the thermal and reactive stability considerably.
- To identify the effect of monolith microreactor properties on the activity of the immobilised lipase.
- To functionalise silica monolith microreactors with gold nanoparticles by two different methods:

A- Simple impregnation of gold nanoparticles into the monolith during the sol formation.

B- Tether thiol groups to the monolith's mesoporous silica structure using 3-(mercaptopropyl)trimethoxysilane, which allows the sulfur groups to act as anchors for the gold nanoparticles. The gold nanoparticles penetrate the monolith, becoming tethered to the thiol groups.

- To test the silica monolith microreactor methodology with model reactions.

1- Hydrolysis activity of 4-nitrophenyl butyrate is used as substrate is shown in Figure 1-21 to evaluate the performance of lipase both in free solution and immobilised lipase in a silica monolith, and utilised the water-decane biphasic system application within the hydrolysis reaction of 4-nitrophenyl butyrate to escalate the lipase interfacial activation. Also, to investigate the effect of the physical properties of the silica based monolith on the immobilized lipase activity.

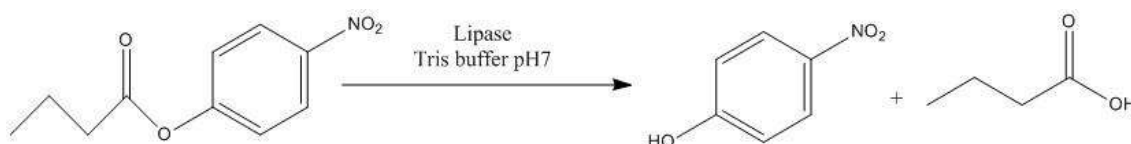


Figure 1-21. The proposed reaction scheme for hydrolysis reaction of 4-nitrophenyl butyrate to 4-nitrophenol

2- Biodiesel production through the transesterification reaction of tributyrin to yield methylbutyrate as shown in Figure 1-22 (This study investigates the efficacy of immobilised lipase silica monolith in effecting biodiesel production *via* catalysing the transesterification reaction of tributyl glycerate [tributyryn]. Tributyrin was selected as a vegetable oil triglyceride mimic since it is miscible with methanol and therefore simplifies the catalytic testing process). Also, optimize the reaction and study the effect of parameter such as molar ratio, temperature and the flow rate of the reaction.

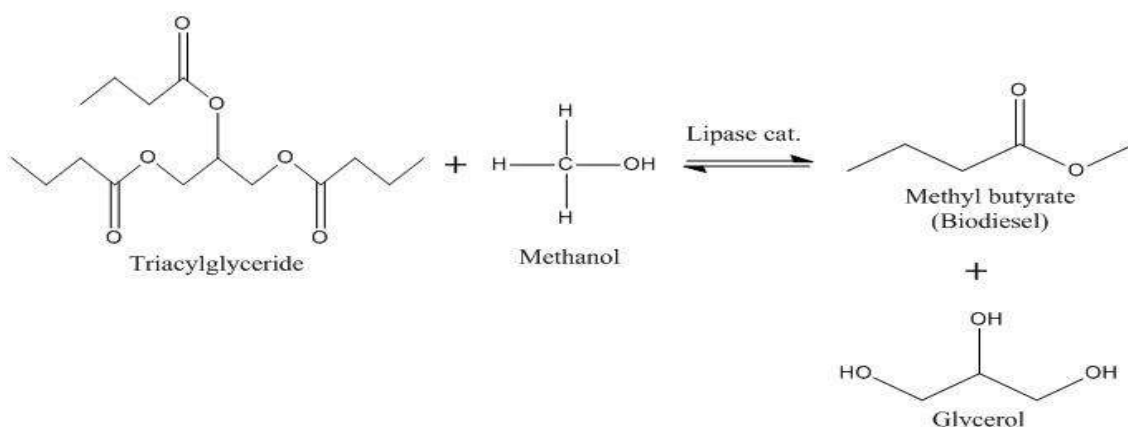


Figure 1-22. The proposed reaction scheme for the transesterification reaction of tributyrin with methanol.

3- Oxidation of cyclohexene through gold functionalised silica monolith microreactors is shown in Figure 1-23. Cyclohexene was applied as a model reaction in selective oxidation studied due to the volume of data that already exists in the literature, which allows for the appropriate choice of reaction condition. In this reaction, two liquid phases were employed: hydrogen peroxide (H_2O_2) and *tert*-butyl hydroperoxide (TBHP).

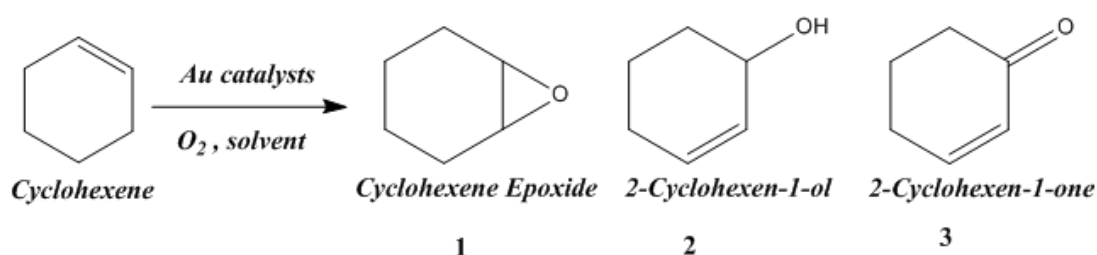


Figure 1-23. The proposed reaction scheme for the selective oxidation of cyclohexene.

1.8 Thesis structure

This thesis is divided into seven chapters. **Chapter 1**, the introduction, explains the background of the study, the literature review, the thesis structure and the research objectives. In **Chapter 2**, the characterisation methods and experimental part used in this thesis are discussed. In **Chapter 3**, using of lipase immobilized silica monolith microreactor for hydrolysis reaction was studied and the microreactor was evaluated kinetically and compared with the free lipase activity while, in **Chapter 4**, a lipase-immobilised silica monolith microreactor was used for biodiesel reactions where the reaction conditions were optimised to obtain the optimum catalytic activity of the lipase silica microreactor. In **Chapter 5**, gold introduced to the silica monolith microreactor which was then used to catalyse oxidation reactions. Finally, **Chapter 6**, summarises and conclude the outcome of this thesis, and **Chapter 7**, offers recommendations for future work.

Chapter 2. Experimental

The main goal of this chapter is to provide the experimental details for the work described in the thesis and in particular to explain the methodology followed to prepare the silica monolith and to incorporate catalysts within. The characterisation techniques applied to evaluate the silica microreactors, including their morphology, porosity, and chemical composition, are also described.

2.1 Chemicals

The solvents and reagents used were purchased from the suppliers as shown in Table 2-1. All chemicals were of analytical grade and used as supplied, without any further purification.

Table 2-1 . Chemicals, reagents and solvents used in the experiment

Chemical	Supplier	Purity/grade
Silica monolith synthesis		
Tetraethyl orthosilicate (TEOS)	Fisher Scientific, Loughborough, UK	99%
Tetramethyl orthosilicate (TMOS)	Fisher Scientific, Loughborough, UK	99%
Acetic acid	Sigma-Aldrich, Poole, UK	≥99%
Nitric acid 70%	Fisher Scientific, Loughborough, UK	-
Ammonia solution	Fisher Scientific, Loughborough	Analytical grade
Hydrochloric acid S.G 1.18 (HCl) 37%	Fisher Scientific, Loughborough	-

Polyethylene oxide MW 100,000 Da	Sigma-Aldrich, Poole, UK	-
Polyethylene oxide MW 200,000 Da	Sigma-Aldrich, Poole, UK	-
Assay of free and immobilized lipase		
Candida antarctica lipase (CAL)	Sigma-Aldrich, Poole, UK	-
Decane	Sigma-Aldrich, Poole, UK	99%
4-nitrophenyl butyrate (4-NPB)	Sigma-Aldrich, Poole, UK	98%
4-nitrophenol (4-NP)	Sigma-Aldrich, Poole, UK	98%
Tris(hydroxymethyl)aminomethane $\text{NH}_2\text{C}(\text{CH}_2\text{OH})_3$	Sigma-Aldrich, Poole, UK	$\geq 99.8\%$
glass capillaries (0.6 /0.05 mm ID and 25 mm length)	Brand GMBH (Germany)	-
Catalytic transesterification		
Tributylin	Sigma-Aldrich, Poole, UK	97%
Methanol	Fisher Scientific, Loughborough, UK	HPLC grade
Methyl butyrate	Sigma-Aldrich, Poole, UK	99%
Selective oxidation of cyclohexene		
$\text{HAuCl}_4 \cdot 3\text{H}_2\text{O}$	Alfa Aesar	99.99%
Ethylene glycol	Fisher Scientific, Loughborough	> 99%

Polyvinylpyrrolidone MW 40,000	Alfa Aesar	-
(mercaptopropyl)trimethoxysilane (3-MPTES)	Sigma-Aldrich, Poole, UK	95%
Acetone	Fisher Scientific, Loughborough, UK	-
Acetonitrile	Fisher Scientific, Loughborough, UK	HPLC super gradient
1,2-Cyclohexanedione	Sigma-Aldrich, Poole, UK	97 %
Cyclohexene oxide	Sigma-Aldrich, Poole, UK	98%
2-Cyclohexen-1one	Sigma-Aldrich, Poole, UK	≥95%
2-Cyclohexen-1-ol	Sigma-Aldrich, Poole, UK	95%
Hydrogen peroxide 30% w/v (100 volumes), extra pure SLR	Fisher Scientific, Loughborough, UK	-
<i>tert</i> -Butyl hydroperoxide solution 5.0-6.0 M in decane	Sigma-Aldrich, Poole, UK	-
Cyclohexene	Sigma-Aldrich, Poole, UK	≥99%
Sodium borohydride	Sigma-Aldrich, Poole, UK	≥98.0%

2.2 General instrumentation and equipment

The instrumentation and equipment used for the experiments are listed in Table 2-2. The instrumental set-up and procedures are described in the subsequent sections.

Table 2-2 Instruments and materials used.

Instrument/material	Supplier
HPLC-UV system	PerkinElmer, California, USA
Scanning electron microscope (SEM)	Carl Zeiss Ltd. (Welwyn Garden City, UK)
BabyBee™ syringe drivers	Bioanalytical Systems Inc., (West Lafayette, USA)
Model 7971 column heater	(Jones Chromatography Ltd)
Chemyx Fusion 100 Syringe Pump	KR Analytical Ltd (Sandbach ,Cheshire)
BIO Wide Pore C18 column 5 μ m, 15 cm \times 2.1 mm	Phenomenex (United Kingdom, Queens Avenue, Hurdsfield Ind. Est).
Brunauer-Emmett-Teller (BET)	Micromeritics Ltd., Dunstable, UK
Hot plate-stirrer	VWR International, LLC, West Chester, PA, USA
Straight connectors	kinesis, Cambridge, UK
Two-piece tight fitting	kinesis, Cambridge, UK
Cuvettes Polystyrol/Polystyrene 10 x 4 x 45 mm	Sarstedt AG and Co , GERMANY
Polytetrafluoroethylene (PTFE)	Adtech Polymer Engineering Ltd., Stroud, UK
Oven	Scientific Laboratory Supplies Ltd, UK

Energy-dispersive X-ray spectroscopy system (EDX)	INCA 350, Oxford Instruments, Abingdon, UK
pH meter	Fisherman Hydrus 300, Thermo Orion, USA
Micropipettes	Eppendorf, UK
Furnace	EF3, Vecstar Furnaces, Chesterfield, UK
Disposable plastic syringe	Scientific Laboratory (Nottingham, UK)
Straight/standard bore 1.5 mm	Kinesis (Cambs, UK)
UVmini-1240 SHIMADZU CORPORATION	Kyoto, Japan

2.3 Silica monolith synthesis

The monolith design was based upon existing designs and dimensions to ensure good thermal control.^{108, 347} The fabrication of mesoporous silica monoliths were prepared by a modification of the method and the experimental conditions established by Nakanishi.³⁴⁸

The reagents of the silica-based monolith were mixed inside a 50 mL polyethylene centrifuge tube. The desired amount of poly(ethylene oxide) (MW 200,000, 0.305 g) was added to a solution of acetic acid 0.02 M, 4 mL, and stirred for one hour (with a magnetic stirrer at 200 rpm) in an ice bath until fully homogeneous to promote the sol gel reaction. The stirring was increased slightly to 300 rpm and then 2 mL of tetramethylorthosilicate (TMOS) was added to the transparent solution and was left for ~60 minutes until a homogenous solution consistency was achieved. While the mixture was stirring, a 1 mL plastic mould (length 6 cm, internal diameter 0.45 cm) was prepared to carry out gelation. The thin end of a moulds were sealed with PTFE tape by winding them tightly until no

leaks were present. The taped end of the tube was then inserted into a red, rubber adapter, which stood up straight. The whole volume of the solution was estimated to fill 4 moulds. Upon achieving a homogenous state, the mixture was left to settle for ~2 minutes to get rid of any bubbles that were formation during mixing. One mL of the solution was subsequently poured by pipette slowly down the sides of each prepared mould and shaken carefully but firmly to get rid of any air bubbles in the tapered end of the mould, ensuring that the remaining solution was left in the ice. Small lids were then placed on the open end of each tube, before placing all tubes upright in a glass beaker, packed with blue roll to prevent movement and left to age for three days in an oven at 40°C. The white semi-solid gel monolith was removed from the mould and washed thoroughly with deionised water to remove any trace residues. The monoliths were then immersed in a conical flask containing ammonium hydroxide solution (1M). This solution was prepared by mixing 24 mL of water with 6 mL of NH_4OH (1M). The solution was heated to ~ 82 °C for 24 hours under reflux, to form a mesoporous network within the material (surface etching). The etching process leads to increase the surface area of the monolithic rods. This was followed by further washing silica rods with deionised water to remove residual ammonium hydroxide and the water was changed every two hours continuously until pH 7 was achieved. Then the rods were dried at 40 °C for one day to allow slow drying then moved to a 100°C oven for another 24 hours to ensure complete drying. The clean and dry monolithic rods were then calcined at 600°C for three hours under air flow to remove the remaining poly (ethylene oxide). Figure 2-1, shows the monolith preparation steps.

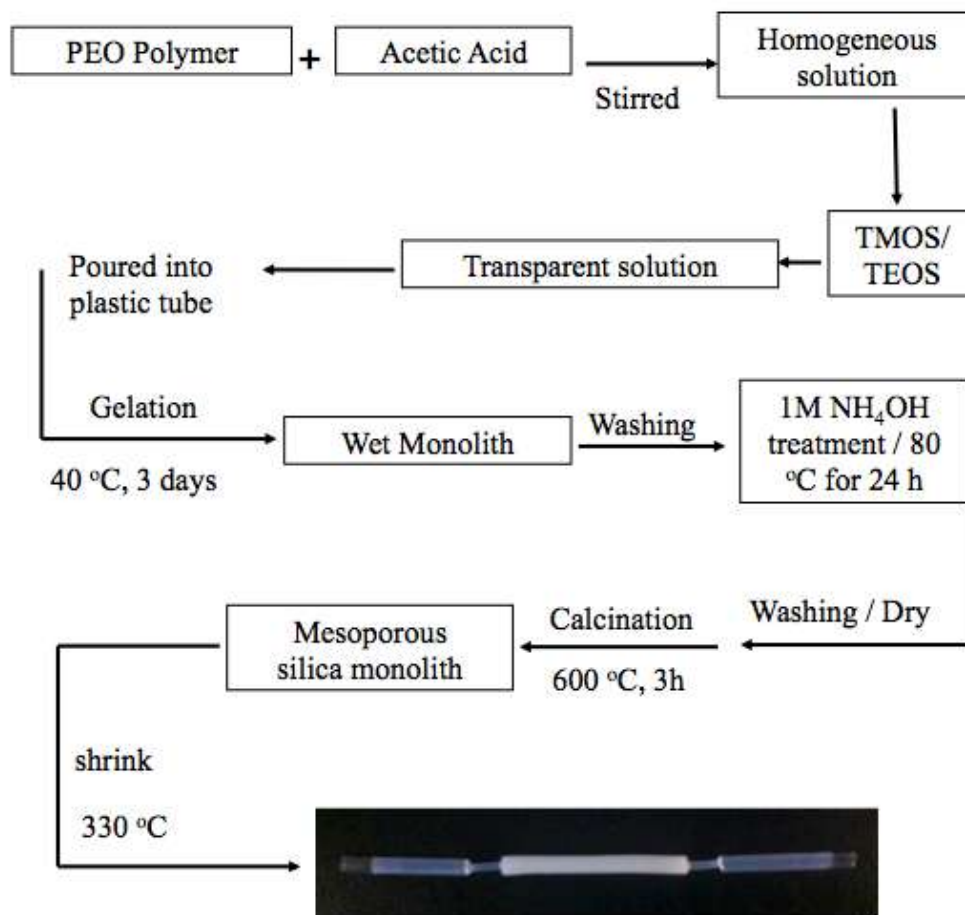


Figure 2-1. Schematic diagram showing the monolith preparation steps.

The desired application for these silica monoliths is as catalyst supports within continuous flow chemical reactors. For both this application and the fluid permeability measurements described here, it is essential they be mounted tightly with no leakage in a flow system. The following method was found to be effective. The silica rod was cut approximately to a 4 cm lengths, and linked to a borosilicate tubes (2.10 mm, i.d and o.d=3.90 mm) aligned inside the shrinkable tube to prevent any dead volume *via* polytetrafluoroethylene (PTFE), heat shrinkable tube ratio of 4:1, internal diameter shrinks from 3.2 mm to 0.94 mm. This was heated in an oven at 350 °C for one hour to seal the tube and encapsulate the monolithic rod. Finally, the monolithic silica rods were ready for either surface modification or for flow through use as shown in Figure 2-2 and then the syringe pump was connected to the tubing using a two-piece finger-tight fitting.

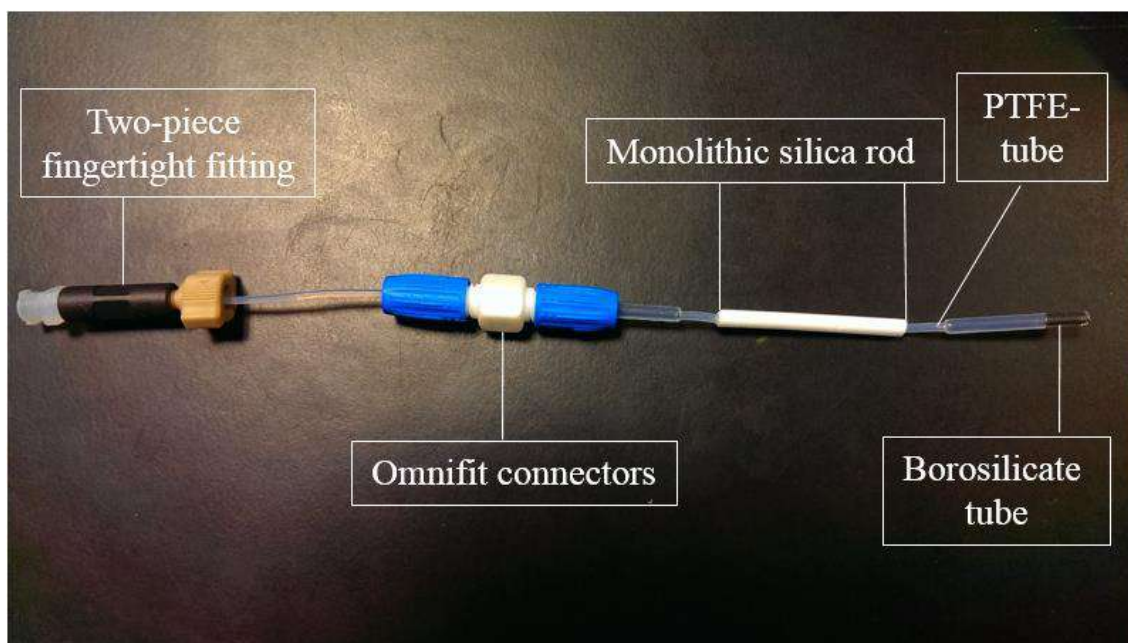


Figure 2-2. A silica monolith contained in a shrinkable tube and connected to the borosilicate tube for flow through use and surface modification.

The range of silica monoliths synthesised by sol-gel methods as described above were prepared using varied masses of polyethylene oxide (PEO) polymer or the triblock polymer F127, with acetic acid (HAC), nitric acid (HNO_3), tetramethoxysilane TMOS or tetraethylorthosilicate TEOS and ammonium hydroxide. The monoliths were produced under identical preparation conditions and were numbered from M1 to M6 depending on polymer masses used as summarized and presented in Table 2-3.

Table 2-3. Summary of monolith preparation conditions.

Sample	polymer	MW	Silane	Preparation conditions
M1	polyethylene oxide	100,000	TMOS	1- PEO 0.282g + ACOH 4 mL (0.02 M) 2- Addition of TMOS 2 mL 3- Gelation three days at 40 °C 4- Treatment of wet monolith with 1N NH ₄ OH at 85 °C 5- Wash and dry at 60 °C 6- Calcine monolith at 600 °C for 3 hours.
M2	polyethylene oxide	100,000	TMOS	1- PEO 0.305g + ACOH 4 mL steps 2,3,4 and 5 have the same preparation conditions for sample 1
M3	polyethylene oxide	200,000	TMOS	1- PEO 0.305g + ACOH 4 mL steps 2,3,4 and 5 have the same preparation conditions for sample 1
M4	polyethylene oxide	200,000	TMOS	1- PEO 0.282g + ACOH 4 mL steps 2,3,4 and 5 have the same preparation conditions for sample 1
M5	polyethylene oxide	100,000	TEOS	1- PEO 0.282g + 1M HNO ₃ 2.537 mL + H ₂ O 0.291 mL 2- Addition of TEOS 2.256 mL steps 3,4 and 5 have the same preparation conditions for sample 1
M6	Co-polymer F-127	13388	TMOS	F-127 0.432g + ACOH 4 mL steps 2,3,4 and 5 have the same preparation conditions for sample 1

2.4 Characterisation of monolithic materials

2.4.1 SEM analysis

Scanning electron microscopy images were acquired *via* a Zeiss EVO 60 instrument and Oxford Instruments Inca System 350 under the pressure of 10^{-2} Pa and an electron acceleration voltage of 20 kV. Samples were adhered to double coated conductive carbon tape and attached to the specimen holder. The morphology of silica monoliths was characterised by scanning electron microscopy (SEM) using Zeiss EVO 60 instrument and Oxford Instruments Inca System 350 under the pressure of 10^{-2} Pa and an electron acceleration voltage of 20 kV. The samples for SEM analysis were coated with a thin layer of gold-platinum (thickness approximately 2 nm) using a SEMPREP 2 Sputter Coater [Nanotech Ltd., Sandy, UK] in order to reduce microscope beam damage, increase thermal conduction, reduce sample charging (increase conduction), improve secondary electron emission and reduce beam penetration with improved edge resolution. The scanning electron micrographs of silica monoliths were obtained using an accelerating voltage of 20 kV and a probe current of 100 pA in high vacuum mode.

2.4.2 BET and BJH analysis

BET surface areas and pore volumes were determined *via* N₂ physisorption using a Micrometrics TriStar porosimeter and was used to measure the surface area, pore size and volume within the monoliths using nitrogen adsorption and desorption isotherms at 77 K. The pore volume and pore size distribution within the monoliths were also determined from the isotherms using the BJH (Barrett-JoynerHalenda) model.

2.5 Calibration curve of 4-nitrophenol

A master stock solution of 4-NP was prepared by made up to 10 mg 4-NP in 10 mL Tris-HCl buffer (pH7, 0.1 M). From the stock solution, serial dilutions of 4-NP analyte were

prepared, (0.02 mg/mL, 0.01 mg/mL, 5 mg/mL, 2.5 mg/mL, and 1.25 mg/mL). These were used to create a calibration curve to measure lipase activity.

2.6 Immobilisation of lipase

After the preparation of six silica monolith microreactors, three were chosen for the immobilization of *Candida antarctica* lipase for biocatalytic reactions (M1, M3, and M5) and those three monoliths have significant different physical properties and were chosen for lipase immobilization in order to explore the effect of their physical properties on the immobilized lipase activity.

The *Candida antarctica* lipase solution was prepared by dissolving 10 mg of the enzyme in 10 mL Tris-HCl buffer (pH7, 0.05M). To manufacture the immobilised lipase microreactor, the solution was pumped through the monolith at a flow rate of $10 \mu\text{L min}^{-1}$ for 16 hours. The lipase infused monolith was then incubated at 4°C for 1 hour before vacuum drying for 30 minutes. To remove all unbound lipase, the microreactor was washed several times with Tris-HCl buffer at the $10 \mu\text{L min}^{-1}$ flow rate. The washing was collected at the end of each washing cycle.

2.6.1 Assay of the free and immobilised lipase activity

The reactant 4-nitrophenyl butyrate (4-NPB) was used to determine the lipase hydrolysis activity of immobilised and free lipase.

Different concentrations of free lipase (0.02 mg/mL, 0.04 mg/mL, 0.08 mg/mL, 0.17 mg/mL, 0.33 mg/mL, 0.58 mg/mL, 0.83 mg/mL, 1.25 mg/mL, and 1.67 mg/mL) were prepared in the aqueous phase. By studying the reaction kinetics of the hydrolysis reaction, the correlation between lipase concentration and activity (initial velocity) was established.

A mobile water/decane biphasic system was used to hydrolyse 4-NPB. The reactant, 4-NPB was found to be soluble in decane, while the reaction product, 4-NP, and the lipase were dissolved in the water phase. UV/Vis spectrometry was used to measure the

maximum absorbance wavelength (λ_{max}) of 4-NP. The free lipase assay was conducted at room temperature. The suspension was agitated by a stirrer set to 200 rpm. The 1 mL mixture comprised 0.6 mL aqueous phase, containing free lipase in Tris-HCl buffer (0.5 M pH7) and 0.4 mL organic phase contained (0.3 – 5) mM of 4-NPB in decane.

At intervals of 1, 5, 10 and 15 minutes, 100 μL of aqueous phase samples were taken by pipette and to stop the reaction were mixed with a 0.1M Tris-HCl buffer solution. The final volume was 1 mL and was contained in disposable plastic UV-Vis cuvette. A calibration curve of 4-NP concentration *vs* absorbance was used to determine 4-NP production, *via* UV-Vis spectrophotometry at 400 nm. Figure 2-3 depicts a scheme of the apparatus used to evaluate the activity of the immobilised lipase. The set up used two syringe pumps to control the flow rate of the aqueous and organic solutions, a capillary mixer and a monolith immobilised lipase microreactor. Lipase-free, Tris-HCl buffer solution and an organic solution (4-NPB in decane) were pumped separately through the capillary mixer and monolith microreactor. The product was collected at a steady rate in a vial from the microreactor outlet. The organic phase was removed from the vial with a pipette. The remaining aqueous phase was treated and analysed using the methodology previously described for the activity assay of free lipase.

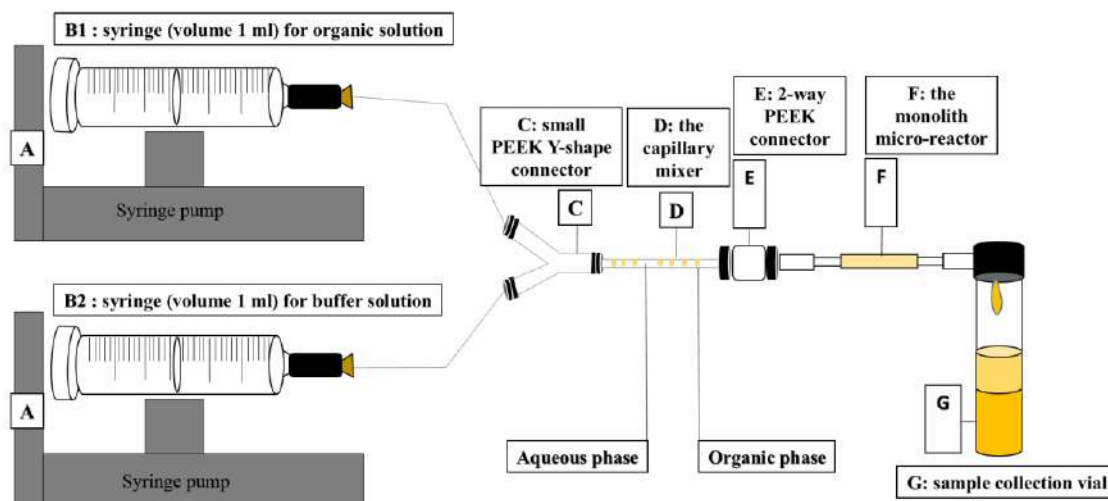


Figure 2-3. Schematic diagram of the reaction system used to assay immobilised lipase activity.

The reaction system to assay the immobilised lipase activity was consisting of (A) syringe pump, (B1) syringe (volume 1 mL) for organic solution and (B2) syringe (volume 1 mL) for buffer solution, (C) small PEEK Y-shape connector (pore size 0.5 mm diameter), (D) the capillary mixer (0.6 mm I.D. and 3 cm length), (E) 2-way PEEK connector (pore size 0.5 mm diameter), (F) the monolith micro-reactor (0.6 mm ID and 4 cm length), (G) sample collection vial. Within the capillary mixer, water was the continuous phase and the organic solution the segmented phase. The length of the organic plugs was ca. 1.5 mm.

The kinetic assay performed for the free lipase to determine V_{\max} and K_m are plotted in the double reciprocal manner suggested by Linweaver and Burk and are a straight fitted to the data by the method of least squares as explained in the introduction section 1.4.9. The kinetic studies for the immobilised lipase was determined by using the Lilly–Hornby model equation as described in the introduction section 1.4.10.

2.6.2 Determination of lipase loading in the immobilized monolith microreactor

The loading amount of candida antractica lipase CAL on silica microreactor supports was determined by calculated the difference between the amounts of lipase before loading solution and the amount of lipase solution remaining after loading immobilised process, and by using the calibration curve of lipase activity with lipase concentration the amount was quantified.

2.7 General procedure for catalytic transesterification:

The transesterification of tributyrin was performed in a flow reactor equipped with a syringe pump placed in the incubator to maintain the temperature as shown in Figure 2-4. A known molar ratio of tributyrin and methanol was charged to the syringe pump and the temperature was set to different temperatures. After the temperature reached the desired value, the syringe pump delivered reagent into the reactor. Samples were taken and the conversion of tributyrin was monitored using high-performance liquid chromatography (HPLC). The conversion of tributyrin and the formation of fatty acid methyl ester and methyl butyrate was calculated by using pre-established calibration curves.

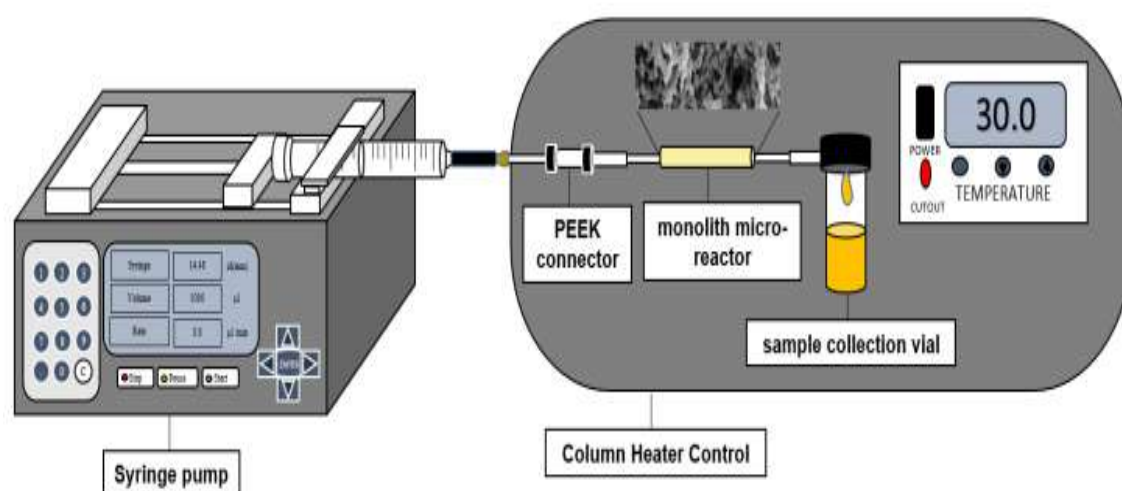


Figure 2-4. Schematic of continuous flow system for silica monolith catalytic testing.

2.7.1 Calibration curve of tributyrin

A master stock solution of tributyrin in methanol was prepared (0.05M). From the stock solution, serial dilutions of tributyrin analyte were prepared, (0.000916 M, 0.00274 M, 0.00457 M, 0.00915 M, 0.0115 M, 0.0115 M, 0.0183 M, and 0.0233 M). These concentration were used to create a calibration curve to determine the unknown concentration of the tributyrin as can be seen in section 4.1.

2.7.2 Calibration curve of methyl butyrate

A master stock solution of methyl butyrate in methanol was prepared (0.5M). From the stock solution, serial dilutions of methyl butyrate were prepared, (0.005 M, 0.01 M, 0.02 M, 0.04 M, 0.06 M, and 0.08 M). These concentrations were used to create a calibration curve to determine the unknown concentration of the methyl butyrate as can be seen in section 4.2.

2.7.3 HPLC conditions and mobile phase combination

In this work, chromatographic analysis was performed using HPLC with a UV detector consisting of an LC 200 series binary pump, a PerkinElmer 785A UV/Visible Detector and a BIO Wide Pore C18 column. The detection absorbance wavelength (λ_{\max}) of the product methyl butyrate (BuME) and the reactant tributyrin (TB) were investigated and set to 210 nm. For tributyrin and methyl butyrate the mobile phases were methanol ultra-pure water (80:20, v/v) run under isocratic conditions at ambient temperature (around 23 °C). The sample injection volume was 20 μL at the flow rate 1 mL min^{-1} .

2.8 Au-nanoparticle synthesis

Au nanoparticles were prepared by adapting the synthetic method described by Liu *et al*³⁴⁹. $\text{HAuCl}_4 \cdot 3\text{H}_2\text{O}$ (24 mg) was dissolved in ethylene glycol 1 mL. To the solution, polyvinylpyrrolidone (22 mg) was added followed by a further 6 mL of ethylene glycol and mixed for 10 min. Sodium borohydride (30 mg) was then added to the mixture and

heated at 80 °C under N₂ for 30 min. The nanoparticles were isolated by the addition of acetone followed by centrifugation at 3500 rpm. This process was repeated three times. The nanoparticles were then dispersed in deionised water. The method was found to produce Au nanoparticles of 2.5 ± 0.7 nm size.

2.8.1 Au nanoparticle - impregnated silica monolith synthesis

Firstly, the silica monolith was prepared by the similar methods as described in section 2.3. The amount of poly(ethylene oxide) was (0.122 g ; MW200, 000, with 1.6 mL of acetic acid (0.02 M) followed by 800 µl of TMOS; however, after addition of the tetramethylorthosilicate one hour after this was homogeneously mixed, the Au nanoparticle suspension in water was also added (0.4 M, 150 µL). The resulting mixture was then mixed until homogenous (30 min). The synthesis was then completed following the same process described above for the Au-free monolith in section 2.3.

2.8.2 Modified Au–thiol functionalized silica monolith

Once synthesised, a mesoporous silica monolith can be functionalized by incorporating a variety of useful functional groups such as: vinyl-, allyl-, amino-propyl and sulfur.^{350, 351} Functionalizing the silica monolith with these examples offers additional binding sites for ligands (vinyl-, allyl- and amino-propyl) that require a specific environment. In the present case thiolation of the monolith was performed to anchor Au nanoparticles. As the Au–S bond is relatively strong and the thiolate ligand is also reasonably durable on the silica surface, the Au nanoparticles are also stabilized.^{323, 352} Typically, functionalization takes place in two steps: (i) functionalizing the surface of the monolith with thiol groups and (ii) anchoring Au nanoparticles to the sulphur containing functional groups. A 0.06 M solution of (3-mercaptopropyl)trimethoxysilane (3-MPTMS) in toluene (4 mL) was passed through the monolith at a flow rate of 40 µL min⁻¹ at 100 °C in one direction, followed by a reverse flow from the opposite direction.³⁵³ The monolith was then washed

by passing toluene (4 mL), methanol (4 mL), and water (4 mL) at a flow rate of $40 \mu\text{L min}^{-1}$. Finally, the Au nanoparticle suspension in water (3 mL, equivalent Au atom content 0.02 M) was passed through the functionalized monolith at a flow rate of $10 \mu\text{L min}^{-1}$ at room temperature. To ensure the removal of polyvinylpyrrolidone, the monolith was washed twice with water (3 mL) at a flow rate of $10 \mu\text{L min}^{-1}$.

2.8.3 Characterisation of Au-catalysts

2.8.4 SEM analysis

Catalyst samples were adhered to double-coated conductive carbon tape and attached to the specimen holder and the following methods carried out as described in section 2.4.1.

2.8.5 BET and BJH analysis

As described in section 2.4.2 of the experiment.

2.8.6 ICP-OES Analysis

Au metal contents were determined by inductively coupled plasma optical emission spectroscopy (ICP-OES, Perkin Elmer Optical Emission Spectrometer Optima 5300 DV) after microwave digestion of the samples in 2 mL HNO₃ (Romil SPA grade 70%), 2 mL HCl (Romil SPA grade 60%) at 200 °C (CEM-MARS microwave reactor) followed by aqueous dilution. Bulk compositions are $\pm 10\%$.

2.8.7 Powder X-ray diffraction (PXRD) and XPS analysis

Powder X-ray diffraction (PXRD) measurements were carried out using monochromated Cu K α radiation ($\lambda = 0.1542 \text{ nm}$) on a PANalytical Empyrean series 2 diffractometer. Subsequent analysis of the diffractograms was performed in HighScore Plus (2013, PANalytical B.V.) with the ICDD's PDF-2 2012 database. X-ray photoelectron spectra were acquired on the UK National EPSRC XPS Users' Service (NEXUS) Kratos Axis Nova XP spectrometer with a monochromated Al K α excitation source (1486.7 eV). Samples were mounted in powdered form on carbon tape, pressed with a spatula, after

pre-attaching the carbon tape to a stainless steel plate containing two holes, that act as wells into which to load the powder. A wide analysis area ($300 \times 700 \mu\text{m}$) X-ray spot and charge compensation was used throughout all measurements. Energies are referenced to adventitious carbon at 284.4 eV. Spectral analysis was performed using CasaXPS.

2.8.8 Catalytic testing

A schematic of the reactor set up is depicted in Figure 2-5. Controlled flow reactions were performed using acetonitrile (5 mL) as the solvent. The reactants 0.35 mmol cyclohexene and 0.35 mmol of the oxidant in solution were mixed with the acetonitrile solvent at room temperature and were passed through the silica monolith at a constant flow rate of $12 \mu\text{L min}^{-1}$ using a Chemyx Fusion 100 Syringe Pump. Two different oxidants were used in this study: hydrogen peroxide, and *tert*-butyl hydroperoxide (TBHP), to maintain constant temperature the monolith was contained in a Model 7971 column heater (Jones Chromatography Ltd) held at $30 \pm 0.1 \text{ }^\circ\text{C}$.

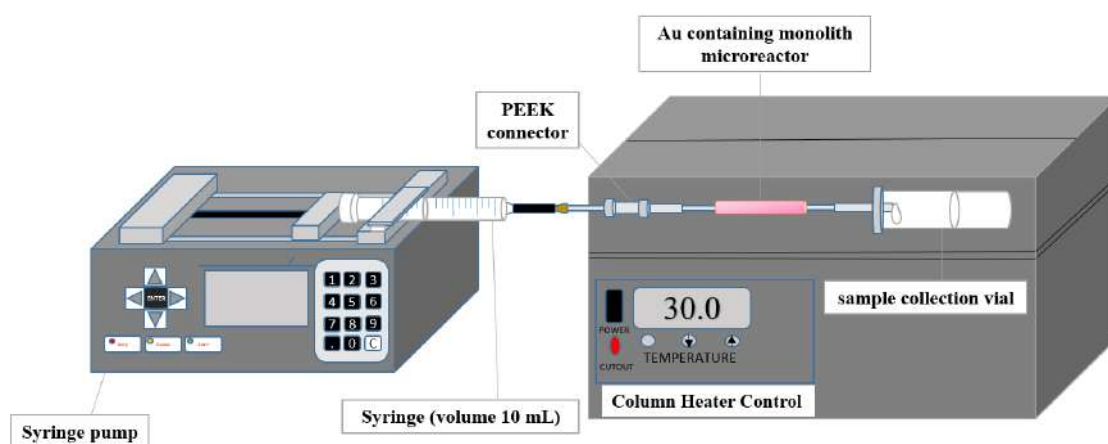


Figure 2-5. Schematic of continuous flow system for silica monolith catalytic testing.

2.8.9 GC-FID conditions

The mixture eluted from the monolith was collected in a vial and analysed by gas chromatography, using a Bruker Scion 456-GC equipped with a flame ionisation detector and a Zebron ZB-5 (5%-phenyl–95%-dimethylpolysiloxane) capillary column. GC–MS was performed using an Agilent 6890 GC equipped with an Agilent 5973N Quadrupole mass spectrometer and an RXI-5MS (5%-phenyl–95%-dimethylpolysiloxane) capillary column. The detection limit for the analytical systems used equates to 0.2% conversion. Conversion and selectivities were calculated using Equation 2-1 and Equation 2-2 :

$$\% \text{ Conversion of cyclohexene} = \left(\frac{C_{S \text{ cyclohexene}} - C_{F \text{ cyclohexene}}}{C_{S \text{ cyclohexene}}} \right) \times 100 \quad \text{Equation 2-1}$$

Where: %Con.cyclohexene – Cyclohexene converted (%)

$C_{S \text{ cyclohexene}}$ – Initial cyclohexene concentration excluding cyclohexene in the monolith after a single pass of the reaction mixture at (M)

$C_{F \text{ cyclohexene}}$ – Final cyclohexene concentration (M)

$$\text{Product selectivity (\%)} = \left(\frac{C_{\text{Individual product}}}{\sum C_{\text{All products}}} \right) \quad \text{Equation 2-2}$$

Turnover frequencies were calculated by assuming the metal surface area can be approximated by using the TEM particle size and assuming all the surface area of a spherical nanoparticle of this diameter is available for reaction, the density of the nanoparticles is 19.3 g mL^{-1} , and the surface packing of gold can be assumed to be close packed, $4.158 \times 10^{-20} \text{ m}^2 \text{ atom}^{-1}$. This likely provides a lower bound as not all of the surface will be accessible so this method can be expected to overestimate the number of surface gold atoms that can contribute.

2.8.10 Calibration curve of Cyclohexene

A master stock solution of Cyclohexene in acetonitrile was prepared (0.1M). From the stock solution, serial dilutions of methyl butyrate were prepared, (0.06 M, 0.02 M, 0.005 M, 0.00125 M, 0.000625 M, and 0.000156 M). These concentrations were used to create a calibration curve to determine the unknown concentration of the Cyclohexene as can be seen in section 5.1.

2.8.11 Calibration curve of Cyclohexene oxide

A master stock solution of Cyclohexene oxide in acetonitrile was prepared (0.1M). From the stock solution, serial dilutions of methyl butyrate were prepared, (0.06 M, 0.02 M, 0.005 M, 0.00125 M, 0.000625 M, and 0.000156 M). These concentrations were used to create a calibration curve to determine the unknown concentration of the Cyclohexene oxide as can be seen in section 5.2.

2.8.12 Calibration curve of 2-Cyclohexene -1-ol

A master stock solution of 2-Cyclohexene -1-ol in acetonitrile was prepared (0.1M). From the stock solution, serial dilutions of methyl butyrate were prepared, (0.06 M, 0.02 M, 0.005 M, 0.00125 M, 0.000625 M, and 0.000156 M). These concentrations were used to create a calibration curve to determine the unknown concentration of the 2-Cyclohexene -1-ol as can be seen in section 5.3.

2.8.13 Calibration curve of 2-Cyclohexen -1-one

A master stock solution of 2-Cyclohexen -1-one in acetonitrile was prepared (0.1M). From the stock solution, serial dilutions of methyl butyrate were prepared, (0.06 M, 0.02 M, 0.005 M, 0.00125 M, 0.000625 M, and 0.000156 M). These concentrations were used to create a calibration curve to determine the unknown concentration of the 2-Cyclohexen -1-one as can be seen in section 5.4.

2.8.14 Calibration curve of Mesitylene

A master stock solution of Mesitylene (external standard) in acetonitrile was prepared (0.1M). From the stock solution, serial dilutions of methyl butyrate were prepared, (0.06 M, 0.02 M, 0.005 M, 0.00125 M, 0.000625 M, and 0.000156 M). These concentrations were used to create a calibration curve to determine the unknown concentration of the Mesitylene as can be seen in section 5.5.

Chapter 3. Development of the Silica Monolith microreactors for hydrolysis reactions

This chapter presents the production of six stable monolithic structures through a sol-gel method using tetramethoxysilane (TMOS) and tetraethyl orthosilicate (TEOS) as precursors and polymers with different average molecular weight as described in chapter 2 section 2.3. Six different conditions were employed to result in silica-monoliths with a range of physical characteristics. Three silica monoliths which have significant different physical properties were chosen for lipase immobilisation in order to explore the effect of their physical properties on the immobilised lipase activity.

Commercial candida antarctica lipase (CAL) was immobilised on the chosen three silica monoliths to generate an active and stable lipase immobilised silica monolith microreactor for bio-catalytic reactions. To evaluate the lipase activation, the hydrolysis of 4-nitrophenyl butyrate was performed using a mobile water-decane biphasic system. Additionally, the free and immobilised lipase was evaluated over extended run times and elevated temperatures. The kinetic studies performed for the free lipase to determine V_{\max} and K_m are plotted in the double reciprocal manner suggested by Lineweaver and Burk. The kinetic studies for the immobilised lipase was determine by the Lilly–Hornby model. The results show that the affinity of free lipase to the substrate is much higher than the affinity of immobilised lipase to the substrate and that could be because, in the case of immobilised lipase, the substrate face some difficulties to reach the lipase immobilised in the mesoporse, but the turn-over number of immobilised lipase is much higher than the free lipase and that could be because of using a flow microreactor system as in the free lipase we used a batch reactor which has high productivity than the batch reactor. The data show that it is better to use a microreactor with small average pore diameter.

3.1 Physical characterisation of monoliths

The monoliths microreactors M1-M6 were measured and evaluated using BET to obtain surface area in (m^2/g), pore volume in (cm^3/g), and pore size in (nm). The results are summarized in Table 3-1.

Table 3-1. Physical characterisation of monolith by BET

Sample	BET Surface Area m^2/g	Pore Volume cm^3/g	Pore Size nm
M1	529 ± 36.22	0.97 ± 0.13	6.5 ± 0.71
M2	470 ± 13.85	0.93 ± 0.02	7.1 ± 0.15
M3	460 ± 28.8	1.04 ± 0.08	8.7 ± 0.35
M4	494 ± 15.24	0.97 ± 0.05	7.2 ± 0.55
M5	218 ± 7.01	1.07 ± 0.05	18.6 ± 0.79
M6	222 ± 12.35	0.69 ± 0.11	16.1 ± 0.92

The range in surface areas, pore volumes and pore sizes obtained from 218-529 m^2/g , 0.69-1.07 cm^3/g , and 6.5-18.6 nm, were found to be significantly larger compared to the variations reported by Fletcher *et al.*¹⁰⁸ This differences could be due to using of TMOS instead of TEOS. It is well known that the hydrolysis rate of TMOS is fast which lead to formation of highly branched clusters linking up and give a monolith structure with mini small pore diameter which could be the reason of the large surface area.¹⁰³ For sample M1 0.282 g PEO polymer was used and underwent the preparation condition indicated in Table 2-3, using 100,000 MW, and the surface area obtained was 529 m^2/g with a pore volume of 0.97 cm^3/g and a pore size of 6.5 nm. This is 13% more than the surface area,

6% less in pore volume and 25% less in the pore size observed when compared to the monolith used using the same concentration of polymer but with 200,000 MW, which can be seen in sample M3. In sample M2, where 0.305 g PEO polymer was used and prepared under the same conditions as in sample M1, the surface area and pore volume obtained was less than the latter at 470 m²/g and 0.93 cm³/g, respectively, while the pore size was larger at 7.1 nm. In sample M5, where 0.282g of PEO polymer was used but with TEOS saline, the surface area indicated 218 m²/g with a pore volume of 1.07 cm³/g and a pore size of 18.6 nm. In sample M6, the surface area indicated 222 m²/g with a pore volume of 0.69 cm³/g and a pore size of 16.1 nm. Thus, sample M5, with 218 m²/g surface area, a pore volume of 1.07 cm³/g and a pore size of 18.6 nm is the best monolith to be used. According to Fletcher *et al.*¹⁰⁸ to use silica monoliths as catalyst support, should contain high specific surface area for maximum catalytic activity, and this can be achieved through obtaining a large value of nm-sized pores. Also, the silica monolith must be highly permeable, and this can be achieved through micron-sized pores. Upon quick observation on Table 3-1, sample M1 has the largest surface area of 529 m²/g.

3.2 Effect of ammonia treatment on the silica microreactors

A high surface area produced by the formation of mesopores on the surface of the monolithic silica is essential. The surface area was therefore measured, and relevant isotherms determined pre- and post-treatment with ammonia at 82 °C for 24 hours. The ammonia treatment was performed after the monolithic rods were well-aged but still wet. The BET method was used to determine the specific surface area for the TMOS (prepared with PEO 100 K) monolithic rods subsequent to ammonia treatment being found to be about 529 m² g⁻¹, compared to TMOS alone, which gave a smaller surface area of 8.37 m² g⁻¹. The presence of the mesopores therefore resulted in a significantly larger surface area.

Figure 3-1 depicts the isotherm curves obtained for two TMOS monolithic silica rods pre- and post-hydrothermal treatment. Figure 3-1 (A) shows the isotherm for the non-treated TMOS silica rod which exhibited an isotherm curve similar to the Type II isotherms discussed in section 1.3.6.2 (see Figure 1-12). IUPAC Type II isotherms are indicative of strong adsorption for macroporous absorbents (pore size > 50 nm). In contrast, Figure 3-1 (B) demonstrates that, when the TMOS monolithic silica rod was subject to ammonia treatment, a Type IV isotherm resulted. All six silica monoliths prepared in this thesis showed Type IV isotherms according to IUPAC classification. This type IV isotherm is typically exhibited by mesoporous materials (2 nm < pore size < 50 nm).

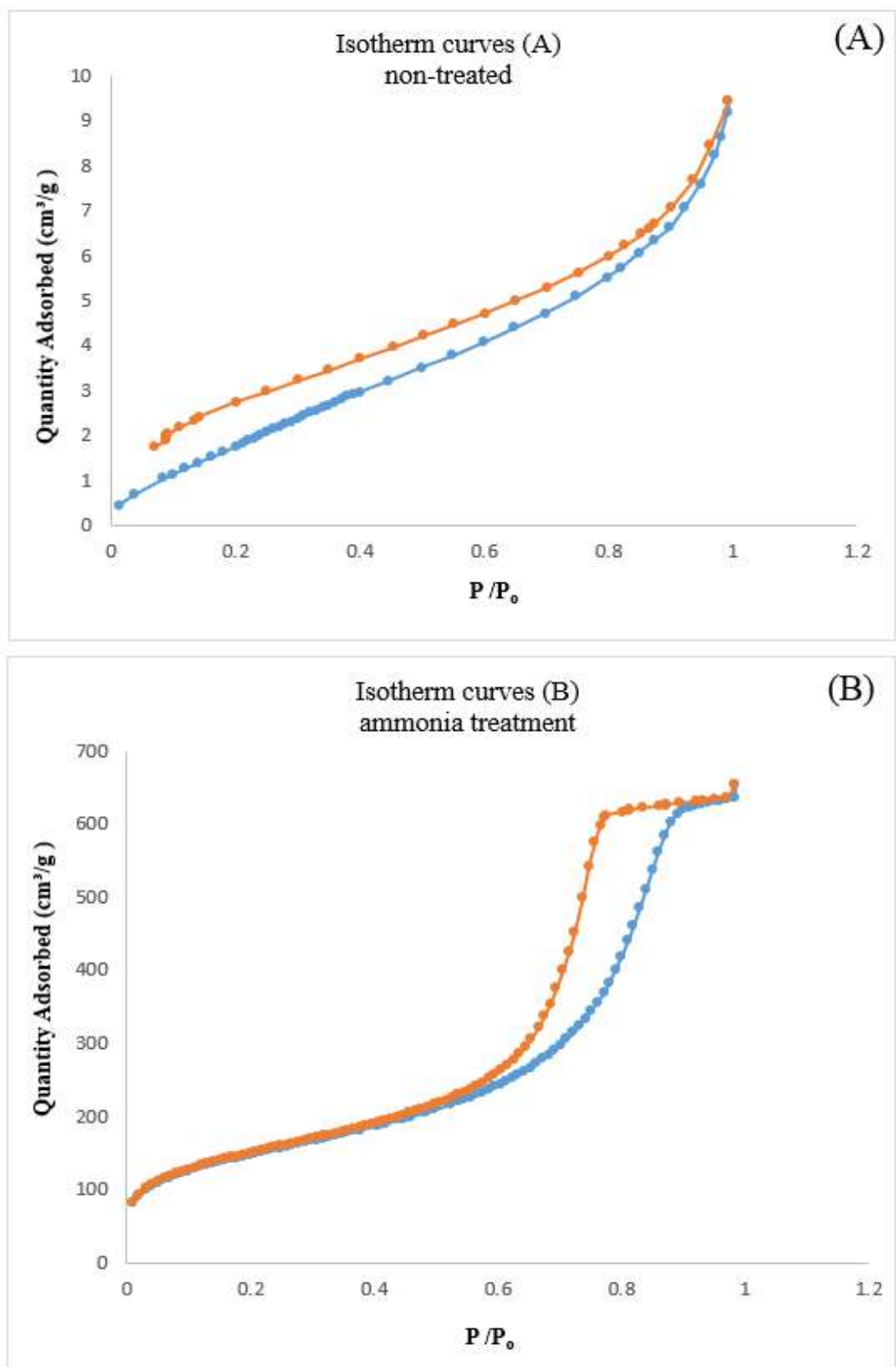


Figure 3-1. Isotherm curves exhibited by two TMOS monolithic silica (M1) rods following the nitrogen physisorption method. The only significant difference in methodology is the absence of hydrothermal treatment (isotherm curve A)/ presence of hydrothermal treatment at 80 °C (isotherm curve B).

These results support the hypothesis that the internal pore structure of the silica-based monolithic rods increased the surface area *via* the creation of mesopores following treatment with ammonia solution, as demonstrated by Nakanishi *et al.*^{110, 111}

This indicates that the presence of the hydrothermal step (ammonia treatment) is critical to the development of mesopores in the monolithic silica material which provide the important significant increase in the surface area.

3.3 Determination of average through pores size by SEM

SEM identification of average particle sizes and pore sizes helped demonstrate the structure produced in the monolith system. This will help identify whether monolith systems have specific morphologies that facilitate microreaction. Further, this will also determine whether the structure possesses ‘air-in-silica’, ‘silica-in-air’ or ‘sponge-like’ quality characteristic’. Figure 3-2 to Figure 3-4 shows SEM images for silica monoliths manufactured by (A) and (B) TMOS and (C) TEOS as silica source, respectively.

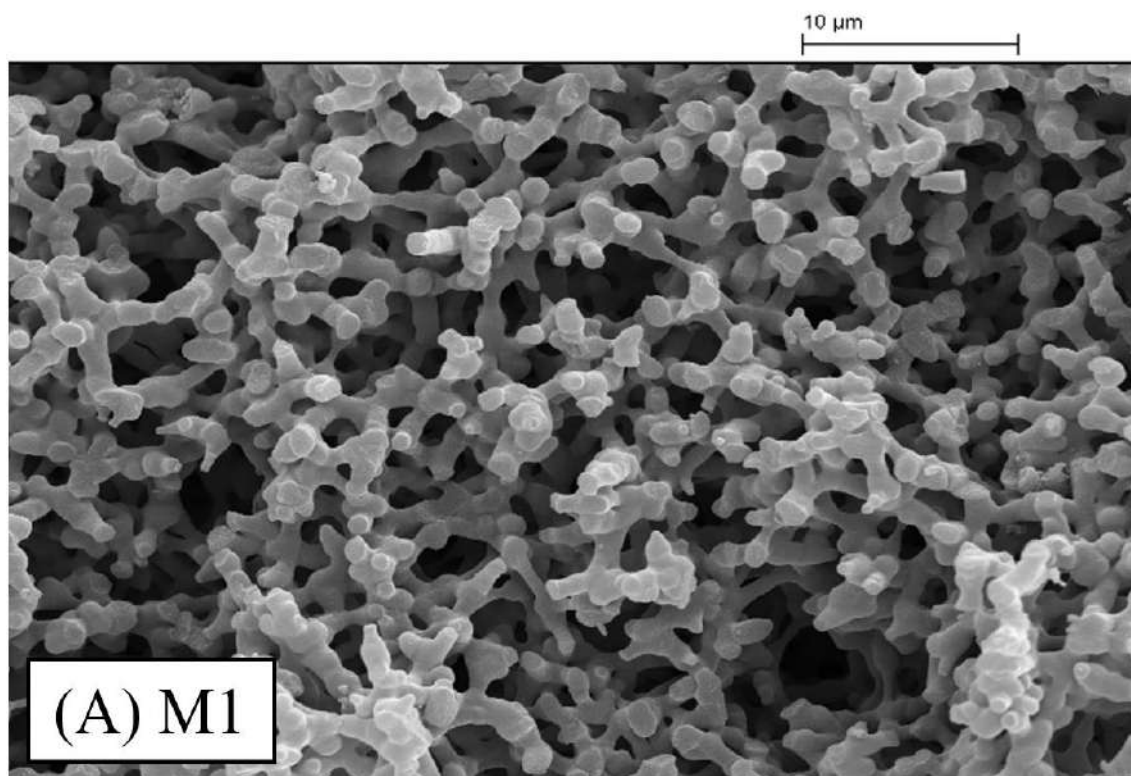


Figure 3-2 .SEM image of (A) the silica monolith after calcination sample. M1

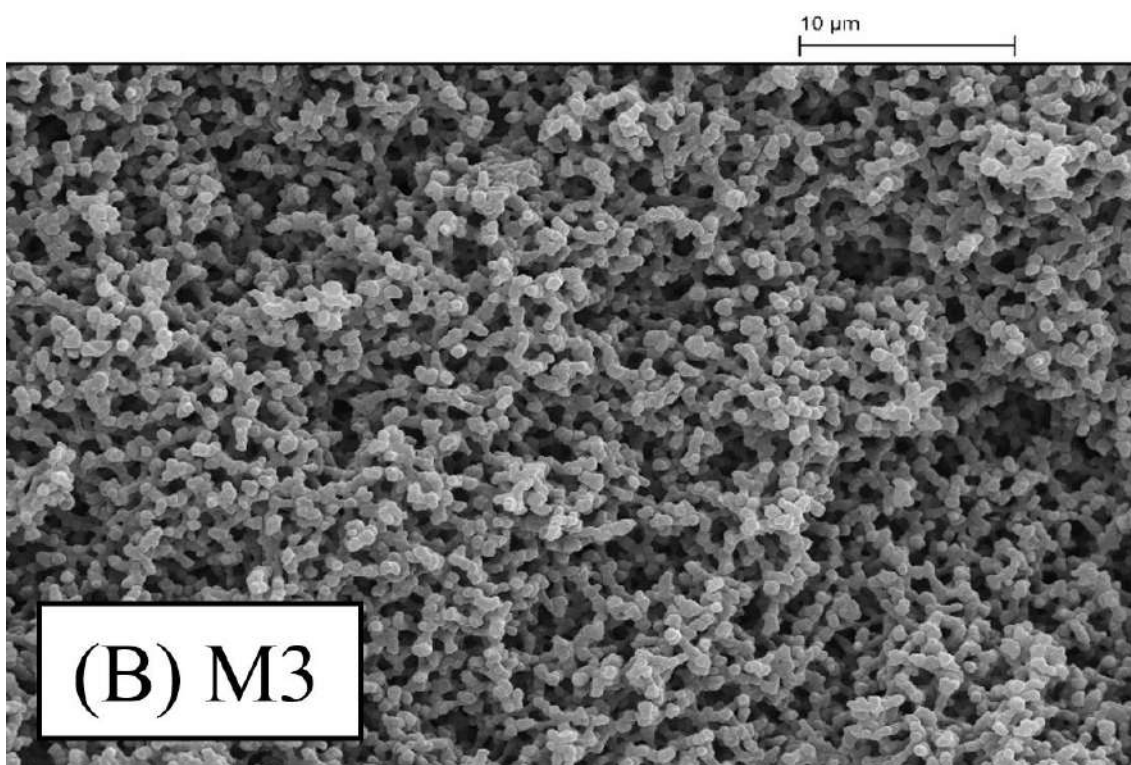


Figure 3-3.SEM image of (B) the silica monolith after calcination sample. M3

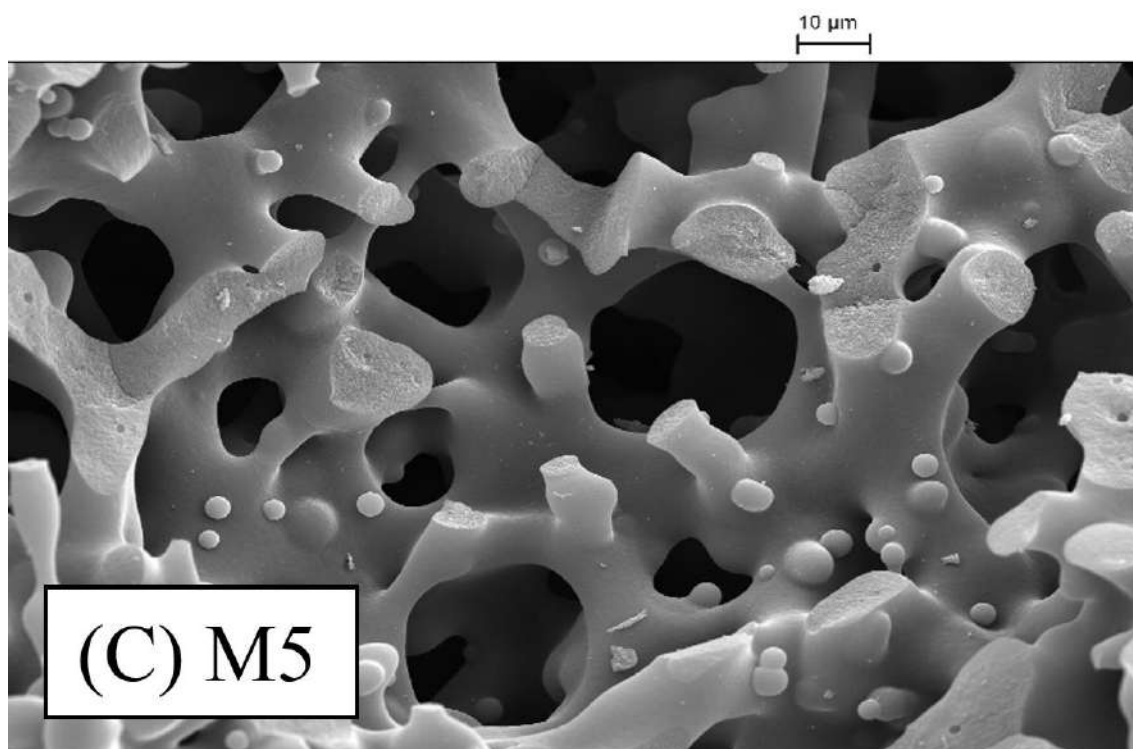


Figure 3-4. SEM image of (C) the silica monolith after calcination sample. M5

SEM images in Figure 3-2 to Figure 3-4 show that all monoliths have “sponge like” bicontinuous monolithic structure. This monolithic structure provides high surface area and pore volume.¹⁰⁸ The SEM measurements suggest that the coral like network is preserved after the immobilisation of lipase in the monolith. The wall thickness appears to be vastly different between the three monoliths. In particular the wall thickness of M5 appears to be substantially larger than that of M1 and M3. The difference could be due to the type and molecular weight of the polymer used and also the silica source, ammonia treatment and calcination temperature and time. Liu *et al.*³⁵⁴ have found that the wall thickness of mesoporous silica increases by increasing the TEOS/TMOS ratio. The above differences are also reflected in the surface area, pore size and pore volume which are shown in Table 3-2. Monolith sample M1 appears to have the highest surface area while M5 has the lowest. As expected M5 has the largest pore size 18.6 nm. As these differences will affect the performance of the monoliths when used as microreactors. Considering the micron-scale pore diameter of each sample, sample M5 has the biggest, followed by

sample M1, while sample M6 which contains the smallest pore diameter. However these pores are on the interior silica surface of the monolith where the lipase are expected to immobilise. There are other larger pores (through pores) where the reaction medium pass through. Manual calculation for pore diameters in SEM pictures was performed for all samples where 12 pore diameters were measured for each sample. The average of pore diameter, standard deviation (SD) and relative standard deviation (RSD) are summarized in Table 3-2.

Table 3-2 .Micron scale pore diameter

Sample	Average pore diameter (μm)	SD	RSD %
M1	2.75	0.44	13.5
M2	1.8	0.36	22.81
M3	1.15	0.07	5.24
M4	2.7	0.81	31
M5	4.15	0.37	18
M6	1.14	0.29	24

3.4 Calibration curve of 4-NP at 400 nm

The maximum absorbance for 4-NP was found to be at 400 nm as shown in Figure 3-5.

Thus all absorbance measurements were taken at 400 nm.

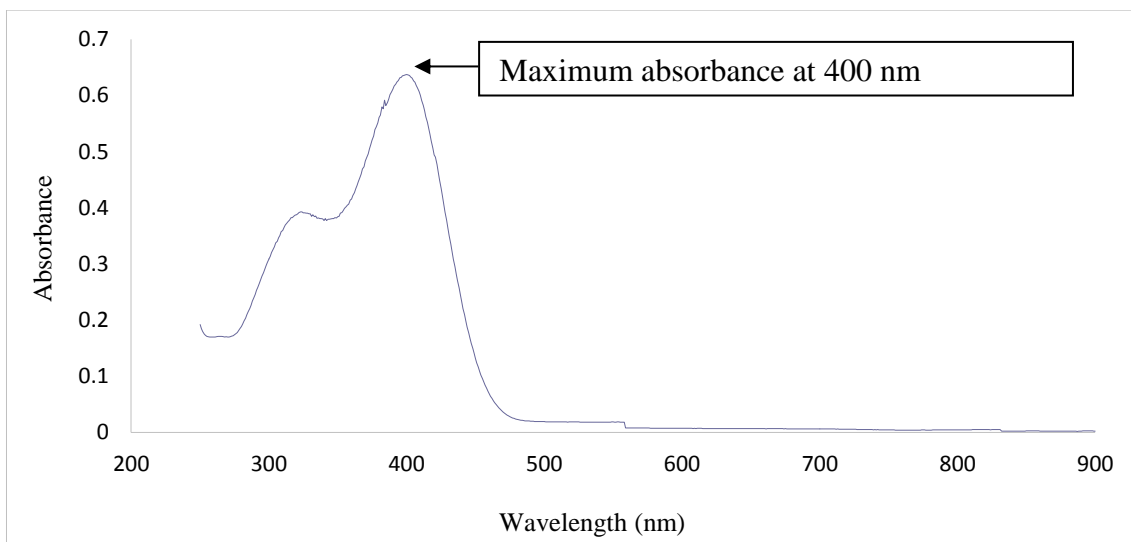


Figure 3-5. An absorption spectrum (λ) for 4-NP.

The absorbance of calibration solutions of 4-NP were measured at wavelength 400 nm to establish the calibration curve of 4-NP as shown in Figure 3-6 which was used to determine the concentration of 4-NP during the activity measurement of lipase as described in experimental procedure. Table 3-3 shows the calibration standards used to establish the calibration curve and the UV response.

Table 3-3. Absorbance of 4-NP measured under varied concentration

Conc. of 4-NP mg/mL	Absorbance
0	0
0.00125	0.117
0.0025	0.229
0.005	0.425
0.01	0.858
0.02	1.737

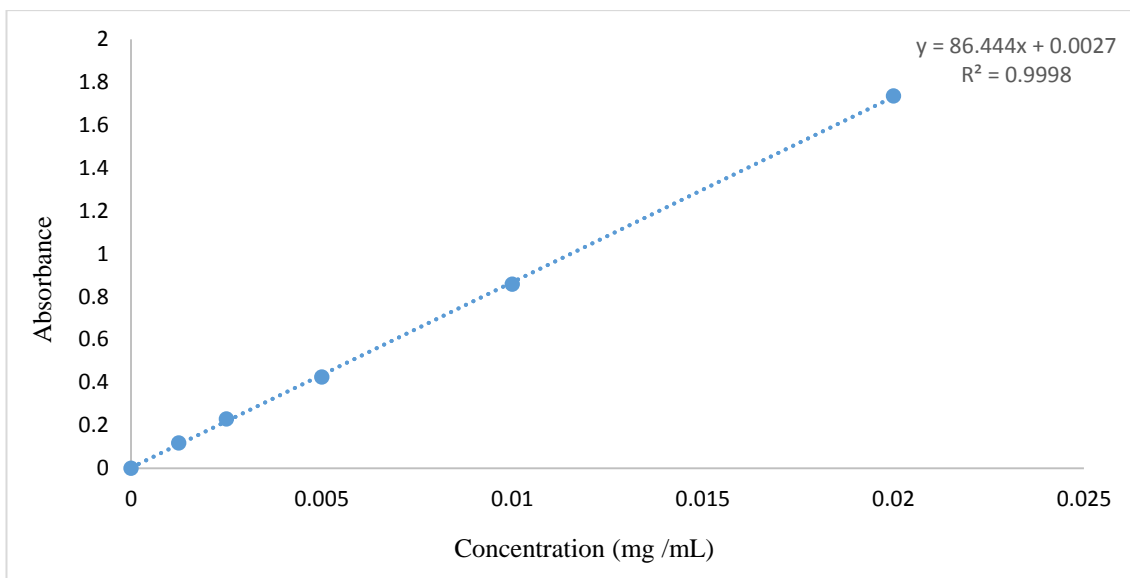


Figure 3-6. Calibration curve of 4-NP at 400 nm.

As shown in Figure 3-6, there is a linear relationship between the concentrations and absorbance as the R square value (0.9998) was close to 1. According to Beer-Lambert law, the absorbance of a solution is directly proportional to the concentration of the absorbing species in the solution and the path length as explained in the Equation 1-3 in the introduction section 1.4.8.1.

Thus molar extinction coefficients can be calculated more accurately from the calibration curve. For 4-NP, the molar extinction coefficients (ϵ) is $86.4 \text{ mol}^{-1} \text{ L cm}^{-1}$.

The uncertainty in the calibration equation, the slope and the y-intercept was calculated. The standard deviation of y axis ($S_{y/x}$) was calculated from the residual values (the difference between each measured y-value and that calculated from the calibration curve), then the error in slope and the error in intercept were calculated. Statistical analysis results of calibration equation are summarized in Table 3-4.

Table 3-4. Estimated error values for calibration equation

Slope	86.4
Error in slope	0.57
Intercept	0.003
Error in intercept	0.005

This value will be used to calculate the concentration of 4-NP ($C = A/ \epsilon$). The error of 4-NP concentration can be calculated from the molar extinction coefficient error and absorbance error (standard deviation/ $\sqrt{3}$) using the error propagation equation).³⁵⁵

$$\frac{\text{Error in concentration}}{\text{Concentration}} = \sqrt{\left(\frac{\text{Error in absorbance}}{\text{Absorbance}}\right)^2 + \left(\frac{\text{Error in molar coefficient}}{\text{Molar coefficient}}\right)^2} \quad \text{Equation 3-1}$$

3.5 Assay of the free lipase activity

The hydrolysis reaction was carried out as explained in section 2.6.1 to establish a correlation between lipase concentration and activity (initial velocity) by studying the kinetics of the reactions. The average absorbance of three replicates of each sample at a given times for free lipase concentrations is shown in Table 3-5.

Table 3-5. Absorbance of 4-NP as a function of time for different free lipase concentrations.

Lipase Conc. mg/mL		Time (min)			
		1	5	10	15
0.02	Abs.	0.005	0.01	0.014	0.02
	Error	0.003	0.001	0.001	0.001
0.04	Abs.	0.006	0.02	0.032	0.042
	Error	0.001	0.001	0.002	0.002
0.08	Abs.	0.019	0.038	0.06	0.085
	Error	0.001	0.002	0.003	0.004
0.17	Abs.	0.021	0.069	0.122	0.171
	Error	0.001	0.003	0.006	0.009
0.33	Abs.	0.034	0.151	0.252	0.325
	Error	0.002	0.008	0.013	0.016
0.58	Abs.	0.049	0.185	0.363	0.493
	Error	0.002	0.009	0.018	0.025
0.83	Abs.	0.062	0.291	0.523	0.661
	Error	0.003	0.015	0.026	0.033
1.25	Abs.	0.067	0.299	0.571	0.711
	Error	0.003	0.015	0.029	0.036
1.67	Abs.	0.086	0.401	0.682	0.851
	Error	0.004	0.02	0.034	0.043

Absorbance results were used to calculate the concentration of 4-NP through Equation 3-2.

$$\text{Conc. of 4-NP (mg/mL)} = (\text{Abs} \div \text{molar coefficient}) \times \text{dilutions factor} \quad \text{Equation 3-2}$$

Where molar coefficients is 86.4 and dilution factor is 91. The error in concentration was calculated by using error propagation equation. The results are summarized in table 3-6.

Table 3-6. Concentration of 4-NP in mg/mL as a function of time for different free lipase concentrations.

Lipase Conc. mg/mL		Time (min)			
		1	5	10	15
0.02	Conc. mg/mL	0.005	0.011	0.015	0.021
	Error	0.002	0.001	0.001	0.001
0.04	Conc. mg/mL	0.006	0.021	0.034	0.044
	Error	0.001	0.001	0.002	0.002
0.08	Conc. mg/mL	0.02	0.04	0.063	0.09
	Error	0.001	0.002	0.003	0.004
0.17	Conc. mg/mL	0.022	0.073	0.129	0.18
	Error	0.001	0.004	0.006	0.009
0.33	Conc. mg/mL	0.036	0.159	0.266	0.342
	Error	0.002	0.008	0.013	0.017
0.58	Conc. mg/mL	0.052	0.195	0.383	0.52
	Error	0.003	0.01	0.019	0.026
0.83	Conc. mg/mL	0.065	0.307	0.551	0.697
	Error	0.003	0.015	0.028	0.035
1.25	Conc. mg/mL	0.071	0.315	0.602	0.749
	Error	0.004	0.016	0.03	0.037
1.67	Conc. mg/mL	0.091	0.423	0.719	0.897
	Error	0.005	0.021	0.036	0.045

Then the concentration of 4-NP was converted from mg/mL to mM, using Equation 3-3

$$\text{Conc. (mM)} = (\text{Conc. (mg/mL)} \div \text{molecular weight of 4 - NP}) \times 1000 \quad \text{Equation 3-3}$$

Where molecular weight of 4-NP is 139.11 g/mol. The results are summarised in Table 3.7.

Table 3-7. Concentration of 4-NP in mM as a function of time for different free lipase concentrations.

Lipase Conc. mg/mL		Time (min)			
		1	5	10	15
0.02	Conc. mM	0.038	0.76	0.106	0.152
	Error	0.002	0.002	0.004	0.005
0.04	Conc. mM	0.045	0.152	0.242	0.318
	Error	0.003	0.005	0.009	0.011
0.08	Conc. mM	0.144	0.288	0.455	0.644
	Error	0.005	0.01	0.016	0.023
0.17	Conc. mM	0.159	0.523	0.924	1.295
	Error	0.006	0.019	0.033	0.047
0.33	Conc. mM	0.258	1.144	1.909	2.462
	Error	0.009	0.041	0.069	0.089
0.58	Conc. mM	0.371	1.401	2.75	3.735
	Error	0.013	0.051	0.099	0.135
0.83	Conc. mM	0.47	2.204	3.962	5.007
	Error	0.017	0.079	0.143	0.181
1.25	Conc. mM	0.508	2.265	4.326	5.386
	Error	0.018	0.082	0.156	0.194
1.67	Conc. mM	0.651	3.038	5.166	6.447
	Error	0.023	0.11	0.186	0.232

The velocity of the reaction (initial velocity) is the slope of the linear phase, expressed as amount of product formed per time as shown from Figure 3-7 to Figure 3-15.

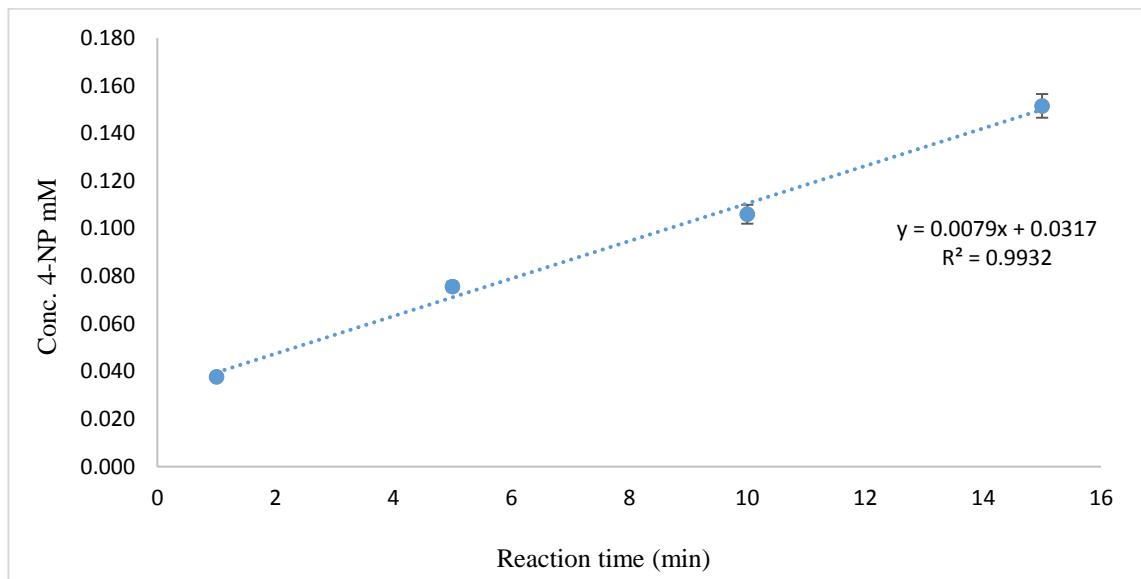


Figure 3-7. The concentration of 4-NP in mM as a function of reaction time in presence of free lipase 0.02 mg/mL.

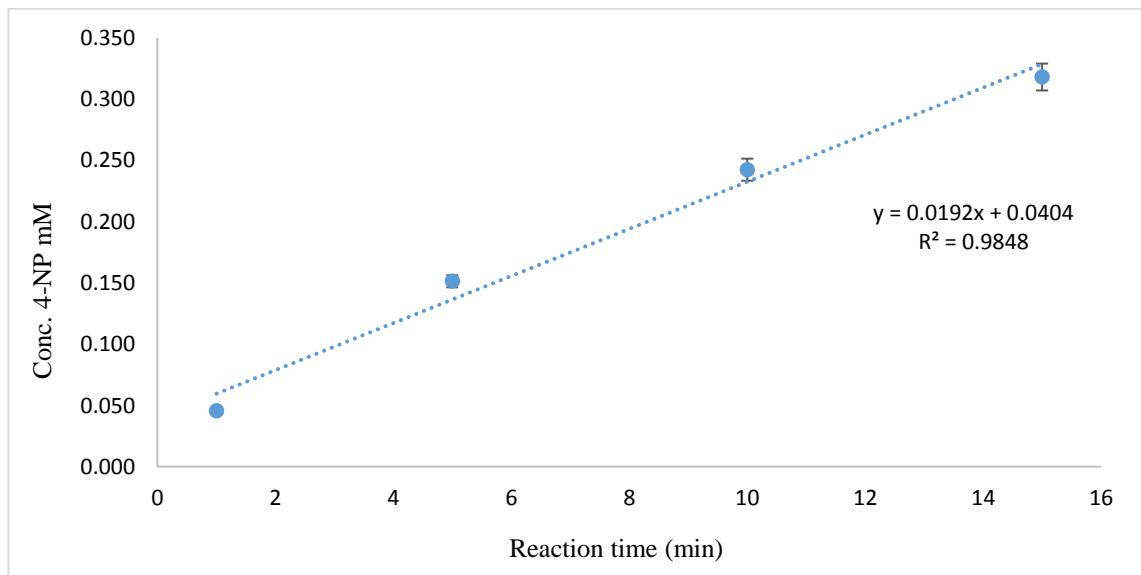


Figure 3-8. The concentration of 4-NP in mM as a function of reaction time in presence of free lipase 0.04 mg/mL.

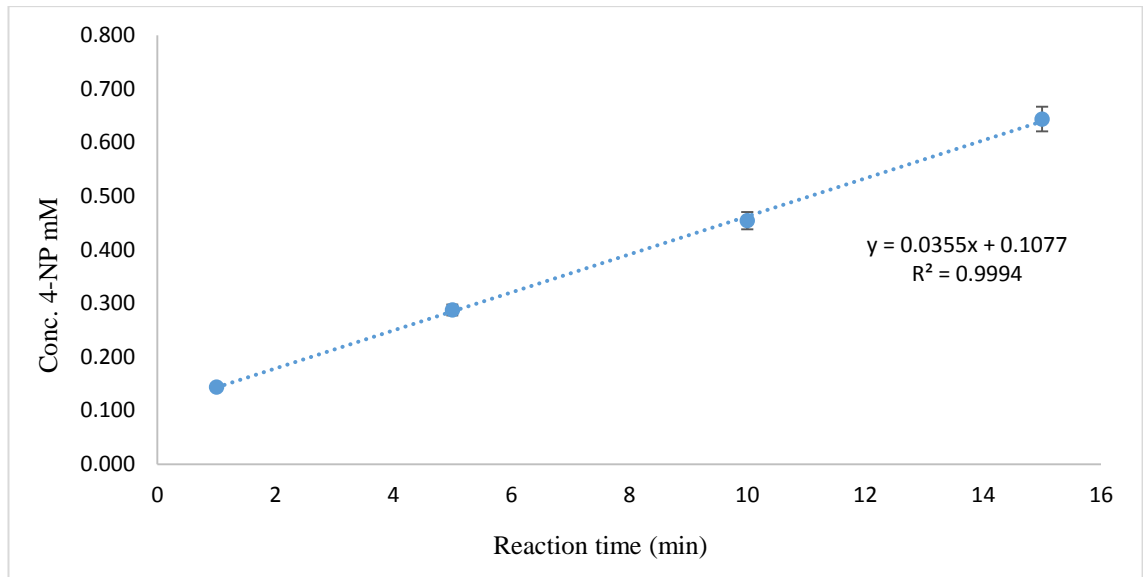


Figure 3-9. The concentration of 4-NP in mM as a function of reaction time in presence of free lipase 0.08 mg/mL.

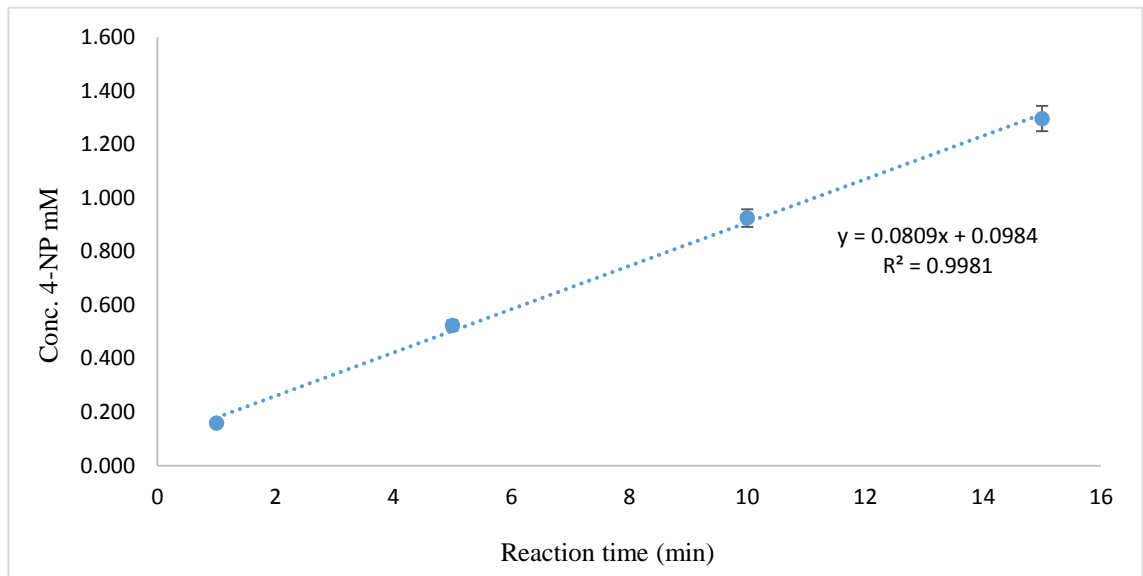


Figure 3-10. The concentration of 4-NP in mM as a function of reaction time in presence of free lipase 0.17 mg/mL.

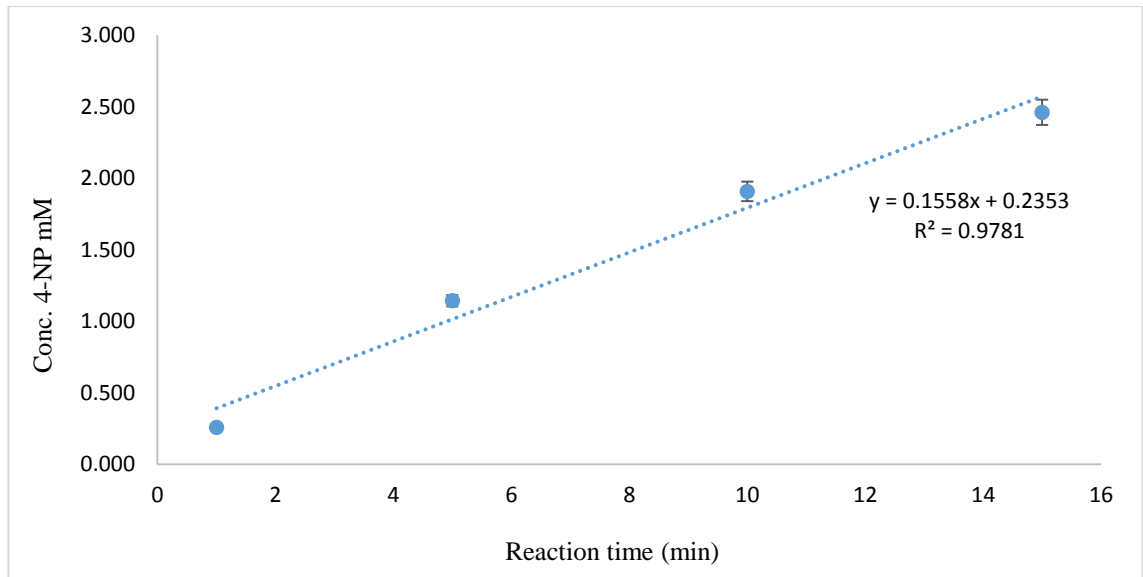


Figure 3-11. The concentration of 4-NP in mM as a function of reaction time in presence of free lipase 0.33 mg/mL.

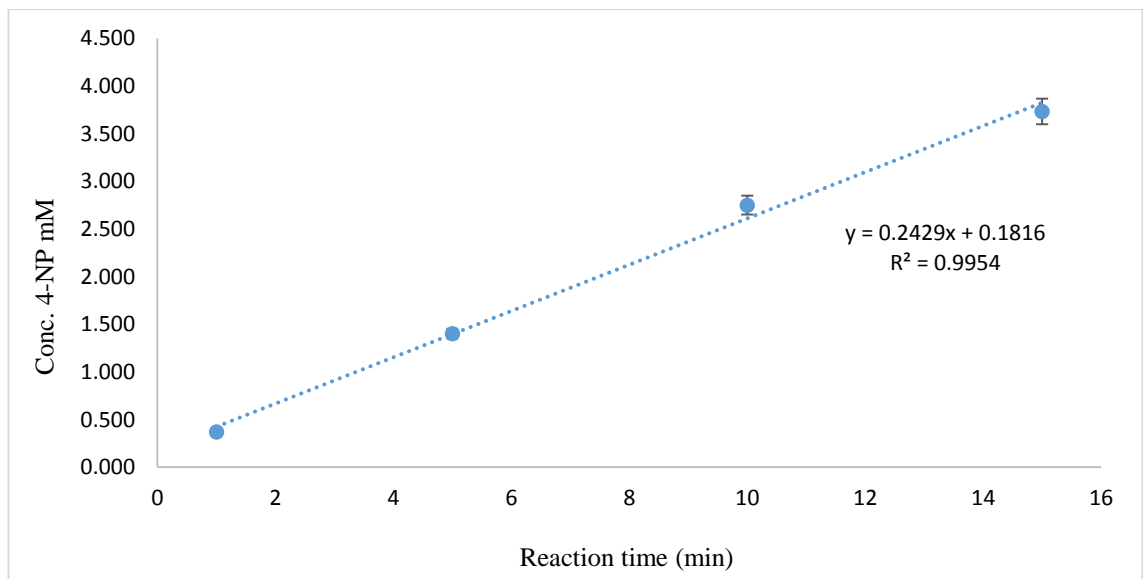


Figure 3-12. The concentration of 4-NP in mM as a function of reaction time in presence of free lipase 0.58 mg/mL.

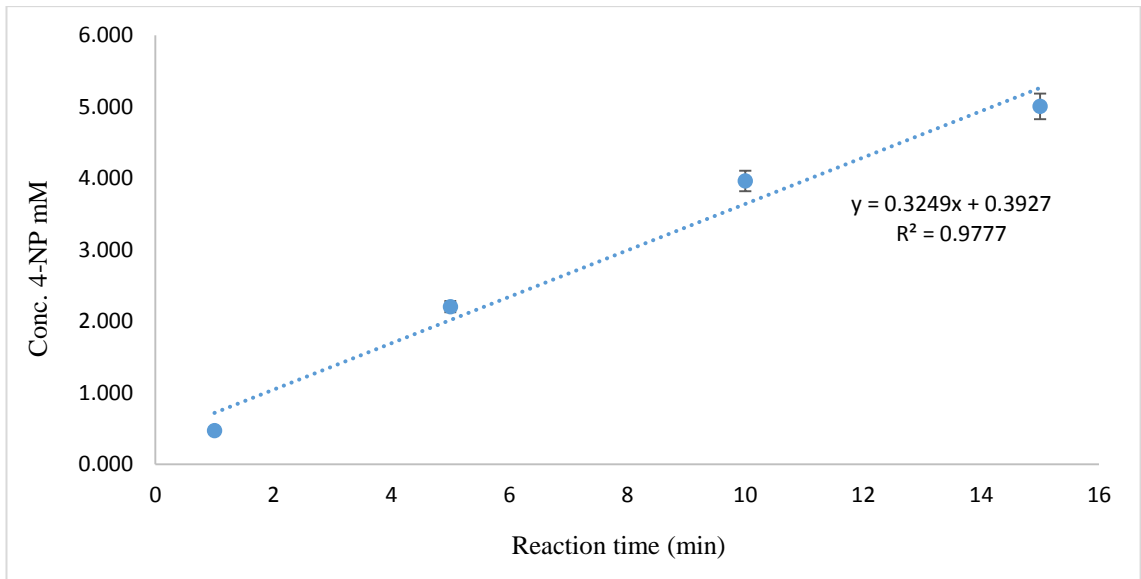


Figure 3-13. The concentration of 4-NP in mM as a function of reaction time in presence of free lipase 0.83 mg/mL.

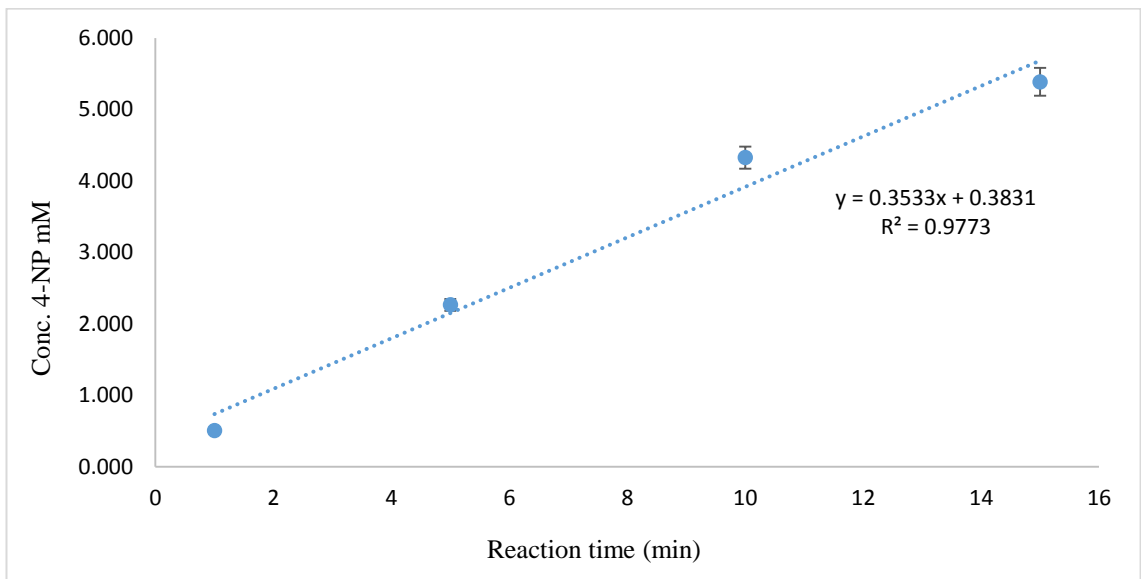


Figure 3-14. The concentration of 4-NP in mM as a function of reaction time in presence of free lipase 1.25 mg/mL.

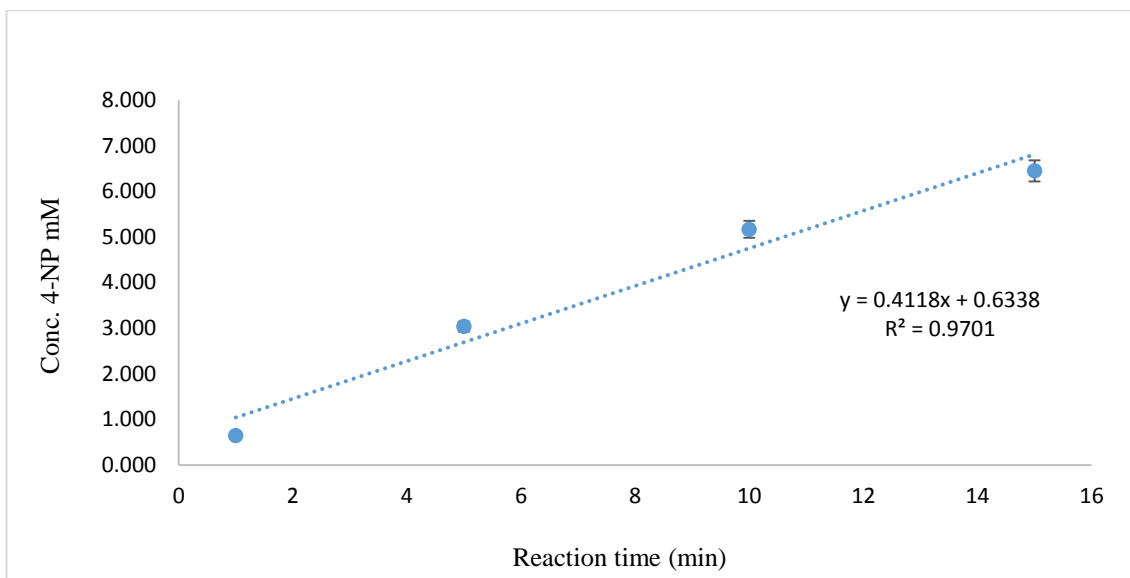


Figure 3-15. The concentration of 4-NP in mM as a function of reaction time in presence of free lipase 1.67 mg/mL.

The initial velocities mmol/min for all lipase concentrations were taken from the gradient of each curve and summarised in Table 3-8.

Table 3-8. Initial velocity (mmol/min) of each lipase concentration

Lipase conc. mg/mL	Initial velocity (mM/min)
0.02	0.008 ± 0.001
0.04	0.019 ± 0.002
0.08	0.035 ± 0.001
0.17	0.081 ± 0.002
0.33	0.156 ± 0.016
0.58	0.243 ± 0.012
0.83	0.325 ± 0.035
1.25	0.353 ± 0.038
1.67	0.412 ± 0.051

The correlation between free lipase concentrations and initial velocities are shown in Figure 3-16.

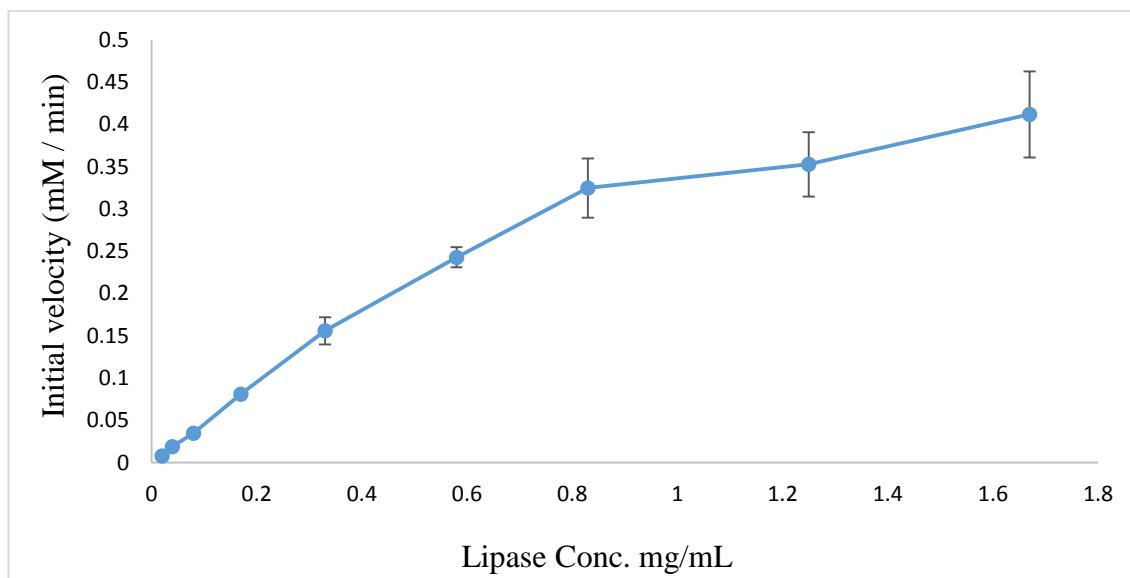


Figure 3-16. The initial velocity (mM/min) plotted versus the concentration of lipase in mg/mL.

From Figure 3-16, it can be seen that the initial velocity increases with increasing free lipase concentration. However, after a certain level between 0.6 mg/mL to 0.8 mg/mL, the increase of free lipase concentration has a little effect on initial velocity. Therefore, to have a linear correlation between the initial velocity and free lipase concentrations, the maximum free lipase concentration of 0.6 mg/mL has been chosen as shown in Figure 3-17.

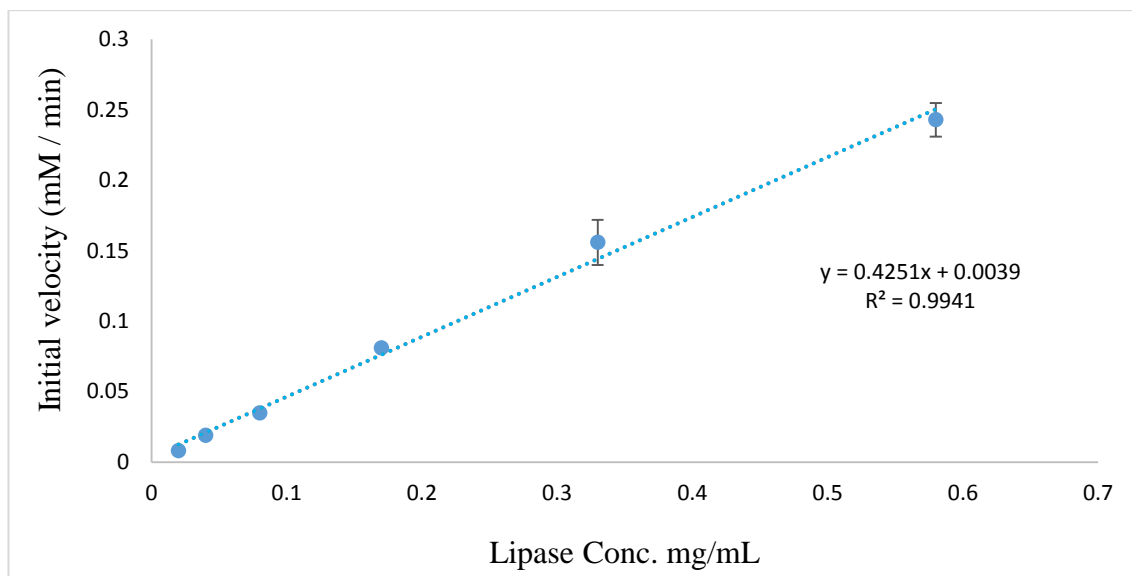


Figure 3-17. The initial velocity (mM/min) were plotted versus the concentration of lipase in mg/mL.

3.6 Kinetic study of free lipase activity

The hydrolysis reaction was carried out as explained in section 2.6.1. The average absorbance of three replicates of each sample at a given times for free lipase 1 mg/mL with 0.3, 0.5, 1, 2, 3, 4 and 5 mM 4-NPB concentrations are shown in Table 3-9.

Table 3-9. Absorbance of 4-NP as a function of time for different free lipase concentrations

Conc. of 4-NPB mM		Time (min)					
		1	2.5	5	10	15	20
0.3	Abs.	0.001	0.002	0.003	0.004	0.006	0.007
	Error	0.000	0.000	0.001	0.000	0.002	0.000
0.5	Abs.	0.004	0.005	0.006	0.01	0.014	0.017
	Error	0.002	0.001	0.000	0.001	0.003	0.002
1	Abs.	0.005	0.009	0.012	0.02	0.032	0.037
	Error	0.001	0.003	0.002	0.000	0.001	0.003
2	Abs.	0.009	0.012	0.021	0.032	0.039	0.063
	Error	0.002	0.003	0.000	0.004	0.001	0.001
3	Abs.	0.014	0.024	0.032	0.05	0.071	0.085
	Error	0.005	0.004	0.000	0.002	0.003	0.000
4	Abs.	0.026	0.037	0.053	0.079	0.109	0.131
	Error	0.004	0.000	0.003	0.001	0.001	0.004
5	Abs.	0.02	0.033	0.044	0.077	0.112	0.136
	Error	0.000	0.003	0.001	0.000	0.002	0.006

As explained earlier the absorbance were used to calculate the concentration of 4-NP by using the Equation 3-2. The results were summarized in Table 3-10.

Table 3-10. Concentration of 4-NP in mg/mL as a function of time

Conc. Of 4-NPB mM		Time (min)					
		1	2.5	5	10	15	20
0.3	Conc. mg/mL	0.001	0.002	0.003	0.004	0.005	0.007
	Error	0.000	0.000	0.001	0.000	0.002	0.000
0.5	Conc. mg/mL	0.003	0.004	0.005	0.009	0.012	0.015
	Error	0.002	0.001	0.000	0.001	0.003	0.002
1	Conc. mg/mL	0.004	0.008	0.010	0.017	0.028	0.032
	Error	0.001	0.003	0.002	0.000	0.001	0.003
2	Conc. mg/mL	0.008	0.010	0.018	0.028	0.034	0.055
	Error	0.002	0.003	0.000	0.004	0.001	0.001
3	Conc. mg/mL	0.012	0.021	0.028	0.043	0.062	0.074
	Error	0.005	0.004	0.000	0.002	0.003	0.000
4	Conc. mg/mL	0.023	0.032	0.046	0.069	0.095	0.114
	Error	0.004	0.000	0.003	0.001	0.001	0.004
5	Conc. mg/mL	0.017	0.029	0.038	0.067	0.097	0.118
	Error	0.000	0.003	0.001	0.000	0.002	0.006

Then the concentration of 4-NP was converted from mg/mL to mM as shown in Table 3-11 by using the Equation 3-3.

Table 3-11. Concentration of 4- NP in mM as a function of time

Conc. Of 4- NPB mM		Time (min)					
		1	2.5	5	10	15	20
0.3	Conc. mM	0.006	0.012	0.019	0.031	0.037	0.050
	Error	0.000	0.000	0.001	0.000	0.002	0.000
0.5	Conc. mM	0.025	0.031	0.037	0.062	0.087	0.106
	Error	0.002	0.001	0.000	0.001	0.003	0.002
1	Conc. mM	0.031	0.056	0.075	0.125	0.200	0.231
	Error	0.001	0.003	0.002	0.000	0.001	0.003
2	Conc. mM	0.056	0.075	0.131	0.200	0.0243	0.393
	Error	0.002	0.003	0.000	0.004	0.001	0.001
3	Conc. mM	0.087	0.150	0.200	0.312	0.443	0.530
	Error	0.005	0.004	0.000	0.002	0.003	0.000
4	Conc. mM	0.162	0.231	0.330	0.493	0.680	0.817
	Error	0.004	0.000	0.003	0.001	0.001	0.004
5	Conc. mM	0.125	0.206	0.274	0.480	0.698	0.848
	Error	0.000	0.003	0.001	0.000	0.002	0.006

The velocity of the reaction (initial velocity) is the slope of the linear phase, expressed as amount of product formed per time as shown in Figure 3-18 to Figure 3-24.

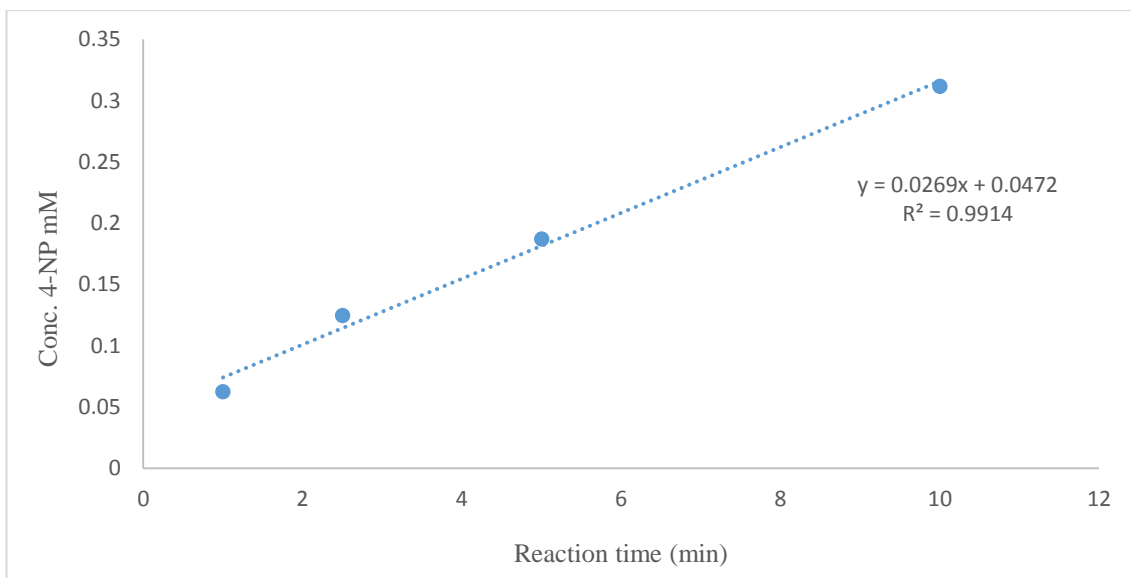


Figure 3-18. The concentration of 4-NP in mM as a function of reaction time in 0.3 mM of 4-NPB.

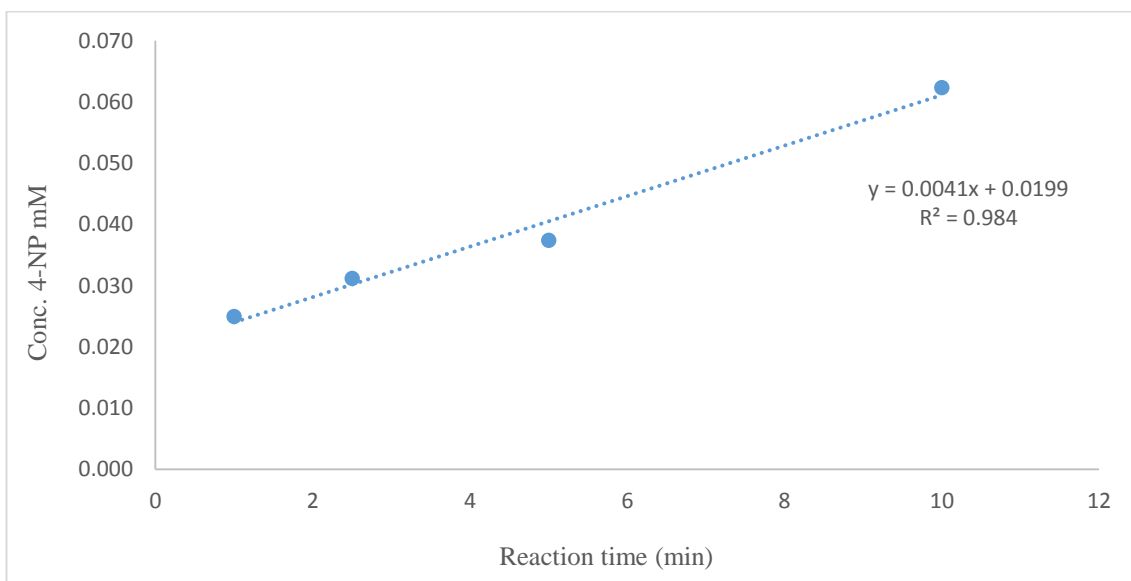


Figure 3-19. The concentration of 4-NP in mM as a function of reaction time in 0.5 mM of 4-NPB.

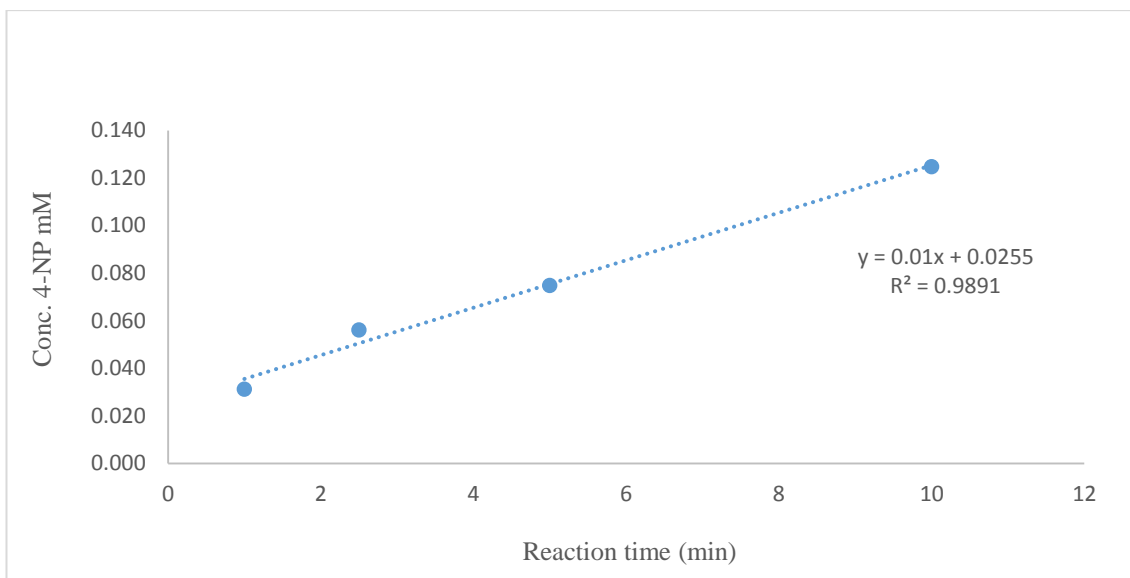


Figure 3-20. The concentration of 4-NP in mM as a function of reaction time in 1 mM of 4-NPB.

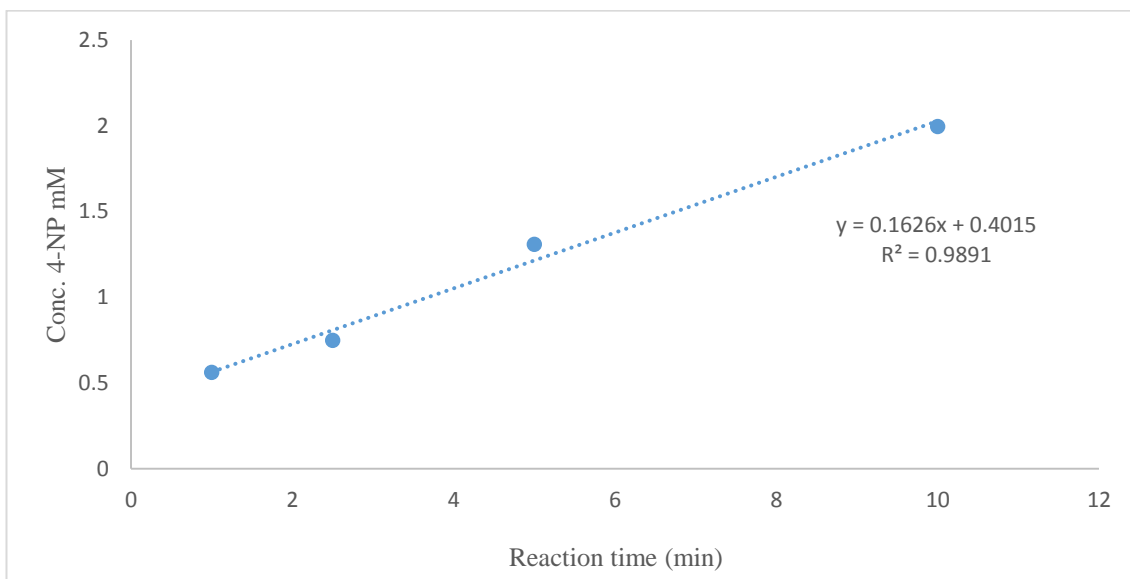


Figure 3-21. The concentration of 4-NP in mM as a function of reaction time in 2 mM of 4-NPB.

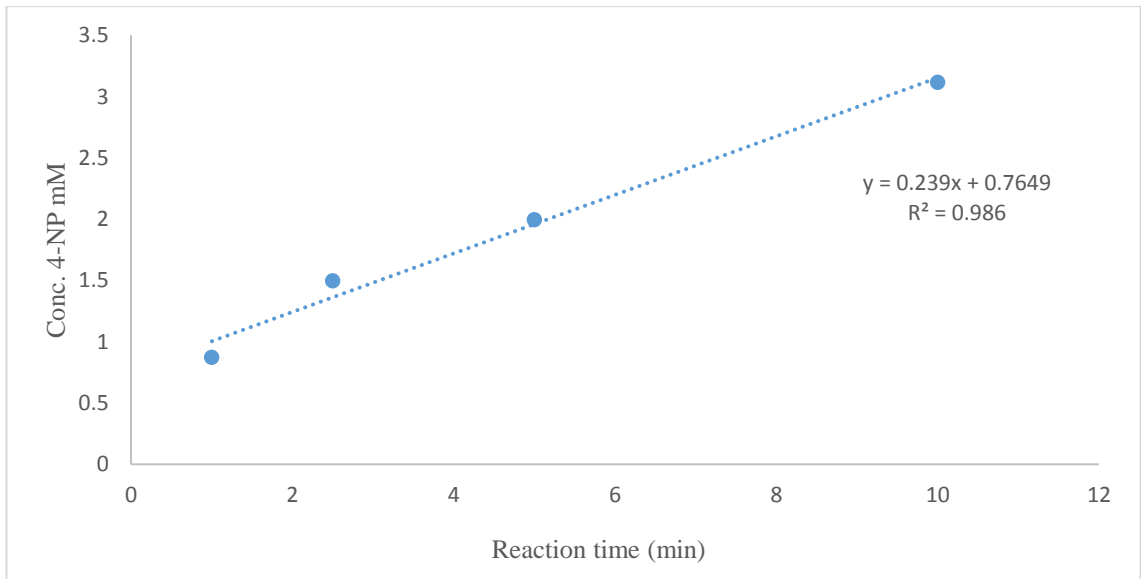


Figure 3-22. The concentration of 4-NP in mM as a function of reaction time in 3 mM of 4-NPB.

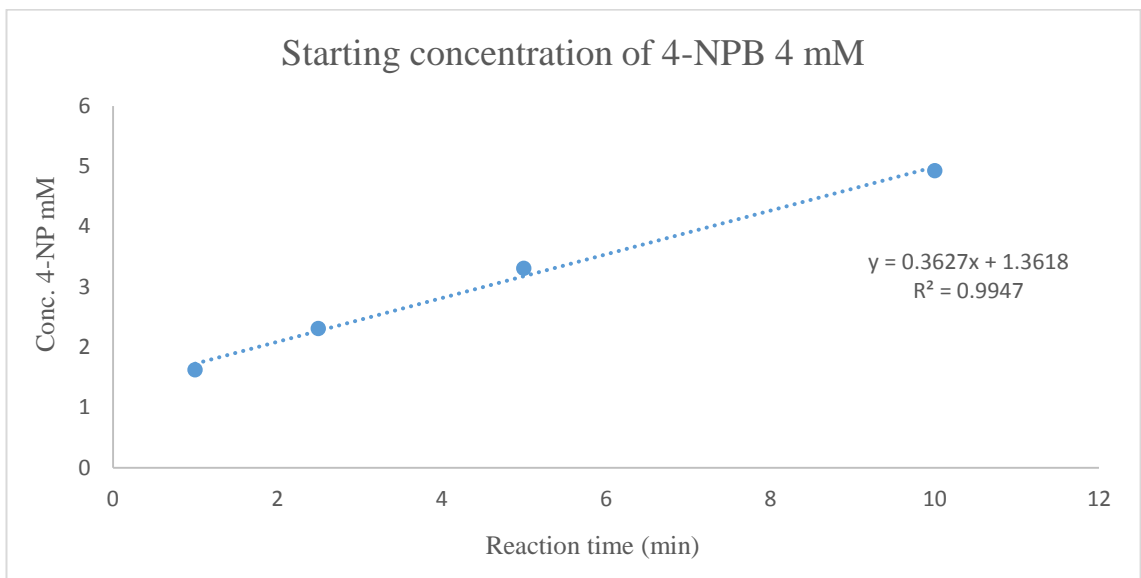


Figure 3-23. The concentration of 4-NP in mM as a function of reaction time in 4 mM of 4-NPB.

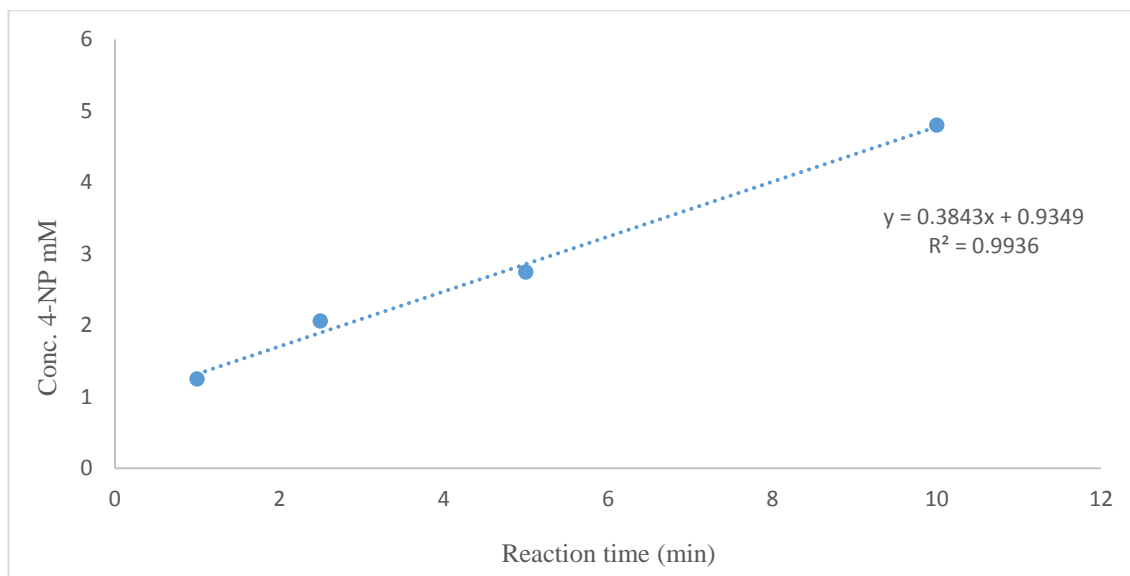


Figure 3-24. The concentration of 4-NP in mM as a function of reaction time in 5 mM of 4-NPB.

The slope of each curve is the initial velocity for the lipase catalyst at specific starting concentration of 4-NPB. The unit of initial velocity is mM min^{-1} . This is the amount of 4-NP produced every minute at a certain starting concentration of 4-NPB. Table 3-12 summarises the initial velocity values at different starting concentrations of 4-NPB. The amount of lipase used in all the reactions was 0.6 mg therefore for ease of calculations, and converted the initial velocity to mg/min which is also summarised in Table 3-12.

Table 3-12. Initial velocity (mmol/min) of each 4-NPB concentration

Concentration of 4-NPB (mM)	Initial velocity (mM /min)	Initial velocity (mg /min)
0.3	0.0027	0.0004
0.5	0.0041	0.0006
1	0.0100	0.0014
2	0.0163	0.0023
3	0.0239	0.0033
4	0.0363	0.0050
5	0.0384	0.0053

An example of the calculation is shown below:

$$\frac{0.0027}{\text{min}} \times \frac{M}{1000 \text{ mM}} = \frac{0.0000027 \text{ mol}}{L \cdot \text{min}} \times \frac{139.11 \text{ g}}{\text{mol}} = \frac{0.00037 \text{ g}}{L \cdot \text{min}} \times \frac{1000 \text{ mg}}{\text{g}} \times \frac{L}{1000 \text{ mL}} = \frac{0.00037 \text{ mg}}{\text{mL} \cdot \text{min}}$$

Therefore for 1 mL reaction volume, the initial velocity is 0.00037 mg/min.

By plotting 1/initial velocity against 1/concentration of 4-NPB, K_m and V_{\max} values for free CAL can be calculated as explained in section 1.4.9 .

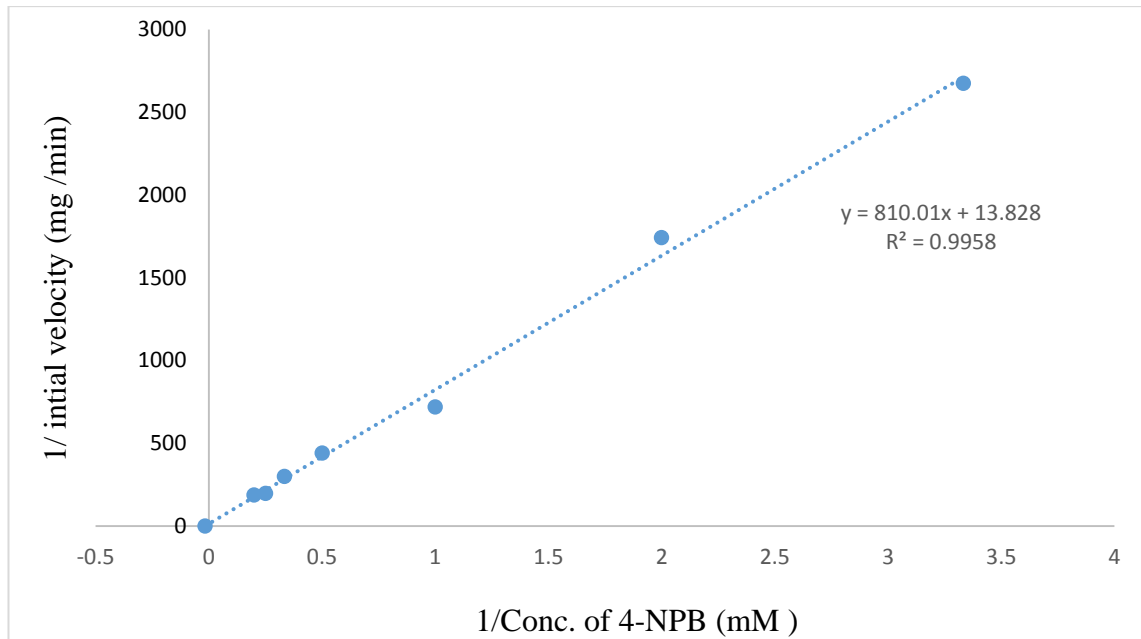


Figure 3-25. Lineweaver–Burk double reciprocal plot for free lipase.

To determine the parameters of the free lipase kinetics the Lineweaver Equation 1-7 as explained in section 1.4.9, was used:

V_{\max} was calculated from the Y-axis intercept = $1/13.82 = 0.0723 \text{ mg min}^{-1}$.

The turn-over number was calculated according to the Equation 1-8.

$k_{\text{cat}} = (V_{\max}/ [\text{lipase}]) = 0.0723 \text{ mg min}^{-1}/0.6 \text{ mg} = 0.120 \text{ min}^{-1}$ (the amount of lipase added to each reaction was constant 0.6 mg).

$K_m = \text{slope} \times V_{\max} = 810.01 \times 0.0723 = 58.57 \text{ mM}$.

The K_m and K_{cat} values will be used to compare the free lipase activity with the immobilised lipase.

3.7 Determination of lipase loading in the immobilised monolith microreactor

The amount of lipase used for immobilisation was 10 mg lipase in 10 mL Tris-HCl buffer pH7. The quantity of the immobilised lipase was determined by calculating the difference between the amount of lipase in the initial loading solution and that in the residual solution collected after the entrapping process, which was quantified using a calibration curve of 4-NP. The 0.6 mL of solution used as aqueous phase in the reaction was added to 0.4 mL organic solution containing 10 mM 4-NPB in decane. The 4-NP was analysed by UV. The results are shown in Table 3-13.

Table 3-13 Analysis of collected solution after the loading of free lipase.

Time min	Absorbance	Conc.4-NP mg/mL	Conc.4-NP mM
1	0.013	0.011	0.081
5	0.029	0.025	0.181
10	0.06	0.052	0.374
15	0.091	0.079	0.567

To determine the initial velocity of the reaction, the concentration of 4-NP in mM was plotted against time as shown in Figure 3-26.

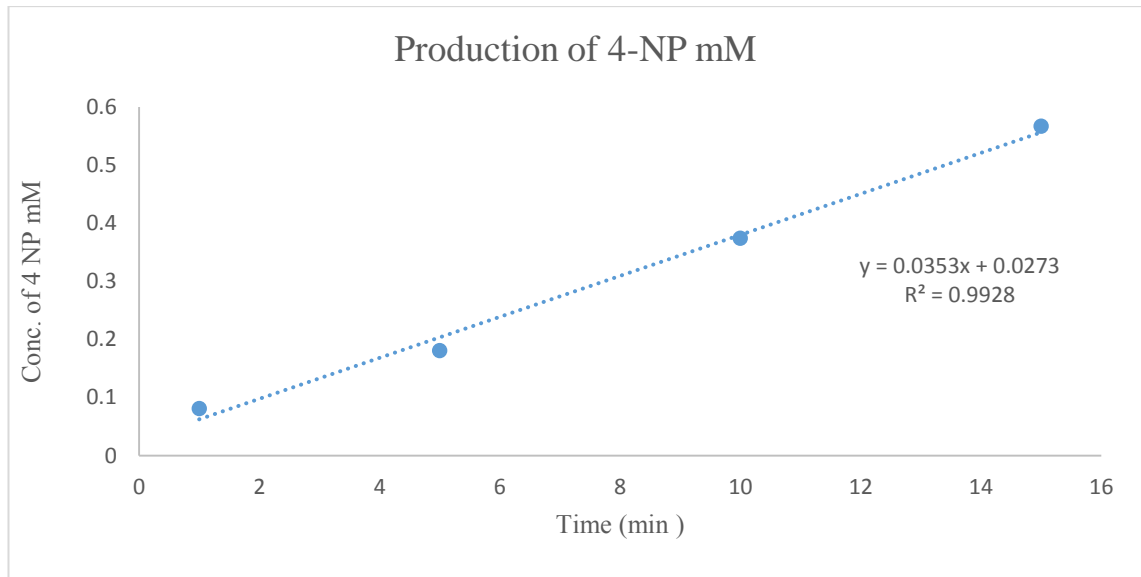


Figure 3-26. The concentration of 4-NP in mM as a function of reaction time in presence of free lipase.

The initial velocity (slope) was found to be 0.0353 mM/min and by using the initial velocity curve equation in Figure 3-17.

$$\text{Un-immobilized Lipase conc.} = (0.0353 - 0.004) / 0.4247 = 0.073 \text{ mg/mL}$$

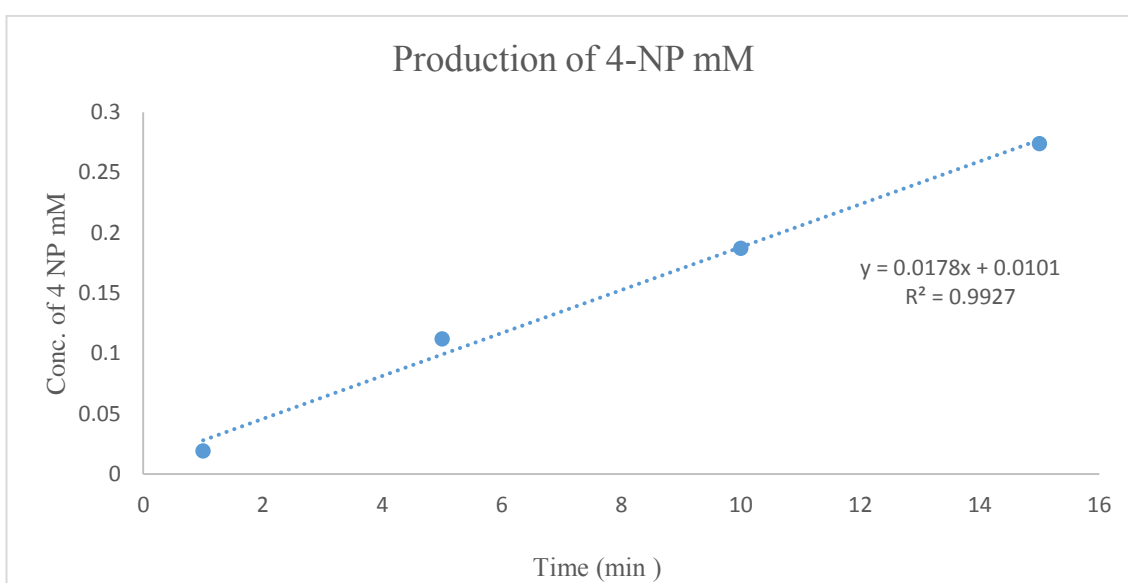
The amount of collected solution was 10 mL therefore the amount of un-immobilised lipase was 0.73 mg. Based on this information, the amount of lipase immobilised in the monoliths was calculated to be: immobilised lipase = 10 – 0.73 = 9.27 mg.

Then the monolith was washed with 10 mL Tris-HCl buffer pH7 0.05 M.

Table 3-14. Analysis of collected solution after the first washing of the immobilised lipase.

Time min	Absorbance	Conc.4-NP mg/mL	Conc.4-NP mM
1	0.003	0.003	0.019
5	0.018	0.016	0.112
10	0.03	0.026	0.187
15	0.044	0.038	0.274

To determine the initial velocity of the reaction, the concentration of 4-NP in mM was plotted against time as shown in Figure 3-27.

**Figure 3-27. The concentration of 4-NP in mM as a function of reaction time after the first washing with Tris-HCL buffer.**

The washing solution was collected and used as aqueous phase in the reaction to check if any lipase leached from the monolith during the washing step or not.

The initial velocity (slope) was found to be 0.0178 mM.

Leached lipase conc. = $(0.0178 - 0.004) / 0.4247 = 0.032$ mg/mL

The amount of washing solutions was 10 mL; therefore, the amount of leached lipase is 0.32 mg. As mentioned earlier the expected amount of total lipase on the monolith was 9.27 mg, so, after washing the total amount of immobilised lipase was estimated = $9.27 - 0.32 = 8.95$ mg.

Then the monolith was washed again with 10 mL Tris-HCl buffer pH7 0.05 M.

Table 3-15. Analysis of collected solution after the second washing of the immobilised lipase.

Time min	Absorbance	Conc. 4-NP mg/mL	Conc. 4-NP mM
1	0.005	0.004	0.031
5	0.012	0.010	0.075
10	0.019	0.016	0.118
15	0.025	0.022	0.156

To determine the initial velocity of the reaction, the concentration of 4-NP in mM was plotted against time as shown in Figure 3-28.

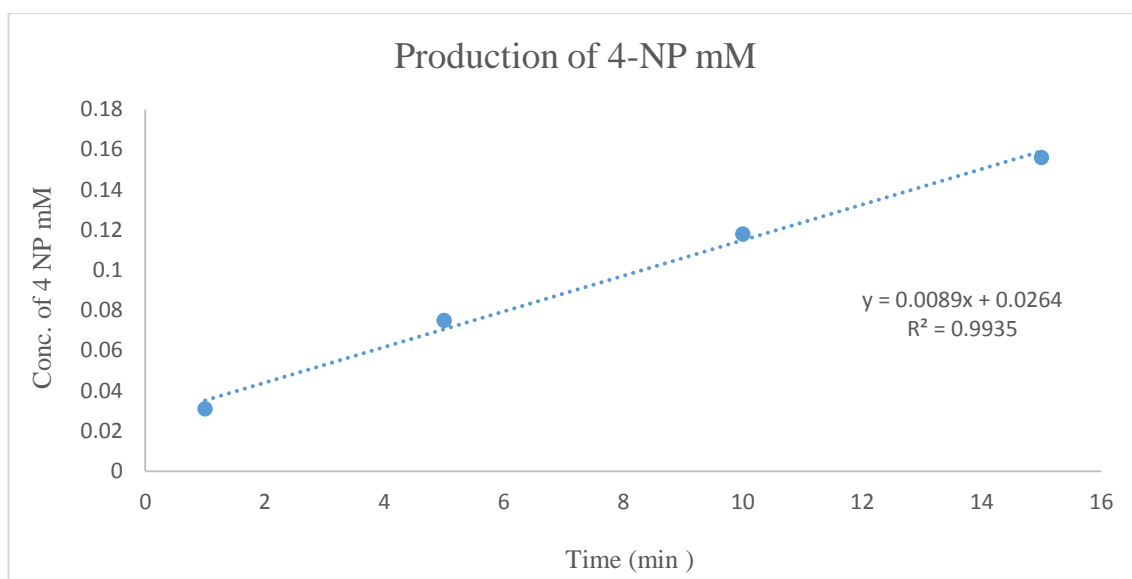


Figure 3-28. The concentration of 4-NP in mM as a function of reaction time after the second washing with Tris-HCL buffer.

The initial velocity (slope) was found to be 0.0089 mM/min by using the initial velocity curve equation in Figure 3-17.

Leached lipase conc. = $(0.0089 - 0.004) / 0.4247 = 0.011$ mg/mL

The amount of washing solutions was 10 mL; therefore, the amount of leached lipase is 0.11 mg. As mentioned earlier the expected amount of total lipase on the monolith was 8.95 mg, so, after washing the total amount of immobilised lipase was estimated = $8.95 - 0.11 = 8.84$ mg.

The same method was used for other monoliths M3 and M5. The results are summarised in Table 3-16.

Table 3-16 Summary of lipase concentration on different monoliths.

Sample	Amount of lipase loading in silica monolith (mg)
M1	8.8
M3	8.2
M5	9.2

3.8 Evaluation of the kinetic parameters for immobilized lipase

Kinetic constants for the immobilized CAL were obtained from the Lilly–Hornby model as explained in section 2.6.1 and the kinetics were calculated as discussed in section 1.4.10 through the following Equation 3-4:

$$C_{in} - C_{out} = K_m \ln \frac{C_{out}}{C_{in}} + \frac{V_{max} V_{void}}{Q} \quad \text{Equation 3-4}$$

Table 3-17. Lilly–Hornby for the immobilised lipase on the silica monolith microreactor (M1)

Abs.	4-NP. mg/mL	4-NP. mM	C _{in}	C _{out}	C _{out} /C _{in} mM	-Ln (C _{out} /C _{in})
0.008	0.008	0.061	0.1	0.039	0.394	0.931
0.027	0.023	0.168	0.3	0.132	0.439	0.824
0.043	0.037	0.268	0.5	0.232	0.464	0.768
0.073	0.063	0.455	1	0.545	0.545	0.607
0.111	0.096	0.692	2	1.308	0.654	0.425

The Lilly-Hornby plot for the immobilised lipase on the silica monolith microreactor (M1) can be seen in Figure 3-29.

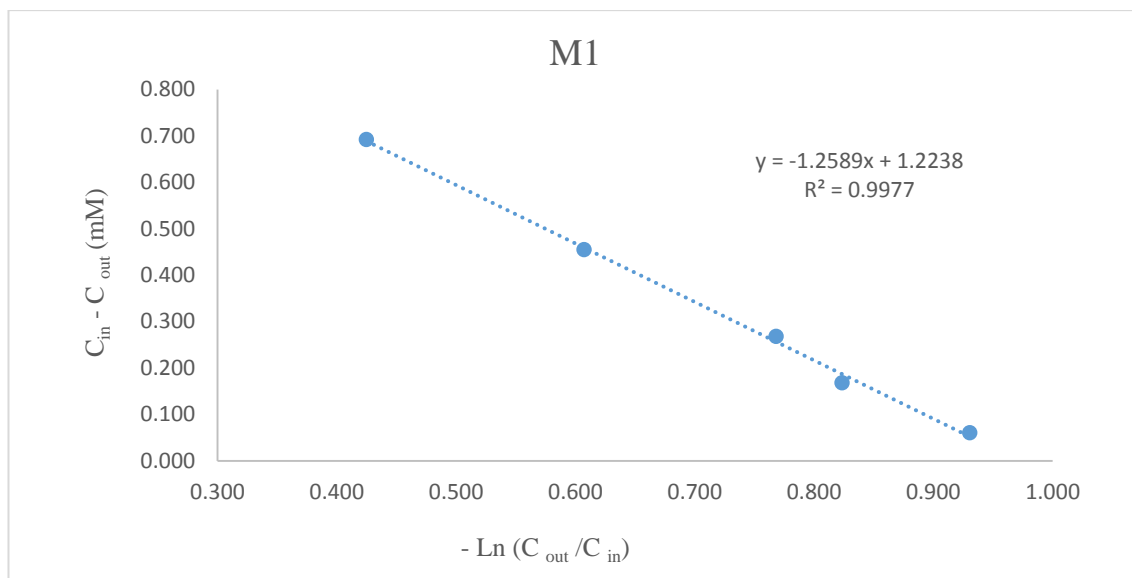


Figure 3-29. Lilly–Hornby plots of the immobilised lipase for immobilised lipase on monolith microreactor (M1).

Table 3-18. Lilly–Hornby for the immobilized lipase on the silica monolith microreactor (M3)

Abs.	4-NP. mg/mL	4-NP. mM	C_{in}	C_{out}	C_{out}/C_{in} mM	$-\ln$ (C_{out}/C_{in})
0.184	0.194	1.393	2	0.607	0.30	1.19
0.235	0.266	1.916	3	1.084	0.36	1.02
0.312	0.329	2.362	4	1.638	0.41	0.89
0.361	0.380	2.733	5	2.267	0.45	0.79

The Lilly-Hornaby plot for the immobilised lipase on the silica monolith microreactor (M3) can be seen in Figure 3-30.

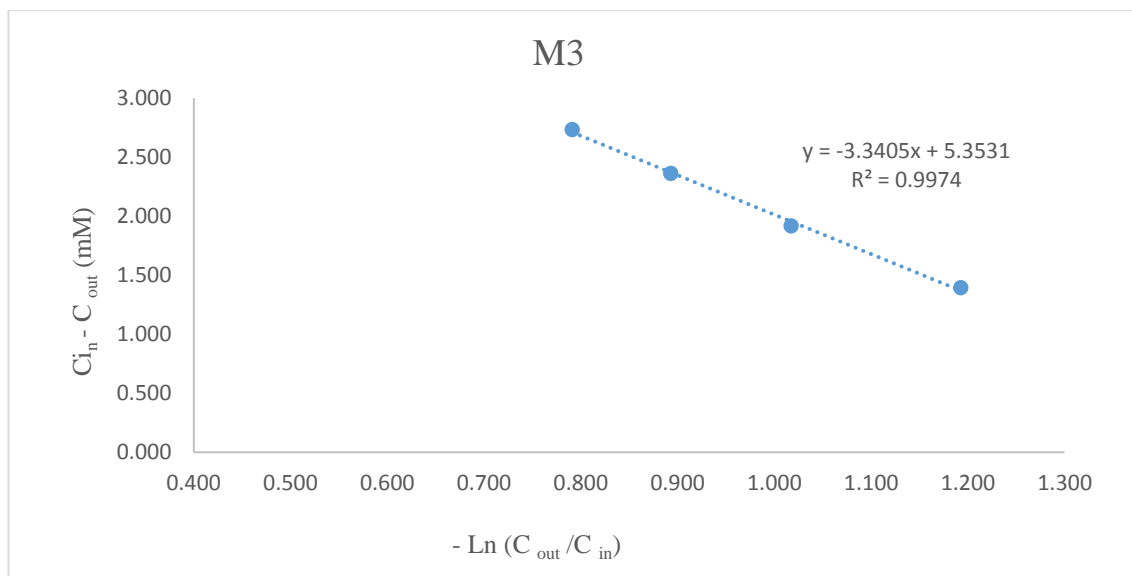


Figure 3-30. Lilly–Hornby plots of the immobilized lipase for immobilised lipase on monolith microreactor (M3).

Table 3-19. Lilly–Hornby for the immobilized lipase on the silica monolith microreactor (M5)

Abs.	4-NP. mg/mL	4-NP. mM	C_{in}	C_{out}	C_{out}/C_{in} mM	$-\ln$ (C_{out}/C_{in})
0.025	0.026	0.189	0.3	0.111	0.37	0.997
0.039	0.041	0.295	0.5	0.205	0.41	0.839
0.069	0.073	0.522	1	0.478	0.48	0.739
0.106	0.112	0.803	2	1.197	0.60	0.513

The Lilly-Hornaby plot for the immobilised lipase on the silica monolith microreactor (M5) can be seen in Figure 3-31.

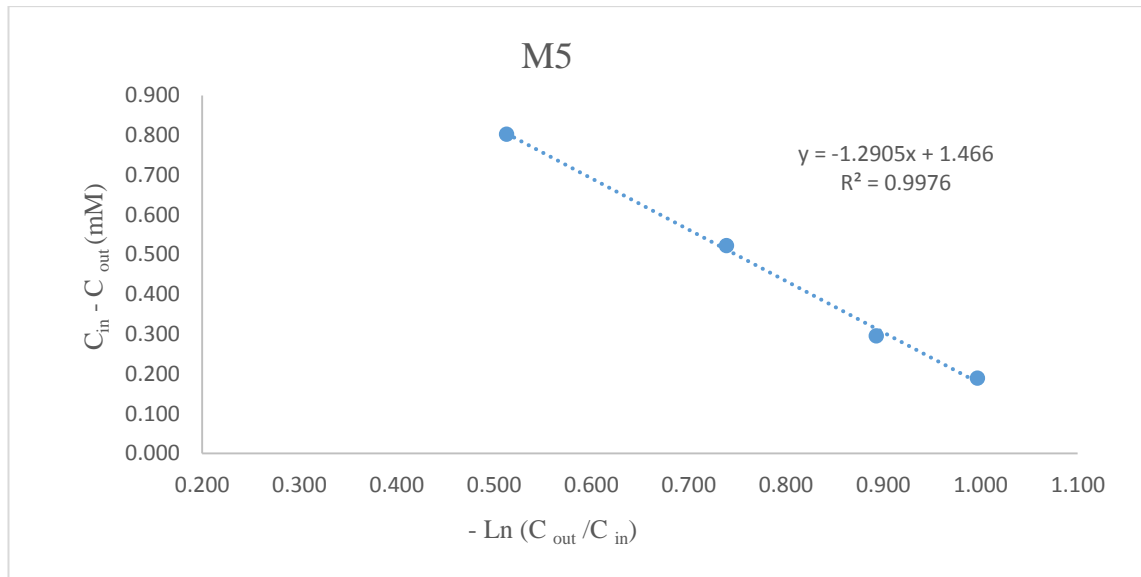


Figure 3-31. Lilly–Hornby plots of the immobilized lipase for immobilised lipase on monolith microreactor (M5).

To calculate the kinetics of the immobilised lipase on the microreactor the Lilly–Hornby plots and equation were used. The K_m can be obtained directly by determination of the slope and the intercept was multiply by the 4-NP molecular weight to convert the concentration from mM to mg/L and to obtained the V_{max} value the concentration of the intercept in mg/L multiply by Q the flow rate 0.0025 mL/min of the flow reaction divided on the V_{void} (0.34 mL) and the K_{cat} was calculated by divide the V_{max} on the lipase concentration. The kinetic constants calculated for free and immobilized lipase are summarized in Table 3-20.

Table 3-20. Kinetic evaluations for free and immobilized lipase

Lipase	Reactions kinetics		
	K_m (mM)	K_{cat} (min^{-1})	V_{max} mg min^{-1}
Free lipase	58.6	0.12	0.072
Immobilised lipase (M1)	1.250	0.139	1.251
Immobilised lipase (M3)	3.340	0.608	5.475
Immobilised lipase (M5)	1.291	0.166	1.499

It can be seen that the immobilised K_m values are 1.240, 3.340 and 1.239 mM for M1, M3 and M5 respectively. These values were found to be 18 to 47 times lower than the K_m for the free CAL in solution (58.6 mM), indicating a favourable affinity between substrate and the substrate binding site of the enzyme. The turn over numbers of immobilised lipase were however much higher than the free lipase indicating that the flow microreactor system offers higher or productivity than the batch reactor. Moreover, M3 shows higher affinity to the substrate than M1 and this could be due to two reasons, the average pore diameters in M3 is smaller than M1 and that increase the contact and interactions between immobilized lipase in the surface with the substrate inside the channel. This may also explain why the activity dropped with the use of the M5 microreactor with the largest average pore diameter. The indication is therefore that it is better to use microreactor with small average pore diameter.

3.9 Conclusions

Different approaches have been reported for producing macro porous silica-monoliths with different physical properties. M1, M2, M3, M4, M5 and M6 were prepared with different surface areas 529 m²/g, 470 m²/g, 460 m²/g, 494 m²/g, 218 m²/g, and 222 m²/g respectively. M1, M3, M5 were used for lipase immobilization to generate active and stable immobilized lipase microreactors for biocatalysis. Homogeneous *Candida antarctica* lipase (CAL) were reported to exhibit high activity for the hydrolysis of 4-NPB in water–decane media and there was a linear relation between the concentrations of free lipase and the initial velocity of the hydrolysis reaction. Accurate methodology was applied to assay the quantity of immobilized lipase on M1, M3 and M5. Immobilised lipase were found to exhibit higher activity than free lipase for the hydrolysis of 4-NPB indicating that using flow microreactor can have a significant effect on the activity of lipase. By decreasing the microreactor average pore diameter, the activity of immobilised lipase increased.

Chapter 4. Development of the Silica Monolith microreactors for biodiesel production

In this study, lipase was trapped into silica monolith channels in order to overcome the high cost of lipase and its recyclability. *Candida antarctica* lipase was used as it is the most effective lipase for triglycerides conversion into biodiesel. The immobilised lipase silica monolith was used as a microreactor for transesterification reaction.

The effect of varying the silica monolith supports on which to immobilise lipase was also investigated. The large surface area and good flow-through and minimal backpressure qualities distinguish silica monoliths as favourable substrates for enzyme immobilisation. The silica scaffold structures also lend themselves to a high loading capacity and remain stable for long periods. Furthermore, the microreactor channels provide a large surface area on which enzymes can be immobilised.

To determine that immobilisation was successful, the amount of free lipase was estimated from its initial velocity in a hydrolysis reaction of 4-nitrophenylbutyrate to 4-nitrophenol, as explained in Chapter 3. The effectiveness of the immobilised lipase microreactor was tested by quantifying the transesterification of tributyrin to methyl butyrate. To determine the identity of the products and their respective quantities, reversed phase liquid chromatography and a UV detector were used.

The majority of the literature addressed immobilised lipase on polymer supports rather than silica supports; few papers that have considered silica supports have not explored the relationship between the physical properties of the support and the lipase activity. Therefore, this is a pioneering study, investigating the physical properties of the silica monolith upon lipase in a biodiesel reaction.

Our results indicate that the activity of immobilised lipase varies in accordance with different monolith structures. As presented in chapter 3, the K_m , K_{cat} and V_{max} values show there is a relationship between monolith pore size and lipase activity. In this chapter, the study is extended to determine the optimal conditions for the reaction. The optimal condition factors, such as the molar ratio of alcohol to oil, temperature and flow rate, were investigated.

4.1 Calibration curve of tributyrin

Before performing the calibration of the HPLC, a sample of diluted tributyrin was tested with UV-visible spectroscopy to obtain the maximum wavelength where the sample absorbs most of the light. Figure 4-1 shows that the maximum wavelength for tributyrin is 210 nm. This wavelength was set on the UV detector for the HPLC studies.

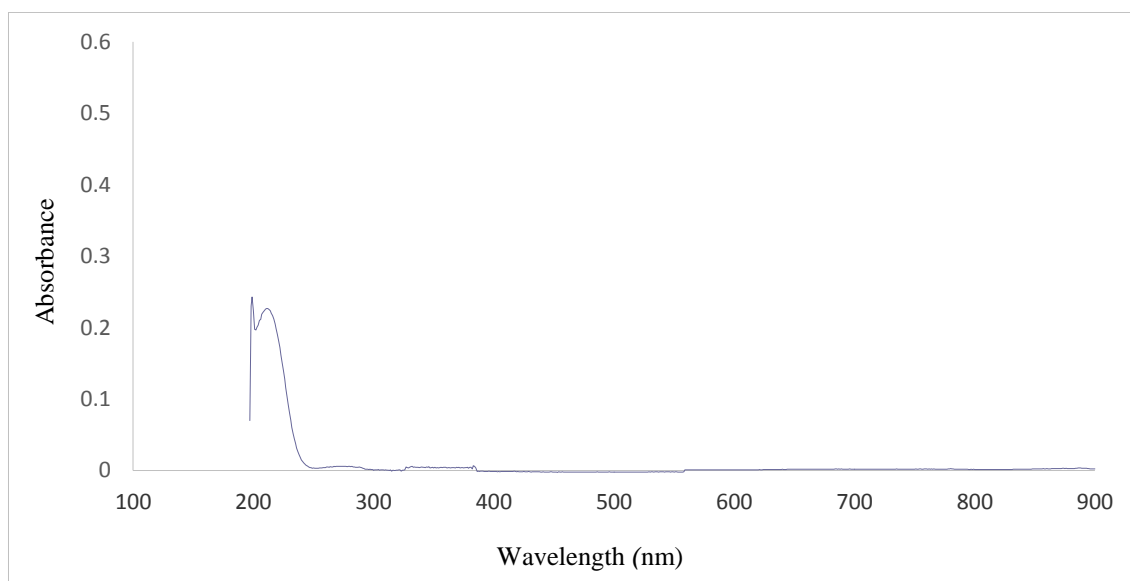
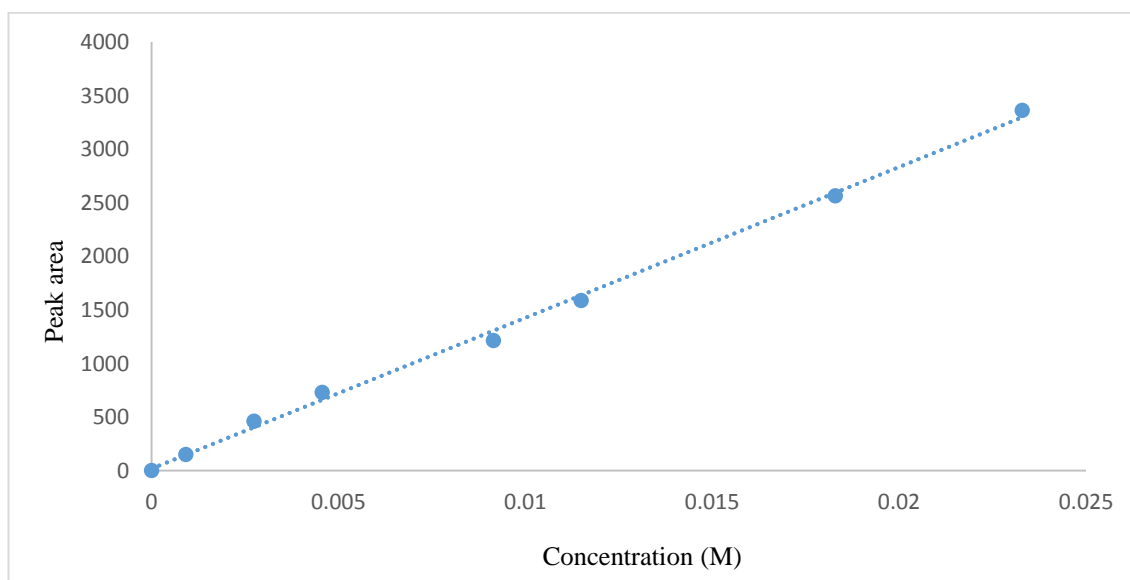


Figure 4-1. Wavelength scan of tributyrin from 199 to 900 nm.

Table 4-1, shows the calibration standards used to establish the calibration curve and the HPLC response.

Table 4-1. The peak area of tributyrin measured under varied concentration

Concentrations (M)	Peak area
0	0
0.000916	151
0.00274	461
0.00457	729
0.00915	1215
0.0115	1586
0.0183	2563
0.0233	3363

**Figure 4-2 . Calibration curve of tributyrin.**

Calibration curves for the reactant showed linearity between concentration and peak area and produced a correlation coefficient (R^2) ≥ 0.997 . Table 4-2 presents the linearity, LOD, standard deviation that were calculated from the calibration curve according to Equation 4-1:

$$y_{LOD} = y_B + 3 S_{yx} \quad \text{Equation 4-1}$$

Table 4-2. Analytical figures for tributyrin

Linearity	$y = 140711x + 19228$
Correlation coefficient	0.9976
Standard deviation of slope S_b	3397
Standard deviation of slope S_a	43
Random error of peak height direction $S_{y/x}$	69
LOD (3sd) (M)	0.00148

Limit of detection (LOD) is calculated from blank signal plus 3 standard deviations of the blank. These values estimated from the intercept and $S_{y/x}$.

4.2 Calibration curve of methyl butyrate

UV-visible spectroscopy study showed that the maximum wavelength for methylbutyrate is 207 nm as shown in the Figure 4-3.

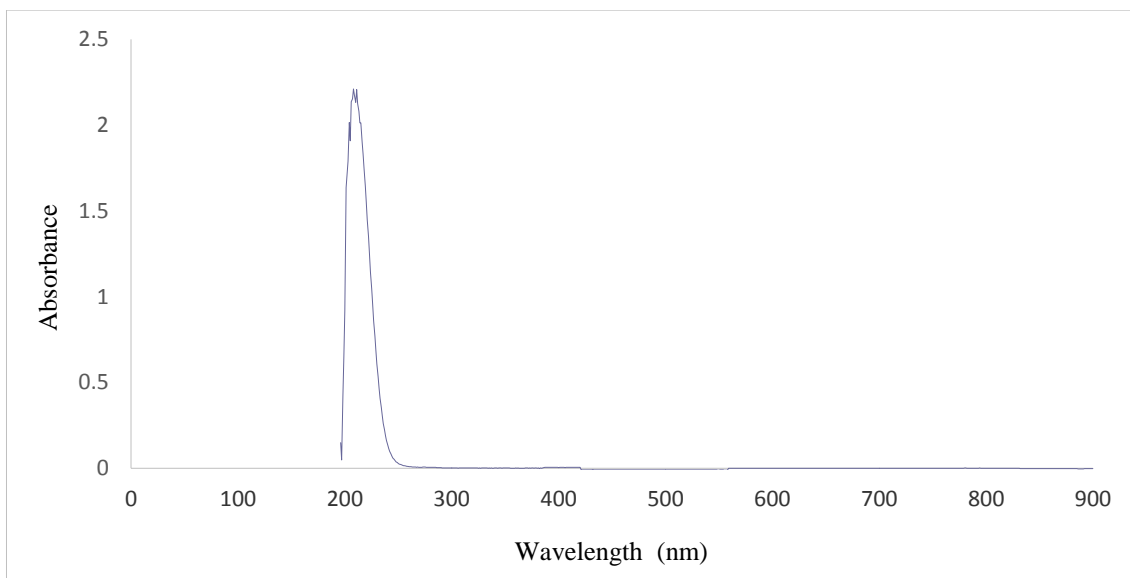


Figure 4-3. Wavelength scan of methyl butyrate from 199 to 900 nm.

Table 4-3, shows the calibration standards used to establish the calibration curve and the HPLC response.

Table 4-3. The peak area of methyl butyrate measured under varied concentration

Concentrations (M)	Peak area
0	0
0.005	320
0.01	505
0.02	903
0.04	1620
0.06	2454
0.08	3187

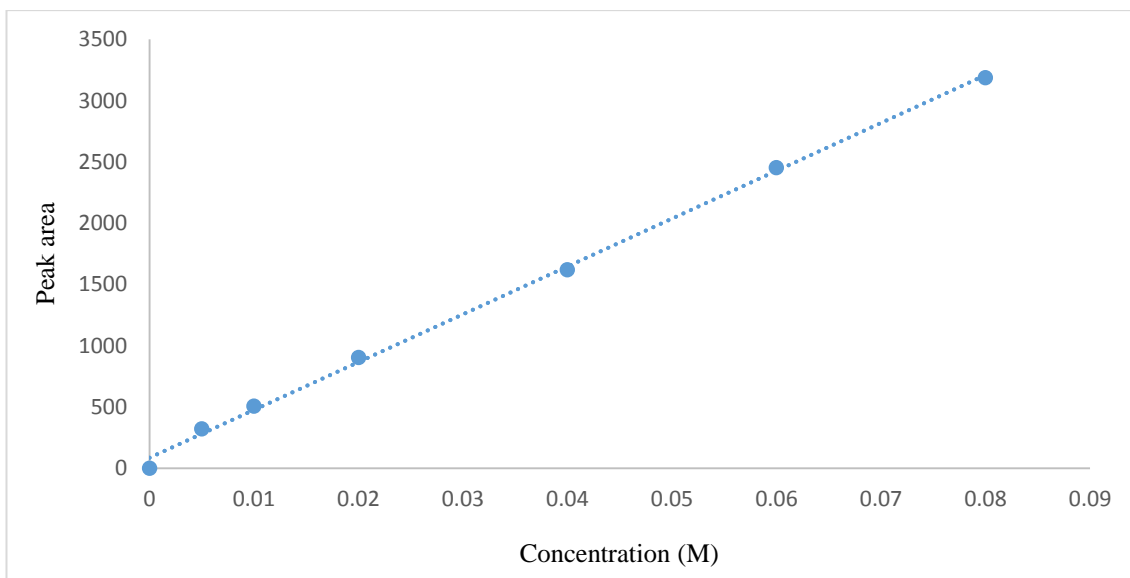


Figure 4-4. Calibration curve of methyl butyrate.

As shown in Figure 4-4, there is a linear relationship between the concentrations and peak area and produced a correlation coefficient ($R^2 \geq 0.998$). Table 4-4 presents the linearity, LOD, standard deviation that were calculated from the calibration curve according to Equation 4-1.

Table 4-4. Analytical figures for methyl butyrate:

Linearity	$y = 39051x + 84.708$
Correlation coefficient	0.9985
Standard deviation of slope S_b	684.4
Standard deviation of slope S_a	28.4
Random error of peak height direction $S_{y/x}$	50.8
LOD (3sd) (M)	0.00391

Limit of detection (LOD) is calculated from blank signal plus 3 standard deviations of the blank. These values estimated from the intercept and $S_{y/x}$.

4.3 Catalytic activity

The reaction mixture was injected into the HPLC before and after the reaction to calculate the conversion of tributyrin. As shown in Figure 4-5, tributyrin peaks at 3.26 min before the reaction was decreased in the end of the reaction while a new peak appeared at 2.00 minutes which is the same retention time of methyl butyrate according to the calibration method.

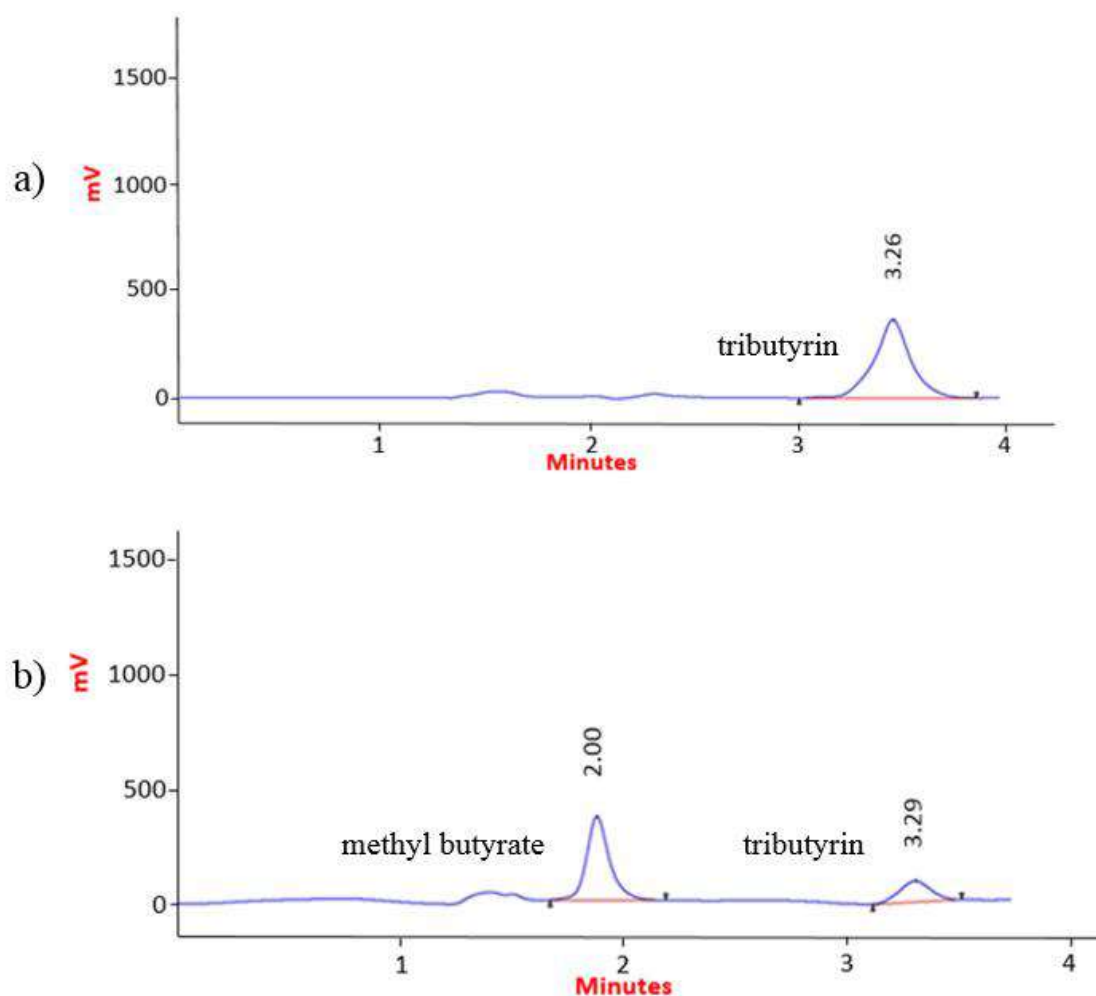


Figure 4-5. HPLC peaks of transesterification reaction of tributyrin (a): before the reaction, (b): after the reaction). Peak at 3.2 min assigned to tributyrin and peak at 2.00 min assigned to methyl butyrate.

4.3.1 Catalytic activity of the lipase immobilised on the silica monolith microreactors (M1, M3 and M5)

For the enzymatic free silica monolith microreactors with molar ratio methanol to tributyrin 2:1 the yield of methyl butyrate was 1.27% while the yields with molar ratio 3:1 was 2.11 %. (Reaction conditions: temperature at 30 °C and flow rate 0.8 µl/min).

In the batch reactor only 21.7 % of methyl butyrate was obtained after 48 hours of reaction. (Reaction conditions: 10 mg of the *Candida antarctica* lipase and the molar ratio for methanol/tributyrin was 3:1, at 30 °C, and stirrer at 2.5 rpm).

The activity of the different lipase microreactors was first investigated to aid the selection of the microreactor and then determine the optimum conditions for the immobilised lipase microreactor. The yield of methyl butyrate obtained from the different microreactors is presented in Figure 4-6, from which it can be seen that the M3 represents the best microreactor for the transesterification reaction between tributyrin and methanol and the yield was calculated using the calibration curve in section 4.1 and section 4.2.

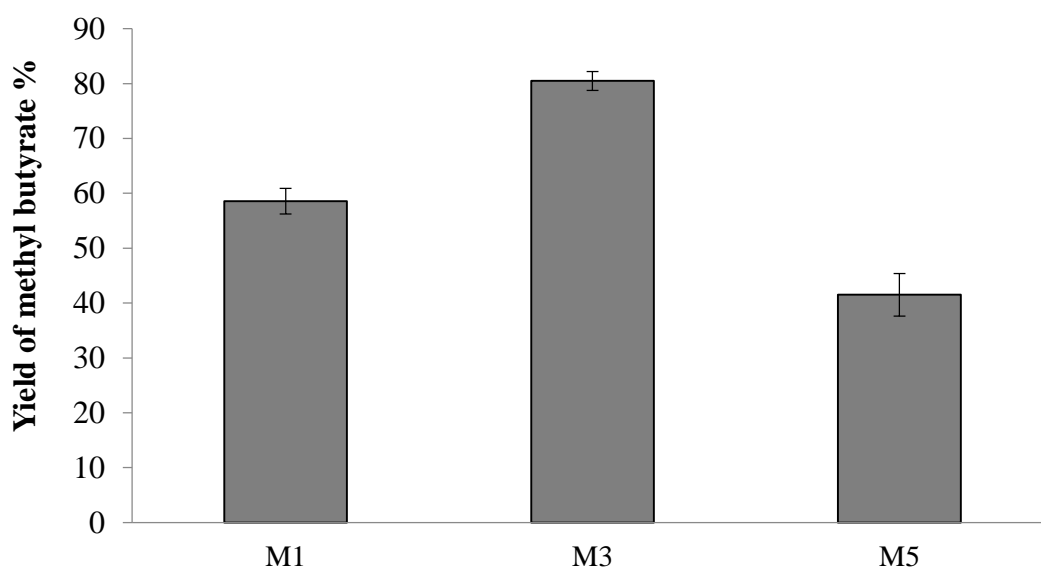


Figure 4-6. Yield of methyl butyrate using different lipase immobilized microreactors. (Reaction conditions: methanol /tributyryn molar ratio 2 :1; Flow rate 0.8 $\mu\text{L}/\text{min}$; 30 $^{\circ}\text{C}$; 20h). The error bars are the standard deviation of the yield % for three experiments.

The difference in activity observed for the microreactors investigated could be attributed to the differences in the physical characteristics of the three materials as well as to the lipase loading. Using M3 gave about a 21 % greater yield compared to M1 although both microreactors have approximately similar amount of immobilised lipase. The average pore diameter in M3 is smaller than M1 which could increase the contact time between the immobilised lipase units with the substrate inside the channels also the high drop in activity when M5 was used which has the largest pore diameter, accordingly M3 was subsequently used for all further experiments. It is worth to note that Anuar *et al*³⁵⁶ achieved 70% conversion of triolein to ethyl oleate using 15 cm lipase immobilised silica monolith microreactor at flow rate 1 $\mu\text{l min}^{-1}$. In this work the monolith is 4 cm long and the flow rate is 0.8 $\mu\text{l min}^{-1}$. Also in the work by Anuar *et al* the method used to immobilise the lipase is complex and time consuming as the silica monolith was grafted first with aminopropyltriethoxy silane then treated with glutaraldehyde as a cross linking reagent to lipase. This also raises questions about the amount of free amine groups left on

the silica monolith which could catalyse the reaction and lead to soap formation which is the main disadvantage of using base catalysts compared to enzyme catalyst in biodiesel production. In this work using aminopropyl group was avoided and the lipase was trapped inside the monolith by the means of the monolith pore size and the electrostatic interaction between the lipase and the silica surface. Because of the high cost of enzymes, it is necessary to optimise the reaction conditions. Therefore, the effect of the molar ratio, temperature, flow rate, time were investigated.

The turn-over frequency was calculated for the three immobilised silica microreactor by using Equation 4-2 and Equation 4-3.

$$\text{TOF} = \frac{\text{TON (Turnover number)}}{\text{Time (h)}} \quad \text{Equation 4-2}$$

$$\text{TON} = \frac{\% \text{ conversion of tributyrin} \times \text{Initial amount of tributyrin (M)}}{\text{Amount of immobilised lipase (g)}} \quad \text{Equation 4-3}$$

The TOF results are summarised in Table 4-5

Table 4-5. The TOF results

Catalyst type	Conversion %	Immobilised lipase (g)	TOF (h ⁻¹)
M1	59	0.0086	8.8
M3	80	0.0082	12.5
M5	42	0.0092	5.8

The data in the table confirm that the immobilised lipase in the M3 monolith is more active than the immobilised lipase in the M1 and M5.

4.3.2 Effect of reaction time

Figure 4-7 and Figure 4-8 shows the change in yield with time for the transesterification reaction with two molar ratio.

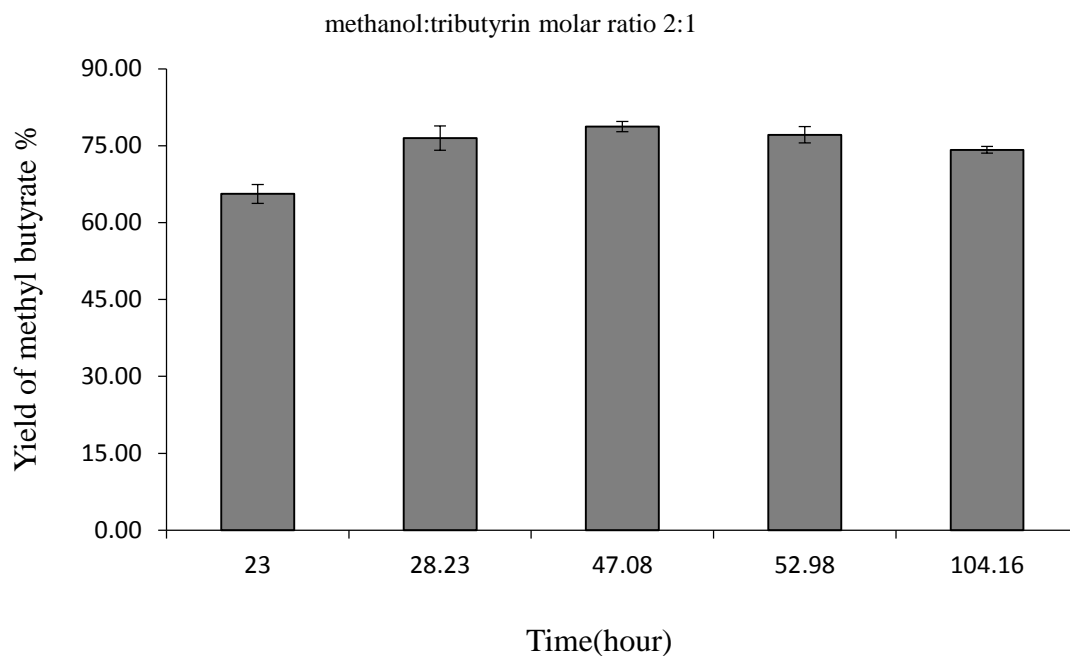


Figure 4-7. Effect of time on the yield of methyl butyrate with two molar ratio methanol: tributyrin 2:1 (Reaction conditions: Flow rate $0.8 \mu\text{l min}^{-1}$; 30°C).

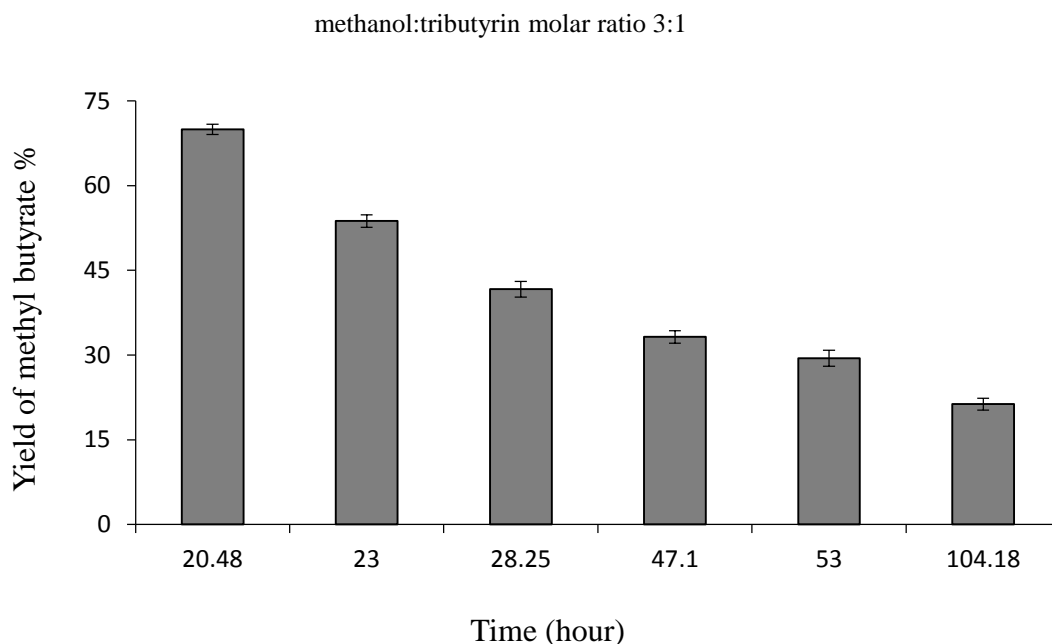


Figure 4-8. Effect of time on the yield of methyl butyrate with two molar ratio methanol: tributyrin 3:1 (Reaction conditions: Flow rate $0.8 \mu\text{l min}^{-1}$; 30°C).

As shown in Figure 4-7 the yield gradually increased from 65% to 74% after 104 h showing that the immobilised lipase is stable at methanol:tributyryn molar ratio 2. While in Figure 4-8 the yield gradually decreased from 70% to 21% after 104 h confirming the deactivation of immobilised lipase at methanol:tributyryn molar ratio 3.

Methanol present as drops in the oil could be at the root of the deactivation of immobilised lipase; methanol with its low solubility together with its high ratio could increase its contact with the enzyme. Methanol deactivation of lipase presents a significant challenge to large-scale biodiesel production.³⁵⁷

4.3.3 Effect of molar ratio of methanol:tributyryn

The effect of the methanol:tributyryn molar ratio on the yield of methyl butyrate was studied because it is an important parameter in the enzymatic transesterification reaction.

The experiments were conducted with various molar ratios and the yield of methyl butyrate is presented in Figure 4-9.

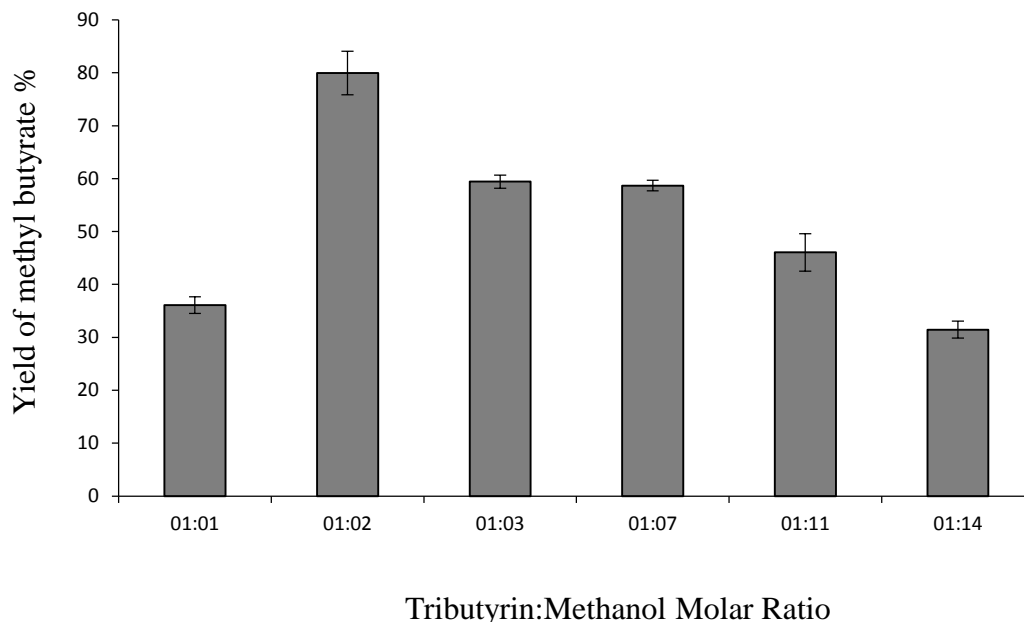


Figure 4-9. Yield of methyl butyrate using different lipase immobilized microreactors. (Reaction conditions: Flow rate 0.8 $\mu\text{L}/\text{min}$; 30 $^{\circ}\text{C}$; 20 h). The error bars are the standard deviation of the yield % for three experiments.

In the transesterification reaction (in accordance with stoichiometry), 3 moles of methanol react with 1 mole of triglyceride to yield 3 moles of fatty acid methyl ester and 1 mole of glycerol. However, the maximum conversion was obtained after 20 hr at a 2:1 methanol:tributyrin molar ratio. For the alkali-catalyzed reaction, an increase in the methanol:oil ratio increases the conversion because excess methanol shifts the equilibrium to the product side. However, a decrease in the conversion at a higher methanol:oil ratio was observed in the enzymatic transesterification of oil, which may be a result of the inhibition of lipase by methanol. These results are in agreement with the results of Du *et al.*³⁵⁸ who reported the deactivation of lipase enzyme at high methanol:oil ratios when soybean oil is transesterified using the Novozyme 435 enzyme. The presence of insoluble methanol in the reaction system could account for the reduced conversion

yield of methyl esters from oil substrates when the molar ratios of oil to alcohol are higher. According to Talampudi *et al.*,³⁵⁹ the active sites of the enzyme become obscured by excess alcohol thereby reducing the oil of the substrate's access to the lipase.

4.3.4 Effect of temperature

The effect of temperature on the transesterification was studied, and the results are shown in Figure 4-10.

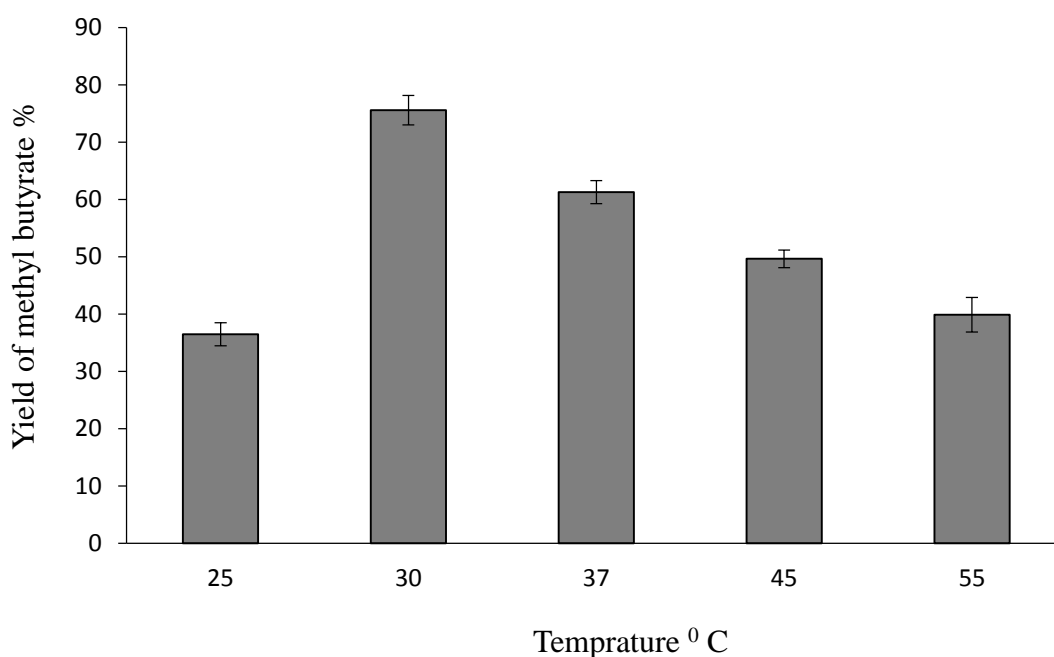


Figure 4-10. Effect of temperature on the yield of methyl butyrate. (Reaction conditions: Flow rate 0.8 μ L/min; 30 °C, methanol:tributyrim molar ratio 2:1).

Along with an increase in temperature for the transesterification of tributyrin from 30 to 55 °C, the conversion decreased. The reduction in the conversion of the reaction was due to the deactivation of lipase at higher temperature. At high reaction temperatures, protein integrity degrades, so lipases are deactivated more quickly in those conditions. Maintaining thermostability in the system is dependent upon ionic interactions and hydrogen bonding, which in turn are influenced by the reaction temperature, therefore reaction temperature determines substrate and enzyme interactions. Kumari *et al.*,³⁶⁰ and Antczak *et al.*,³⁶¹ described an increase in biodiesel conversion yield, reaching a

maximum of 87%, as a result of increasing the reaction temperature from 30 to 40° C. However, in research wherein Lipozyme was used to convert waste cooking oil to methyl esters, the conversion yield decreased when the temperature was raised from 40° C to 70°. ³⁶² The phenomenon has also been described by Rodrigues *et al*, ³⁶³ who used Lipozyme RM-IM to reach a peak conversion yield of 53% in converting canola oil to methyl esters at 35° C, but production diminished in higher reaction temperatures. In a study by Nie *et al*, that used Novozyme 435 to convert soybean oil to methyl esters, a maximum biodiesel conversion yield of 90% was achieved when the reaction temperature was at 40° C, but production dropped off at higher temperatures. ³⁶⁴

4.3.5 Effect of flow rate

Another important parameter affecting the conversion efficiency in flow microreactor is substrate flow rate. Figure 4-11 showed the conversion decreasing with increasing flow rate. The highest conversion (80%) was obtained at a flow rate of 0.8 µL/min. The increase in substrate flow rate caused a reduction in the residence time of substrate in the microreactor, which resulted in poor contact between lipases and substrates.

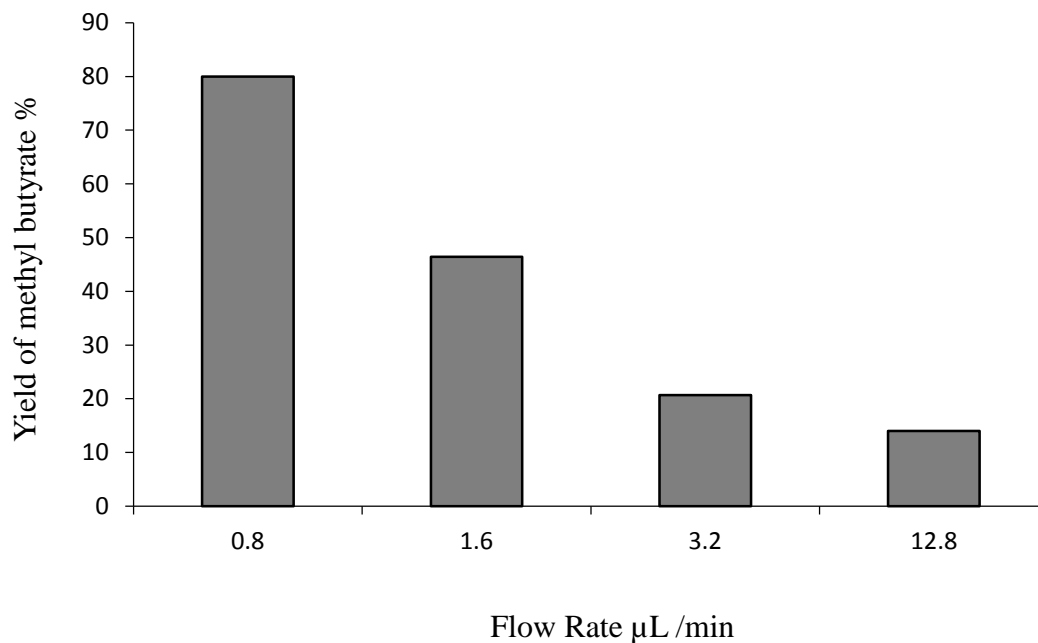


Figure 4-11. Effect of time on the yield of methyl butyrate. (Reaction conditions: Flow rate 0.8 μL/min; 30 °C).

4.4 Conclusions

A lipase-immobilised silica microreactor has shown good activity for transesterification reaction of tributyrin at 30° C. Increasing the temperature up to 55° C leads to decreasing the activity from 76 % to 40 % conversion. It is known that methanol and high temperatures deactivate the lipase. Finally, the molar ratio of methanol to tributyrin has been studied and the highest activity was obtained with 2:1 methanol to butyrin molar ratio. These results show the ability of using such system for biodiesel production. However, more studies need to be done to investigate other factors especially when oils with long triglycerides chain are used.

Chapter 5. Selective Oxidation of Cyclohexene through Gold functionalised Silica Monolith Microreactors

In this chapter a simple reproducible method was used to synthesise a mesoporous silica monolithic reactors and investigated two strategies for evenly functionalizing them with gold nanoparticles along their length. In this way of project aiming to combine (i) a continuous flow monolithic system, which offers a variety of operational and economic benefits with (ii) the unique catalytic properties of Au in selective oxidation catalysis. Two different methods were used to achieve even Au nanoparticle distribution within the monoliths. Firstly, simple impregnation of Au nanoparticles into the monolith during the formation of the monolith ensures even/random positioning of the nanoparticles as a result of solution phase mixing. Secondly, tethering thiol groups into the mesoporous structure of the monolith using 3-(mercaptopropyl)trimethoxysilane (3-MPTMS) allow the sulfur groups to act as anchors for the Au nanoparticles which can then be passed through the monolith and be tethered to the thiol groups. As the small thiol groups can diffuse readily through the monolith and react with surface hydroxyls to produce an even coverage, this allows Au nanoparticles to be flowed through the reactor until some saturation coverage of the thiols is reached. At this point the even distribution of the thiol groups confers a similarly even distribution within the monolith upon the anchored gold nanoparticles. As will be shown, both methods succeed in distributing the gold evenly along the length of the reactor. However, the impregnated method heat treatment during synthesis, results in heavily agglomerated Au nanoparticles. In contrast, the material containing thiol groups that can act as anchoring sites for the Au nanoparticles led to a material that was not only evenly dispersed along the length of the monolith but also exhibits a smaller particle size and more uniform particle size distribution. The materials synthesised were tested for the selective oxidation of cyclohexene.³⁶⁵

The oxidation of cyclohexene has been utilised as a model reaction in selective oxidation studies.^{345, 366, 367} Two common liquid phase oxidants were employed: hydrogen peroxide (H_2O_2) and *tert*-butyl hydroperoxide (TBHP).³⁶⁸⁻³⁷⁰ The Au-free monoliths were found to be catalytically inert at 30 °C. The presence of Au was the minimum necessary requirement for the selective oxidation reaction to proceed. Both Au functionalized monoliths were found to be active for the selective oxidation of cyclohexene with the thiol functionalized monolith being more active as compared to the impregnated monolith due to the better dispersity and higher surface area of Au. The oxidation reaction on the Au–thiol functionalised monolith was found to depend on the type of oxidant used with TBHP being more active than H_2O_2 , results suggest this can be attributed to the thiol modifier (containing propyl groups) rendering the silica surface of the monolith more hydrophobic than the hydroxyl termination of the bare silica surface and so favouring the organic oxidant.

5.1 Calibration curve of Cyclohexene

Table 5-1. Shows the calibration standards used to establish the calibration curve and the HPLC response.

Table 5-1. The peak area of Cyclohexene measured under varied concentration (n=1)

Concentrations (M)	Peak area
0	0
0.000156	12.2
0.000625	45.1
0.00125	130
0.005	619.2
0.02	2873.3
0.06	8612.3
0.1	15002.7

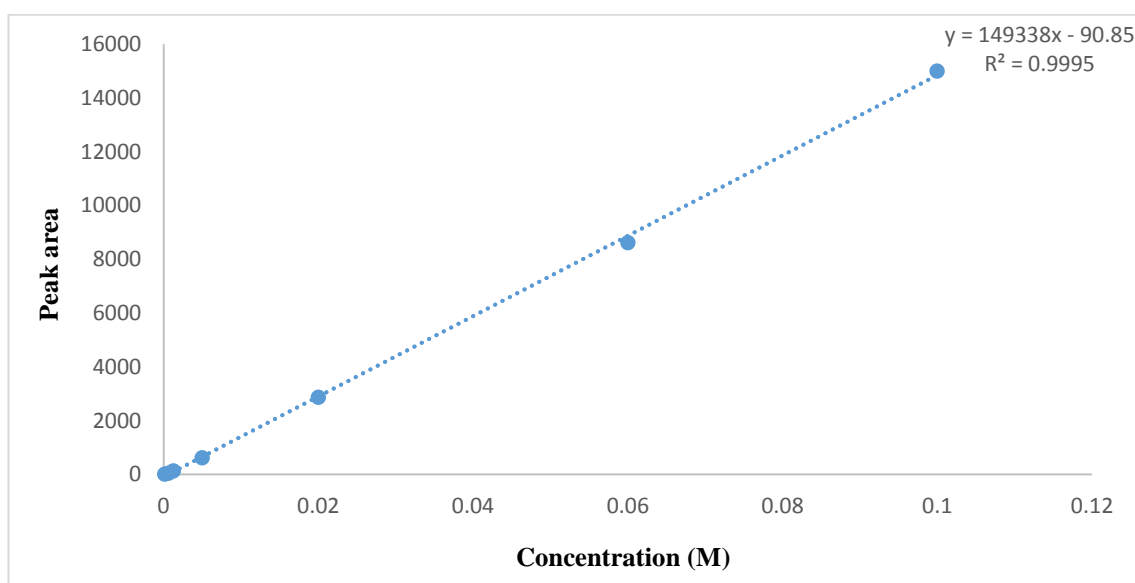


Figure 5-1. Calibration curve of Cyclohexene.

As shown in Figure 5-1, there is a linear relationship between the concentrations and peak area and produced a correlation coefficient (R^2) ≥ 0.9995 .

5.2 Calibration curve of Cyclohexene oxide

Table 5-2. Shows the calibration standards used to establish the calibration curve and the HPLC response.

Table 5-2. The peak area of Cyclohexene oxide measured under varied concentration (n=1)

Concentrations (M)	Peak area
0	0
0.000156	16.7
0.000625	81.8
0.00125	173.7
0.005	676.2
0.02	2938.2
0.06	8965.6
0.1	14874

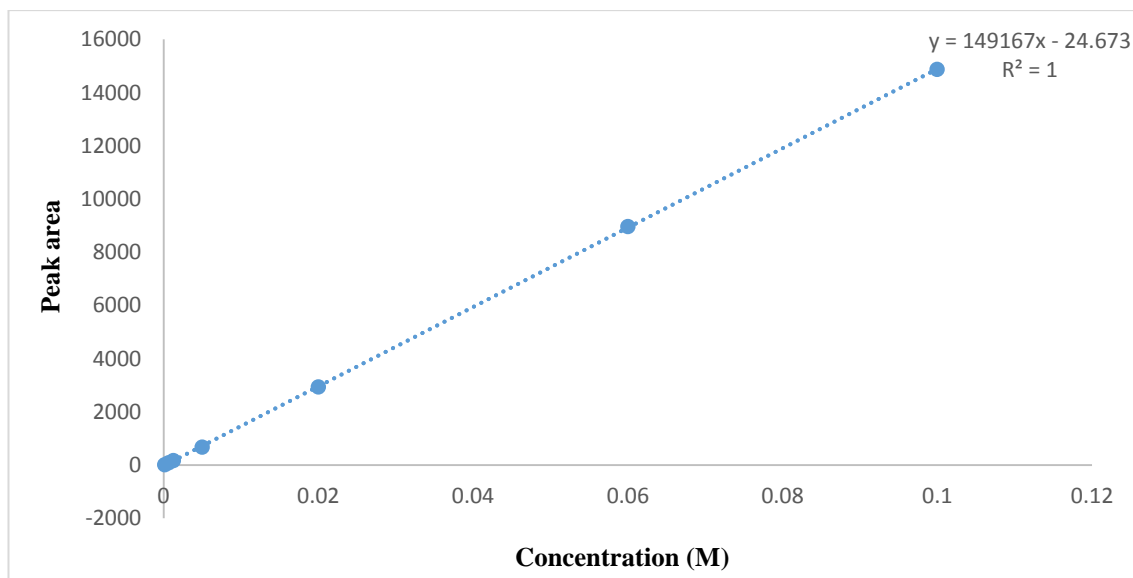


Figure 5-2. Calibration curve of Cyclohexene oxide.

As shown in Figure 5-2, there is a linear relationship between the concentrations and peak area and produced a correlation coefficient (R^2) 1.

5.3 Calibration curve of 2-Cyclohexene -1-ol

Table 5-3. Shows the calibration standards used to establish the calibration curve and the HPLC response.

Table 5-3. The peak area of 2-Cyclohexene -1-ol measured under varied concentration (n=1)

Concentrations (M)	Peak area
0	0
0.000156	21.7
0.000625	81
0.00125	167.4

0.005	649.6
0.02	3063.5
0.06	9437.6
0.1	15140.9

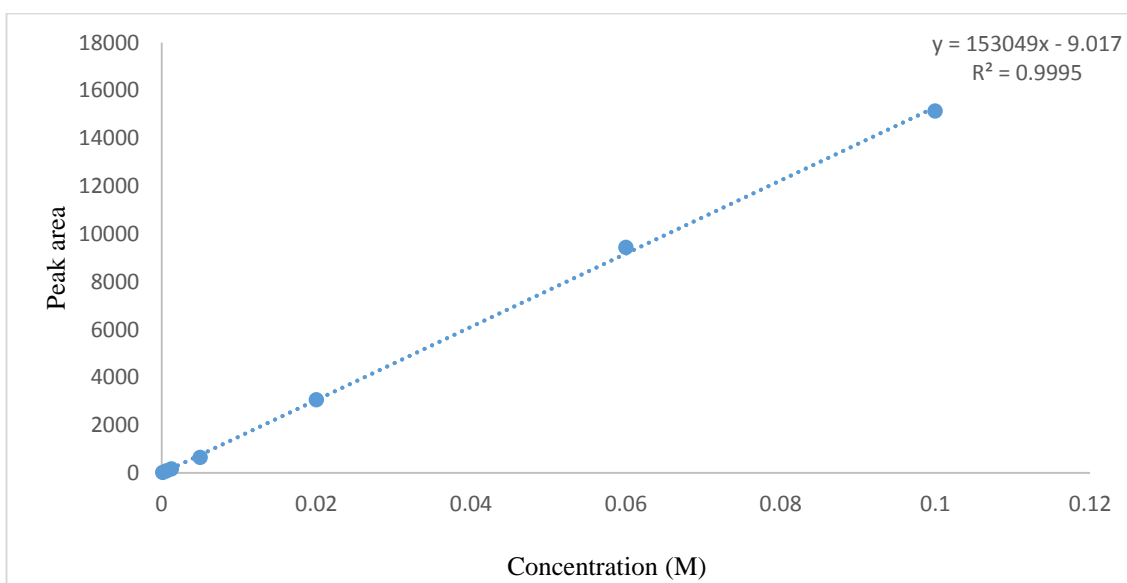


Figure 5-3. Calibration curve of Cyclohexene -1-ol.

As shown in Figure 5-3, there is a linear relationship between the concentrations and peak area and produced a correlation coefficient (R^2) 0.9995.

5.4 Calibration curve of 2-Cyclohexene -1-one

Table 5-4. Shows the calibration standards used to establish the calibration curve and the HPLC response.

Table 5-4. The peak area of 2-Cyclohexene -1-one measured under varied concentration (n=1)

Concentrations (M)	Peak area
0	0
0.000156	24.7
0.000625	94.7
0.00125	200.3
0.005	516.1
0.02	3436.8
0.06	10632.2
0.1	17590.4

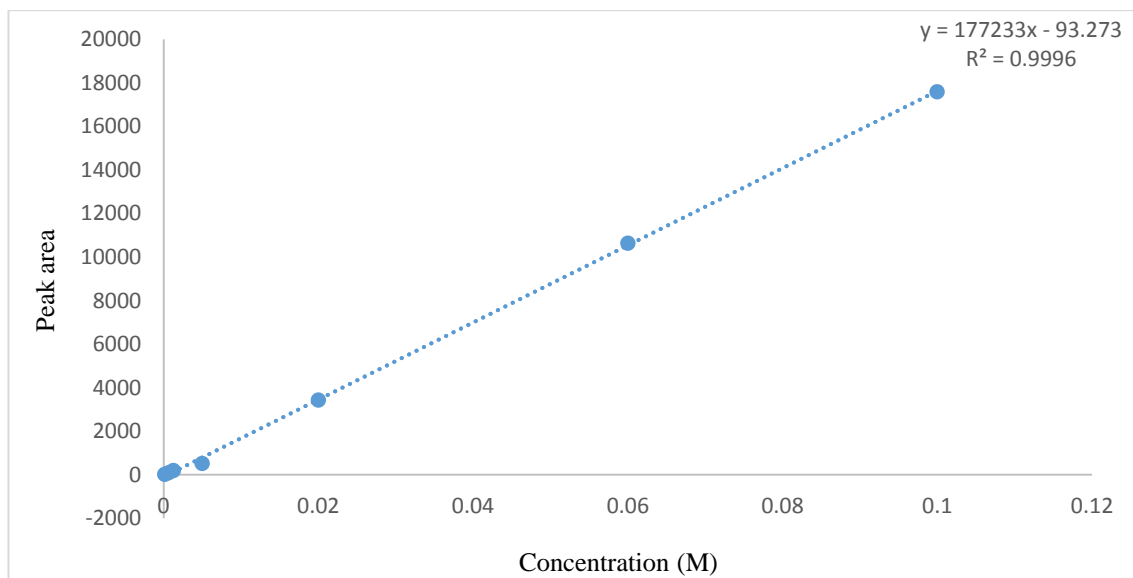


Figure 5-4. Calibration curve of Cyclohexene 1-one.

As shown in Figure 5-4, there is a linear relationship between the concentrations and peak area and produced a correlation coefficient (R^2) 0.9996.

5.5 Calibration curve of Mesitylene (External standard)

Table 5-5. Shows the calibration standards used to establish the calibration curve and the HPLC response

Table 5-5. The peak area of Mesitylene measured under varied concentration (n=1)

Concentrations (M)	Peak area
0	0
0.000156	47.2
0.000625	168.7
0.00125	516

0.005	1393.9
0.02	5628.7
0.06	17070.8
0.1	27814.8

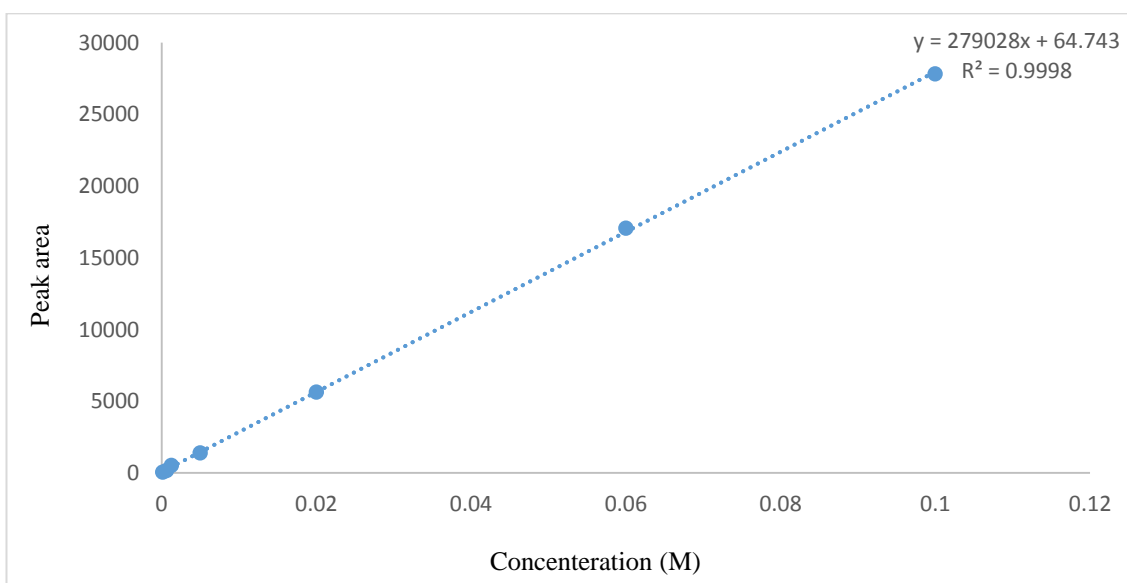


Figure 5-5. Calibration curve of Mesitylene (External standard).

As shown in Figure 5-5, there is a linear relationship between the concentrations and peak area and produced a correlation coefficient (R^2) 0.9998.

5.6 Characterisation of Au monolith microreactors with BET

The Au monolith microreactors in this experiment were measured and evaluated using BET to obtain surface area in (m^2/g), pore volume in (cm^3/g), and pore size in (nm). The results are summarized in Table 5-6.

Table 5-6. Physical characterisation of monolith (n=1)

Sample	BET Surface Area m^2/g	Pore Volume cm^3/g	Pore Size nm
Au-thiol monolith	160	0.6	16.2
Au- impregnated monolith	191	0.7	15.4
Au -free monolith	210	0.9	11.6

The BET measurements in Table 5-6, suggest that the Au doped monoliths have a lower surface area and pore volume while the overall pore size is increased. This is understood in terms of restricted diffusion of N_2 molecules in the micropores of the monolith due to blocking with Au nanoparticles during the N_2 physisorption measurement.³⁷¹⁻³⁷³

Blocking the small pores of the mesostructure with Au particles or particle aggregates leads to a lower overall monolith surface area. On the other hand blocking the small pores will increase the average pore size of the monolith as diffusion of particles takes place

only at the larger unblocked pores. Interestingly, this effect appears to be more pronounced in the case of the thiol-functionalised Au monolith as compared to the impregnated one. This suggests that a larger number of Au nanoparticles must be present, which amplifies the blocking effect. To further elucidate this point TEM and ICP-OES measurements were performed.

5.7 Determination of silica Au monolith microreactors by SEM

As discussed earlier, silica monoliths in general may adapt a variety of structural morphologies depending on the synthesis procedure followed. These morphologies are governed primarily on the molecular weight of the starting polymer precursor as well as the ratio of water to silane. Alteration of the above parameters may lead to a variety of polymorphs, namely: (i) air-in-silica, (ii) silica-in-air and (iii) bicontinuous.¹⁰⁸ In this work, the ‘sponge like’ bicontinuous monolithic structure reported by Fletcher *et al.*¹⁰⁸ was targeted as it maximises the available surface area and pore volume. The bicontinuous monolith structure can be obtained under specific reaction conditions and is characterized by ‘continuous mutually conjugated domains and hyperbolic interfaces’.¹⁰²

SEM images in Figure 5-6 to Figure 5-8 show that this was successfully achieved by following the synthetic protocol described in section 2.3, which can be seen to lead to a ‘coral-like’ structure seen in the Au-free monolith in Figure 5-6(a).³⁷⁴ The image is typical of the bicontinuous monolithic morphology.^{108, 375-377} The SEM measurements suggest that the coral like network is preserved when Au is incorporated in the monolith by either method (Figure 5-7(b) and Figure 5-8 (c)). The Au nanoparticles, highlighted by red circles in Figure 5-7(b), and Figure 5-8(c), appear as bright spots within the SiO₂ network. Critically, the particles observed in Figure 5-7(b) appear much larger than those in Figure 5-8 (c) which suggests heavy agglomeration of Au in the case of the Au-impregnated monolith.

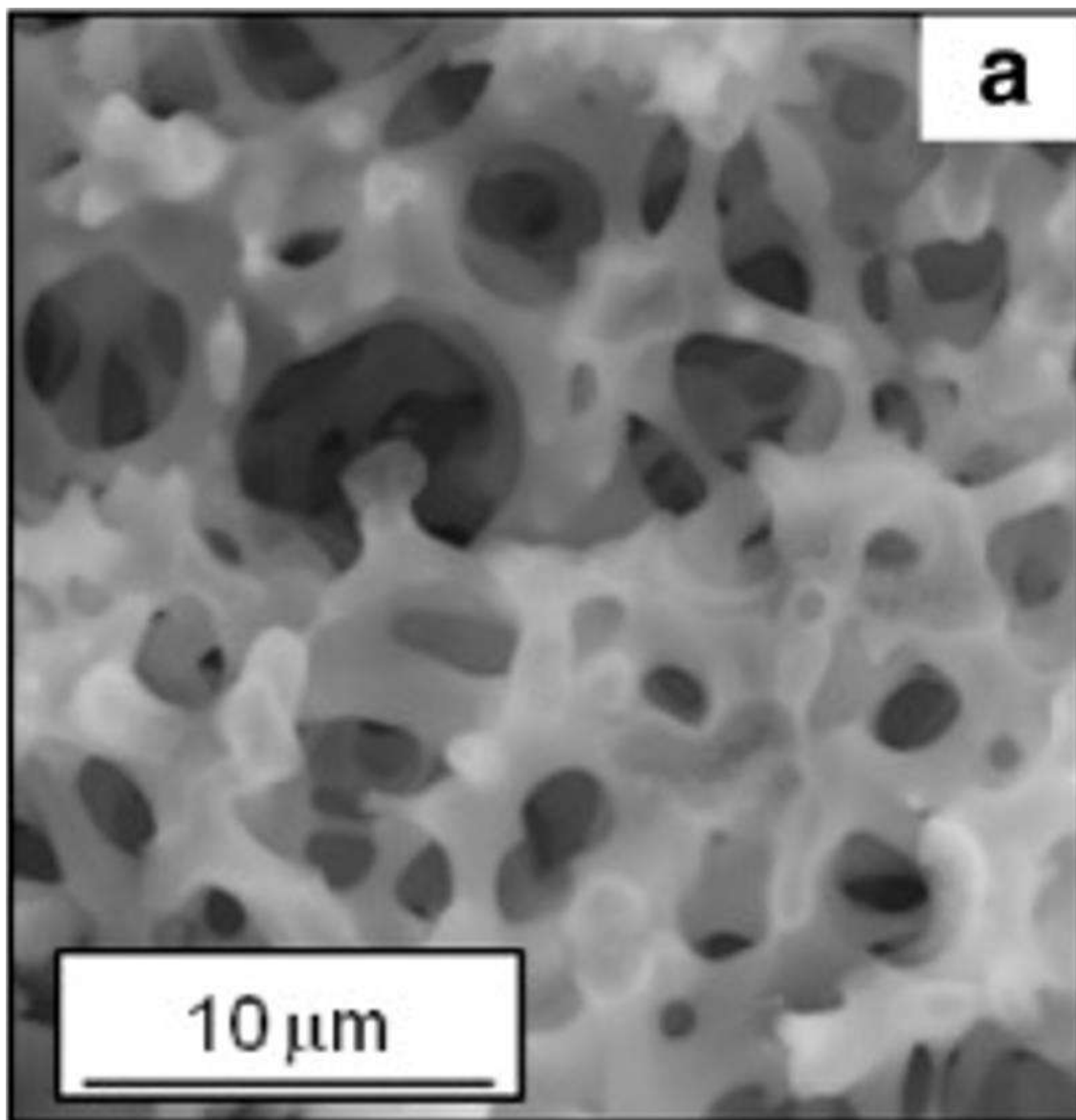


Figure 5-6. SEM image of (a) Au-free monolith.

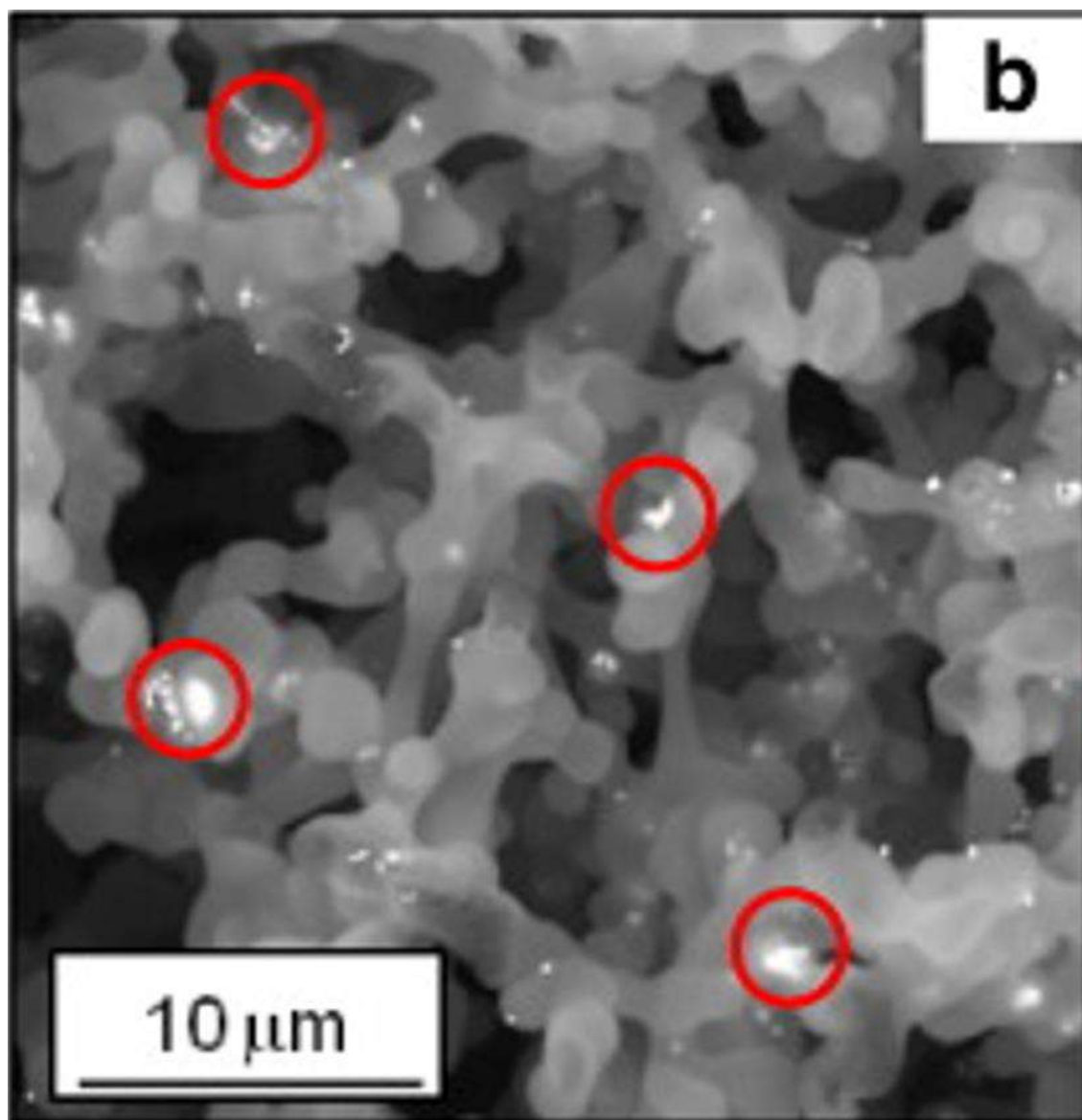


Figure 5-7. SEM image of (b) Au-impregnated monolith.

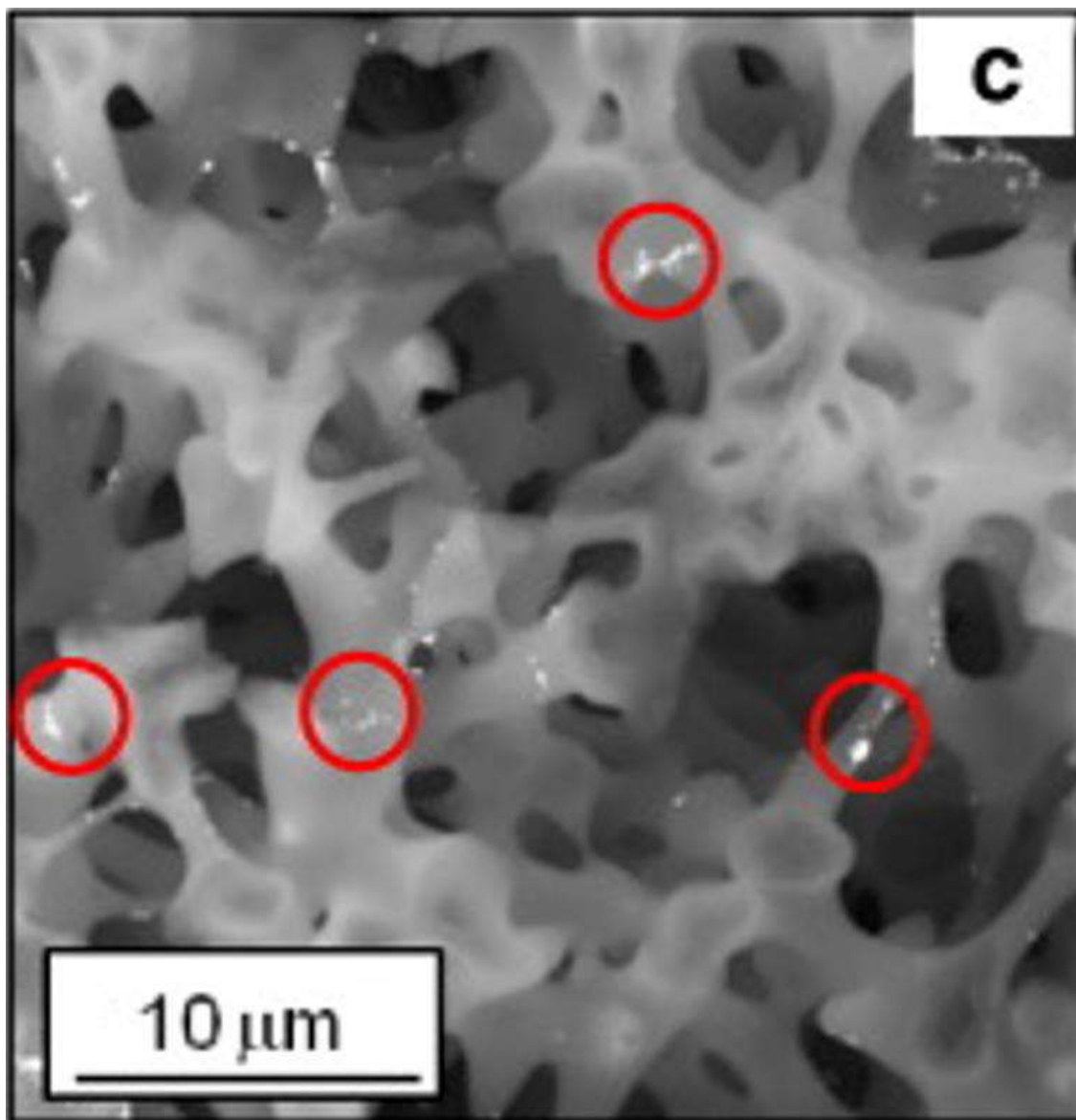


Figure 5-8. SEM image of (c) Au-thiol functionalised monolith.

5.8 ICP-OES analysis for Au-impregnated and Au-modified monolith microreactors

Figure 5-9 shows the elemental (ICP-OES) analysis for the two Au based monoliths. The analysis was performed by dissecting the monolith rod into four sections of 1 cm length. From each section, a piece of ~ 0.1 cm was cut and digested following the method described in section 2.8.6. The key point to note is that in both cases the Au content appears to be nearly homogeneous across the length of each monolith, as was desired. The final weight % loading determined by ICP-OES is similar in both cases: the impregnated monolith had an Au content of 2.7 wt.% \pm 0.2% across the monolith rod, while for the thiol-functionalised monolith there was an Au content of 1.2 wt.% \pm 0.3%. This similarity in Au content (around a factor of two) confirms that the very significant differences in agglomeration are unlikely to be due merely to different Au loadings. It should also be noted that there is a small loss of Au from the nominal loading of 4.7 wt.% in the case of the impregnated method (likely due to washing steps removing any free material during the synthesis), but for the thiol-functionalised monolith, a saturation (based on the number of thiol groups) is reached despite washing through a large excess of Au nanoparticles (which if all incorporated would yield a 9.4% nominal loading). In the latter case, it should be noted that, to minimise waste of valuable Au the nanoparticles not tethered within one monolith could be collected after pumping through the first monolith and used directly to load further monoliths with Au nanoparticles.

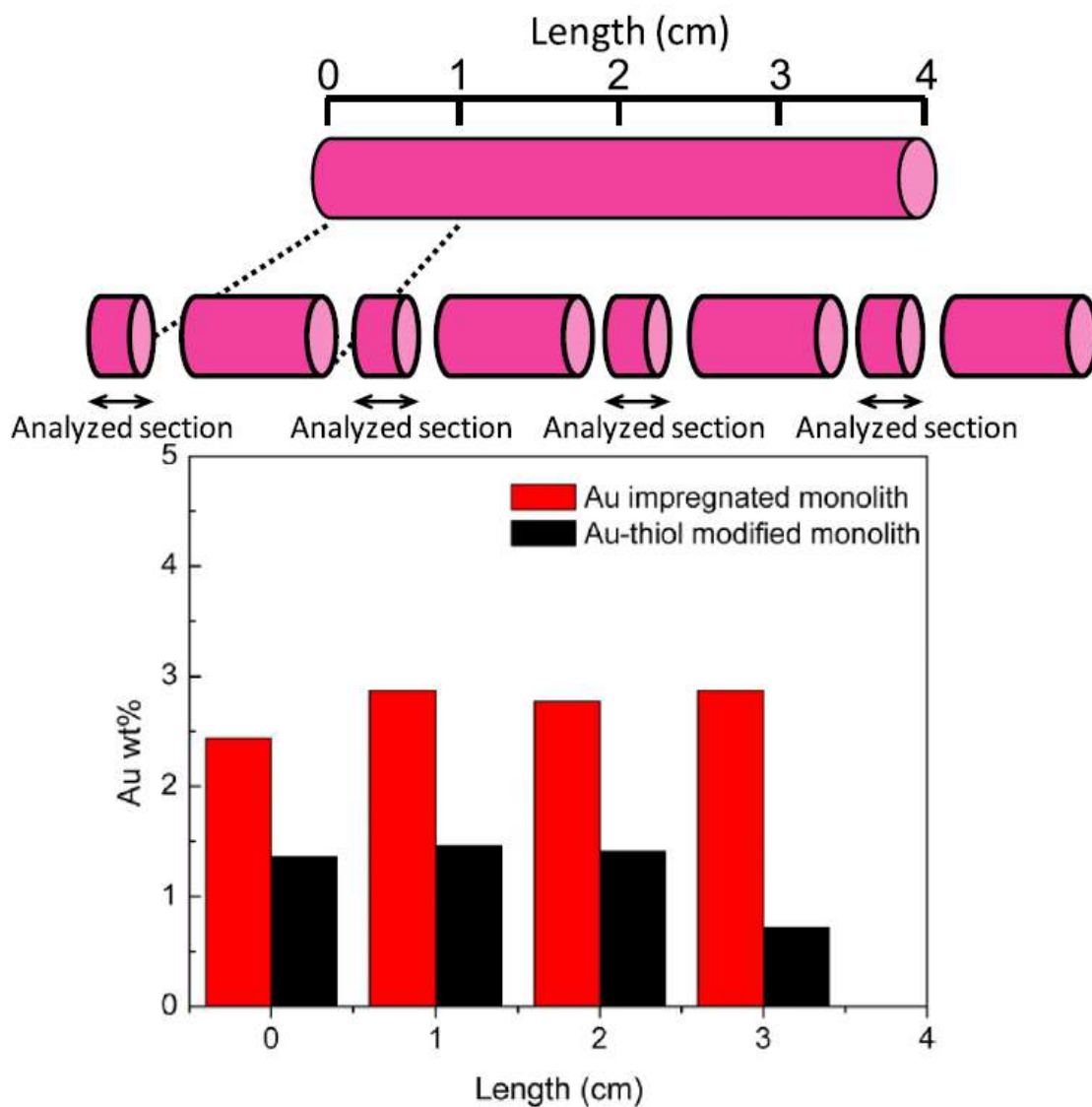


Figure 5-9. ICP-OES results taken at 1 cm at different position a cross sections of the two monoliths. (n=1)

5.9 Characterisation of Au monolith microreactors with TEM

Figure 5-10 (a) and Figure 5-11(b) shows representative TEM images and the particle size histograms for the two Au monoliths. It can be seen that the Au nanoparticles of the thiol functionalised Au monolith have a relatively narrow particle size distribution (average size of 6.8 ± 1.4 nm). Impregnation of the monolith with Au nanoparticles led to a vastly broader particle size distribution (average size 49.5 ± 26.5 nm diameter) with a maximum size of 110 nm, due to severe agglomeration. The difference in Au particle size between the two monoliths is attributed to the heat treatment. The monolith synthetic protocol requires calcination at 600 °C to produce the final material. In the case of the impregnated monolith the Au nanoparticles are present in the monolith when the calcination process takes place leading to strong agglomeration of the particles. In the case of the thiol functionalised monolith, the Au nanoparticles and thiol groups are added to the monolith after the calcination step; thus, they are protected from agglomeration which led to a more uniform particle size distribution.³⁷⁸

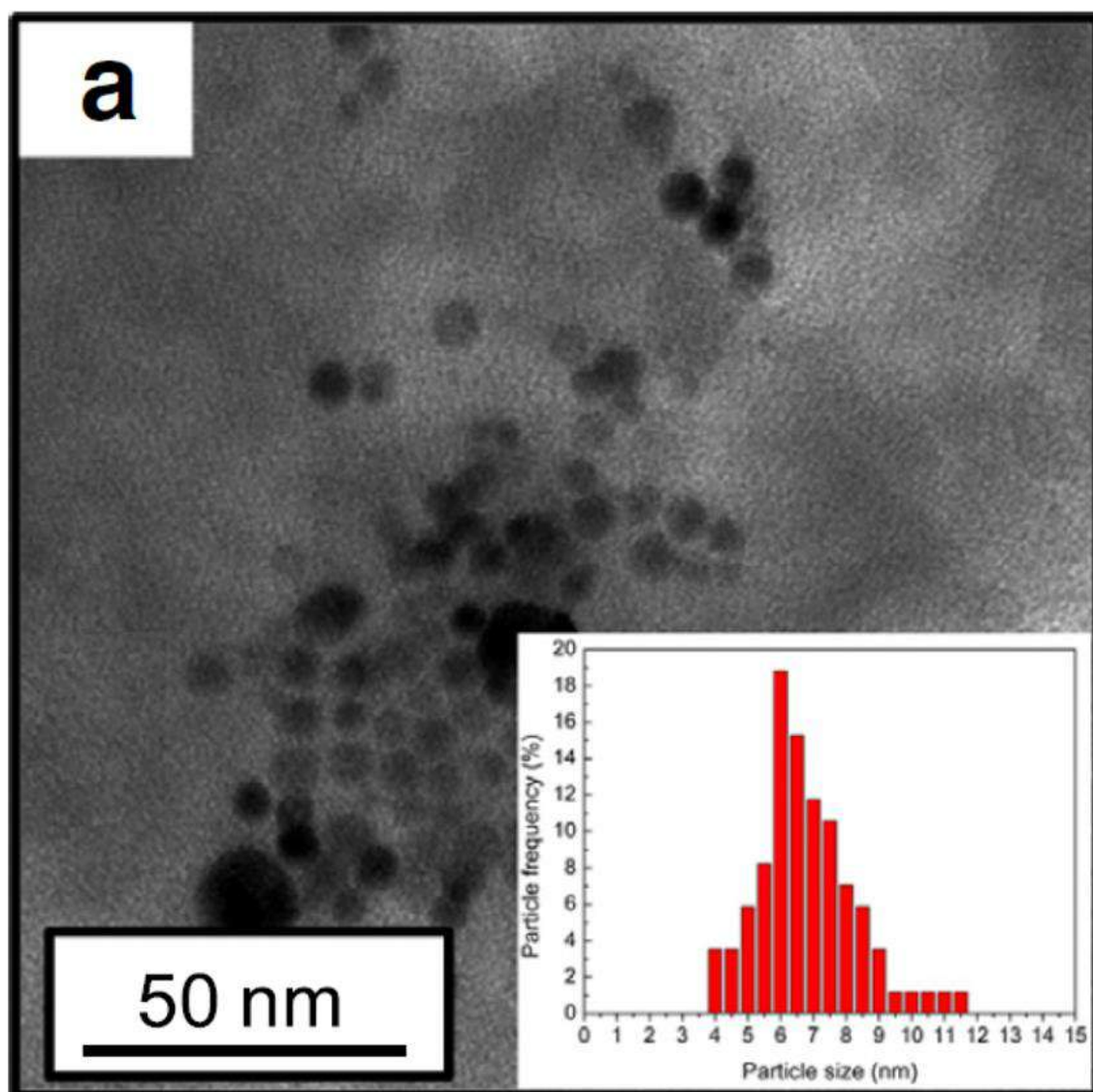


Figure 5-10. TEM and particle size distribution diagrams of: (a) Au thiol-functionalised monolith. (n=1).

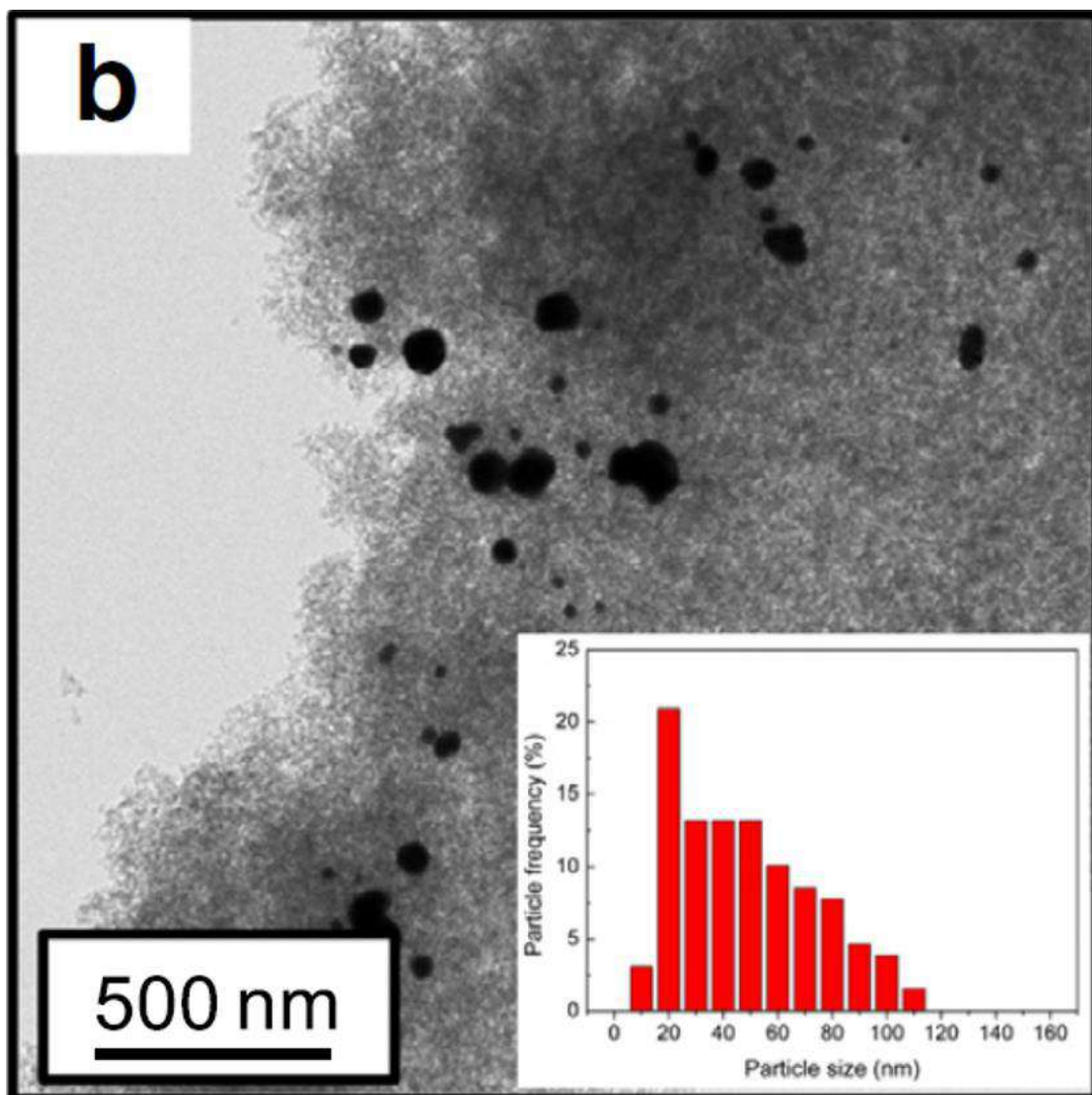


Figure 5-11. TEM and particle size distribution diagrams of: (b) Au-impregnated monolith. (n=1).

5.10 Characterisation of Au monolith microreactors with PXRD

Further confirmation of the general trend in particle size difference between the two monoliths was obtained *via* PXRD measurements. Figure 5-12 shows that the Au particles present in both samples possess the same four crystal planes with the {111} plane being the most dominant in both cases. The broadening of the peaks in the case of the thiol modified Au monolith suggests that the Au particle size is smaller than that of the impregnated monolith.³⁷⁹

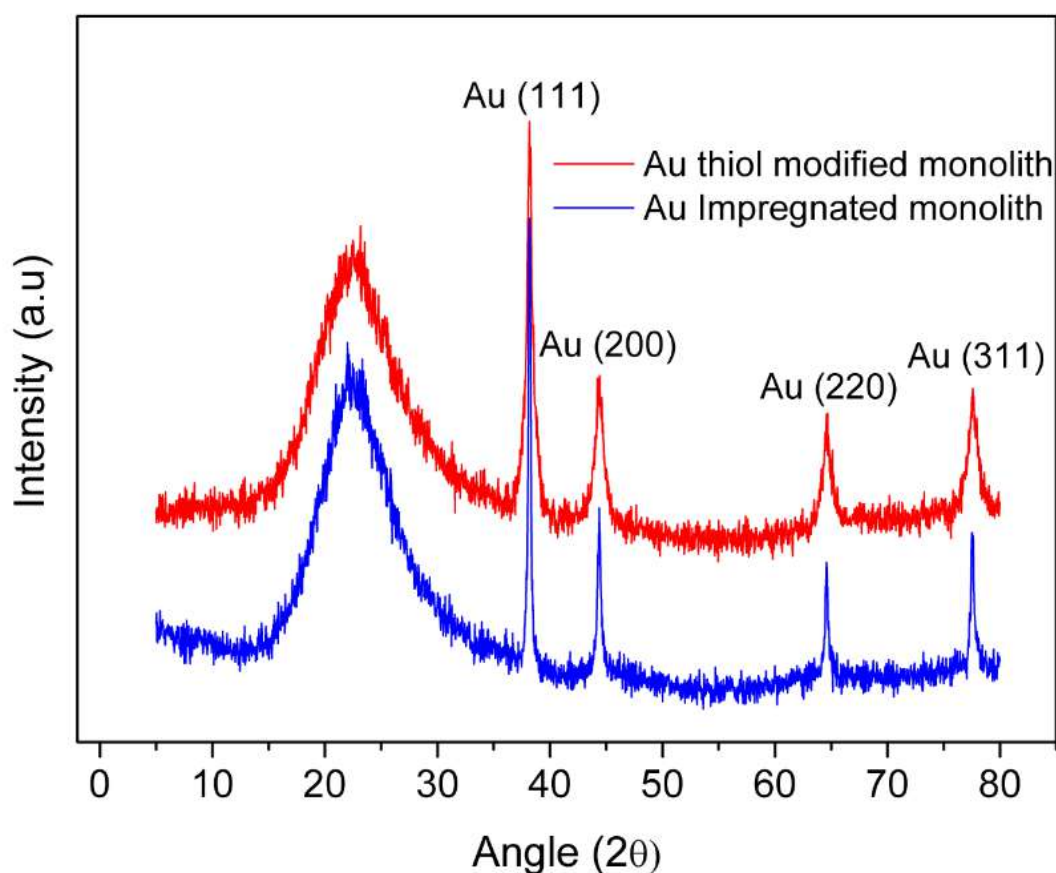


Figure 5-12. For gold catalyst monoliths thiol-modified (top) monoliths impregnated (bottom): (a) PXRD data, specific dominant crystallographic planes are indicated on the figure. In each case data for two samples are offset for clarity. XPS binding energy scale corrected to C 1s at 284.4 eV.

By utilising Scherrer's equation, an average crystallite size was obtained Table 5-7. As can be seen, the trend in particle sizes for the Au–thiol monolith is concordant between the PXRD and TEM.

Table 5-7. Au particle size distribution *via* TEM and PXRD

Catalyst type	TEM (nm)	PXRD (nm)
Au – impregnated monolith	49.5 ± 26.5	22.0 ± 10.0
Au-thiol modified monolith	6.8 ± 1.4	11.0 ± 5.0

It is worth noting that the TEM particle size is a number average (counted once per particle), whereas PXRD is an electron weighted average; PXRD therefore is relatively biased towards large particles³⁸⁰ in the case of the thiol modified small particles, this likely accounts for the numerical difference between the two methods. For the impregnated sample a large range of particle sizes and the possibility of many particles are present as agglomerates, which may also lead to an apparent numerical inconsistency, but this time due to the difference between apparent particle size inferred from contrast in bright field TEM images *vs.* PXRD which measures crystallite rather than particle size. The key point however is both techniques indicate the general result that the thiol modified monolith method affords much improved size control and thus leads to smaller particles.

5.11 Characterisation of Au monolith microreactors with XPS

Clearly, despite the relatively higher Au content of the impregnated monolith, the available Au surface area is relatively lower as compared to the thiol functionalized monolith due to the severe agglomeration of the Au nanoparticles.

This effect is also seen very dramatically in the XP spectra shown in Figure 5-13(b) which show, after correction to the Si 2p substrate signal, that the XPS visible Au is 8 times greater for the thiol modified sample as compared to the impregnated one, despite the slightly lower bulk gold content of the former. This confirms the loss of surface Au (and consequent loss of catalytic sites) as a result of Au agglomeration in the impregnated catalyst, since the Au signal will largely originate from near the surface of the nanoparticles; hence gold buried deep with the larger agglomerated particles will not be seen (emitted electrons have a kinetic energy of 1403 eV, corresponding to a typical mean free path escape depth of 1.8 nm).³⁸¹

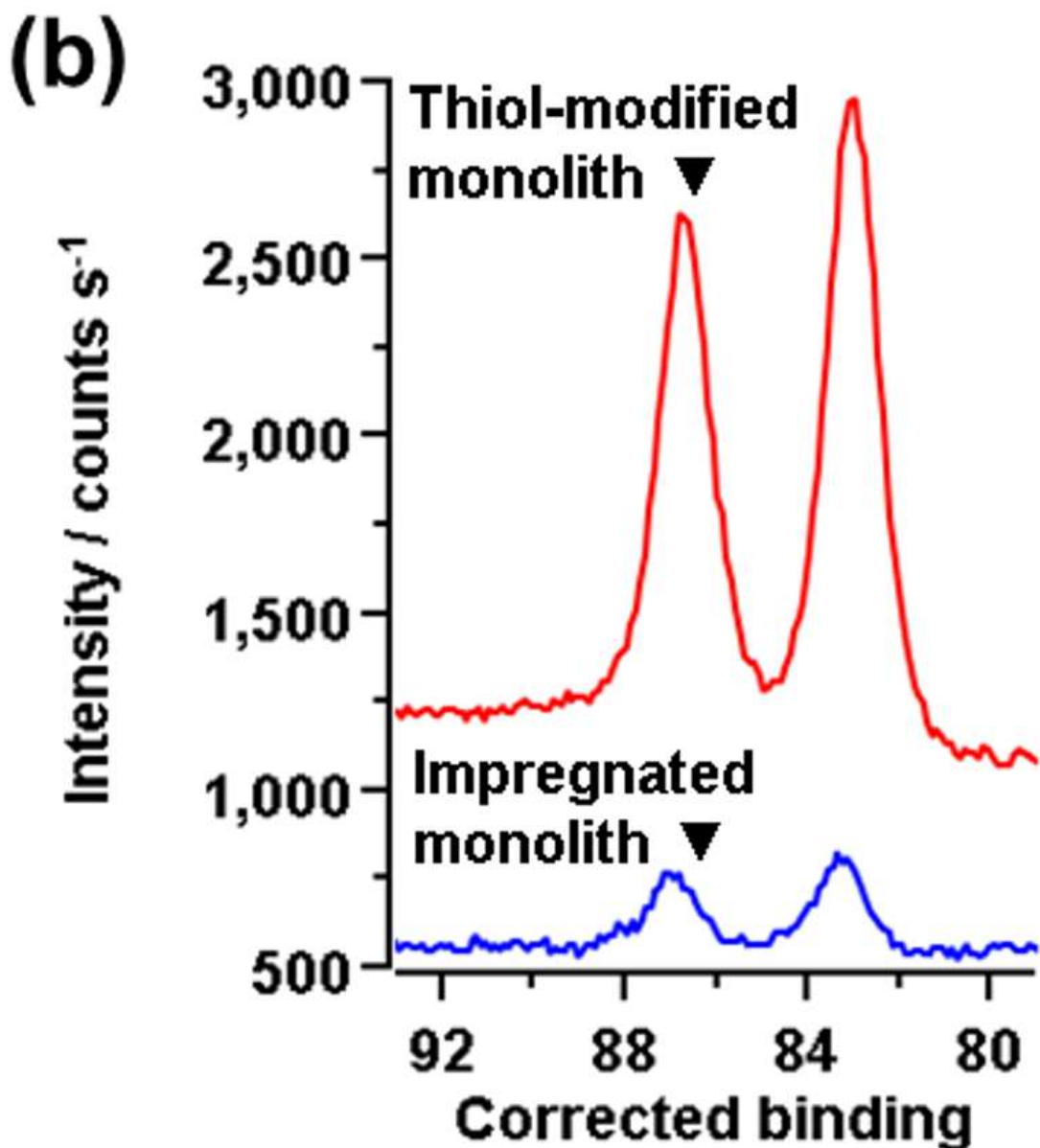


Figure 5-13. For gold catalyst monoliths thiol-modified (top) monoliths impregnated (bottom): (b) Au 4f region XP spectra. In each case data for two samples are offset for clarity. XPS binding energy scale corrected to C 1s at 284.4 eV.

Additionally, Figure 5-14(c) shows the S 2p XP spectra which clearly demonstrate the successful functionalization of the monolith with the thiol groups.

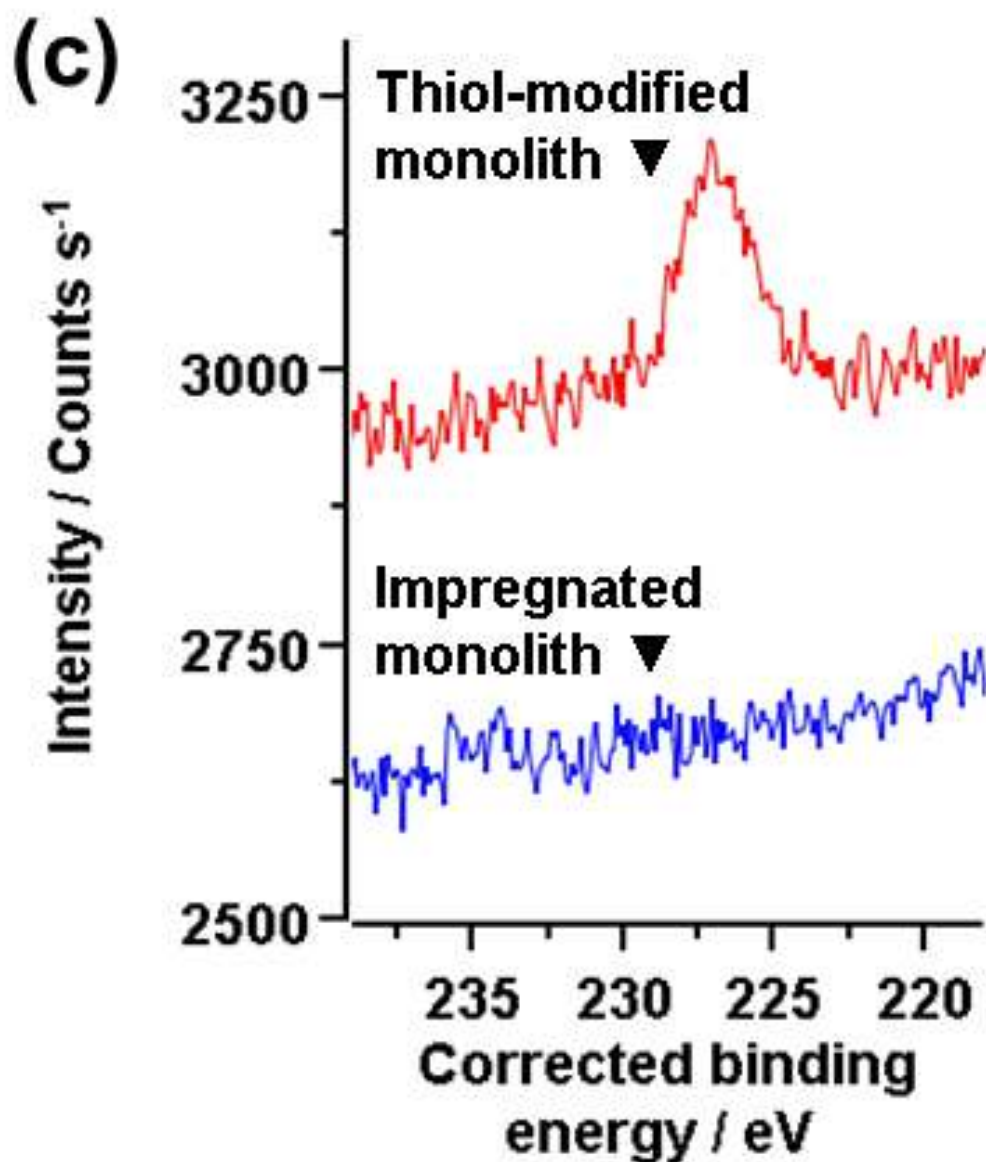


Figure 5-14. For gold catalyst monoliths thiol-modified (top) monoliths impregnated (bottom): (c) S 2s region XP spectra. In each case data for two samples are offset for clarity. XPS binding energy scale corrected to C 1s at 284.4 eV.

5.12 Catalytic activity of oxidation of cyclohexene

The reaction mixture was injected into the GC-FID before and after the reaction to calculate the conversion of cyclohexene and the selectivities. As shown in Figure 5-15.

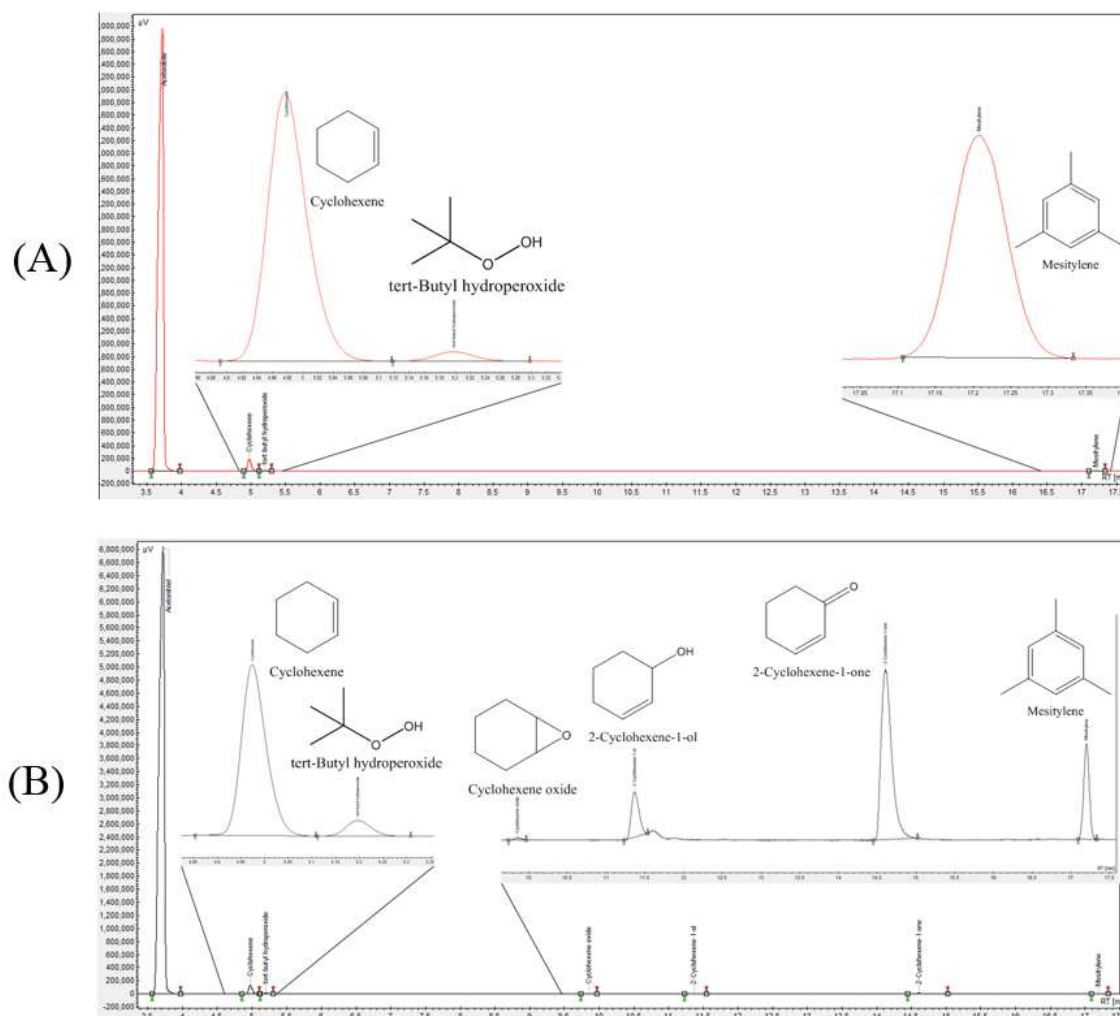


Figure 5-15. GC peaks of epoxidation reaction of Cyclohexene (A): before the reaction. Peak at 3.72 min assigned to solvent (Acetonitrile, peak at 4.96 min assigned to Cyclohexene, peak at 5.25 min assigned to *tert*-Butyl hydroperoxide, and peak at 17.20 min assigned to Mesitylene (external standard). (B) : after the reaction. Peak at 3.72 min assigned to solvent (Acetonitrile), peak at 4.97 min assigned to Cyclohexene, peak at 5.25 min assigned to *tert*-Butyl hydroperoxide, peak at 9.86 min assigned to Cyclohexene oxide, peak at 11.34 min assigned to 2-Cyclohexene-1-ol, peak at 14.78 min assigned to 2-Cyclohexene-1-one, and peak at 17.20 min assigned to Mesitylene (external standard).

The Au free and the two Au containing monoliths were tested for the selective oxidation of cyclohexene using acetonitrile as the solvent at the very mild temperature of 30 °C as explained in section 2.8.8. The reaction was studied using two different oxidants: *tert*-butyl hydroperoxide (TBHP) and hydrogen peroxide (H₂O₂).³⁶⁸

The molar ratio of reagent to oxidant was kept to 1:1. The results are summarised in Table 5-8. The pure silica monolith was found to be inactive for the selective oxidation of cyclohexene at 30 °C with both TBHP and H₂O₂. The impregnated monolith was found to lead to low conversion of cyclohexene ($\leq 3\%$ conversion) using both oxidants. This is attributed to the relatively low surface area of the heavily agglomerated Au nanoparticles present in this monolith. Under these low conversions, the selectivity of the reaction was found to be different when the two oxidants were used with H₂O₂ favouring cyclohexene oxide (58.4% selectivity) while TBHP favouring the formation of 2-cyclohexen-1-ol (51.5% selectivity).

Table 5-8. Cyclohexene oxidation on Au impregnated and Au free monoliths using *tert*-butyl hydroperoxide (TBHP) and hydrogen peroxide (H₂O₂) as the oxidants at 30 °C.

Catalyst type	Oxidant	Conv. %	TOF	Cyclohexene oxide (S) %	2-Cyclohexene-1-one (S) %	2-Cyclohexene-1-ol (S)%
Au-free monolith	TBHP	< 0.2	n/a	0	0	0
Au-impregnated monolith	TBHP	3.1	184	30.2	18.3	51.5
Au-modified monolith	TBHP	18.3	342	2.5	81.5	16.0
Au-free monolith	H ₂ O ₂	< 0.2	n/a	0	0	0
Au-impregnated monolith	H ₂ O ₂	2.8	167	8.4	18.5	23.1
Au-modified monolith	H ₂ O ₂	2.7	51	56.7	22.7	20.6

Where:

S — % selectivity, Conv. — % conversion, TOF — turnover-frequency (cyclohexene molecules per surface Au atom, per hour).

As might be expected owing to the higher surface area, the thiol functionalised monolith was found to be relatively more reactive than the impregnated monolith with the conversion reaching 18.3% when TBHP was used as the oxidant. This also confirms that there is no strongly deleterious poisoning effect resulting from the presence of a small number of sulphur binding sites present in the material. Normalization to the metal surface area in the form of turnover frequencies (TOFs), also given in Table 5-8, gives additional insight into the mechanism by which the mass activity enhancement observed may be occurring. TOF values are in the high end of the range expected for room temperature cyclohexene oxidation using peroxide oxidants; speculatively this is perhaps due to less mass transfer limitations in a flow reactor, rather than the batch systems commonly reported.³⁶⁸

However, it is interesting to note that TOF values are relatively comparable for either oxidant in the case of the impregnated monolith, but differ somewhat between the two oxidants in the case of the thiol modified monolith. As can be seen, the thiol-modified TOF values fall on either side of the impregnated TOF values (suggesting in general terms much of the mass activity enhancement seen is likely due to higher surface area) speculate that the difference in the case of the thiol-modified monolith with different oxidants may be due to the presence of the thiol-anchoring agent which induces an increased hydrophobicity in the silica monolith^{382, 383} limiting the access of H₂O₂, thus lowering the rate of reaction. The slight increase of TOF (factor of two) when using organic TBHP as oxidant with the thiol modified monolith compared to the impregnated monolith could either be due again to the hydrophobicity, or due to better access of reactants within the monolith structure, large Au agglomerates can be expected to potentially cause more blockages in the pore structure. Both these factors can be seen as potentially contributory to the mechanism by which method of dispersing small gold nanoparticles within the monolith structure leads to a substantial improvement in mass activity for practical

chemical processing. The results suggest that tailoring the selectivity of the selective oxidation reaction is driven by both the oxidizing agent and the method used to functionalise the monolith with Au nanoparticles. Furthermore, the XPS data of both monolith catalysts (Figure 5-13(b)) are indicative of Au in the metallic state with very limited variation in the peak centres: Au 4f_{7/2} 283.1 and 283.3 eV for the modified and unmodified catalysts respectively; shifts for oxidation to Au (I) are typically 1 eV or more.³²⁷ XPS, therefore, excludes that the possibility the improved catalysis observed is due to changes in the electronic structure rather than simply as a result of the dramatically improved particle size control when using the thiol-modified monolith.

5.13 Conclusions

In summary, have shown how two simple methods can be used to prepare mesoporous monolithic reactors functionalised evenly along their length with Au nanoparticles. These methods consist of (i) impregnation of Au nanoparticles in the porous network during monolith synthesis, (ii) functionalising the monolith with sulphur groups and then passing Au along the monolith, forming Au-thiol bonds. While both methods successfully achieved even distribution of gold nanoparticles along the length of the monolithic microreactor, the two methods were found to lead to very different Au particle sizes and therefore available catalytic Au surface area, as seen by the XPS and TEM. It was found that a pure silica monolith was inactive for the oxidation reaction. The incorporation of Au proved essential in utilising the monoliths for continuous flow selective oxidation catalytic microreactors. The Au-free monoliths were found to be unreactive at 30 °C. The thiol-functionalised was found to be more active when using TBHP as oxidant as compared to the impregnated monolith due to the better dispersity and higher surface area of Au and in spite of the presence of sulfur. Additionally, the oxidation reaction on the Au-thiol functionalized monolith was found to depend on the type of oxidant used with *tert*-butyl hydroperoxide being more active than H₂O₂, likely due to the thiol induced hydrophobicity of the monolith. Overall the results point to the use of post synthetic surface modification to anchor nanoparticles as a highly effective strategy for evenly incorporating catalytically active nanoparticles within monolithic flow reactors.

Chapter 6. Conclusions and Future work

As a general conclusion for this thesis, silica monoliths were utilised as flow microreactors and were found to offer more effective control over chemical reactions compared to traditional batch chemistry. Their high-surface area and excellent thermal transfer characteristics create a new dimension in reaction control. The production of a stable monolithic structure through a sol-gel method was investigated. Different approaches have been utilized to produce macroporous silica-monoliths with different physical properties. Six silica monoliths were prepared with different physical properties of surfaces area, and pore size. Three of them were used for lipase immobilisation to generate active and stable immobilised lipase microreactors for biocatalysis. The kinetic behaviour of immobilised lipase and free lipase were studied in the hydrolysis reaction of 4-NPB in water–decane media. The kinetic studies revealed that immobilised lipase in silica monoliths was more active than free lipase when the physical properties of the monolith were adjusted to increase the pore size. It was found that increasing the average pore size helped to overcome the lipase aggregation and pore blocking and thus increased the lipase specific activity and the accessibility of the substrate to the biphasic system compared to other published work.

The effectiveness of the immobilised lipase microreactor was tested for the transesterification of tributyrin (TB). TB was quantitatively transformed into methyl butyrate when using flow rates of $0.8 \mu\text{L min}^{-1}$. The immobilised lipase microreactor was also shown to be reusable without loss of activity for 105 hours when operated at 30°C and flow rates of $0.8 \mu\text{L min}^{-1}$. The reaction was optimized with respect to temperature, flow rate and oil/methanol ratio. It was found that increasing methanol and temperatures deactivate the lipase. The highest activity was obtained at a 2:1 methanol to tributyrin

molar ratio. The silica monolithic microreactor channels provide a large surface area for enzyme immobilisation.

The work was extended to utilise the advantages of the microreactor in an oxidation reaction. This was done by immobilising gold nano particles by two different methods. Both methods were found suitable (i) impregnation of Au nanoparticles in the porous network during monolith synthesis, and (ii) functionalising the monolith with sulfur groups and then passing Au along the monolith, forming Au-thiol bonds. While both methods successfully achieved even distribution of gold nanoparticles along the length of the monolithic microreactor, the two methods were found to lead to very different Au particle sizes and therefore available catalytic Au surface areas, as seen by XPS and TEM analysis. It was found that a pure silica monolith was inactive for the oxidation reaction. The oxidation reaction of cyclohexene was performed with gold nanoparticles immobilised in a silica monolith microreactor. The incorporation of Au proved essential in utilising the monoliths for continuous flow selective oxidation catalytic microreactors. The Au-free monoliths were found to be unreactive at 30° C. The thiol functionalised was found to be more active as compared to the impregnated monolith due to the better dispersity and higher surface area of Au and in spite of the presence of sulfur. Additionally, the oxidation reaction on the Au-thiol-functionalised monolith was found to depend on the type of oxidant used with *tert*-butyl hydroperoxide being more active than H₂O₂ due to the thiol-induced hydrophobicity of the monolith. Overall, the results point to the use of post-synthetic surface modification to anchor nanoparticles as a highly effective strategy for evenly incorporating catalytically active nanoparticles within monolithic flow reactors.

The primary and critical finding of this project has been that the flow system design was revealed as a highly useful tool. It is notable that, if subjected to further development,

considerable value could be achieved in contributions to further analyses of flow organic reaction. The successful achievement of the transesterification and oxidation reactions took place in flow, and there is the possibility of several other reactions for this flow system setup.

The work described in the earlier chapters is only one step towards the use of a silica monolith as a microreactor for a range of reactions. The use of an immobilised catalyst is well known in the field of heterogeneous catalysis and it has its advantages and disadvantages. Combining the advantages of flow microreactor reactor technology with the advantages of heterogeneous catalysis was the main theme of this thesis and it proved to be more efficient when the microreactor is fabricated in certain ways. Therefore, the first prospective future work which could add to the subject is to study the fabrication process in more detail and obtain silica monoliths with different physical characteristics. Then, similar methodology used in this thesis can be applied in grafting the catalyst and studying its activity within the microreactor. This should reveal more information about the relation between the silica monoliths and immobilised functional sites activity. In order to build on the progress made in the current study, is to use silica monoliths as microreactors support in the design of cooperative heterogeneous catalysts. The primary obstacle for the present study will revolve around the identification of the suitable functional groups and their ideal concentrations. Despite this, surface organisation will be the critical stage that determines the design of effective cooperative and bifunctional (or even polyfunctional) catalytic microreactors.

The idea of developing a polyfunctional solid catalyst comes from the biodiesel chapter. Using used oil as a biodiesel source is always a challenge because it consists of high concentrations of free fatty acids which needs an acid catalyst to form an ester. At the same time, a base catalyst is still required for the transesterification reaction. Therefore,

a polyfunctional catalyst that is able to catalyse both ester and transesterification reactions in one pot will be an advantage. A monolith and base groups such as amine groups in the second half of the silica monolith could be used for biodiesel production from used oil in a continuous process. Silica monoliths with bi-metals can be used as well. In this work, a silica monolith with nano gold was utilised for oxidation reactions. However, there could be an advantage in adding another oxidizing metal to enhance the oxidation reaction rate. Most of these catalysts were tried in batch phases so using a silica monolith as a microreactor will allow these bi-metals to be studied in continuous phase, thus adding another dimension to their activity.

Chapter 7. References

1. A. Stankiewicz and J. A. Moulijn, *Re-engineering the chemical processing plant: process intensification*, CRC Press, 2003.
2. P. L. Mills, D. J. Quiram and J. F. Ryley, *Chemical Engineering Science*, 2007, **62**, 6992-7010.
3. D. Patel, S. Kellici and B. Saha, *Processes*, 2014, **2**, 311.
4. R. Schütte, M. Matlosz, A. Renken, M. Liauw and O. Langer, IMRET 9, *Potsdam/Berlin, Germany*, 2006.
5. P. Watts and S. J. Haswell, *Chemical Society Reviews*, 2005, **34**, 235-246.
6. W. Ehrfeld, V. Hessel and H. Löwe, *Microreactors: New Technology for Modern Chemistry*, Wiley, 2000.
7. P. D. I. Fletcher, S. J. Haswell, E. Pombo-Villar, B. H. Warrington, P. Watts, S. Y. F. Wong and X. Zhang, *Tetrahedron*, 2002, **58**, 4735-4757.
8. K. F. Ehmann, D. Bourell, M. L. Culpepper, T. J. Hodgson, T. R. Kurfess, M. Madou, K. Rajurkar and R. DeVor, *Micromanufacturing: International research and development*, Springer Science and Business Media, 2007.
9. J. Schrickel and C. AG, *Chimica Oggi-Chemistry Today*, 2013, **31**, 3.
10. R. Knitter and M. A. Liauw, *Lab on a Chip*, 2004, **4**, 378-383.
11. R. J. Jackman, T. M. Floyd, R. Ghodssi, M. A. Schmidt and K. F. Jensen, *Journal of Micromechanics and Microengineering*, 2001, **11**, 263.
12. D. Roberge, *Green Processing and Synthesis*, 2012, **1**, 129-130.
13. J. R. Anderson, D. T. Chiu, R. J. Jackman, O. Cherniavskaya, J. C. McDonald, H. Wu, S. H. Whitesides and G. M. Whitesides, *Analytical Chemistry*, 2000, **72**, 3158-3164.
14. T. Wirth, *Microreactors in organic chemistry and catalysis*, John Wiley and Sons, 2013.
15. M. P. C. Marques and P. Fernandes, *Molecules*, 2011, **16**, 8368.
16. B. H. Jo, L. M. Van Lerberghe, K. M. Motsegood and D. J. Beebe, *Microelectromechanical Systems, Journal of*, 2000, **9**, 76-81.
17. H. Kawazumi, A. Tashiro, K. Ogino and H. Maeda, *Lab on a Chip*, 2002, **2**, 8-10.
18. G. Velze-Casquillas, M. Le Berre, M. Piel and P. T. Tran, *Nano Today*, 2010, **5**, 28-47.
19. K. F. Jensen, *MRS bulletin*, 2006, **31**, 101-107.
20. C.-C. Lee, G. Sui, A. Elizarov, C. J. Shu, Y.-S. Shin, A. N. Dooley, J. Huang, A. Daridon, P. Wyatt, D. Stout, H. C. Kolb, O. N. Witte, N. Satyamurthy, J. R. Heath, M. E. Phelps, S. R. Quake and H.-R. Tseng, *Science*, 2005, **310**, 1793-1796.
21. P. D. I. Fletcher, S. J. Haswell, E. Pombo-Villar, B. H. Warrington, P. Watts, S. Y. F. Wong and X. L. Zhang, *Tetrahedron*, 2002, **58**, 4735-4757.
22. L. Martínez-Latorre, P. Ruiz-Cebollada, A. Monzón and E. García-Bordejé, *Catalysis Today*, 2009, **147**, S87-S93.
23. C. Alépée, L. Vulpescu, P. Cousseau, P. Renaud, R. Maurer and A. Renken, *Measurement and Control*, 2000, **33**, 265-268.
24. E. Iannone, *Labs on chip: Principles, Design and Technology*, CRC Press, 2014.
25. A. Phommahaxay, G. Lissorgues, L. Rousseau, T. Bourouina and P. Nicole, *arXiv preprint arXiv:0711.3276*, 2007.
26. X. Yao, Y. Zhang, L. Du, J. Liu and J. Yao, *Renewable and Sustainable Energy Reviews*, 2015, **47**, 519-539.
27. E. R. Murphy, J. R. Martinelli, N. Zaborenko, S. L. Buchwald and K. F. Jensen, *Angewandte Chemie International Edition*, 2007, **46**, 1734-1737.

28. S. Loebbecke, J. Antes, W. Ferstl, D. Boskovic, T. Tuercke, M. Schwarzer and H. Krause, 2007.
29. T. Bayer, J. Jenck and M. Matlosz, *Chemical Engineering and Technology*, 2005, **28**, 431-438.
30. R. D. Chambers and R. C. H. Spink, *Chemical Communications*, 1999, 883-884.
31. R. C. R. Wootton, R. Fortt and A. J. de Mello, *Lab on a Chip*, 2002, **2**, 5-7.
32. B. P. Mason, K. E. Price, J. L. Steinbacher, A. R. Bogdan and D. T. McQuade, *Chemical Reviews*, 2007, **107**, 2300-2318.
33. N. G. Anderson, *Organic Process Research and Development*, 2001, **5**, 613-621.
34. C. Wiles and P. Watts, *European Journal of Organic Chemistry*, 2008, **2008**, 1655-1671.
35. A. I. Stankiewicz and J. A. Moulijn, *Chemical Engineering Progress*, 2000, **96**, 22-34.
36. V. Hessel, J. C. Schouten and A. Renken, *Micro process engineering: a comprehensive handbook*, John Wiley and Sons, 2009.
37. R. M. Tiggelaar, P. v. Male, J. W. Berenschot, J. G. E. Gardeniers, R. E. Oosterbroek, M. H. J. M. d. Croon, J. C. Schouten, A. v. d. Berg and M. C. Elwenspoek, *Sensors and Actuators A: Physical*, 2005, **119**, 196-205.
38. C. S. Martínez-Cisneros, S. G.-d. Pedro, M. Puyol, J. García-García and J. Alonso-Chamarro, *Chemical Engineering Journal*, 2012, **211-212**, 432-441.
39. K. Jain, C. Wu, S. V. Atre, G. Jovanovic, V. Narayanan, S. Kimura, V. Sprenkle, N. Canfield and S. Roy, *International Journal of Applied Ceramic Technology*, 2009, **6**, 410-419.
40. H. Löwe, V. Hessel and A. Mueller, *Pure and Applied Chemistry*, 2002, **74**, 2271-2276.
41. Y.-S. Lee, J. M. Jeong, H. W. Kim, Y. S. Chang, Y. J. Kim, M. K. Hong, G. B. Rai, D. Y. Chi, W. J. Kang, J. H. Kang, D. S. Lee, J.-K. Chung, M. C. Lee and Y.-G. Suh, *Nuclear Medicine and Biology*, 2006, **33**, 677-683.
42. J. N.-S. M. BENKE, *Materials Science and Engineering*, 2014, **39**, 89-101.
43. R. Porta, M. Benaglia and A. Puglisi, *Organic Process Research and Development*, 2016, **20**, 2-25.
44. T. W. Phillips, I. G. Lignos, R. M. Maceiczky, A. J. deMello and J. C. deMello, *Lab on a Chip*, 2014, **14**, 3172-3180.
45. S. Marre, J. Baek, J. Park, M. G. Bawendi and K. F. Jensen, *Journal of the Association for Laboratory Automation*, 2009, **14**, 367-373.
46. S. Marre, J. Park, J. Rempel, J. Guan, M. G. Bawendi and K. F. Jensen, *Advanced Materials*, 2008, **20**, 4830-4834.
47. A. J. deMello, *Nature*, 2006, **442**, 394-402.
48. C.-Y. Lee, C.-L. Chang, Y.-N. Wang and L.-M. Fu, *International Journal of Molecular Sciences*, 2011, **12**, 3263-3287.
49. X. C. i Solvas, R. A. Lambert, L. Kulinsky, R. H. Rangel and M. J. Madou, *Micro and Nano Systems*, 2009, **1**, 2-11.
50. P. Löb, K. S. Drese, V. Hessel, S. Hardt, C. Hofmann, H. Löwe, R. Schenk, F. Schönfeld and B. Werner, *Chemical Engineering and Technology*, 2004, **27**, 340-345.
51. V. Hessel, S. Hardt, H. Löwe and F. Schönfeld, *AIChE Journal*, 2003, **49**, 566-577.
52. K. F. Jensen, 2005.
53. V. Hessel, H. Löwe and F. Schönfeld, *Chemical Engineering Science*, 2005, **60**, 2479-2501.

54. B. Ahmed-Omer, J. C. Brandt and T. Wirth, *Organic and Biomolecular Chemistry*, 2007, **5**, 733-740.
55. M. Baumann, I. R. Baxendale, S. V. Ley, C. D. Smith and G. K. Tranmer, *Organic Letters*, 2006, **8**, 5231-5234.
56. J. A. Banister, P. D. Lee and M. Poliakoff, *Organometallics*, 1995, **14**, 3876-3885.
57. J. L. F. C. Lima, J. L. M. Santos, A. C. B. Dias, M. F. T. Ribeiro and E. A. G. Zagatto, *Talanta*, 2004, **64**, 1091-1098.
58. K. F. Bolton, A. J. Canty, J. A. Deverell, R. M. Guijt, E. F. Hilder, T. Rodemann and J. A. Smith, *Tetrahedron Letters*, 2006, **47**, 9321-9324.
59. M. Brivio, W. Verboom and D. N. Reinhoudt, *Lab on a Chip*, 2006, **6**, 329-344.
60. K. J. Shaw, P. T. Docker, J. V. Yelland, C. E. Dyer, J. Greenman, G. M. Greenway and S. J. Haswell, *Lab on a Chip*, 2010, **10**, 1725-1728.
61. T. P. Petersen, A. Ritzén and T. Ulven, *Organic Letters*, 2009, **11**, 5134-5137.
62. M. E. Sacks, S.-I. Lee and J. A. Biesenberger, *Chemical Engineering Science*, 1973, **28**, 241-257.
63. M. Baumann and I. R. Baxendale, *Beilstein Journal of Organic Chemistry*, 2015, **11**, 1194-1219.
64. K. Geyer and P. H. Seeberger, *VDIBERICHT*, 2008, **2039**, 91.
65. G. Jas and A. Kirschning, *Chemistry—A European Journal*, 2003, **9**, 5708-5723.
66. N. Rott, *Annual Review of Fluid Mechanics*, 1990, **22**, 1-12.
67. N. Ryan and M. Johnson, *AIChE Journal*, 1959, **5**, 433-435.
68. Cheremisinoff, N.P. and Cheremisinoff, P.N., 1981. Cooling towers selection, design and practice.
69. J. D. Adams and H. T. Soh, *Journal of the Association for Laboratory Automation*, 2009, **14**, 331-340.
70. F. Smith, *IMA Journal of Applied Mathematics*, 1982, **28**, 207-281.
71. P. Hänggi and F. Marchesoni, *arXiv preprint cond-mat/0502053*, 2005.
72. A. E. Kamholz and P. Yager, *Biophysical Journal*, 2001, **80**, 155-160.
73. S. A. Peyman, A. Iles and N. Pamme, *Chemical Communications*, 2008, 1220-1222.
74. M. Vojtišek, A. Iles and N. Pamme, *Biosensors and Bioelectronics*, 2010, **25**, 2172-2176.
75. V. Chiroli, M. Benaglia, A. Puglisi, R. Porta, R. P. Jumde and A. Mandoli, *Green Chemistry*, 2014, **16**, 2798-2806.
76. A. Sachse, A. Galarneau, B. Coq and F. Fajula, *New Journal of Chemistry*, 2011, **35**, 259-264.
77. R. M. Heck, S. Gulati and R. J. Farrauto, *Chemical Engineering Journal*, 2001, **82**, 149-156.
78. G. Guiochon, *Journal of Chromatography A*, 2007, **1168**, 101-168.
79. C. Triantafillidis, M. S. Elsaesser and N. Husing, *Chemical Society Reviews*, 2013, **42**, 3833-3846.
80. L. Kiwi-Minsker, *CHIMIA International Journal for Chemistry*, 2002, **56**, 143-147.
81. F. Svec and Z. Deyl, *Capillary electrochromatography*, Elsevier, 2001.
82. S. Hjerten, J.-L. Liao and R. Zhang, *Journal of Chromatography A*, 1989, **473**, 273-275.
83. F. Svec and J. M. Fréchet, *Analytical Chemistry*, 1992, **64**, 820-822.
84. H. Zou, X. Huang, M. Ye and Q. Luo, *Journal of Chromatography A*, 2002, **954**, 5-32.
85. S. M. Fields, *Analytical Chemistry*, 1996, **68**, 2709-2712.

86. H. Minakuchi, K. Nakanishi, N. Soga, N. Ishizuka and N. Tanaka, *Analytical Chemistry*, 1996, **68**, 3498-3501.
87. M. T. Alotaibi, M. J. Taylor, D. Liu, S. K. Beaumont and G. Kyriakou, *Surface Science*, 2016, **646**, 179-185.
88. R. E. Trubac, F. M. Dautzenberg, T. A. Griffin, B. Paikert, V. R. Schmidt and R. A. Overbeek, *Catalysis Today*, 2001, **69**, 17-24.
89. M. Kato, K. Sakai-Kato and T. Toyo'oka, *Journal of Separation Science*, 2005, **28**, 1893-1908.
90. M. M. Manfe, K. Kulkarni and A. Kulkarni, *Int. J. Adv. Eng. Res. Stud.(E-ISSN2249-8974)*, 2011.
91. D. Mangelings and Y. Vander Heyden, *Journal of Chromatographic Science*, 2009, **47**, 407-417.
92. H. Zhong, G. Zhu, P. Wang, J. Liu, J. Yang and Q. Yang, *Journal of Chromatography A*, 2008, **1190**, 232-240.
93. E. Tronconi, A. Cavanna, C. Orsenigo and P. Forzatti, *Industrial and Engineering Chemistry Research*, 1999, **38**, 2593-2598.
94. A. M. Siouffi, *Journal of Chromatography A*, 2003, **1000**, 801-818.
95. R. Miyamoto, Y. Ando, C. Kurusu, H. z. Bai, K. Nakanishi and M. Ippommatsu, *Journal of separation science*, 2013, **36**, 1890-1896.
96. Q. S. Qu, S. Wang, D. Mangelings, C. Y. Wang, G. J. Yang, X. Y. Hu and C. Yan, *Electrophoresis*, 2009, **30**, 1071-1076.
97. H. Minakuchi, K. Nakanishi, N. Soga, N. Ishizuka and N. Tanaka, *Journal of Chromatography A*, 1998, **797**, 121-131.
98. M. Niederberger and N. Pinna, *Metal oxide nanoparticles in organic solvents: synthesis, formation, assembly and application*, Springer Science and Business Media, 2009.
99. A. M Frolova, M. A Chukhlieb, A. V Drobot, A. P Kryshnal, L. P Loginova and A. P Boichenko, *The Open Surface Science Journal*, 2009
100. O. Núñez, K. Nakanishi and N. Tanaka, *Journal of Chromatography A*, 2008, **1191**, 231-252.
101. L. Xu and H. K. Lee, *Journal of Chromatography A*, 2008, **1195**, 78-84.
102. B. Gawel, K. Gawel and G. Øye, *Materials*, 2010, **3**, 2815-2833.
103. C. J. Brinker and G. W. Scherer, *Sol-gel science: the physics and chemistry of sol-gel processing*, Academic press, 2013.
104. K. Sinkó, *Materials*, 2010, **3**, 704.
105. M. Motokawa, H. Kobayashi, N. Ishizuka, H. Minakuchi, K. Nakanishi, H. Jinnai, K. Hosoya, T. Ikegami and N. Tanaka, *Journal of Chromatography A*, 2002, **961**, 53-63.
106. K. Nakanishi, *Journal of Porous Materials*, 1997, **4**, 67-112.
107. S. Shrinivasan, M. C. Breadmore, B. Hosticka, J. P. Landers and P. M. Norris, *Journal of Non-Crystalline Solids*, 2004, **350**, 391-396.
108. P. D. Fletcher, S. J. Haswell, P. He, S. M. Kelly and A. Mansfield, *Journal of Porous Materials*, 2011, **18**, 501-508.
109. N. Tanaka, H. Kobayashi, N. Ishizuka, H. Minakuchi, K. Nakanishi, K. Hosoya and T. Ikegami, *Journal of Chromatography A*, 2002, **965**, 35-49.
110. R. Takahashi, K. Nakanishi and N. Soga, *Faraday Discussing.*, 1995, **101**, 249-263.
111. K. Nakanishi, R. Takahashi, T. Nagakane, K. Kitayama, N. Koheiya, H. Shikata and N. Soga, *Journal of Sol-Gel Science and Technology*, **17**, 191-210.
112. Y. Wei, T. E. Parmentier, K. P. de Jong and J. Zečević, *Chemical Society Reviews*, 2015, **44**, 7234-7261.

113. F. Akhtar, L. Andersson, S. Ogunwumi, N. Hedin and L. Bergström, *Journal of the European Ceramic Society*, 2014, **34**, 1643-1666.
114. W. M. Carty and P. W. Lednor, *Current Opinion in Solid State and Materials Science*, 1996, **1**, 88-95.
115. A. Inayat, B. Reinhardt, H. Uhlig, W.-D. Einicke and D. Enke, *Chemical Society Reviews*, 2013, **42**, 3753-3764.
116. K. Nakanishi, H. Minakuchi, N. Soga and N. Tanaka, *Journal of Sol-Gel Science and Technology*, **8**, 547-552.
117. N. Ishizuka, H. Minakuchi, K. Nakanishi, K. Hirao and N. Tanaka, *Colloids and Surfaces A: Physicochemical and Engineering Aspects*, 2001, **187-188**, 273-279.
118. D. M. Smith, G. W. Scherer and J. M. Anderson, *Journal of Non-Crystalline Solids*, 1995, **188**, 191-206.
119. G. W. Scherer and D. M. Smith, *Journal of Non-Crystalline Solids*, 1995, **189**, 197-211.
120. I. D. Wilson, *Handbook of methods and instrumentation in separation science, vol 1*, Elsevier, Boston, MA, 2009.
121. J. M. Armenta, B. Gu, P. H. Humble, C. D. Thulin and M. L. Lee, *Journal of Chromatography A*, 2005, **1097**, 171-178.
122. I. Gusev, X. Huang and C. Horváth, *Journal of Chromatography A*, 1999, **855**, 273-290.
123. F. Svec, *Journal of Chromatography A*, 2010, **1217**, 902-924.
124. F. Svec, *Journal of separation science*, 2004, **27**, 747-766.
125. Y. Li and M. L. Lee, *Journal of separation science*, 2009, **32**, 3369-3378.
126. F. Svec and J. M. J. Fréchet, *Chemistry of Materials*, 1995, **7**, 707-715.
127. I. Nischang, *Journal of Chromatography A*, 2013, **1287**, 39-58.
128. V. F. Samanidou, A. S. Ioannou and I. N. Papadoyannis, *Journal of Chromatography B*, 2004, **809**, 175-182.
129. K. Cabrera, G. Wieland, D. Lubda, K. Nakanishi, N. Soga, H. Minakuchi and K. K. Unger, *TrAC Trends in Analytical Chemistry*, 1998, **17**, 50-53.
130. E. C. Peters, F. Svec and J. M. J. Fréchet, *Chemistry of Materials*, 1997, **9**, 1898-1902.
131. E. Alzahrani and K. Welham, *Analyst*, 2011, **136**, 4321-4327.
132. L. Z. Fan, Y. S. Hu, J. Maier, P. Adelhelm, B. Smarsly and M. Antonietti, *Advanced Functional Materials*, 2007, **17**, 3083-3087.
133. F. C. Leinweber and U. Tallarek, *Journal of Chromatography A*, 2003, **1006**, 207-228.
134. D. Cabooter, K. Broeckhoven, R. Sterken, A. Vanmessen, I. Vandendael, K. Nakanishi, S. Deridder and G. Desmet, *Journal of Chromatography A*, 2014, **1325**, 72-82.
135. I. M. Lazar, L. Li, Y. Yang and B. L. Karger, *Electrophoresis*, 2003, **24**, 3655-3662.
136. M.-C. Hennion, *Journal of Chromatography A*, 1999, **856**, 3-54.
137. S. Xie, F. Svec and J. M. J. Fréchet, *Chemistry of Materials*, 1998, **10**, 4072-4078.
138. E. C. Peters, F. Svec, J. M. Fréchet, C. Viklund and K. Irgum, *Macromolecules*, 1999, **32**, 6377-6379.
139. M. Kele and G. Guiochon, *Journal of Chromatography A*, 2002, **960**, 19-49.
140. S. L. Cohen and B. T. Chait, *Analytical Chemistry*, 1996, **68**, 31-37.
141. C. F. Poole, *TrAC Trends in Analytical Chemistry*, 2003, **22**, 362-373.
142. Y. Ueki, T. Umemura, J. Li, T. Odake and K.-i. Tsunoda, *Analytical Chemistry*, 2004, **76**, 7007-7012.

143. N. J. Simpson, *Solid-phase extraction: principles, techniques, and applications*, CRC Press, 2000.
144. P. K. Jal, S. Patel and B. K. Mishra, *Talanta*, 2004, **62**, 1005-1028.
145. E. Alzahrani and K. Welham, *Analyst*, 2012, **137**, 4751-4759.
146. C. Viklund, E. Pontén, B. Glad, K. Irgum, P. Hörstedt and F. Svec, *Chemistry of Materials*, 1997, **9**, 463-471.
147. N. Shinozaki, R. Takahashi, S. Sato and T. Sodesawa, *Journal of Sol-Gel Science and Technology*, 2007, **43**, 275-282.
148. R. Sharma, S. Dwivedi, K. Hristovski, Y. Wu, R. Srinivasan, A. Mishra, J. H. Clark, G. A. Kraus, P. R. Seidl and A. Stankiewicz, *Green Materials for Sustainable Water Remediation and Treatment*, Royal Society of Chemistry, 2013.
149. M. J. Telepchak, G. Chaney and T. F. August, *Forensic and Clinical Applications of Solid Phase Extraction*, Springer, 2004.
150. J. E. Sandoval and J. J. Pesek, *Analytical Chemistry*, 1991, **63**, 2634-2641.
151. J. M. Herrero-Martínez, A. Méndez, E. Bosch and M. Rosés, *Journal of Chromatography A*, 2004, **1060**, 135-145.
152. M. M. Sanagi, A. A. Naim, A. Hussain and N. Dzakaria, *Malaysian Journal of Analytical Sciences*, 2001, **7**, 337-343.
153. C. W. Klampfl, *Journal of Chromatography A*, 2004, **1044**, 131-144.
154. Q. Wei, *Surface modification of textiles*, Elsevier, 2009.
155. N. Kanellopoulos, *Nanoporous materials: Advanced techniques for characterization, modeling, and processing*, CRC Press, 2011.
156. J. L. Williams, *Catalysis Today*, 2001, **69**, 3-9.
157. S. Roy, T. Bauer, M. Al-Dahhan, P. Lehner and T. Turek, *AIChE Journal*, 2004, **50**, 2918-2938.
158. T. A. Nijhuis, M. T. Kreutzer, A. C. J. Romijn, F. Kapteijn and J. A. Moulijn, *Chemical Engineering Science*, 2001, **56**, 823-829.
159. F. Svec, *Journal of Separation Science*, 2004, **27**, 1419-1430.
160. K. Cabrera, *Journal of Separation Science*, 2004, **27**, 843-852.
161. N. Tanaka, H. Kobayashi, K. Nakanishi, H. Minakuchi and N. Ishizuka, *Analytical Chemistry*, 2001, **73**, 420 A-429 A.
162. M. Bedair and Z. El Rassi, *Electrophoresis*, 2004, **25**, 4110-4119.
163. H. Fu, W. Jin, H. Xiao, C. Xie, B. Guo and H. Zou, *Electrophoresis*, 2004, **25**, 600-606.
164. F. Svec and A. A. Kurganov, *Journal of Chromatography A*, 2008, **1184**, 281-295.
165. E. F. Hilder, F. Svec and J. M. J. Fréchet, *Journal of Chromatography A*, 2004, **1044**, 3-22.
166. T. Nema, E. C. Y. Chan and P. C. Ho, *Talanta*, 2010, **82**, 488-494.
167. D. S. Peterson, T. Rohr, F. Svec and J. M. J. Frechet, *Analytical Chemistry*, 2002, **74**, 4081-4088.
168. G. Emig, *Chemie in unserer Zeit*, 1987, **21**, 128-137.
169. J. Hagen, *Industrial catalysis: a practical approach*, John Wiley and Sons, 2015.
170. G. V. Smith and F. Notheisz, *Heterogeneous catalysis in organic chemistry*, Academic Press, 1999.
171. E. Klemm, H. Doering, A. Geisselmann and S. Schirrmeister, *Chemical Engineering and Technology*, 2007, **30**, 1615-1621.
172. T. Chinnusamy, S. Yudha, M. Hager, P. Kreitmeier and O. Reiser, *ChemSusChem*, 2012, **5**, 247-255.
173. O. Deutschmann, H. Knözinger, K. Kochloefl and T. Turek, *Ullmann's Encyclopedia of Industrial Chemistry*, 2009.

174. I. Chorkendorff and J. W. Niemantsverdriet, *Concepts of modern catalysis and kinetics*, John Wiley and Sons, 2006.
175. G. Rothenberg, *Catalysis: Concepts and Green Applications*, 2008, 127-187.
176. M. Misson, H. Zhang and B. Jin, *Journal of The Royal Society Interface*, 2015, **12**, 20140891.
177. M. Adamczak and S. H. Krishna, *Food Technology and Biotechnology*, 2004, **42**, 251-264.
178. R. K. Singh, M. K. Tiwari, R. Singh and J.-K. Lee, *International Journal of Molecular Sciences*, 2013, **14**, 1232-1277.
179. A. S. Bommarius and B. R. Riebel-Bommarius, *Biocatalysis: fundamentals and applications*, John Wiley and Sons, 2004.
180. O. Kirk and M. W. Christensen, *Organic Process Research and Development*, 2002, **6**, 446-451.
181. B. Joseph, P. W. Ramteke and G. Thomas, *Biotechnology Advances*, 2008, **26**, 457-470.
182. A. A. Mendes and H. F. d. Castro, *Brazilian Archives of Biology and Technology*, 2005, **48**, 135-142.
183. S. Sharma and S. S. Kanwar, *The Scientific World Journal*, 2014, **2014**.
184. A. Rajendran, A. Palanisamy and V. Thangavelu, *Brazilian Archives of Biology and Technology*, 2009, **52**, 207-219.
185. C. Ke, Y. Fan, Y. Chen, L. Xu and Y. Yan, *RSC Advances*, 2016, **6**, 19413-19416.
186. W. Aehle, *Enzymes in industry: production and applications*, John Wiley and Sons, 2007.
187. P. Villeneuve, J. M. Muderhwa, J. Graille and M. J. Haas, *Journal of Molecular Catalysis B: Enzymatic*, 2000, **9**, 113-148.
188. R. Sharma, Y. Chisti and U. C. Banerjee, *Biotechnology Advances*, 2001, **19**, 627-662.
189. S. V. Ley, D. E. Fitzpatrick, R. M. Myers, C. Battilocchio and R. Ingham, *Angewandte Chemie International Edition*, 2015, **54**, 10122-10136.
190. P. Watts and C. Wiles, *Chemical Communications*, 2007, DOI: 10.1039/B609428G, 443-467.
191. M. C. Franssen, P. Steunenberg, E. L. Scott, H. Zuilhof and J. P. Sanders, *Chemical Society Reviews*, 2013, **42**, 6491-6533.
192. B. Averill, J. Moulijn, R. van Santen and P. van Leeuwen, *Catalysis: An Integrated Approach: An Integrated Approach*, Elsevier, 1999.
193. Y. Yeşiloğlu, *Process Biochemistry*, 2005, **40**, 2155-2159.
194. S. Li, J. Hu and B. Liu, *Biosystems*, 2004, **77**, 25-32.
195. N. Ortega, M. Perez-Mateos, M. C. Pilar and M. D. Busto, *Journal of Agricultural and Food Chemistry*, 2009, **57**, 109-115.
196. E. Y. Ozmen and M. Yilmaz, *Colloids and Surfaces B: Biointerfaces*, 2009, **69**, 58-62.
197. S. Y. Chang, N.-Y. Zheng, C.-S. Chen, C.-D. Chen, Y.-Y. Chen and C. R. C. Wang, *Journal of the American Society for Mass Spectrometry*, 2007, **18**, 910-918.
198. F. X. Malcata, H. R. Reyes, H. S. Garcia, C. G. Hill Jr and C. H. Amundson, *Journal of the American Oil Chemists' Society*, 1990, **67**, 890-910.
199. A. Bastida, P. Sabuquillo, P. Armisen, R. Fernandez-Lafuente, J. Hugué and J. M. Guisan, *Biotechnology and Bioengineering*, 1998, **58**, 486-493.
200. R. Fernandez-Lafuente, *Enzyme and Microbial Technology*, 2009, **45**, 405-418.
201. E. Ruckenstein and X. Wang, *Biotechnology and Bioengineering*, 1993, **42**, 821-828.

202. J. Yang, X. Ma, Z. Zhang, B. Chen, S. Li and G. Wang, *Biotechnology Advances*, 2010, **28**, 644-650.
203. M. T. Reetz, A. Zonta and J. Simpelkamp, *Biotechnology and Bioengineering*, 1996, **49**, 527-534.
204. J.-P. Chen and W.-S. Lin, *Enzyme and Microbial Technology*, 2003, **32**, 801-811.
205. C. Mateo, J. M. Palomo, G. Fernandez-Lorente, J. M. Guisan and R. Fernandez-Lafuente, *Enzyme and Microbial Technology*, 2007, **40**, 1451-1463.
206. J. Alemán, A. V. Chadwick, J. He, M. Hess, K. Horie, R. G. Jones, P. Kratochvíl, I. Meisel, I. Mita and G. Moad, *Pure and Applied Chemistry*, 2007, **79**, 1801-1829.
207. J. F. Díaz and K. J. Balkus Jr, *Journal of Molecular Catalysis B: Enzymatic*, 1996, **2**, 115-126.
208. P. H. Pandya, R. V. Jasra, B. L. Newalkar and P. N. Bhatt, *Microporous and Mesoporous Materials*, 2005, **77**, 67-77.
209. A. Popat, S. B. Hartono, F. Stahr, J. Liu, S. Z. Qiao and G. Q. M. Lu, *Nanoscale*, 2011, **3**, 2801-2818.
210. M. T. Reetz, A. Zonta and J. Simpelkamp, *Angewandte Chemie*, 1995, **107**, 373-376.
211. M. T. Reetz, P. Tielmann, W. Wiesenhöfer, W. Könen and A. Zonta, *Advanced Synthesis and Catalysis*, 2003, **345**, 717-728.
212. F. Beisson, A. Tiss, C. Rivière and R. Verger, *European Journal of Lipid Science and Technology*, 2000, **102**, 133-153.
213. E. J. Herrera-López, *Lipases and Phospholipases: Methods and Protocols*, 2012, 525-543.
214. K. F. Tipton, *Enzyme assays*. Oxford Univ. Press, Oxford, UK, 1992, 1-58.
215. E. Mateos-Díaz, J. A. Rodríguez, M. de los Ángeles Camacho-Ruiz and J. C. Mateos-Díaz, *Lipases and Phospholipases: Methods and Protocols*, 2012, 89-100.
216. D. Guieysse, G. Sandoval, L. Faure, J.-M. Nicaud, P. Monsan and A. Marty, *Tetrahedron: Asymmetry*, 2004, **15**, 3539-3543.
217. J. C. Mateos, K. Ruiz, J. A. Rodriguez, J. Cordova and J. Baratti, *Journal of Molecular Catalysis B: Enzymatic*, 2007, **49**, 104-112.
218. L. Ramírez, J. Arrizon, G. Sandoval, A. Cardador, R. Bello-Mendoza, P. Lappe and J. Mateos-Díaz, *Applied biochemistry and biotechnology*, 2008, **151**, 711-723.
219. R. Eienthal and M. J. Danson, *Enzyme assays: a practical approach*, Oxford University Press, USA, 2002.
220. F. M. Everaerts, J. L. Beckers and T. P. Verheggen, *Isotachopheresis: theory, instrumentation and applications*, Elsevier, 2011.
221. V. Henri, *Lois générales de l'action des diastases*, Librairie Scientifique A. Hermann, 1903.
222. L. Michaelis and M. L. Menten, *Biochem.*"Die kinetik der invertinwirkung."*Biochem. z* 49.333-369 (1913): 352
223. J. M. Berg, J. L. Tymoczko and L. Stryer, *Biochemistry*, Parts 1-34, 2002.
224. A. G. Hadd, D. E. Raymond, J. W. Halliwell, S. C. Jacobson and J. M. Ramsey, *Analytical Chemistry*, 1997, **69**, 3407-3412.
225. D. C. Duffy, H. L. Gillis, J. Lin, N. F. Sheppard and G. J. Kellogg, *Analytical Chemistry*, 1999, **71**, 4669-4678.
226. E. A. Schilling, A. E. Kamholz and P. Yager, *Analytical Chemistry*, 2002, **74**, 1798-1804.
227. Q. Xue, A. Wainright, S. Gangakhedkar and I. Gibbons, *Electrophoresis*, 2001, **22**, 4000-4007.
228. J. Wang, M. P. Chatrathi, B. Tian and R. Polsky, *Analytical Chemistry*, 2000, **72**, 2514-2518.

229. C. B. Cohen, E. Chin-Dixon, S. Jeong and T. T. Nikiforov, *Analytical Biochemistry*, 1999, **273**, 89-97.
230. A. G. Hadd, S. C. Jacobson and J. M. Ramsey, *Analytical Chemistry*, 1999, **71**, 5206-5212.
231. C. Wang, R. Oleschuk, F. Ouchen, J. Li, P. Thibault and D. J. Harrison, *Rapid Communications in Mass Spectrometry*, 2000, **14**, 1377-1383.
232. H. Mao, T. Yang and P. S. Cremer, *Analytical Chemistry*, 2002, **74**, 379-385.
233. D. S. Peterson, T. Rohr, F. Svec and J. M. J. Fréchet, *Analytical Chemistry*, 2002, **74**, 4081-4088.
234. M. Lilly, W. Hornby and E. Crook, *Biochemical Journal*, 1966, **100**, 718.
235. P. He, G. Greenway and S. J. Haswell, *Process Biochemistry*, 2010, **45**, 593-597.
236. A. Demirbas, *Biodiesel*, Springer, 2008.
237. B. K. Barnwal and M. P. Sharma, *Renewable and Sustainable Energy Reviews*, 2005, **9**, 363-378.
238. M. S. Mannan, Y. Wang, C. Zhang and H. H. West, *Proceedings of Hazard XIX*, 2006, 982-989.
239. S. Howell, *US Biodiesel Standards-An Update of Current Activities*, Report 0148-7191, SAE Technical Paper, 1997.
240. M. Nieves-Soto, C. A. Guerrero-Fajardo, I. Contreras-Andrade, M. A. Sánchez-Castillo, O. M. Hernández-Calderón and T. Viveros-García, *Biodiesel current technology: ultrasonic process a realistic industrial application*, INTECH Open Access Publisher, 2012.
241. W. Körbitz, *Renewable Energy*, 1999, **16**, 1078-1083.
242. A. K. Agarwal and L. Das, *Journal of Engineering for Gas Turbines and Power*, 2001, **123**, 440-447.
243. M. P. Dorado, E. Ballesteros, J. M. Arnal, J. Gómez and F. J. López, *Fuel*, 2003, **82**, 1311-1315.
244. D. Oliveira, M. Luccio, C. Faccio, C. D. Rosa, J. P. Bender, N. Lipke, C. Amroginski, C. Dariva and J. V. Oliveira, in *Twenty-Sixth Symposium on Biotechnology for Fuels and Chemicals*, eds. B. H. Davison, B. R. Evans, M. Finkelstein and J. D. McMillan, Humana Press, Totowa, NJ, 2005, pp. 553-560.
245. F. Ma and M. A. Hanna, *Bioresource Technology*, 1999, **70**, 1-15.
246. E. Lotero, Y. Liu, D. E. Lopez, K. Suwannakarn, D. A. Bruce and J. G. Goodwin, *Industrial and Engineering Chemistry Research*, 2005, **44**, 5353-5363.
247. D. Y. C. Leung, X. Wu and M. K. H. Leung, *Applied Energy*, 2010, **87**, 1083-1095.
248. S. A. Singh, N. R. Singh and R. Yadav, *J. Chem*, 2010, **2**, 304-308.
249. M. Zabeti, W. M. A. Wan Daud and M. K. Aroua, *Fuel Processing Technology*, 2009, **90**, 770-777.
250. G. Vicente, M. Martínez and J. Aracil, *Bioresource Technology*, 2004, **92**, 297-305.
251. I. M. Atadashi, M. K. Aroua, A. R. Abdul Aziz and N. M. N. Sulaiman, *Journal of Industrial and Engineering Chemistry*, 2013, **19**, 14-26.
252. A. Sivasamy, K. Y. Cheah, P. Fornasiero, F. Kemausor, S. Zinoviev and S. Miertus, *ChemSusChem*, 2009, **2**, 278-300.
253. B. Bharathiraja, M. Chakravarthy, R. R. Kumar, D. Yuvaraj, J. Jayamuthunagai, R. P. Kumar and S. Palani, *Renewable and Sustainable Energy Reviews*, 2014, **38**, 368-382.
254. B. Freedman, R. O. Butterfield and E. H. Pryde, *Journal of the American Oil Chemists' Society*, 1986, **63**, 1375-1380.

255. D. M. Reinoso, M. L. Ferreira and G. M. Tonetto, *Journal of Molecular Catalysis A: Chemical*, 2013, **377**, 29-41.
256. H. C. Joshi, *Optimization and characterization of biodiesel production from cottonseed and canola oil*, ProQuest, 2008.
257. T. Čerče, S. Peter and E. Weidner, *Industrial and Engineering Chemistry Research*, 2005, **44**, 9535-9541.
258. A. Šalić and B. Zelić, *goriva i maziva*, 2011, **50**, 98-110.
259. J. Sun, J. Ju, L. Ji, L. Zhang and N. Xu, *Industrial and Engineering Chemistry Research*, 2008, **47**, 1398-1403.
260. G. Guan, K. Kusakabe, K. Moriyama and N. Sakurai, *Industrial and Engineering Chemistry Research*, 2009, **48**, 1357-1363.
261. C. Bertoldi, C. da Silva, J. P. Bernardon, M. L. Corazza, L. C. Filho, J. V. Oliveira and F. C. Corazza, *Energy and Fuels*, 2009, **23**, 5165-5172.
262. C. M. Trentin, A. P. Lima, I. P. Alkimim, C. da Silva, F. de Castilhos, M. A. Mazutti and J. V. Oliveira, *The Journal of Supercritical Fluids*, 2011, **56**, 283-291.
263. E. Santacesaria, M. Di Serio, R. Tesser, M. Tortorelli, R. Turco and V. Russo, *Chemical Engineering and Processing: Process Intensification*, 2011, **50**, 1085-1094.
264. N. Canter, *Tribology and Lubrication Technology*, 2006, **62**, 15.
265. Z. Wen, X. Yu, S.-T. Tu, J. Yan and E. Dahlquist, *Bioresource Technology*, 2009, **100**, 3054-3060.
266. G. N. Jovanovic, B. K. Paul, J. Parker and A. Al-Dhubabian, United States Patent Application. 2009, US2009/0165366A1
267. P. Sun, B. Wang, J. Yao, L. Zhang and N. Xu, *Industrial and Engineering Chemistry Research*, 2010, **49**, 1259-1264.
268. E. E. Kalu, K. S. Chen and T. Gedris, *Bioresource Technology*, 2011, **102**, 4456-4461.
269. F. Avellaneda and J. Salvadó, *Fuel Processing Technology*, 2011, **92**, 83-91.
270. A. L. Machsun, M. Gozan, M. Nasikin, S. Setyahadi and Y. J. Yoo, *Biotechnology and Bioprocess Engineering*, 2010, **15**, 911-916.
271. K. Jähnisch, V. Hessel, H. Löwe and M. Baerns, *Angewandte Chemie International Edition*, 2004, **43**, 406-446.
272. P. Ejikeme, I. Anyaogu, C. Ejikeme, N. Nwafor, C. Egbuonu, K. Ukogu and J. Ibemesi, *Journal of Chemistry*, 2010, **7**, 1120-1132.
273. M. Canakci and J. Van Gerpen, *Transactions of the ASAE*, 2001, **44**, 1429.
274. M. K. Lam, K. T. Lee and A. R. Mohamed, *Biotechnology Advances*, 2010, **28**, 500-518.
275. Y. C. Sharma, B. Singh and J. Korstad, *Fuel*, 2011, **90**, 1309-1324.
276. J. A. Melero, J. Iglesias and G. Morales, *Green Chemistry*, 2009, **11**, 1285-1308.
277. F. Su, C. Peng, G.-L. Li, L. Xu and Y.-J. Yan, *Renewable Energy*, 2016, **90**, 329-335.
278. D. T. Johnson and K. A. Taconi, *Environmental Progress*, 2007, **26**, 338-348.
279. K. R. Jegannathan, S. Abang, D. Poncelet, E. S. Chan and P. Ravindra, *Critical Reviews in Biotechnology*, 2008, **28**, 253-264.
280. X. Miao, R. Li and H. Yao, *Energy Conversion and Management*, 2009, **50**, 2680-2684.
281. C. Li, T. Tan, H. Zhang and W. Feng, *Journal of Biological Chemistry*, 2010, **285**, 28434-28441.
282. M. Turner, V. B. Golovko, O. P. H. Vaughan, P. Abdulkin, A. Berenguer-Murcia, M. S. Tikhov, B. F. G. Johnson and R. M. Lambert, *Nature*, 2008, **454**, 981-983.

283. G. C. Bond and D. T. Thompson, *Catalysis Reviews*, 1999, **41**, 319-388.
284. J. H. Clements, *Industrial and Engineering Chemistry Research*, 2003, **42**, 663-674.
285. G. Ertl, H. Knozinger, F. Schuth and J. Weitkamp, *METODOLOGÍA DOCENTE*.
286. A. G. Sault, R. J. Madix and C. T. Campbell, *Surface science*, 1986, **169**, 347-356.
287. B. Hammer and J. K. Norskov, *Nature*, 1995, **376**, 238-240.
288. G. J. Hutchings, *Catalysis Today*, 2005, **100**, 55-61.
289. A. S. K. Hashmi and G. J. Hutchings, *Angewandte Chemie International Edition*, 2006, **45**, 7896-7936.
290. G. Schmid and B. Corain, *European Journal of Inorganic Chemistry*, 2003, 3081-3098.
291. M.-C. Daniel and D. Astruc, *Chemical Reviews*, 2004, **104**, 293-346.
292. W. Abidi and H. Remita, *Recent Patents on Engineering*, 2010, **4**, 170-188.
293. S. K. Ghosh and T. Pal, *Chemical Reviews*, 2007, **107**, 4797-4862.
294. G. Schmid, R. Pfeil, R. Boese, F. Bandermann, S. Meyer, G. Calis and J. W. van der Velden, *Chemische Berichte*, 1981, **114**, 3634-3642.
295. G. Schmid, *Chemical Society Reviews*, 2008, **37**, 1909-1930.
296. D. Astruc and F. Chardac, *Chemical Reviews*, 2001, **101**, 2991-3024.
297. S. R. K. Perala and S. Kumar, *Langmuir*, 2013, **29**, 9863-9873.
298. J. Turkevich, P. C. Stevenson and J. Hillier, *Discussions of the Faraday Society*, 1951, **11**, 55-75.
299. M. Zhao, L. Sun and R. M. Crooks, *Journal of the American Chemical Society*, 1998, **120**, 4877-4878.
300. A. Corma and H. Garcia, *Chemical Society Reviews*, 2008, **37**, 2096-2126.
301. R. Zanella, A. Sandoval, P. Santiago, V. A. Basiuk and J. M. Saniger, *The Journal of Physical Chemistry B*, 2006, **110**, 8559-8565.
302. P. Floris, B. Twamley, P. N. Nesterenko, B. Paull and D. Connolly, *Microchimica Acta*, 2013, **181**, 249-256.
303. M. Hussain, D. Fino and N. Russo, *Chemical Engineering Journal*, 2014, **238**, 198-205.
304. F. Al Badran, S. Awdry and S. T. Kolaczowski, *Catalysis Today*, 2013, **216**, 229-239.
305. W. Eck, G. Craig, A. Sigdel, G. Ritter, L. J. Old, L. Tang, M. F. Brennan, P. J. Allen and M. D. Mason, *ACS Nano*, 2008, **2**, 2263-2272.
306. S. Guo, Y. Huang, Q. Jiang, Y. Sun, L. Deng, Z. Liang, Q. Du, J. Xing, Y. Zhao, P. C. Wang, A. Dong and X.-J. Liang, *ACS Nano*, 2010, **4**, 5505-5511.
307. L. Calzolari, F. Franchini, D. Gilliland and F. Rossi, *Nano Letters*, 2010, **10**, 3101-3105.
308. D. F. Moyano and V. M. Rotello, *Langmuir*, 2011, **27**, 10376-10385.
309. G. Lü, R. Zhao, G. Qian, Y. Qi, X. Wang and J. Suo, *Catalysis Letters*, 2004, **97**, 115-118.
310. C. M. Alexander, M. M. Maye and J. C. Dabrowiak, *Chemical Communications*, 2011, **47**, 3418-3420.
311. J. A. Khan, R. A. Kudgus, A. Szabolcs, S. Dutta, E. Wang, S. Cao, G. L. Curran, V. Shah, S. Curley and D. Mukhopadhyay, *PLoS One*, 2011, **6**, e20347.
312. Y. Liu, H. Tsunoyama, T. Akita, S. Xie and T. Tsukuda, *ACS Catalysis*, 2011, **1**, 2-6.
313. N. S. Patil, B. S. Uphade, P. Jana, S. K. Bharagava and V. R. Choudhary, *Journal of Catalysis*, 2004, **223**, 236-239.

314. I. Hussain, S. Graham, Z. Wang, B. Tan, D. C. Sherrington, S. P. Rannard, A. I. Cooper and M. Brust, *Journal of the American Chemical Society*, 2005, **127**, 16398-16399.
315. M. Grzelczak, J. Pérez-Juste, P. Mulvaney and L. M. Liz-Marzán, *Chemical Society Reviews*, 2008, **37**, 1783-1791.
316. S. Roux, B. Garcia, J.-L. Bridot, M. Salomé, C. Marquette, L. Lemelle, P. Gillet, L. Blum, P. Perriat and O. Tillement, *Langmuir*, 2005, **21**, 2526-2536.
317. C. J. Ackerson, P. D. Jadzinsky and R. D. Kornberg, *Journal of the American Chemical Society*, 2005, **127**, 6550-6551.
318. G. Frens, *Nature*, 1973, **241**, 20-22.
319. K. Aslan and V. H. Pérez-Luna, *Langmuir*, 2002, **18**, 6059-6065.
320. S.-Y. Lin, Y.-T. Tsai, C.-C. Chen, C.-M. Lin and C.-h. Chen, *The Journal of Physical Chemistry B*, 2004, **108**, 2134-2139.
321. M. Brust, M. Walker, D. Bethell, D. J. Schiffrin and R. Whyman, *Journal of the Chemical Society, Chemical Communications*, 1994, 801-802.
322. M. J. Hostetler, J. E. Wingate, C.-J. Zhong, J. E. Harris, R. W. Vachet, M. R. Clark, J. D. Londono, S. J. Green, J. J. Stokes, G. D. Wignall, G. L. Glish, M. D. Porter, N. D. Evans and R. W. Murray, *Langmuir*, 1998, **14**, 17-30.
323. J. C. Love, L. A. Estroff, J. K. Kriebel, R. G. Nuzzo and G. M. Whitesides, *Chemical Reviews*, 2005, **105**, 1103-1170.
324. G. Perego, *Catalysis Today*, 1998, **41**, 251-259.
325. G. Arrhenius, *Journal of Chemical Education*, 1955, **32**, 228.
326. T. Carlson, *Inc., Stroudsburg*, 1978.
327. M. Casaletto, A. Longo, A. Martorana, A. Prestianni and A. Venezia, *Surface and Interface Analysis*, 2006, **38**, 215-218.
328. M. P. Seah and D. Briggs, *Practical Surface Analysis: Auger and X-ray Photoelectron Spectroscopy*, John Wiley and Sons, 1990.
329. S. Hüfner, *Photoelectron spectroscopy: principles and applications*, Springer Science and Business Media, 2013.
330. D. B. Williams and C. B. Carter, *Micron*, 1997, **28**, 75-75.
331. M. Welna, A. Szymczycha-Madeja and P. Pohl, *Quality of the trace element analysis: sample preparation steps*, INTECH Open Access Publisher, 2011.
332. J. Sneddon and M. D. Vincent, *Analytical Letters*, 2008, **41**, 1291-1303.
333. V. R. Choudhary and D. K. Dumbre, *Topics in Catalysis*, 2009, **52**, 1677-1687.
334. R. A. Sheldon and H. Van Bekkum, *Fine chemicals through heterogeneous catalysis*, John Wiley and Sons, 2008.
335. L. Hu, L. Shi, H. Hong, M. Li, Q. Bao, J. Tang, J. Ge, J. Lu, X. Cao and H. Gu, *Chemical Communications*, 2010, **46**, 8591-8593.
336. S. Tang, Y. Guo, C. Xiong, S. Liu, X. Liu and S. Jiang, *Analyst*, 2014, **139**, 4103-4117.
337. J. Randon, S. Hugué, C. Demesmay and A. Berthod, *Journal of Chromatography A*, 2010, **1217**, 1496-1500.
338. W. Sun, Q. Li, S. Gao and J. K. Shang, *Chemical Engineering Journal*, 2012, **185-186**, 136-143.
339. G. Kyriakou, S. K. Beaumont, S. M. Humphrey, C. Antonetti and R. M. Lambert, *ChemCatChem*, 2010, **2**, 1444-1449.
340. S. K. Beaumont, G. Kyriakou and R. M. Lambert, *Journal of the American Chemical Society*, 2010, **132**, 12246-12248.
341. G. Wang, D. Kundu and H. Uyama, *Journal of Colloid and Interface Science*, 2015, **451**, 184-188.

342. R. Poupart, B. Le Droumaguet, M. Guerrouache and B. Carbonnier, *Materials Chemistry and Physics*, 2015, **163**, 446-452.
343. I. Miguel-García, M. Navlani-García, J. García-Aguilar, Á. Berenguer-Murcia, D. Lozano-Castelló and D. Cazorla-Amorós, *Chemical Engineering Journal*, 2015, **275**, 71-78.
344. P. Landon, J. Ferguson, B. E. Solsona, T. Garcia, A. F. Carley, A. A. Herzing, C. J. Kiely, S. E. Golunski and G. J. Hutchings, *Chemical Communications*, 2005, 3385-3387.
345. M. D. Hughes, Y.-J. Xu, P. Jenkins, P. McMorn, P. Landon, D. I. Enache, A. F. Carley, G. A. Attard, G. J. Hutchings, F. King, E. H. Stitt, P. Johnston, K. Griffin and C. J. Kiely, *Nature*, 2005, **437**, 1132-1135.
346. N. S. Patil, R. Jha, B. S. Uphade, S. K. Bhargava and V. R. Choudhary, *Applied Catalysis A: General*, 2004, **275**, 87-93.
347. P. He, S. J. Haswell, P. D. Fletcher, S. M. Kelly and A. Mansfield, *Beilstein Journal of Organic Chemistry*, 2011, **7**, 1150-1157.
348. K. Nakanishi and N. Soga, *Journal of Non-Crystalline Solids*, 1992, **139**, 1-13.
349. J. Liu, S. Zou, S. Li, X. Liao, Y. Hong, L. Xiao and J. Fan, *Journal of Materials Chemistry A*, 2013, **1**, 4038-4047.
350. J. Ou, Z. Liu, H. Wang, H. Lin, J. Dong and H. Zou, *Electrophoresis*, 2015, **36**, 62-75.
351. R. Göbel, P. Hesemann, A. Friedrich, R. Rothe, H. Schlaad and A. Taubert, *Chemistry—A European Journal*, 2014, **20**, 17579-17589.
352. E. Skrzyńska, J. Ftouni, A.-S. Mamede, A. Addad, M. Trentesaux, J.-S. Girardon, M. Capron and F. Dumeignil, *Journal of Molecular Catalysis A: Chemical*, 2014, **382**, 71-78.
353. C. D. Pina, E. Falletta and M. Rossi, *Chemical Society Reviews*, 2012, **41**, 350-369.
354. J. Liu, L. Zhang, Q. Yang and C. Li, *Microporous and Mesoporous Materials*, 2008, **116**, 330-338.
355. J. N. Miller and J. C. Miller, *Statistics and Chemometrics for Analytical Chemistry*, Pearson/Prentice Hall, 2005.
356. S. T. Anuar, Y.-Y. Zhao, S. M. Mugo and J. M. Curtis, *Journal of Molecular Catalysis B: Enzymatic*, 2013, **92**, 62-70.
357. M. Lotti, J. Pleiss, F. Valero and P. Ferrer, *Biotechnology Journal*, 2015, **10**, 22-30.
358. W. Du, D. Liu, L. Li and L. Dai, *Biotechnology Progress*, 2007, **23**, 1087-1090.
359. S. Tamalampudi, M. R. Talukder, S. Hama, T. Numata, A. Kondo and H. Fukuda, *Biochemical Engineering Journal*, 2008, **39**, 185-189.
360. V. Kumari, S. Shah and M. N. Gupta, *Energy and Fuels*, 2007, **21**, 368-372.
361. M. Szcześna Antczak, A. Kubiak, T. Antczak and S. Bielecki, *Renewable Energy*, 2009, **34**, 1185-1194.
362. N. Dizge and B. Keskinler, *Biomass and Bioenergy*, 2008, **32**, 1274-1278.
363. R. C. Rodrigues, G. Volpato, K. Wada and M. A. Z. Ayub, *Journal of the American Oil Chemists' Society*, 2008, **85**, 925-930.
364. K. Nie, F. Xie, F. Wang and T. Tan, *Journal of Molecular Catalysis B: Enzymatic*, 2006, **43**, 142-147.
365. L. Wang, H. Wang, P. Hapala, L. Zhu, L. Ren, X. Meng, J. P. Lewis and F.-S. Xiao, *Journal of Catalysis*, 2011, **281**, 30-39.
366. K. Zhu, J. Hu and R. Richards, *Catalysis Letters*, 2005, **100**, 195-199.
367. P. Wu, Z. Xiong, K. P. Loh and X. S. Zhao, *Catalysis Science and Technology*, 2011, **1**, 285-294.

368. E. L. Pires, J. C. Magalhães and U. Schuchardt, *Applied Catalysis A: General*, 2000, **203**, 231-237.
369. A. Corma, P. Esteve and A. Martínez, *Journal of Catalysis*, 1996, **161**, 11-19.
370. N. Yu, Y. Ding, A.-Y. Lo, S.-J. Huang, P.-H. Wu, C. Liu, D. Yin, Z. Fu, D. Yin, C.-T. Hung, Z. Lei and S.-B. Liu, *Microporous and Mesoporous Materials*, 2011, **143**, 426-434.
371. W. Chen, J. Zhang, Y. Di, Z. Wang, Q. Fang and W. Cai, *Applied Surface Science*, 2003, **211**, 280-284.
372. W. Chen, J. Zhang, L. Shi, Y. Di, Q. Fang and W. Cai, *Composites Science and Technology*, 2003, **63**, 1209-1212.
373. C. Huo, J. Ouyang and H. Yang, *Scientific Reports*, 2014, **4**.
374. S. Altmaier and K. Cabrera, *Journal of Separation Science*, 2008, **31**, 2551-2559.
375. J. Le Bideau, M. Y. Miah, A. Vioux, F. Fajula and A. Galarneau, *Journal of Materials Chemistry*, 2010, **20**, 964-971.
376. A. Ghanem and T. Ikegami, *Journal of Separation Science*, 2011, **34**, 1945-1957.
377. D. Zhao, J. Sun, Q. Li and G. D. Stucky, *Chemistry of Materials*, 2000, **12**, 275-279.
378. G. M. Veith, A. R. Lupini, S. Rashkeev, S. J. Pennycook, D. R. Mullins, V. Schwartz, C. A. Bridges and N. J. Dudney, *Journal of Catalysis*, 2009, **262**, 92-101.
379. R. Munirathinam, J. Huskens and W. Verboom, *Advanced Synthesis and Catalysis*, 2015, **357**, 1093-1123.
380. G. Somorjai and S. Beaumont, *Topics in Catalysis*, 2015, **58**, 560-572.
381. A. Jablonski, National Institute of Standards and Technology, 2010.
382. A. Venkateswara Rao and R. R. Kalesh, *Science and Technology of Advanced Materials*, 2003, **4**, 509-515.
383. C. Xie, J. Hu, H. Xiao, X. Su, J. Dong, R. Tian, Z. He and H. Zou, *Journal of Separation Science*, 2005, **28**, 751-756.

Publication and presentations

Publication:

Alotaibi M, Tylor M , Liu D, Beaumont S, Kyriakou G "Selective oxidation of cyclohexene through gold functionalized silica monolith microreactors." *Surface Science* 646 (2016): 179-185.

Conferences:

1. 2nd SCI/RSC Symposium on Continuous Processing and Flow Chemistry in Novartis, Horsham, UK, September 2013. "Monolith based immobilised lipase microreactors for biocatalytic reactions".
2. 13th International Conferences on MicroREaction Technologyn (IMRET 13) in Budapest, Hungary , June 2014. "Monolith based immobilised lipase microreactors for biocatalytic reactions".
3. The 9th Saudi Students Conference in the UK, at the International Convention Centre (ICC) in Birmingham, Febrauary 2016. "Selective oxidation of cyclohexene through gold functionalized silica monolith microreactors".